



Biochemical Characterization of RHO GTPases- IQGAPs and NPM1-US11/Rev interactions

Inaugural-Dissertation

for the attainment of the title of doctor
in the Faculty of Mathematics and Natural Sciences
at the Heinrich Heine University Düsseldorf

presented by

Kazem Nouri

from

Kazeroon, Iran

Düsseldorf, November 2015

From the Institute of Biochemistry and Molecular Biology II
At Medical Faculty of the Heinrich-Heine University Düsseldorf

Published by permission of the
Faculty of Mathematics and Natural Sciences
at Heinrich-Heine University Düsseldorf

Supervisor: Prof. Dr. Reza Ahmadian
Co-supervisor: Prof. Dr. Lutz Schmitt

Date of the oral examination:

Summary

Proteins can be assembled into specific complexes especially by scaffold proteins, which safeguard as control elements the strength, efficiency, fidelity and specificity of signal transduction within the cells. A variety of scaffold proteins, *e.g.*, IQ domain GTPase-activating protein 1 (IQGAP1), nucleophosmin (NPM1), and nucleolin (NCL), has been reported to directly bind small GTPases of the RAS and RHO family and to control their signaling processes. RHO- and RAS-related proteins, which normally act as molecular switches in diverse biological processes, are frequently dysregulated in diseases, such as cardiovascular and infectious diseases, developmental and neurological disorders, and cancer. Deciphering new functional control mechanisms and defining new targets is essential for the rational development of highly selective drugs that attenuate signal transduction rather than inhibiting it. An essential prerequisite to elucidate the mechanism behind functions of scaffold proteins is the dissection of their individual domains and the analysis of their interactions with desired protein partners; and this was the aim of the present dissertation. Comprehensive investigation of IQGAP1 interaction with the RHO family proteins revealed for the first time that IQGAP1 association with RAC- and CDC42-related proteins underlies a two-step mechanism, first a low-affinity, nucleotide-independent binding of the GAP-related domain outside the switch regions, and second a high-affinity, GTP-dependent binding of the GTPase binding domain to the switch regions of RAC- and CDC42-related proteins. These results provide the field with new insights into interaction characteristics of RHO GTPases with IQGAP1, which is a critical mechanism in temporal regulation and integration of IQGAP1-mediated cellular responses. In contrast, a proposed physical interaction of NPM1 and NCL with the RAS isoforms (HRAS, NRAS, and KRAS) was not verified in this study but instead new interactions of their domains were explored in-depth. NPM1 interactions with HIV-1 Rev and HSV-1 US11, two functionally homologous viral proteins, in the presence and in the absence of a blocking cyclic peptide (CIGB-300), provided unprecedented insights into the key role of NPM1 in viral infections that may represent a novel promising target for antiviral therapeutic intervention. The identification of a direct interaction between NCL and the fragile X mental retardation protein (FMRP) pointed to a novel mechanism underlying a transient nucleocytoplasmic and nucleolar translocation and regulating different processes, *e.g.*, ribosome biogenesis.

Zusammenfassung

Proteine können in spezifischen Komplexen durch sog. Adaptor- bzw. Gerüstproteine „vernetzt“ werden, die in den Zellen als Kontrollelemente Stärke, Effizienz und Spezifität eines Signaltransduktionswegs kontrollieren/regulieren. Verschiedenen Studien zufolge regulieren/kontrollieren eine Reihe von Gerüstproteinen, u.a. *IQ domain GTPase-activating protein 1* (IQGAP1), Nucleophosmin (NPM1), und Nucleolin (NCL) die Signalprozesse kleiner GTPasen der RAS- und Rho-Familie, indem sie direkt mit ihnen interagieren. RAS- und RHO-verwandte Proteine, die als molekulare Schalter normalerweise in diversen biologischen Prozessen agieren, sind sehr häufig bei kardiovaskulären und neuronalen Erkrankungen, Infektionserkrankungen, Entwicklungsstörungen und Tumorerkrankungen fehlreguliert. Die Entschlüsselung neuer funktionaler Kontrollmechanismen und die Definition neuer Targets sind essentiell für die rationale Entwicklung hochselektiver Pharmazeutika, welche die Signaltransduktion abschwächt, aber nicht vollständig inhibiert. Eine wesentliche Voraussetzung zur Aufklärung der Funktion der Gerüstproteine ist ihre Zerlegung in einzelnen Domänen und die Untersuchung deren Interaktionen mit den entsprechenden Bindungspartnern, was das Hauptziel der vorliegenden Dissertation darstellte. Umfassende Untersuchungen der IQGAP1-Interaktion mit den Proteinen der RHO-Familie haben hierbei gezeigt, dass die Assoziation von IQGAP1 mit RAC- und CDC42-verwandten Proteinen einem zwei-Schritt Mechanismus unterliegt. Dieser umfasst eine niederaffine Nukleotid-unabhängige Bindung an die GAP-verwandte Domäne außerhalb der Schalterregionen, gefolgt von einer hochaffinen, GTP-abhängigen Bindung der GTPase-Bindungsdomäne an die Schalterregionen von RAC- und CDC42-verwandten Proteinen. Diese Resultate tragen zum besseren Verständnis der Bindungseigenschaften von RHO-GTPasen mit IQGAP1 und somit der zeitlichen Regulation und Integration IQGAP1-vermittelter zellulärer Antworten. Demgegenüber stehen die Gerüstproteine NPM1 und NCL, deren vorgeschlagenen physikalischen Interaktionen mit den RAS-Isoformen (HRAS, NRAS, und KRAS) in dieser Arbeit nicht bestätigt werden konnten. Eingehende Untersuchungen einzelner Domänen von NPM1 und NCL identifizierten stattdessen neue Interaktionen. Die NPM1-Interaktionen mit HIV1-1 Rev und HSV-1 US11, zwei funktionell homologe virale Proteine, in der An- und Abwesenheit eines blockierenden zyklischen Peptids (CIGB-300), lieferten neue Einblicke in die Schlüsselrolle von NPM1 bei viralen Infektionen. Letzteres repräsentiert derzeit eine neue und viel versprechende Zielstruktur für die Entwicklung antiviraler Wirkstoffe. Die Charakterisierung der direkten Interaktion zwischen NCL und *fragile X mental retardation protein* (FMRP) weist auf einem wichtigen Mechanismus hin, dem eine vorübergehende nukleozytoplasmatische und nukleoläre Translokation von NCL zugrunde liegt und hierbei unterschiedliche Prozesse, wie beispielsweise die *Ribosomen-Biogenese*, reguliert wird.

TABLE OF CONTENTS

Chapter I	1
General introduction	1
1 RAS Superfamily	2
1.1 Classification of RAS Small GTPases	2
1.2 Structural properties of the RAS GTPases	3
2 Small GTPases of the RHO family	5
2.1 Biological functions and role in human diseases	6
2.2 RHO mutations in tumor progression	7
2.3 Structural features of RHO proteins.....	8
2.4 Regulation of RHO proteins activity by nucleotide binding	8
2.5 RHO GTPases and their effectors	9
3 Protein scaffolds	10
3.1 IQGAPs.....	11
3.1.1 IQGAP1 domain organization and interacting partners.....	13
3.1.2 IQGAP1-RHO interaction and regulating cellular functions	13
3.2 Nucleophosmin and nucleolin.....	15
3.2.1 Structural features	15
3.2.2 Interacting partners.....	16
3.2.3 Role in cell signaling and human diseases.....	17
3.2.4 Role in viral infection.....	18
3.3 Fragile X mental retardation (FMRP)	22
4 Aims of this thesis	23
Chapter II	24
Classical RHO Proteins: Biochemistry of Molecular Switch Function and Regulation	24
Chapter III	39
Juvenile myelomonocytic leukemia displays mutations in components of the RAS pathway and the PRC2 network.....	39
Chapter IV	66
IQGAP1 interaction with RHO family proteins revisited: kinetic and equilibrium evidence for two distinct binding sites	66
Chapter V	99
Biophysical Characterization of Nucleophosmin Interactions with Human Immunodeficiency Virus Rev and Herpes Simplex Virus US11	99

Chapter VI	130
Subcellular Fractionation and Localization Studies Reveal a Direct Interaction of the Fragile X Mental Retardation Protein (FMRP) with Nucleolin	130
Chapter VII	142
The Centrosomal Adaptor TACC3 and the Microtubule Polymerase chTOG Interact <i>via</i> Defined C-terminal Subdomains in an Aurora-A Kinase-independent Manner	142
Chapter VIII	180
5 Discussion	181
5.1 Classical RHO proteins and Juvenile myelomonocytic leukemia (JMML)	182
5.2 RHO family GTPases and IQGAP1 interaction	184
5.3 Nucleophosmin and viral infection	187
5.4 Nucleolin and FMRP interaction	190
6 References	192
7 Acknowledgments	207
8 Curriculum Vitae	208
9 Declaration	210

LIST OF FIGURES

Figure 1. RAS superfamily of small G proteins.....	3
Figure 2. Motifs and structure of the RAS superfamily proteins.	5
Figure 3. Phylogenetic tree of the RHO family proteins.	7
Figure 4. RHO Proteins as molecular switches.....	9
Figure 5. IQGAP isoforms and their tissue expression.....	12
Figure 6. Schematic representation of the protein interaction domains of IQGAP1.	13
Figure 7. Functional domains organization of nucleophosmin (NPM1), and nucleolin (NCL).....	16
Figure 8. Nucleophosmin signaling	18
Figure 9. Model for the molecular mechanism of RAC1/CDC42 interaction with IQGAP1	187
Figure 10. Model for the regulation of nuclear export and import of Rev and US11.....	190

LIST OF ABBREVIATIONS

aa	amino acids
ACK	CDC42-associated tyrosine kinase
AD	acidic domain
ARF	ADP ribosylation factor
Arp2 /3	actin-related proteins 2/3
aSEC	analytical SEC
CBB	coomassie brilliant blue
CDC42	cell division control protein 42 homolog
CHD	calponine homology domain
CRIB	CDC42/RAC-interactive binding
DNA	deoxyribonucleic acid
e.g.	exempli gratia, for example
ERK	extracellular regulated kinase
FL	full-length
FMRP	fragile X mental retardation protein
GAP	GTPase-activating protein
GAR	glycine-arginine rich
GBD	GTPase-binding domain
GDI	guanine nucleotide dissociation inhibitor
GDP	guanosine diphosphate
GEF	guanine-nucleotide-exchange factor
GRD	GAP-related domain
GTP	guanosine triphosphate
GTPases	guanosine triphosphatases
HBD	histone binding domain
HCC	hepatocellular carcinoma
HGF	hepatocyte growth factor
HIV-1	human immunodeficiency virus type 1
HRAS	harvey rat sarcoma
HRBD	histone and RNA-binding domains
HSC	hepatic stellate cell
HSV-1	herpes simplex virus type 1
HVR	hypervariable region
IP	immunoprecipitation
IQ	protein sequences containing Iso/Leu and Gln residues
IQGAPs	IQ-domain GTPase- activating proteins
ITC	isothermal titration calorimetry
JMML	juvenile myelomonocytic leukemia
kDa	kilo dalton
KRAS	kirsten rat sarcoma
Lis1	lissencephaly 1
MALS	multi angle light scattering
MAPK	mitogen-activated protein kinase
MEK	MAPK/ERK kinase
NCL	nucleolin
NES	nuclear export signal
NF1	neurofibromatosis type 1
NLS	nuclear localization signals

NoLS	nucleolar localization signal
NPM1	nucleophosmin
OD	oligomerization domain
PAK	p21-activated kinase
PD	pull-down
PKC	protein kinase C
RAC	RAS-related C3 botulinum toxin substrate
RAF	rapidly accelerated fibrosarcoma
RAN	RAS-related nuclear protein
RAS	rat sarcoma
RBD	RNA binding domain
RHO	RAS homolog
RNA	ribonucleic acid
RRM	RNA recognition motifs
SEC	size exclusion chromatography
WASP	wiskott–aldrich-syndrome protein
WT	wild type
WW	tryptophan-containing protein domain

Amino Acid	Three letter code	One letter code
alanine	ala	A
arginine	arg	R
asparagine	asn	N
aspartic acid	asp	D
cysteine	cys	C
glutamine	gln	Q
glutamic acid	glu	E
glycine	gly	G
histidine	his	H
isoleucine	ile	I
leucine	leu	L
lysine	lys	K
methionine	met	M
phenylalanine	phe	F
proline	pro	P
serine	ser	S
threonine	thr	T
tryptophan	trp	W
tyrosine	tyr	Y
valine	val	V

Chapter I

General introduction

Kazem Nouri

1 RAS Superfamily

As of today the RAS superfamily of small guanosine triphosphatases (GTPases) comprise over 167 human members, which are small proteins between 20-25 kDa in size and classified by a conserved structural domain. In the beginning, *RAS* genes were identified as viral oncogenes found in the Harvey murine sarcoma virus (Ha-MuSV) and the Kirsten murine sarcoma virus (Ki-MuSV), which encode a 21 kDa phosphoprotein and induce tumor formation in new-born rodents [1-3]. Shortly after that it was shown that transforming genes are detected in human tumor cell lines and these oncogenes originated from genes called *HRAS* and *KRAS* [4]. The first human *RAS* gene was identified in human bladder carcinoma cell line and it was shown that bladder cancer *HRAS* gene is activated by a codon 12 mutation [5-7]. In 1982, transforming genes in human cancer cell lines identified as *HRAS* and *KRAS* sequences and this finding led to beginning of an intensive focus on studying biology, biochemistry, and structure of the RAS proteins. Normal cellular *RAS* genes were cloned, sequenced, and it was found very soon that they encode 21 kDa proteins, which bind the guanine nucleotides GDP and GTP, have GTPase activity, and are localized at the inner leaflet of the plasma membrane [3,8]. Later, it was shown that *HRAS* C-terminus, especially Cys186 is required for its posttranslational modification, membrane association, and transformation [3]. They show high-affinity binding for GDP and GTP, and have low intrinsic nucleotide exchange and GTP hydrolysis reactions. Their GDP/GTP exchange activity is controlled by guanine-nucleotide-exchange factors (GEFs) and GTPase-activating proteins (GAPs) as regulatory proteins [9]. So, these proteins act as molecular switches, have diverse regulatory functions, and control a wide variety of processes within the cell.

1.1 Classification of RAS Small GTPases

The human RAS superfamily is divided into five classical subfamilies, including RAS, RHO, RAB, RAN, and ARF (**Fig. 1**) [10-12]. Most of the biological and biochemical processes in the cells are accomplished by the crosstalk of different proteins and it is not easy to define the unique function of a certain small GTPase family alone [13]. The RAB family is by far the largest family. RAB GTPases and their effectors coordinate consecutive stages of transport such as intracellular vesicular transport and the protein trafficking between different organelles in the endocytic and secretory pathways [14]. There is only one copy of the RAS-like nuclear (RAN) protein in the human genome, but it is the most highly expressed protein in human. It functions as a positional marker of the genome and regulates the nucleocytoplasmic transport of RNAs and proteins through NPC (nuclear pore complex) [15]. The ADP ribosylation factor (ARF) family is by far the most diverse and divergent family of the RAS superfamily. ARF family members are also a central

role player in the membrane trafficking and phospholipid metabolism pathways of eukaryotic cells [16,17], and eventually the RHO proteins, which are the main focus of this thesis, are mostly known to direct the reorganization of the actin cytoskeleton at a specific time and site in the cell [18,19].

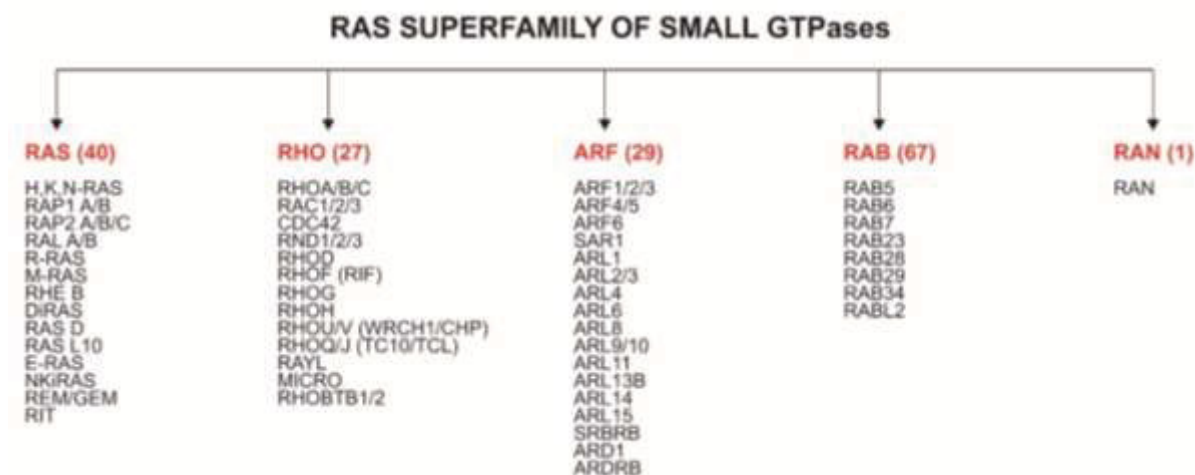


Figure 1. RAS superfamily of small G proteins. RAS superfamily consists of 167 human members which is divided to five subfamily, including RAS, RHO, RAB, ARF, and RAN. Numbers indicate the orthologues found in each subfamily. Modified from [20].

1.2 Structural properties of the RAS GTPases

By comparing the amino acid sequences of RAS proteins from different species, it has been shown that these proteins are highly conserved with a homology of 30–55%. Among RAS proteins, each protein shares quite high amino acid identity (~50%), while RAB and RHO/RAC/CDC42 proteins share ~30% amino acid identity with RAS proteins [21,22]. All these proteins share a core GDP/GTP-binding (G) domain (RAS residues 5-166; approximately 19 kDa) that has a universal structure and carries out the basic functions of nucleotide binding and hydrolysis [11]. This domain is the basis for the molecular switch function of almost all RAS-like proteins cycling between an active GTP-bound state, and an inactive GDP-bound, which are highly conserved in all GTPases [11,23,24]. They share five conserved GDP/GTP-binding (G) motifs. G1 (L1) box or the “Walker A motif” with the consensus sequence GX4GKS/T (residues 10-17 in HRAS), is a glycine-rich phosphate binding (P) loop, which provides the highest contribution to high-affinity binding of the nucleotides. This motif comprises three vital residues: codon 12 encoding for Gly12 that is the most frequently mutated RAS codon in human tumors [25,26]; Lys16 is responsible for the formation of a ring-like structure, which wrap around the β - and γ -phosphate oxygen and generate a positively charged environment; Ser17 with its hydroxyl group coordinates the Mg^{2+} ion and the β -phosphate oxygen [27-29]. G2 box or L2 (residues 32-40 in HRAS) also called effector binding site or switch I, contains a threonine (Thr35 in HRAS), that is conserved in almost

all members of RAS superfamily. Switch I region overlaps with G2 box and locates between $\alpha 1$ helix and $\beta 2$ strand. This conserved residue is crucial for sensing the presence of the γ -phosphate of GTP and coordinates the magnesium (Mg^{2+}) ion. It is absolutely crucial for the functional dynamics of the switch I region, and is therefore essential for the interaction with effector proteins [30]. Switch II region comprises part of $\alpha 2$ helix and G3 motif. G3 box, L4 or “Walking B motif” is the DX2G motif (residues 53-62 in HRAS), close to “switch II” region with a conserved aspartate (Asp 57 in HRAS) in the vicinity of the Mg^{2+} ion and a Gly (Gly60 in HRAS) that coordinates the γ -phosphate by a main chain hydrogen bond, and is a key sensor for the conformational change of the switch II region [31]. G4 is the N/TKXD motif (residues 112-119 in HRAS), where an aspartate (Asp 119 in HRAS) binds to the nitrogen atoms of the base with two hydrogen bonds, and an asparagine and a lysine (116 and 117 in HRAS) contacting the oxygen of the purine, which are important in conferring the specificity to the guanine base [10]. G5 box is the SAK motif (residues 144-146 in HRAS), where a serine side chain (145 in HRAS) stabilizes the neighbor loop in a tight turn, and an alanine (146 in HRAS) that binds the guanine base and is another determinant for the guanine-specificity of RAS [10,30,32]. The conformations of switch I and switch II largely change when the G domain cycles between the GDP-bound and GTP-bound states. The conformational change can best be interpreted as a “loaded spring” mechanism. Presence of the GTP γ -phosphate causes the switch I and switch II regions to locate in the position close to the nucleotide. Once the γ -phosphate is cleaved off after GTP hydrolysis, the switch regions relax into the “open”-GDP specific conformation. Such GTP-induced conformational changes are crucial for the function of molecular switch (**Fig. 2**) [11,33,34].

In addition, small GTPases belonging to RAS, RHO/RAC/CDC42, and RAB proteins have sequences at their carboxyl (C) terminal that undergo posttranslational modifications with lipid, such as palmitoyl, geranylgeranyl, farnesyl, methyl moieties, and proteolysis. Indeed the main difference between RAS superfamily members comes from the carboxyl (C) terminal hypervariable region (HVR; residues 165-185 in HRAS; 173-189 in RHOA; 181-212 in RAB5) [35-37]. HVR is important for membrane association of small GTPases and probably plays a role in selectivity for different binding partners [38]. In the case of RHO GTPases, the HVR is sufficient for association of the proteins with the membrane without any posttranslational modification [39].

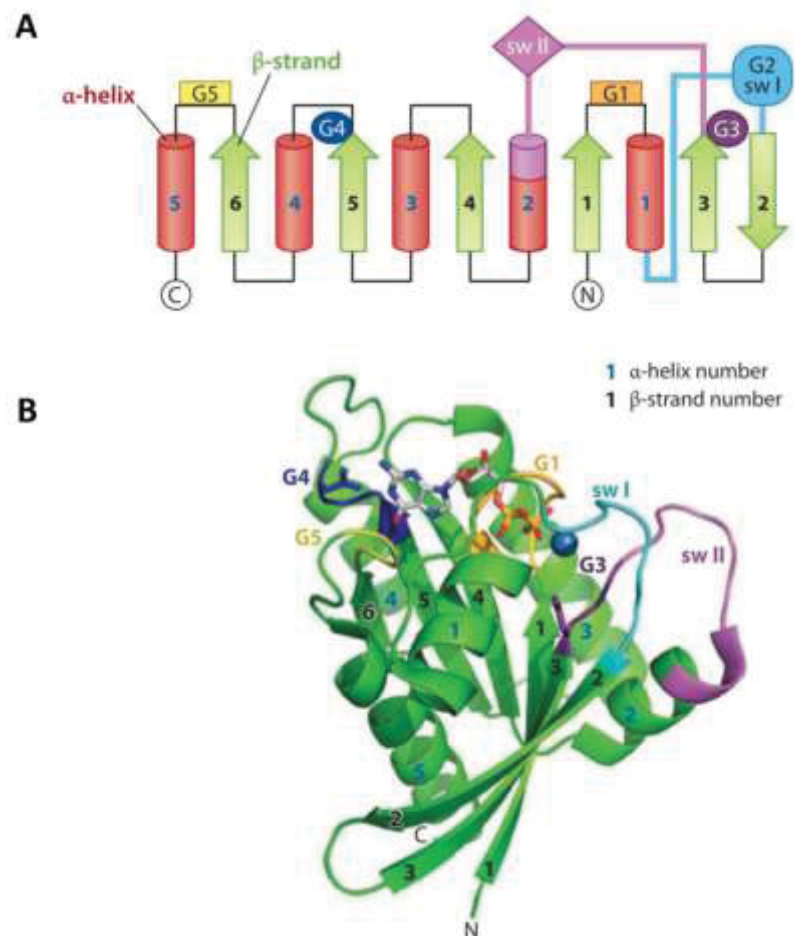


Figure 2. Motifs and structure of the RAS superfamily proteins. (A) Topology diagram for G-domains of the RAS superfamily. α -helices are shown in red and β -strands in green, and N and C termini are indicated. **(B)** Three dimensional structure of the G-domain with labeled position of the conserved nucleotide binding motifs (same color code like in (a)), P loop is shown in orange [34].

2 Small GTPases of the RHO family

RHO (RAS homologous) family proteins are involved in a variety of cellular processes by modulating cytoskeletal organization, cell polarity, transcription, cell cycle progression, and hematopoiesis [40,41]. So far, 22 human proteins of the RHO family have been identified, that can be divided into six distinct subfamilies based on their sequence homology and biological functions: (1) RHO-related group, i.e. RHOA, RHOB, RHOC; (2) the RAC-related group, i.e. RAC1 (and its splice variant RAC1b), RAC2, RAC3, RHOG; (3) the CDC42-related group, i.e. CDC42 (and its brain-specific C-terminal splice variant G25K), TC10, TCL, RHOU/WRCH1, RHOV/CHP; (4) RHOD, i.e. RHOD, RIF; (5) RND, i.e. RND1, RND2, RND3; (6) RHOBTB group, i.e. RHOBTB1, RHOBTB2, and RHOH/TTF (**Fig. 3**) [18,40,42,43] (**chapter 2**).

2.1 Biological functions and role in human diseases

The RHO family GTPases play an important role in diverse cellular processes and progression of different diseases, such as cardiovascular diseases, developmental and neurological disorders, tumor invasion and metastasis as well as regulating liver regeneration [44-51]. They are main regulators of cytoskeletal dynamics and stimulate various cellular processes, including migration, neuronal development, morphogenesis, cell polarity, cell division and adhesion, cytokinesis, embryonic development, immune response, wound healing, tumor formation, and metastasis [40,52-54]. Moreover, they regulate microtubule dynamics, vesicle transport, gene expression, and cell cycle progression [54]. Of the RHO GTPase family members, RAC1, RHOA, and CDC42 have been most extensively studied and characterized. Activation of RAC1 results in the membrane ruffling and lamellipodia formation, while CDC42 leads to the formation of filopodia [54]. RHOA promotes the formation of actin stress fibers and focal adhesion assembly [55,56]. Other RHO GTPases such as TC10 (RHOQ), WRCH1 (RHOU), RIF (RHOF), and RHOD also promote filopodia formation [57-59]. RHO GTPases are also implicated in various aspects of neuronal development, including neurite extension, axon specification, and axon guidance, hence perturbations in RHO GTPase signaling may lead to cognitive disorders [60]. Numbers of enzymatic activities which are involved in lipid metabolism or implicated in changes to the actin cytoskeleton are also influenced by RHO GTPases [61,62]. It has been shown that RHOA, RAC1, and CDC42 contribute to G1 cell cycle progression of fibroblasts and epithelial cells in culture, and all of them when expressed in quiescent fibroblasts are able to stimulate entry into G1 and progression to S phase [63,64]. Some effects of RHO GTPases on G1 progression, seems to be vital for adhesion- or anchorage-dependent signals for cell proliferation. Since one of the hallmarks of cancer is loss of anchorage, this motivates many scientists to inspect the possible involvement of RHO GTPase pathways dysregulation to tumor progression [65]. RHO-like proteins can potentially influence the invasiveness of tumor cells in many different ways [54,66,67].

In addition, it has been shown that dysregulation or dysfunction of RHO signaling pathways results in number of other clinical symptoms such as X-linked genetic diseases, mental retardation, and neurodegenerative diseases such as amyotrophic lateral sclerosis (ALS), Alzheimer's disease, Huntington's disease and Parkinson's disease as well as human immunodeficiency syndrome [66,68-72].

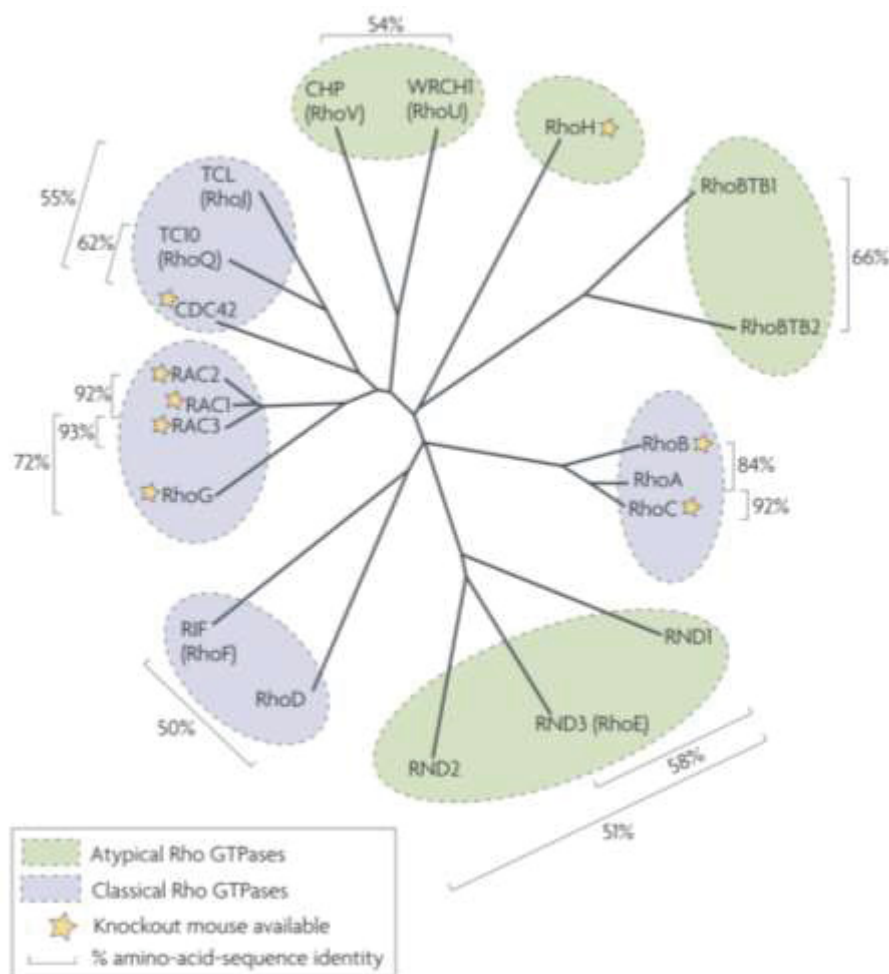


Figure 3. Phylogenetic tree of the RHO family proteins. The unrooted phylogenetic tree is based on the ClustalW alignment of the amino-acid sequences of the 20 RHO GTPase proteins. RHO family can be roughly divided into six major groups: RHO-, RAC-, CDC42-, RND-, RHOBTB-, and RHOD-related groups, where RHOH cannot assign as a defined group [40].

2.2 RHO mutations in tumor progression

There are different levels of RAS and RHO cross-talks at the levels of GAP or scaffolding proteins. While *HRAS*, *NRAS*, and *KRAS* regularly acquire transforming missense mutations in human cancer, slight is known of the oncogenic roles of RHO GTPases or the coexistence of *RAS* and *RHO* mutations in tumors. The mutation in RHOH/TTF has been shown to be involved in lymphoma development [73]. In addition to that, recently a mutant form of RAC1 with the amino acid substitution N92I beside the NRAS Q61K mutation in a human sarcoma cell line, HT1080, has been discovered and have been shown that this mutation renders RAC1 constitutively active and highly oncogenic [74]. Further screening for RAC1, RAC2, and RAC3 mutations among cancer cell lines as well as public databases, identified additional transforming mutations of RAC1 and RAC2 including RAC1 P29S, RAC1 C157Y, RAC2 P29L, and RAC2 P29Q [74]. Furthermore, RAC1 P29S mutation in melanoma and its possible role in resistance to RAF inhibitors by maintaining

activation of the MAPK signaling pathway has been reported [75]. Most recent report of mutation in RHO proteins is the RAC2 D63V mutation in Juvenile myelomonocytic leukemia (JMML) [76]. Juvenile myelomonocytic leukemia (JMML) is a rare but aggressive form of childhood leukemia that results from infiltration of overproduced myelomonocytic cells to organs such as liver, spleen, and intestine and exhibits both myelodysplastic and myeloproliferative properties [77]. Pathological studies revealed that the JMML initiated by germline or somatic RAS-activating mutations [78]. JMML is considered as a unique example of RAS-driven oncogenesis since it is thought to be initiated by mutations, usually described as mutually exclusive, in *NRAS* and *KRAS* genes or RAS-pathway regulators (PTPN11, NF1 or CBL) [79] but genetic profiling of the JMML patient with *NRAS* mutation has shown the second mutation which belongs to RHO GTPase (RAC2) [76] (see **chapter 3**).

2.3 Structural features of RHO proteins

RHO proteins are defined by the presence of a RHO-type GTPase-like domain. These proteins normally comprise a conserved GDP/GTP-binding domain (called G domain) and a C-terminal hypervariable region ending with a consensus sequence known as CAAX (C is cysteine, A is any aliphatic amino acid, and X is any amino acid) [11,18]. The G domain of RHO proteins is highly conserved among RHO family members and its structure is slightly different from what was described above for the RAS superfamily proteins (**Fig. 2**). One of the main differences between RHO family proteins and other small GTPases, which indeed distinguishes these proteins from other small GTPases, is an additional 12-amino acid “insert region”, (residues 124-135) in the RHO family proteins. This region is located between the fifth β strand and the fourth α helix in G domain [80]. All RHO family members have conserved motifs for high affinity binding to GDP and GTP. Furthermore, the majority of RHO members undergo post-translational modification such as phosphorylation, acetylation, ubiquitination, farnesylation, geranylgeranylation, palmitoylation, endoproteolysis, and carboxyl methylation at their C-terminal HRV that facilitates their membrane anchorage [18,81].

2.4 Regulation of RHO proteins activity by nucleotide binding

As indicated before, similar to other RAS superfamily members, RHO family proteins also share a core G domain with five conserved sequence motifs (G1–G5), which are required for nucleotide binding and hydrolysis [34]. Membrane-associated RHO GTPases act, with some exceptions [82], as molecular switches by cycling between an inactive GDP-bound state and an active GTP-bound state (**Fig. 4**). The role of the RHO family proteins as signaling molecules in controlling a wide range of fundamental cellular processes is mostly dependent on this functional molecular switch

[83]. This cycle underlies two critical intrinsic functions, the GDP-GTP exchange and GTP hydrolysis [82], and is controlled by at least three classes of regulatory proteins: guanine nucleotide exchange factors (GEFs), GTPase-activating proteins (GAPs), and guanine nucleotide dissociation inhibitor (GDI) (**Fig. 4**) [83,84]. GEFs accelerate the intrinsic nucleotide exchange by several orders of magnitude, resulting in the formation of the GTP-bound active state [82,85]. GAPs stimulate the intrinsic GTP hydrolysis activity and leading to a rapid inactivation of RHO proteins [84,86,87]. GDIs have been suggested to selectively bind to prenylated RHO proteins and to sequester the RHO proteins from the membrane by binding to the lipid anchor and by creating an inactivated cytosolic pool [88,89]. RHO proteins, in their active GTP-bound, associate with and in turn activate a wide variety of downstream effector molecules and subsequently activate signaling cascades (**Fig. 4**) [90,91] (more detailed information in **chapter 2**).

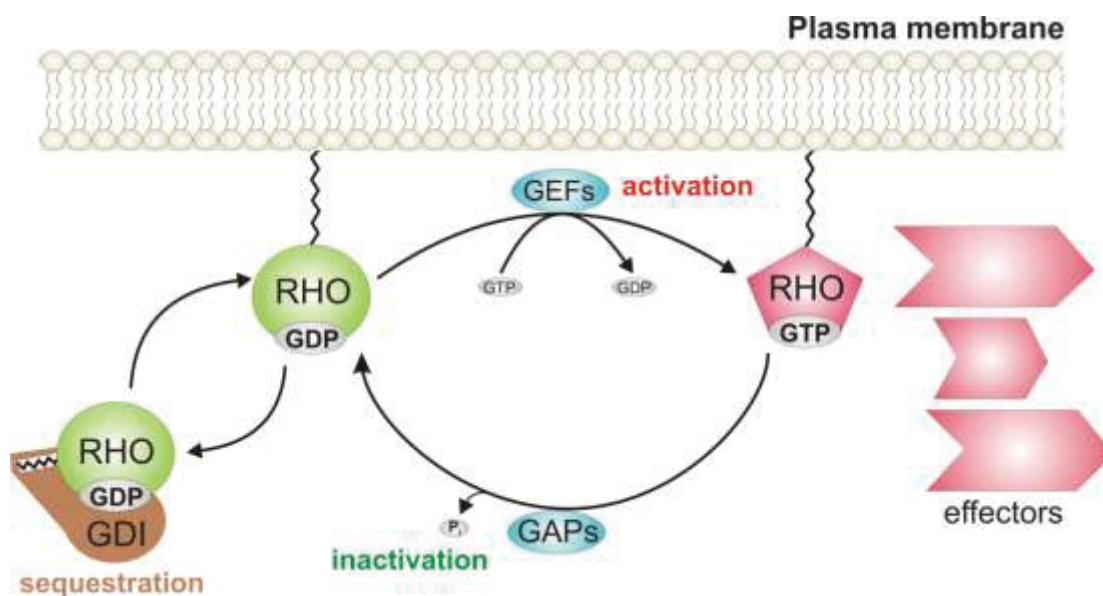


Figure 4. RHO Proteins as molecular switches. Most members of the RHO family act as molecular switches by cycling between an inactive, GDP-bound state and an active GTP-bound state. They interact specifically with three structurally and functionally unrelated classes of proteins. Guanine nucleotide exchange factors (GEFs), which activate the RHO proteins by accelerating the slow intrinsic exchange of GDP for GTP and turn on the signal transduction. GTPase-activating proteins (GAPs) negatively regulate the switch by stimulating the slow intrinsic GTP hydrolysis activity of the RHO proteins and turn off the signal transduction. Guanine nucleotide dissociation inhibitors (GDIs), which solubilize prenylated RHO proteins in cytosol and keep them in inactive state. The active GTP-bound RHO proteins interact with, and activate the downstream effectors to induce a variety of intracellular responses.

2.5 RHO GTPases and their effectors

GTP-bound RHO proteins interact with effector molecules to activate downstream cellular responses [92]. The crystal structures of several RHO proteins have revealed that the conformational differences between the GTP-bound and the GDP-bound forms are restricted to switch regions I and II. Activation of RHO proteins typically induce a conformational change,

providing common elements of the switch regions that are specifically recognized by the downstream interacting partners, although certain effectors may bind outside of switch regions [83,93,94]. In addition to switch regions, other regions are required for specific interaction of RHO proteins with distinct binding partners. Each protein may recognize several effectors, and some effectors may be recognized by multiple family members. To date more than 30 potential effectors for RHO, RAC, and CDC42 have been identified [18,54,90,91]. Many of RAC- and CDC42-binding proteins such as activated CDC42-associated tyrosine kinase (ACK), and Wiskott–Aldrich-syndrome protein (WASP) contain the conserved GTPase-binding consensus site, so-called CRIB (CDC42/RAC-interactive binding) motif [95]. Binding of RHO to its effector proteins require quite different GTPase regions compared to RAC and CDC42. One group of effectors, including protein kinase N (PKN)/PRK1 and PRK2, rhotekin and rhophilin, bind to RHO *via* RHO effector homology (REM) domain, which contains three repeats of a leucine-zipper-like motif termed HR1RHO effectors [96]. ROCK and kinectin are in another class of RHO effectors so-called ROK-kinectin homology proteins (RKH), and finally citron kinase is known as class III of RHO effectors [91,97-99]. p67^{phox} is one of the first targets of RAC which was identified. p67^{phox} is an essential structural component of the phagocyte NADPH oxidase complex [100]. RAC is involved in the assembly and activation of NADPH oxidase complex *via* direct interaction with p67^{phox} and possibly gp91^{phox} [101]. The p21-activated kinase (PAK) family of serine/threonine kinases is another well-known effector that can be activated by both RAC and CDC42. So far, six members of this family (PAK1–6) have been identified and it has been shown that they play critical roles in actin cytoskeleton dynamic regulation and gene expression [102,103]. In addition to classical regulators and effectors of RHO GTPases, the interaction with other scaffold proteins, like IQGAP1, as a crucial interacting partner of RHO family proteins has been investigated in recent years [118,119].

3 Protein scaffolds

The spatial and temporal organization of molecules within a cell is critical for coordinating many activities carried out by the cell. Signaling molecules interact together to form large complexes, which are normally not diffuse in the cytoplasm, but are rather attached to the cell membranes. The complex is called signalsome or transducisome. In signalsome, a protein that binds to more than one protein and has no enzymatic activity is defined as a scaffold protein or adaptor protein [104]. Cells have developed this class of proteins in order to physically assemble the relevant molecular components. These proteins simultaneously bind multiple components, assemble them into specific complexes, and thereby enhance signaling efficiency and fidelity, increase signaling sensitivity, and coordinate different signaling pathways [105].

Many scaffold proteins with diverse functions in different signaling pathways have been identified. For instance, the importance of scaffold proteins such as IQGAP1 [45,106,107], kinase suppressor of RAS (KSR) [108], MEK partner-1 (MP-1) [109], β -arrestins, and similar expression to FGF (Sef) [110], are well investigated in mitogen activated protein kinase (MAPK) signaling pathways specially MEK/ERK pathway [111]. Galectin-1 (Gal-1), Galectin-3 (Gal-3), nucleophosmin (NPM1), and nucleolin (NCL) are other protein scaffolds which participate in facilitating or enhancing RAS nanoclustering [112-115]. Gal-1 increases nanoclustering of active form of HRAS and its level may modulate HRAS signaling activity [115]. In contrast to Gal-1, cytosolic Gal-3 associates more with GTP bound form of KRAS nanoclusters [114]. NPM1 and NCL are other protein scaffolds for KRAS nanoclusters, and the latter is involved in ribosome biogenesis most likely in the complex with FMRP (fragile X mental retardation protein). These proteins are shuttling proteins between nucleolus and cytoplasm and can interact with KRAS, but not HRAS on the plasma membrane [112]. Furthermore, it has been shown that increasing cytosolic NPM1 or NCL concentration, stabilizes KRAS localization to the plasma membrane and enhances KRAS nanoclustering [112].

3.1 IQGAPs

IQ-domain GTPase-activating proteins (IQGAPs) belong to a recently identified protein family, which is an evolutionary conserved multidomain protein family in eukaryotes, from *Saccharomyces cerevisiae* to mammals. The multiple domains in IQGAPs interact with wide variety of binding partners, regulate numerous signaling pathways, and subsequently playing an important role in different biological processes [48,106,116-119]. IQGAPs have high sequences similarity to the RAS GAPs and four isoleucine/glutamine-containing domains (IQ), and the name "IQGAP" came from these two structural features.

In mammals, three isoforms of IQGAPs are expressed: IQGAP1, IQGAP2, and IQGAP3 (**Fig. 5A**). These homologues have similar domain compositions but different subcellular localization, tissue expression (**Fig. 5B**), and functions. Among these Isoforms, IQGAP1 is ubiquitously expressed and is the most investigated member. IQGAP1 *via* many different mechanisms coordinate communication between binding partners, including serving as a scaffold. IQGAP2 is expressed predominantly in the liver and also in stomach and platelet, and has 62% sequence identity to IQGAP1. IQGAP3 is enriched in brain and lung tissue [107,120-122]. Recent differential gene and protein expression analysis revealed a reciprocal expression of IQGAPs in hepatic stellate cells (HSC), with highly expression of IQGAP2 in quiescent HSC and IQGAP1 in activated HSC (**chapter 4**), and also in hepatocellular carcinoma (HCC) [123]. In spite of having RASGAP homology domain,

none of these three isoforms have GAP activity. In contrast, IQGAP proteins exhibit an inhibitory effect on the intrinsic GTPase activity of RHO GTPases CDC42 and RAC1, thereby stabilize them in their active GTP-bound form [124,125]. Lack of GAP function is apparently owing to absence of arginine finger in their GAP-related domain, which is involved evolutionarily in GAP activity of RASGAPs [126,127].

IQGAPs participate in many essential cellular activities in different organisms including cytokinesis in yeast and *Dictyostelium* [116], cell–cell adhesion through binding to E-cadherins as well as β -catenins [48,128], and regulate cell adhesion via binding to RAP1 [129]. Moreover they contribute in cancer cell invasion and metastasis and also as a scaffold for the mitogen-activated protein (MAP) kinase pathway by interactions with MAPK/ERK kinase (MEK1/2), B-RAF and extracellular signal-regulated kinase 2 (Erk2) [130,131].

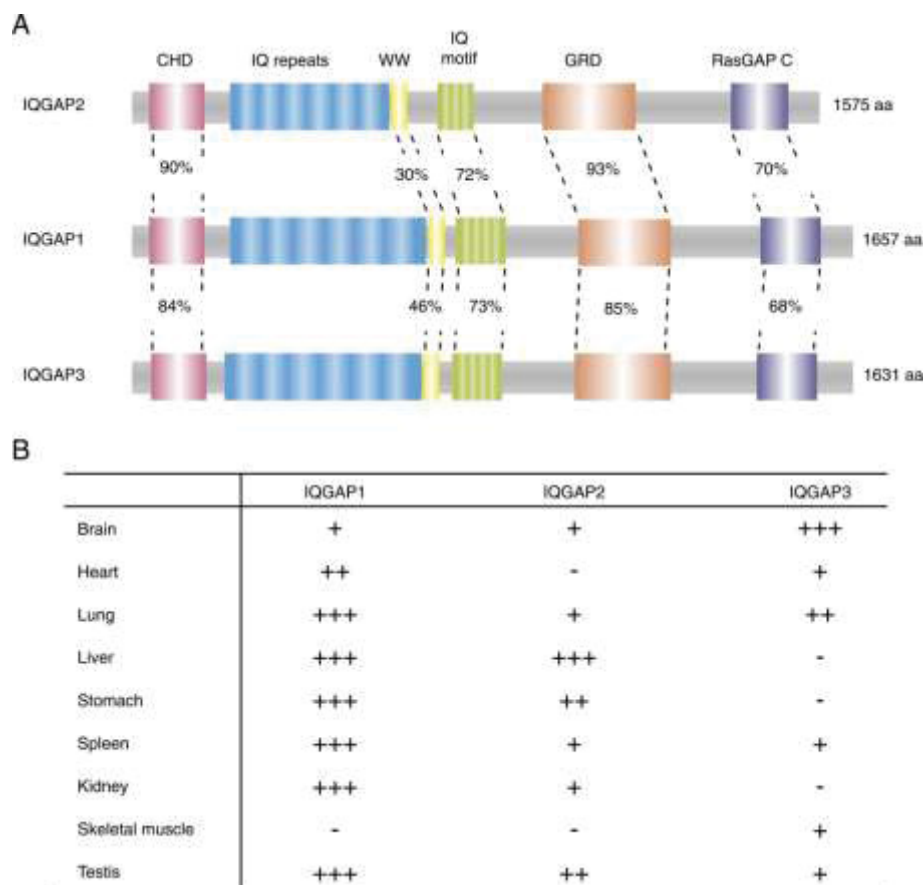


Figure 5. IQGAP isoforms and their tissue expression. (A) Schematic representation of the IQGAP proteins. IQGAPs contain several domains that mediate protein–protein interactions. They are consisting of five distinct domains; calponin homology domain (CHD), the WW domain, the IQ domain (which contains four tandem IQ motifs), the GTPase-activating protein (GAP)-related domain (GRD), and the RASGAP-C terminus. The amino acid homologies are indicated. **(B)** The tissue expression pattern of IQGAP family members [117]. The plus number reflects the expression level.

3.1.1 IQGAP1 domain organization and interacting partners

IQGAP1 is ubiquitously expressed and best-investigated member of the IQGAP family. It is a large multidomain scaffolding protein with 1657 amino acids (190 kDa). Since its discovery 20 years ago [132], more than 100 interacting partners have been identified, that some of them are illustrated in **Figure 6** [118,119]. The N-terminal calponin homology domain (CHD) shares homology with the Ca^{2+} and calmodulin-binding protein calponin. CHD interacts with F-actin [133], also weakly with calmodulin and Ca^{2+} ions [134,135]. This followed by a long coiled-coil (CC) region. So far, only Ezrin and adaptor protein ShcA have been identified to bind to a distinct part of this region containing six LNEALDEGDAQ consensus sequence repeats [118,135,136]. Whereas the proline rich region with two conserved tryptophans (WW) interacts with components of the MAPK pathway such as ERK1 and 2 [137]. This domain is followed by IQ motifs comprising Iso/Leu and Gln residues that mediate interactions with Ca^{2+} -binding proteins, including calmodulin [45,138] and S100 family proteins [139]. RAS GAP-related domain (GRD), and originally called RASGAP C terminal domain which we called a GTPase-binding domain (GBD) are known as RAC- and CDC42-like binding sites. At the very C-terminus, the C domain interacts with CLIP-170 [140], beta-catenin, E-cadherin [48,141,142], and the important tumor suppressor protein adenomatous polyposis coli (APC) [143].

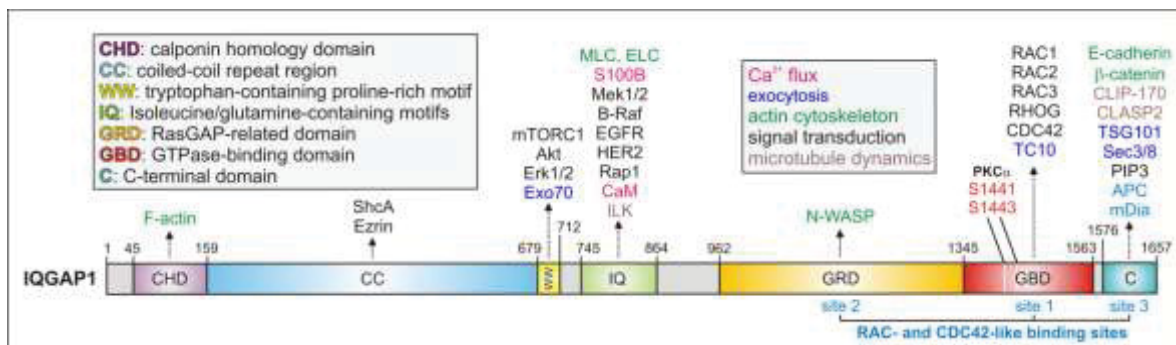


Figure 6. Schematic representation of the protein interaction domains of IQGAP1. Functional domain organization of IQGAP1 protein and the binding sites of some well-investigated binding partners are shown. It encompasses calponin homology domain (CHD), coiled-coil (CC) region, tryptophan-containing proline-rich (the WW domain), the IQ domain with four tandem IQ motifs, the GTPase-activating protein (GAP)-related domain (GRD), GTPase-binding domain (GBD), and C-terminal domain (C). Each domain has diverse interacting partners. The numbers indicate the N- and C-terminal amino acids of the respective domains.

3.1.2 IQGAP1-RHO interaction and regulating cellular functions

Accumulating evidence supports diverse roles for the IQGAP1 interaction with CDC42 [144] and RAC1 [145] in vertebrates, including regulation of cell-cell adhesion [146], cell polarity and migration, neuronal motility [147], invasion of *Salmonella typhimurium* [148], and tumor cell invasion [149]. IQGAP2 and IQGAP3 are also able to bind RHO proteins [120,125,150]. The

interaction with the active, GTP-bound form of CDC42 and RAC1 suggests that IQGAP1 acts as a downstream effector [151,152]. However, the nature of such a protein-protein recognition process has remained obscure. Physical interaction of IQGAP1 with small GTPases, like RAC1 and CDC42, play vital controlling roles in actin polymerization at the leading edge of migrating cells, where they localize with IQGAP1 [153,154]. Filamin-A is an actin crosslinking protein, which forms a complex with IQGAP1 and activated β_1 integrin to recruit RACGAP1. RACGAP1-IQGAP1 interaction negatively regulates RAC1 and promotes RHOA activation [155,156]. Since depletion of filamin-A, IQGAP1 or RACGAP1, caused uncontrolled membrane protrusion and disrupted directional cell migration [156], it has been suggested that IQGAP1 regulates cell motility at the leading edge [133]. Current evidence indicates that R-spondins (RSPOs)-leucine-rich repeat-containing G-protein coupled receptor 4 (LGR4) recruits IQGAP1 into the Wnt signaling complex and potentiates both the canonical and noncanonical pathways of Wnt signaling [157]. IQGAP1 also plays a critical role in cell polarity by associating with Wnt/RSPO and activation of the RAC1, and CDC42 proteins [157].

While modulation of the cytoskeletal architecture was initially thought to be the primary function of the interaction of IQGAP1 with RHO proteins, it is now clear that they have some critical physiological roles beyond the cytoskeleton [119]. Hepatocyte growth factor (HGF) enhances barrier function in endothelial cells [158]. It has been reported that IQGAP1 functions as a scaffold between microtubules and actin to stimulate enhanced barrier functions downstream of HGF [158,159]. CDC42 promotes the interaction of PTP μ with IQGAP1 to stimulate actin remodeling and, eventually, neurite outgrowth [160]. The complex of active CDC42, Lis1, and CLIP-170 with IQGAP1 seems to be crucial for cerebellar neuronal motility [147]. Another example is in the pancreatic β -cells. Analysis of the insulin secretory pathway has shown that IQGAP1 scaffolds CDC42, RAB27a, and coronin-3 and this complex controls endocytosis of insulin secretory membranes [161]. Apart from that, immunoprecipitation studies have recently shown that IQGAP1 binds to both RHOA and p190A-RHOGAP to inactivate RHOA and modulates contractility of airway smooth muscle cells [162]. *Wu et al.* also have found RHOC and IQGAP1 in immunoprecipitates. This study has shown that isoform-specific interaction of RHO proteins with IQGAP1 regulates cancer cell proliferation and reveals that IQGAP1 is a downstream effector of RHOC in the regulation of gastric cancer cells migration activity [163,164]. From IQGAP family, IQGAP1 has been precisely implicated as a drug target although the molecular mechanism of the IQGAP1 functions is unclear. A prerequisite to elucidate the mechanism behind IQGAP1 functions is the dissection of its distinct domains and the analysis of their interactions with desired protein partners.

Work from several laboratories has shown that the C-terminal half of IQGAP1 (GRD-C, aa 863-1657), including GRD, GBD, and C (**Fig. 6**), binds physically to active, GTP-bound forms of CDC42 and RAC1 [150,165,166]. IQGAP1 GRD, which is structurally a homologous but functionally an inactive RASGAP [167] also undergoes interaction with RAC1 and CDC42, although with a lower affinity than the larger protein fragment, containing GRD, GBD, and C [167]. These works together with homology modeling, based on the RHOGAP in complex with RHOA [168] and CDC42 [169], provided a structural model of IQGAP1 GRD that contacts the switch regions of the GTP-bound CDC42 [167,170,171]. On the contrary, in this study new model was proposed that the C-terminal half of IQGAP1 utilize at least three functionally distinct units, including GRD, GBD, and C, to achieve the interaction with RAC1- and CDC42-like proteins. GRD undergoes a low-affinity, GDP-/GTP-independent complex with RAC1 and CDC42 proteins outside their switch regions. GBD only binds to the RAC1 and CDC42 proteins if they are active and exist in the GTP-bound forms, and the C-terminal region of IQGAP1 may potentiate the IQGAP1 interaction with RAC1 and CDC42 proteins by probably extending the resident time of the respective proteins complexes (**chapter 4**).

3.2 Nucleophosmin and nucleolin

Nucleophosmin (NPM1, also known as B23, numatrin, NO38), and nucleolin (NCL, C23), are multifunctional phosphoprotein predominately localized in nucleoli, where they play key roles in RNA regulatory mechanisms including transcription, ribosome assembly and biogenesis, mRNA stability and translation, and microRNA processing [172-175]. They also act as a nucleolar chaperon of histones [172,176-178]. Moreover, they have been reported to undergo a large variety of posttranslational modifications such as phosphorylation [179,180], ADP-ribosylation [181], glycosylation [182], glutamylation, and acetylation [183-185]. Mechanistic relationships between differential modifications, localizations, and functions of these proteins are still unclear. It is, however, clear that NCL and NPM1 undergo multiple interactions with diverse host proteins and microbial effectors in different subcellular compartments.

3.2.1 Structural features

NPM1 (294 aa) is a 37 kDa protein that contains an N-terminal oligomerization domain, a central histone binding domain, and a C-terminal RNA binding domain (**Fig. 7**) [186]. It also has two nuclear exports signals (NESs) at the N-terminus, two central nuclear localization signals (NLSs), and one nucleolar localization signal (NoLS) at the very C-terminus (**Fig. 7**). NPM1 exists in two splicing variants, B23.1 (major form) and B23.2 (minor form). B23.2 is identical to B23.1 but contains a C-terminal 35 amino acids extension [177,186].

A sequence comparison of NCL (710 aa, 77 kDa) reveals a high degree of identity in the different kingdoms. It contains an N-terminal domain (aa 1-284) with four acidic motifs, one nuclear localization signal (NLS), a large central region (aa 307-647) containing four RNA recognition motifs (RRM 1-4), and a C-terminal arginine-glycine-glycine-rich (RGG, also called glycine-arginine rich or GAR) region (aa 645-710) (**Fig. 7**) [187].

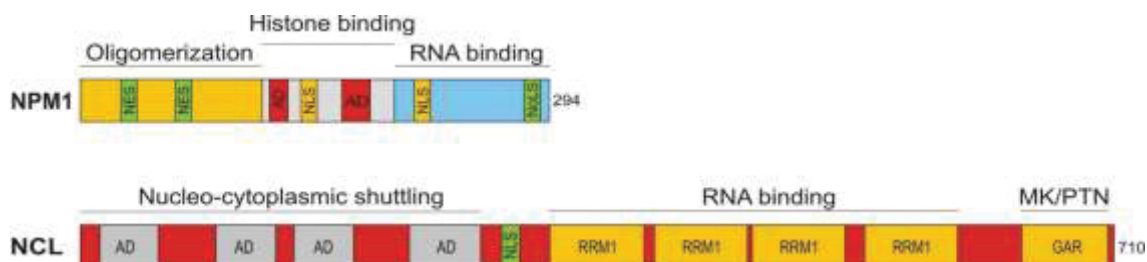


Figure 7. Functional domains organization of nucleophosmin (NPM1), and nucleolin (NCL). NES, nuclear export signal; AD, acidic domain; NLS, nuclear localization signal; NoLS, nucleolar localization signal; RRM (or RBD), RNA recognition motifs (also called RNA binding domain), and GAR (or RGG), glycine-arginine-repeat (arginine-glycine-glycine domain).

3.2.2 Interacting partners

NCL, and also NPM1, belong to the most abundant non-ribosomal proteins of the nucleolus, but are also found in the nucleoplasm and at the nuclear membrane, as well as in the cytoplasm and at endomembrane and the plasma membrane [188]. NPM1 and NCL are interacting partners [189] and also interact with many other nucleolar and viral proteins. These proteins include the tumor suppressors ARF (p19ARF in mouse, p14ARF in human) [190,191], the SUMO1/sentrin/SMT3 specific peptidases 3 and 5 (SEN3-5) [192], F-box and WD repeat domain containing 7 (Fbw7g) [193], p21/WAF/CIP (p21) [194,195], nucleolar cell cycle related protein p120 [189,196], and ribosomal protein S9 [197], and some viral proteins which are reported to accumulate in the nucleolus by the help of NPM1 [198].

As it was mentioned before, both NCL and NPM1 bind KRAS and mediates recruitment of KRAS into nanoclusters on the inner leaflet of the plasma membrane [112]. Furthermore, it has been shown that NPM1 is a negative regulator of the small GTPase RAC1 [199]. It has also been identified that ROCK II kinase, an effector of RHO small GTPase, as a protein that localizes to centrosomes, physically interacts with NPM1 and this play role in the regulation of centrosome duplication [200].

NCL participates in the dynamic intracellular localization of telomerase complex [201], inhibits Mdm2 and thereby leads to p53 stabilization [202]. At the outer leaflet it participates in the interaction with lactoferrin [203], Midkine [204], Pleiotrophin [205], and Urokinase-type plasminogen activator [206]. Most recently, the direct interaction of the N-terminus of FMRP with

the arginine-glycine-glycine (RGG) domain of NCL has also been reported and proposing that the transient nucleolar localization of FMRP in a complex with NCL and possibly ribosomes, regulate translation of target mRNAs [188] (**chapter 6**).

3.2.3 Role in cell signaling and human diseases

NPM1 and NCL are involved in the regulation of a wide spectrum of cellular processes *via* binding to many partners in distinct cellular compartments, including nucleolar factors, transcription factors, nuclear factors, and proteins involved in cell proliferation, mitosis, and the response to oncogenic stress.

NPM1 was first identified as a nucleolar phosphoprotein and was shown to be critical in the regulation of proliferation, cell growth, and transformation [178,207]. NPM1 is directly involved in human tumorigenesis [178] but its physiological function thereby is controversial as it has been shown to have both oncogenic and tumor suppressor functions [208]. The upregulation of NPM1 occurs in various tumors, and it has been proposed as a marker for gastric [209], colon [210], ovarian [211], and prostate [212] carcinomas. Recent studies indicate that about 35% of adult acute myeloid leukemia (AML) has mutations in exon 12 of the NPM1 gene [213]. Therefore, understanding the function(s) and the mechanism(s) of NPM1 regulation may provide new insights into the molecular pathogenesis of human cancer.

To date, several distinct cellular functions for NPM1 upregulation have been described (**Fig. 8**). Following is a brief description of some of these functions. NPM1 has been proposed as a nucleolar receptor for PI(3,4,5)P3 in the cells. NPM1 directly interacts caspase-activated DNase (CAD) and inhibits active CAD in a PI(3,4,5)P3 dependent manner and leads to antiapoptotic actions [214]. Furthermore, NPM1 by binding PI(3,4,5)P3 and suppressing p21^{WAF1} causes inhibition of DNA synthesis and cell proliferation [215]. It also interacts tumor-suppressor ARF which leads to inhibition of Mdm2 and to stabilization of p53 transcriptional responses, such as apoptosis or cell cycle arrest [216]. Ubiquitin-like protein/sentrin-specific proteases (Ulp/SENPs) process all lately synthesized small ubiquitin-like modifier proteins (SUMOs). SENP3 and SENP5 physically interact with NPM1 and regulate SUMO deconjugation. This may be a main facet of NPM1 function that by affecting H3-H4 and Cenp-A and by inhibiting GCN5 and pRb resulting in histone acetylation, chromatin assembly, and translation [192]. It has also been reported that phosphorylation of NPM1 at Thr199 plays a vital role in the RNF168 and RNF8-dependent DNA repair pathway *via* recruiting to DNA double-strand breaks (DSBs) [217]. It has been suggested that balance between SIRT1 and p300 activity is critical for maintaining NPM1 acetylation status in the cells. Acetylated NPM1 directly regulates the transcriptional activity of defined genes such as

AP2 α , NF κ B, AR, Miz1, and c-Myc which are associated with oral cancer [218]. NPM1 is also important for Bax-mediated cell death. NPM1-Bax interaction increases accumulation of mitochondrial Bax, organelle injury, and cell death [219].

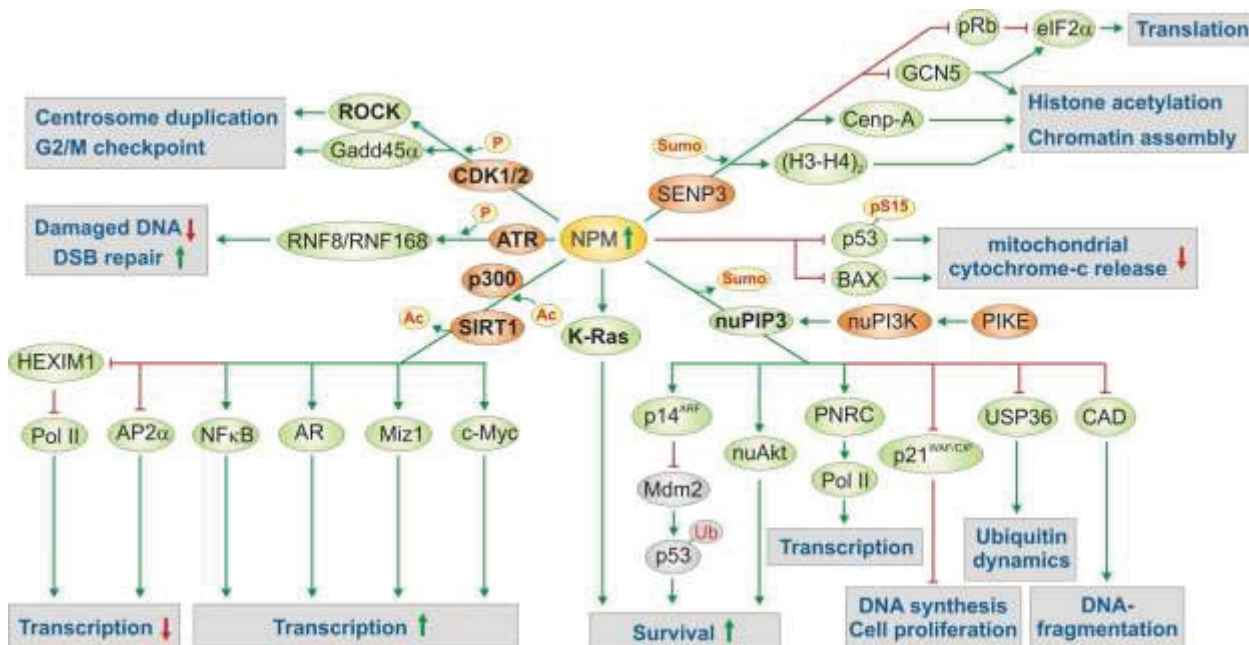


Figure 8. Nucleophosmin signaling. NPM1 overexpression in tumor cells or under external stress leads to regulation of variety of cellular processes.

NCL is an abundant nucleolar protein, which is highly expressed in stem cells and cancer cells. Similar to NPM1, NCL also contributes widely to RNA regulatory mechanisms and *via* its different RNA modulatory functions and its ability to associate with target RNAs. NCL is increasingly involved in pathological processes, especially cancer and viral infection.

NCL stimulates survival and cell proliferation related carcinogenesis, but the mechanisms are not well understood [174,187]. In various tumor cell lines and in activated endothelial cells, expression of surface NCL is enhanced [220,221]. Moreover, it has been reported that NCL targeting with a specific antibody results in the activation of endothelial cell apoptosis *via* reducing antiapoptotic Bcl-2 mRNA [222]. Apart from its functions at the cell surface, it has been shown that NCL has vital role in the apoptotic process which is linked to regulation of proteins like p53, Bcl-2, and retinoblastoma [223,224]. Recent studies revealed the potential role of NCL in parkinson disease (PD) pathogenesis as well [225].

3.2.4 Role in viral infection

NPM1 and NCL have emerged as an essential host factor for multiple aspects of microbial infection, adhesion at cell surface, entry, intracellular trafficking, regulation of transcription and

translation, and nucleo-cytoplasmic shuttling [172-174,176]. It is increasingly evident that these two proteins function as a host-specific target for a large number of viruses and pathogenic bacteria which have raised interest in targeting them therapeutically.

NCL is involved as a pro-viral host target in different processes during infection of many viruses, including Herpes simplex virus type 1 (HSV-1), Influenza A viruses (IAV), Cytomegalovirus (CMV), and Severe acute respiratory syndrome coronavirus (SARS) [226-231]. NCL is a host component that interacts with Hepatitis C virus (HCV) NS5B and is indispensable for HCV replication [226,227]. NCL interaction with UL24 of HSV-1 [232,233] and with UL44 and UL83 of CMV [228,231] appears to be important for efficient viral DNA replication. A direct interaction of NCL with UL24 has not been shown yet. However, it is known that the conserved N-terminal domain of UL24 is sufficient to induce the spatial redistribution of NCL [234]. UL12 and US11 binding to NCL has been reported to be required for efficient nuclear egress of HSV-1 nucleocapsids in infected cells [229,230]. US11 displays striking functional similarities to HIV-1 Rev and human T-cell leukemia/lymphoma virus type I (HTLV-I) Rex proteins [235]. Remarkably, it can substitute for Rev and Rex and interferes with the life cycle of these retroviruses [230], suggesting a possible role for NCL in HIV-1 and HTLV-I replication. NCL is an integral element of internal ribosome entry site-mediated translation of HCV [236]. The growth factors pleiotrophin and midkine have been reported to interfere with HIV infection by competitively associating with C-terminal end of NCL, an arginine-glycine-rich (called RGG or GAR) region [204,205]. The GAR domain of surface NCL has been suggested to be also involved in the interaction with the elongation factor Tu of *Francisella tularensis* [237,238] and the TNF α -inducing protein (Tip α), which is a secreted protein of *Helicobacter pylori* [239]. This interaction has been implicated to cause a cancer-oriented microenvironment that increases the risk of gastric cancer [240]. NCL has been most recently reported as the only protein target receptor of human respiratory syncytial virus (RVS) at the apical surface of epithelial cells [241]. Similarly, the adhesin intimin- γ of the EHEC pathogen has been implicated as a ligand for NCL function as a host cell surface receptor [242].

NPM1 appears also to be such a host-directed antimicrobial drug-target protein that acts strikingly as an emerging receptor for a multitude of viruses, including Adeno-associated virus (AAV) [243], Adenovirus [244,245], Epstein-Barr virus (EBV) [246,247], Hepatitis B virus (HBV) [248,249], Hepatitis C virus (HCV) [250], Hepatitis delta virus (HDV) [251], Herpes simplex virus 1 (HSV-1) [252], Human immunodeficiency virus type 1 (HIV-1) [253-255], Human T-cell leukemia virus type 1 (HTLV-1) [256], Japanese encephalitis virus (JEV) [257], Kaposi's sarcoma herpes virus (KSHV) [258], and Newcastle disease virus (NDV) [198].

NPM1 is a replication protein (Rep) interacting partner which plays a role in Adeno-associated virus (AAV) amplification and affecting Rep function and virion assembly [243]. It interacts with adenovirus basic core proteins and functions as a chaperone in the viral chromatin assembly process in infected cells [244]. Epstein-Barr virus (EBV) is a gamma herpes virus that infects more than 95% of the world's adult population. The EBV EBNA1 protein plays important roles in latent infection of this virus. NPM1 is recruited by EBNA1 to the FR element and is required for EBNA1-mediated transcriptional activation [247]. NPM1 is a host factor that increases HBV capsid assembly of Hepatitis B virus (HBV) by interaction with the HBV core protein 149 (Cp149) *via* its RNA binding domain [248,249]. Furthermore, NPM1 make a complex with Hepatitis C virus core protein which this complex formation may describe the pleiotropic effects of core protein on gene expression and cellular function in HCV-infected cells [250]. Hepatitis delta virus (HDV) encodes two isoforms of delta antigens (HDAGs); the small form and the large form, which they are needed for HDV RNA replication and virion assembly, respectively. It has been shown that the association of NPM1 and NCL with the small HDAG may characterize an important mechanism for HDV RNA replication [251].

Viral proteins such as HSV-1 UL24 [252], Rex protein of human T-cell leukemia virus [256], Rev protein [253], and Tat protein of HIV-1 [255] are reported to accumulate in the nucleolus by interaction with NPM1 *via* their nucleolar localization signals (NoLSs) [198]. After entering the Rev to the nucleus, NPM1 facilitates transport of Rev to the nucleolus. It is shown that NPM1 is necessary for the Rev nucleolar localization through interaction with its respective basic domain [253,259]. However, this interaction is currently not well understood and awaits detailed molecular investigations. Along with this line, the direct interaction between Rev and NPM1 variants has been done *in vitro* in order to map binding epitope of NPM1 for Rev. It is shown that Rev undergoes high-affinity binding to two domains of NPM1, OD and HBD, in an RNA-independent manner [260] (**chapter 5**). Furthermore, it has been revealed that proapoptotic CIGB-300 pseudopeptide, which specifically interacts NPM1 *in vivo* [261-263], bound to NPM1 oligomerization domain *in vitro* as well, and blocked Rev and US11 association with NPM1. Moreover, HIV-1 virus production is significantly reduced in the cells treated with CIGB-300 [260] (**chapter 5**). Rex is the post-transcriptional regulator of human T-cell leukemia virus type I (HTLV-I). It is suggested that NPM1 functions as a shuttle protein for the import of HTLV-I Rex from the cytoplasm to the nucleolus to allow further circles of export of the viral mRNAs containing Rex-responsive element [256]. Japanese encephalitis virus (JEV) is the arthropod-borne virus which causes significant morbidity and mortality in mammals and birds. It is shown that NPM1 plays critical role in the JEV replication [257]. Oncogenic Kaposi's sarcoma herpesvirus (KSHV) is the

etiological agent of Kaposi's sarcoma, Primary effusion lymphoma (PEL) and Multicentric castlemans disease (MCD). NPM1, *via* functional interactions with v-cyclin and Latency-associated nuclear antigen (LANA), regulates oncogenic Kaposi's sarcoma herpesvirus (KSHV) latency [258]. NPM1 has been reported to interact with Newcastle disease virus (NDV) matrix (M) protein and this association represents a direct role for NPM1 in NDV replication [198]. In addition, NPM1 interaction with UL24 of HSV-1 seems to promote nuclear egress of nucleocapsids during HSV-1 infection, possibly through effects on nucleoli [252]. Furthermore it has recently been shown that NPM1 interacts with HSV-1 US11 *in vitro* and in the cell, but the biological function of this interaction remains to be elucidated yet (**chapter 5**). As it was mentioned before, in addition to UL24, US11 is also shown to interact with NCL [230]. US11 protein acts as an inhibitor of an antiviral host defense system. dsRNA and IFN activate the ribosome-associated PKR (protein kinase R) which in turn inhibits translation and induces autophagy [264,265]. US11 hijacks dsRNA and PKR, and counteracts the host defense.

3.2.4.1 HIV-1 Rev

Besides the three common polyproteins (Gag, Pol, and Env) in all retroviruses, the human immunodeficiency virus (HIV) genome encodes six more regulatory proteins. Among these regulatory proteins, Rev, which is translated from fully spliced viral mRNAs, is one of the crucial proteins for viral replication in human cells [253,266,267]. It interposes during the late phase of the viral replicative cycle and its posttranscriptional activity permits synthesis of structural and enzymatic viral proteins needed for production of infectious viral particles [268,269]. Rev is typically 116 amino acids and has RNA binding domains composed of arginine-rich motif (ARM or R-rich), which binds to different HIV-1 RNA stem loop structures. The RNA binding domain of Rev also functions as a nuclear/nucleolar targeting signal and can deliver cytoplasmic protein to the nucleus or nucleolus. Rev is located predominantly in the nucleus of the cells infected with the virus and transfected cells but due to the nucleocytoplasmic shuttling, in addition to nucleoplasm it localizes in the nucleolus and also to a lesser extent, in the cytoplasm [270,271].

3.2.4.2 HSV-1 US11

Herpes simplex virus type 1 (HSV-1) is a nearly 152 kb double-stranded DNA virus. It encodes at least 80 polypeptides which are expressed as three, immediate early (IE), early (E), and late (L), classes of genes. The *US11* gene of HSV-1 is a so-called nonessential gene, since it is not necessary for virus growth in animal models as well as in tissue culture [272-274]. The US11 protein is a highly basic phosphoprotein expressed late during infection. HSV-1 has three different strains (F, 17 and KOS strain) that US11 protein from these strains showed more than 97% identity with

different copies of XPR repeats, in the C-terminal half, (F strain: 21; 17 strain: 24; KOS strain: 20), where X is most commonly an acidic or uncharged polar amino acid (P; Proline and R; Arginine). US11 is a tegument protein and approximately 600 to 1,000 molecules per virion are presented [274-276]. It is localized in the nucleus, specially accumulated in the nucleolus, and the cytoplasm [277]. US11 can associate strongly with ribosomes and has been found in rRNA and polysome-containing fractions [274-276]. Although, US11 is unessential for virus growth, but it plays a role in cells subjected to thermal stress [278,279] and in the replication of HSV-1 in the adrenal gland, an organ vital for viral penetration into the brain and spinal cord [273,280]. US11 shows anti-apoptotic activity, remarkably against heat-induced apoptosis, which seems to be placed at mitochondrial level or upstream signaling [281]. Moreover, it is involved in the antiviral response by inhibiting activation of the cellular PKR kinase in response to dsRNA [265].

3.3 Fragile X mental retardation (FMRP)

FMRP is ubiquitously expressed with higher abundance in the brain and testis [282,283]. It localizes predominantly in different cellular compartments, including mitochondria and nucleoli [188]. FMRP is a regulator of protein translation and associates with the translation machinery [284-286]. It is associated with messenger ribonucleoprotein (mRNP) particles and large polyribosomal complexes in the cytoplasm of numerous cell types [287-295]. This protein consists of an N-terminal dimerization domain [296,297], a central region containing two K homology (KH1 and KH2) domains [298], and a C-terminus encompassing the arginine-glycine-glycine (RGG) region [299]. The N-terminal and central regions of FMRP are highly conserved among the fragile X related proteins (FXRPs), while the C-terminal shows significant variability [283,300,301]. FMRP is known to play roles in nucleocytoplasmic shuttling of mRNA [288,302,303], which is accomplished by a non-canonical nuclear localization signal (NLS) and a nuclear export signal (NES) [303-305]. Different mechanisms for the nuclear export of FMRP such as involving CRM1/Exportin1 [305] and/or the nuclear export factor family proteins have been suggested [303,306].

4 Aims of this thesis

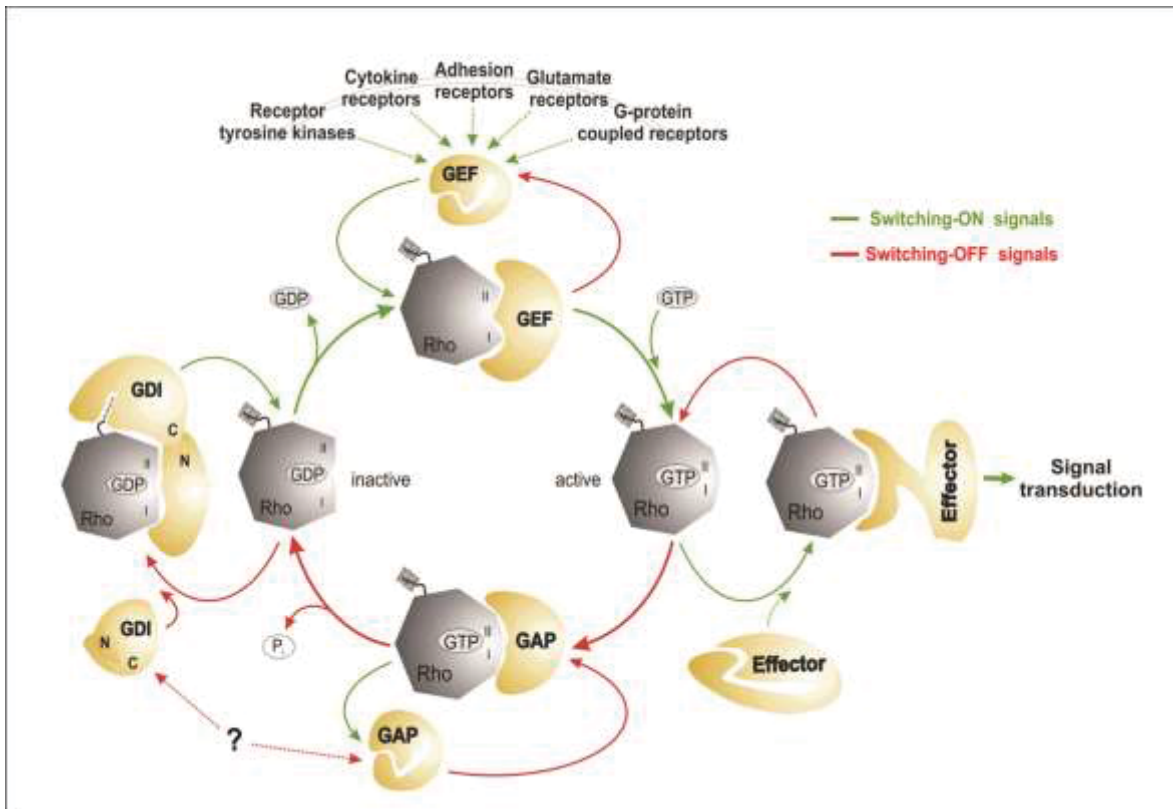
The RHO family of GTPases is known to play an important role in diverse cellular processes and progression of different diseases, such as cardiovascular diseases, developmental and neurological disorders, and cancer. The formation of the active GTP-bound state of RHO GTPases is accompanied by a conformational change in two regions (known as switch I and II) which provides a platform for the selective interaction with structurally and functionally diverse effectors, e.g. the IQ motif-containing GTPase activating protein 1 (IQGAP1). This class of proteins activates a wide variety of downstream signaling cascades thereby regulating many important physiological and pathophysiological processes in eukaryotic cells. IQGAP1 is a ubiquitously expressed scaffold protein and has been implicated as a drug target although the molecular mechanism of the IQGAP1 functions is unclear. A prerequisite to achieve this aim is the dissection of its distinct domains and the analysis of their interactions with desired protein partners. Aim of this thesis was to better understand the structure and functions of RHO proteins in diseases, to comprehensively investigate the structure-function relationship and the mode of interaction of the small GTPases of the RHO family with their effector IQGAP1, and to explore the molecular mechanism, binding domains and interacting residues. Addressing these issues is of fundamental importance and will ultimately advance our knowledge in the field of signal transduction and disclose molecular details of dysregulated signaling pathways.

Nucleophosmin (NPM1) is another multifunctional scaffold protein which is increasingly emerged as a potential cellular factor that directly associates with viral proteins in different subcellular compartments, although the significance of these interactions in each case is still not clear. Another aim of this thesis was to investigate the physical interaction of NPM1 with human Human immunodeficiency virus type 1 (HIV-1)-Rev and Herpes simplex virus type 1 (HSV-1)-US11 proteins in order to perform binding epitope mapping of NPM1 and elucidate their probable function in viral infection. Deciphering new functional control mechanisms and defining new targets are essential for the rational development of antiviral agents.

Chapter II

Classical RHO Proteins: Biochemistry of Molecular Switch Function and Regulation

Graphical abstract



Status: Published in Wittinghofer, A (ed) RAS Superfamily small G Proteins, Biology and Mechanism, Vol. 1 Springer (2014), Chapter 14, pp 327-340

Impact factor: not available (book chapter)

Own Proportion to this work: 25 %

Writing the guanine nucleotide exchange factors (GEFs) section

Chapter 14

Classical Rho Proteins: Biochemistry of Molecular Switch Function and Regulation

Si-Cai Zhang, Kazem Nouri, Ehsan Amin, Mohamed S. Taha, Hossein Nakhaeizadeh, Saeideh Nakhaei-Rad, Radovan Dvorsky, and Mohammad Reza Ahmadian

Abstract Rho family proteins are involved in an array of cellular processes by modulating cytoskeletal organization, transcription, and cell cycle progression. The signaling functions of Rho family proteins are based on the formation of distinctive protein–protein complexes with their regulators and effectors. A necessary precondition for such differential interactions is an intact molecular switch function, which is a hallmark of most members of the Rho family. Such classical Rho proteins cycle between an inactive GDP-bound state and an active GTP-bound state. They specifically interact via a consensus-binding sites called switch I and II with three structurally and functionally unrelated classes of regulatory proteins, such as guanine nucleotide dissociation inhibitors (GDIs), guanine nucleotide exchange factors (GEFs), and GTPase-activating proteins (GAPs). Extensive studies in the last 25 years have provided invaluable insights into the molecular mechanisms underlying regulation and signal transduction of the Rho family proteins. In this chapter, we will review common features of Rho protein regulations and highlight specific aspects of their structure–function relationships.

Keywords Effector • GAP • GDI • GEF • Rho GTPase • Switch region

Abbreviations

A	Aliphatic amino acid
Bcr	Breakpoint cluster region protein
C	Cysteine
CZH	CDM-zizimin homology

S.-C. Zhang • K. Nouri • E. Amin • M.S. Taha • H. Nakhaeizadeh • S. Nakhaei-Rad • R. Dvorsky • M.R. Ahmadian (✉)
Institute of Biochemistry and Molecular Biology II, Medical Faculty, Heinrich-Heine-University, 40225 Düsseldorf, Germany
e-mail: reza.ahmadian@uni-duesseldorf.de

A. Wittinghofer (ed.), *Ras Superfamily Small G Proteins: Biology and Mechanisms I*, 327
DOI 10.1007/978-3-7091-1806-1_14, © Springer-Verlag Wien 2014

Db1	Diffuse B-cell lymphoma
DH	Dbl homology domain
DHR1&2	DOCK-homology regions 1 and 2
ERM	Ezrin/radixin/moesin
GAPs	GTPase-activating proteins
GDI	Guanine nucleotide dissociation inhibitors
GDP	Guanosine diphosphate
GEFs	Guanine nucleotide exchange factors
Gln	Glutamine
Gly	Glycine
GTP	Guanosine triphosphate
p75 ^{NTR}	Neurotrophin receptor p75
PAK1	p21-activated kinase 1
PH	Pleckstrin homology domain
PKA	Protein kinase A
PKC	Protein kinase C
P-loop	Phosphate-binding loop
X	Any amino acid

14.1 General Introduction

The role of the Rho family proteins as signaling molecules in controlling a large number of fundamental cellular processes is largely dependent on a functional molecular switch between a GDP-bound, inactive state and a GTP-bound, active state (Dvorsky and Ahmadian 2004). This function underlies a so-called GTPase cycle consisting of two different, slow biochemical reactions, the GDP/GTP exchange and the GTP hydrolysis. The cellular regulation of this cycle involves guanine nucleotide exchange factors (GEFs), which accelerate the intrinsic nucleotide exchange, and GTPase-activating proteins (GAPs), which stimulate the intrinsic GTP hydrolysis activity (Cherfils and Zeghouf 2013). Rho protein function requires both posttranslational modification by isoprenyl groups and membrane association. Therefore, Rho proteins underlie a third control mechanism that directs their membrane targeting to specific subcellular sites. This mechanism is achieved by the function of guanine nucleotide dissociation inhibitors (GDIs), which bind selectively to prenylated Rho proteins and control their cycle between cytosol and membrane. Activation of Rho proteins results in their association with effector molecules that subsequently activate a wide variety of downstream signaling cascades (Bishop and Hall 2000; BurrIDGE and Wennerberg 2004), thereby regulating many important physiological and pathophysiological processes in eukaryotic cells (Etienne-Manneville and Hall 2002; Heasman and Ridley 2008) (see Chap. 16). In the following, the biochemical properties of the Rho proteins and their regulatory cycles will be described in detail. Figure 14.1 schematically summarizes the regulatory mechanism of the Rho proteins.

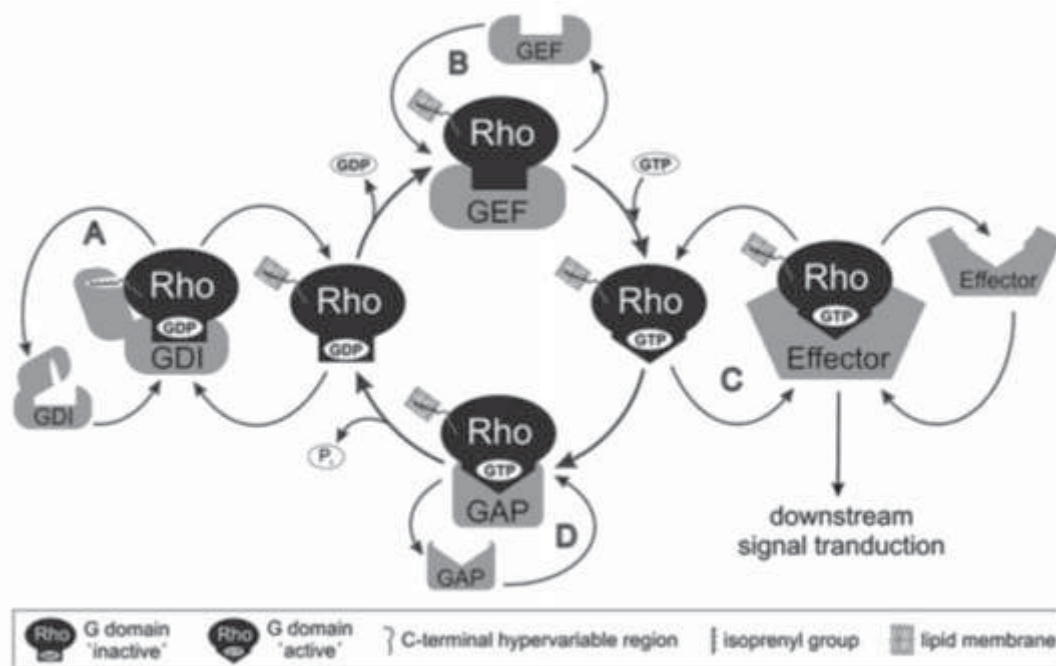


Fig. 14.1 Molecular principles of regulation and signaling of Rho Proteins. Most members of the Rho family act as molecular switches by cycling between an inactive, GDP-bound state and an active GTP-bound state. They interact specifically with four structurally and functionally unrelated classes of proteins: (a) In resting cells, guanine nucleotide dissociation inhibitors (GDIs) sequester the Rho proteins from the membrane by binding to the lipid anchor and create an inactivated cytosolic pool. (b) In stimulated cells, different classes of membrane receptors activate guanine nucleotide exchange factors (GEFs), which in turn activate their substrate Rho proteins by accelerating the slow intrinsic exchange of GDP for GTP and turn on the signal transduction. (c) The active GTP-bound Rho proteins interact with and activate their targets (the downstream effectors) to evoke a variety of intracellular responses. (d) GTPase-activating proteins (GAPs) negatively regulate the switch by stimulating the slow intrinsic GTP hydrolysis activity of the Rho proteins and turn off the signal transduction

14.2 Rho Family and the Molecular Switch Mechanism

Members of the GTP-binding proteins of the Rho family have emerged as key regulatory molecules that couple changes in the extracellular environment to intracellular signal transduction pathways. So far, 20 human members of the Rho family have been identified, which can be divided into six distinct subfamilies based on their sequence homology: (1) Rho (RhoA, RhoB, RhoC); (2) Rac (Rac1, Rac1b, Rac2, Rac3, RhoG); (3) Cdc42 (Cdc42, G25K, TC10, TCL, RhoU/Wrch1, RhoV/Chp); (4) RhoD (RhoD, Rif); (5) Rnd (Rnd1, Rnd2, Rnd3); (6) RhoH/TTF (Boureaux et al. 2007; Jaiswal et al. 2013a, b; Wennerberg and Der 2004).

Rho family proteins are approximately 21–25 kDa in size typically containing a conserved GDP/GTP-binding domain (called G domain) and a C-terminal hypervariable region ending with a consensus sequence known as CAAX (C is cysteine, A is any aliphatic amino acid, and X is any amino acid). The G domain consists of five conserved sequence motifs (G1-G5) that are involved in nucleotide binding and

hydrolysis (Wittinghofer and Vetter 2011). In the cycle between the inactive and active states at least two regions of the protein, switch I (G2) and Switch II (G3), undergo structural rearrangements and transmit the “OFF” to “ON” signal to downstream effectors (Fig. 14.1) (Dvorsky and Ahmadian 2004). Subcellular localization of Rho proteins at different cellular membranes, that is known to be critical for their biological activity, is achieved by a series of posttranslational modifications at a cysteine residue in the CAAX motif, including isoprenylation (geranylgeranyl or farnesyl), endoproteolysis, and carboxyl methylation (Roberts et al. 2008).

A characteristic region of Rho family GTPases is the insert helix (amino acids 124–136, RhoA numbering) that may play a role in effector activation and downstream process (Thapar et al. 2002). Although the function of the insert helix has not been elucidated yet, it has been reported to be involved in the Rho-dependent activation of ROCK (Zong et al. 2001), phospholipase D (Walker and Brown 2002) and mDia (Lammers et al. 2008; Rose et al. 2005), and in the Rac-dependent activation of p67phox (Joneson and Bar-Sagi 1997; Karnoub et al. 2001; Nisimoto et al. 1997) and Plexin B1 (Bouguet-Bonnet and Buck 2008).

Although the majority of the Rho family proteins are remarkably inefficient GTP hydrolyzing enzymes, in quiescent cells they rest in an inactive state because the GTP hydrolysis is in average two orders of magnitude faster than the GDP/GTP exchange (Jaiswal et al. 2013a, b). Such different intrinsic activities provide the basis for a two-state molecular switch mechanism, which highly depends on the regulatory functions of GEFs and GAPs that directly control ON and OFF states of classical type of Rho proteins (Fig. 14.1). Eleven out of twenty members of the Rho family belong to these classical molecular switches, namely RhoA, RhoB, RhoC, Rac1, Rac2, Rac3, RhoG, Cdc42, G25K, TC10, and TCL (Jaiswal et al. 2013a, b).

The atypical Rho family members, including Rnd1, Rnd2, Rnd3, Rac1b, RhoH/TTF, Wrch1, RhoD, and Rif, have been proposed to accumulate in the GTP-bound form in cells due to various biochemical properties (Jaiswal et al. 2013a, b). Rnd1, Rnd2, Rnd3, and RhoH/TTF represent a completely distinct group of proteins within the Rho family (Riou et al. 2010; Troeger et al. 2013), as they do not share several conserved and essential amino acids, including Gly-12 (Rac1 numbering) in the G1 motif (also called phosphate-binding loop or P-loop) and Gln-61 (Rac1 numbering) in the G3 motif or switch II region. The role of these residues in GTP hydrolysis is well described for Ras oncogene in human cancers (Chaps. 6 and 7). Thus, they can be considered as GTPase-deficient Rho-related GTP-binding proteins (Fiegen et al. 2002; Garavini et al. 2002; Gu et al. 2005; Li et al. 2002) (see also Chap. 15). Another example is Rac1b, which is an alternative splice variant of Rac1 and contains a 19-amino acid insertion next to the switch II region (Jordan et al. 1999). Rac1b exhibits different biochemical properties as compared to the other Rac isoforms (Fiegen et al. 2004; Haeusler et al. 2006), including an accelerated GEF-independent GDP/GTP exchange and an impaired GTP hydrolysis (Fiegen et al. 2004). RhoD and Rif are involved in the regulation of actin dynamics (Fan and Mellor 2012; Gad and Aspenstrom 2010) and exhibit a strikingly faster nucleotide exchange than GTP hydrolysis similarly to Rac1b and thus persist

mainly in the active state under resting conditions (Jaiswal et al. 2013a, b). Wrch1, a Cdc42-like protein that has been reported to be a fast cycling protein (Shutes et al. 2006), resembles in this context Rac1b, RhoD, and Rif (Jaiswal et al. 2013a, b). These atypical members of the Rho family with their distinctive biochemical features do not follow the classical switch mechanism and may thus require additional forms of regulation.

14.3 Guanine Nucleotide Dissociation Inhibitors

Multiple functions have been originally described for the Rho-specific GDIs, including the inhibition of the GDP/GTP exchange (Hiraoka et al. 1992; Ohga et al. 1989), the intrinsic and GAP-stimulated GTP hydrolysis (Chuang et al. 1993; Hancock and Hall 1993; Hart et al. 1992), and the interaction with the downstream effectors (Pick et al. 1993). However, it is generally accepted that in resting cells, RhoGDIs target the isoprenyl anchor and sequester Rho proteins from their site of action at the membrane in the cytosol (Boulter and Garcia-Mata 2010; Garcia-Mata et al. 2011).

RhoGDIs undergo a high affinity interaction with the Rho proteins using an N-terminal regulatory arm contacting the switch regions and a C-terminal domain binding the isoprenyl group (Tnimov et al. 2012). In contrast to the large number of RhoGEFs and RhoGAPs, there are only three known RhoGDIs in human (DerMardirossian and Bokoch 2005). RhoGDI-1 (also called RhoGDI α) is ubiquitously expressed (Fukumoto et al. 1990), whereas RhoGDI-2 (also called RhoGDI β , LyGDI, or D4GDI) is predominantly found in hematopoietic tissues and lymphocytes (Leonard et al. 1992; Scherle et al. 1993) and RhoGDI-3 (also called RhoGDI γ) in lung, brain, and testis (Adra et al. 1997; Zalzman et al. 1996).

Despite intensive research over the last two decades, the molecular basis by which GDI proteins associate and extract the Rho GTPases from the membrane remains to be investigated. The neurotrophin receptor p75 (p75^{NTR}) and ezrin/radixin/moesin (ERM) proteins have been proposed to displace the Rho proteins from the RhoGDI complex resulting in reassociation with the cell membrane (Takahashi et al. 1997; Yamashita and Tohyama 2003). Another regulatory mechanism is RhoGDI phosphorylation. RhoGDI has been shown to be phosphorylated by serine/threonine p21-activated kinase 1 (PAK1), protein kinase A (PKA), protein kinase C (PKC), and the tyrosine kinase Src, thereby decreasing the ability of RhoGDI to form a complex with the Rho proteins, including RhoA, Rac1, and Cdc42 (DerMardirossian et al. 2004, 2006).

14.4 Guanine Nucleotide Exchange Factors

GEFs are able to selectively bind to their respective Rho proteins and accelerate the exchange of tightly bound GDP for GTP. A common mechanism utilized by GEFs is to strongly reduce the affinity of the bound GDP, leading to its displacement and the subsequent association with GTP (Cherfils and Chardin 1999; Guo et al. 2005). This reaction involves several stages, including an intermediate state of the GEF in the complex with the nucleotide-free Rho protein. This intermediate does not accumulate in the cell and rapidly dissociates because of the high intracellular GTP concentration leading to the formation of the active Rho-GTP complex. The main reason therefore is that the binding affinity of nucleotide-free Rho protein is significantly higher for GTP than for the GEF proteins (Cherfils and Chardin 1999; Hutchinson and Eccleston 2000). Cellular activation of the Rho proteins and their cellular signaling can be selectively uncoupled from the GEFs by overexpressing dominant negative mutants of the Rho proteins (e.g., threonine 17 in Rac1 and Cdc42 or threonine 19 in RhoA to asparagine) (Heasman and Ridley 2008). Such mutations decrease the affinity of the Rho protein to nucleotide resulting in a so-called dominant negative behavior (Rossman et al. 2002). As a consequence, dominant negative mutants form a tight complex with their cognate GEFs and thus prevent them from activating the endogenous Rho proteins.

RhoGEFs of the diffuse B-cell lymphoma (Dbl) family directly activate the proteins of the Rho family (Cook et al. 2013; Jaiswal et al. 2013a, b). The prototype of this GEF family is the Dbl protein, which was isolated as an oncogenic product from diffuse B-cell lymphoma cells in an oncogene screen (Eva et al. 1988; Srivastava et al. 1986), and has been later reported to act on Cdc42 (Hart et al. 1991). The Dbl family consists of 74 members in human (Jaiswal et al. 2013a, b) with evolutionary conserved orthologs in fly (23 members), yeast (6 members), worm (18 members) (Schmidt and Hall 2002; Venter et al. 2001), and slime mold (45 members) (Vlahou and Rivero 2006). Human Dbl family proteins have recently been grouped into functionally distinct categories based on both their catalytic efficiencies and their sequence–structure relationship (Jaiswal et al. 2013a, b). The members of the Dbl family are characterized by a unique Dbl homology (DH) domain (Aittaleb et al. 2010; Erickson and Cerione 2004; Hoffman and Cerione 2002; Jaiswal et al. 2011; Viaud et al. 2012). The DH domain is a highly efficient catalytic machine (Rossman et al. 2005) that is able to accelerate the nucleotide exchange of Rho proteins up to 10^7 -fold (Jaiswal et al. 2011, 2013a, b), as efficiently as the RanGEF RCC1 (Klebe et al. 1995) and *Salmonella typhimurium* effector SopE (see below) (Bulgin et al. 2010; Rudolph et al. 1999). The DH domain is often preceded by a pleckstrin homology (PH) domain indicating an essential and conserved function. A model for PH domain-assisted nucleotide exchange has been proposed for some GEFs, such as Dbl, Dbs, and Trio (Rossman et al. 2005). Herein the PH domain serves multiple roles in signaling events anchoring GEFs to the membrane (via phosphoinositides) and directing them

towards their interacting GTPases which are already localized to the membrane (Rossman et al. 2005).

In addition to the DH-PH tandem, Dbl family proteins are highly diverse and contain additional domains with different functions, including SH2, SH3, CH, RGS, PDZ, and IQ domains for interaction with other proteins; BAR, PH FYVE, C1, and C2 domains for interaction with membrane lipids; and other functional domains like Ser/Thr kinase, RasGEF, RhoGAP, and RanGEF (Cook et al. 2013). These additional domains have been implicated in autoregulation, subcellular localization, and connection to upstream signals (Dubash et al. 2007; Rossman et al. 2005). Spatiotemporal regulation of the Dbl proteins has been implicated to specifically initiate activation of substrate Rho proteins (Jaiswal et al. 2013a, b) and to control a broad spectrum of normal and pathological cellular functions (Dubash et al. 2007; Hall and Lalli 2010; Mulinari and Hacker 2010; Mulloy et al. 2010; Schmidt and Hall 2002). Thus, it is evident that members of the Dbl protein family are attractive therapeutic targets for a variety of diseases (Bos et al. 2007; Loirand et al. 2008; Vigil et al. 2010).

Apart from conventional Dbl family RhoGEFs there are two additional proteins families, which do not share any sequence and structural similarity with each other. The dedicator of cytokinesis (DOCK) or CDM-zizimin homology (CZH) family RhoGEFs are characterized by two conserved regions, known as the DOCK-homology regions 1 and 2 (DHR1 and DHR2) domains (Meller et al. 2005; Rittinger 2009). This type of GEFs employs their DHR2 domain to activate specially Rac and Cdc42 proteins (Meller et al. 2005). Another Rho protein-specific GEF family, represented by the SopE/WxxxE-type exchange factors, is classified as type III effector proteins of bacterial pathogens (Bulgin et al. 2010). They mimic functionally, but not structurally, eukaryotic GEFs by efficiently activating Rac1 and Cdc42 and thus induce “the trigger mechanism of cell entry” (see Chap. 4) (Bulgin et al. 2010; Rudolph et al. 1999).

14.5 GTPase-Activating Proteins

Hydrolysis of the bound GTP is the timing mechanism that terminates signal transduction of the Rho family proteins and returns them to their GDP-bound inactive state (Jaiswal et al. 2012). The intrinsic GTP hydrolysis (GTPase) reaction is usually slow, but can be stimulated by several orders of magnitude through interaction with Rho-specific GAPs (Eberth et al. 2005; Fidyk and Cerione 2002; Zhang and Zheng 1998). The RhoGAP family is defined by the presence of a conserved catalytic GAP domain which is sufficient for the interaction with Rho proteins and mediating accelerated catalysis (Scheffzek and Ahmadian 2005). The GAP domain supplies a conserved arginine residue, termed “arginine finger”, into the GTP-binding site of the cognate Rho protein, in order to stabilize the transition state and catalyze the GTP hydrolysis reaction (Nassar et al. 1998; Rittinger et al. 1997). A similar mechanism is utilized by other small GTP-binding proteins

(Scheffzek and Ahmadian 2005), including Ras, Rab, and Arf, although the sequence and folding of the respective GAP families are different (Ismail et al. 2010; Pan et al. 2006; Scheffzek et al. 1997). Masking the catalytic arginine finger is an elegant mechanism for the inhibition of the GAP activity. This has been recently shown for the tumor suppressor protein DLC1, a RhoGAP, which is competitively and selectively inhibited by the SH3 domain of p120RasGAP (Jaiswal et al. 2014).

RhoGAP insensitivity can be achieved by the substitution of either the catalytic arginine of the GAP domain (Fidyk and Cerione 2002; Graham et al. 1999) or amino acids critical for the GTP hydrolysis in Rho proteins, e.g., Glycine 12 and Glutamine 61 in Rac1 and Cdc42 or Glycine 14 and Glutamine 63 in RhoA, which are known as the constitutive active mutants (Ahmadian et al. 1997; Graham et al. 1999). Most remarkably, a similar mechanistic strategy has been mimicked by bacterial GAPs (see Chap. 4), such as the *Salmonella typhimurium* virulence factor SptP, the *Pseudomonas aeruginosa* cytotoxin ExoS, and *Yersinia pestis* YopE, even though they do not share any sequence or structural similarity to eukaryotic RhoGAP domains (Evdokimov et al. 2002; Stebbins and Galan 2000; Wurtele et al. 2001).

The first RhoGAP, p50RhoGAP, was identified by biochemical analysis of human spleen cell extracts in the presence of recombinant RhoA (Garrett et al. 1989). Since then more than 80 RhoGAP containing proteins have been identified in eukaryotes, ranging from yeast to human (Lancaster et al. 1994; Moon and Zheng 2003). The RhoGAP domain (also known as Bcr-homology, BH domain) containing proteins are present throughout the genome and rarely cluster in specific chromosomal regions (Peck et al. 2002). The majority of the RhoGAP family members are frequently accompanied by several other functional domains and motifs implicated in tight regulation and membrane targeting (Eberth et al. 2009; Moon and Zheng 2003; Tcherkezian and Lamarche-Vane 2007). Numerous mechanisms have been shown to affect the specificity and the catalytic activity of the RhoGAPs, e.g., intramolecular autoinhibition (Eberth et al. 2009), posttranslational modification (Minoshima et al. 2003), and regulation by interaction with lipid membrane (Ligeti et al. 2004) and proteins (Yang et al. 2009).

14.6 Conclusions

Abnormal activation of Rho proteins has been shown to play a crucial role in cancer, infectious and cognitive disorders, and cardiovascular diseases. However, several tasks have to be yet accomplished in order to understand the complexity of Rho proteins signaling: (1) The Rho family comprises of 20 signaling proteins, of which only RhoA, Rac1, and Cdc42 have been comprehensively studied so far. The functions of the other less-characterized members of this protein family await detailed investigation. (2) Despite intensive research over the last two decades, the mechanisms by which RhoGDIs associate and extract the Rho proteins from the

membrane and the factors displacing the Rho protein from the complex with RhoGDI remain to be elucidated. (3) For the regulation of the 22 Rho proteins, a tremendous number of their regulatory proteins (>74 GEFs and >80 GAPs) exist in the human genome. How these regulators selectively recognize their Rho protein targets is not well understood and majority of GEFs and GAPs in humans so far remain uncharacterized. (4) Most of the GEFs and GAPs themselves need to be regulated and require activation through the relief of autoinhibitory elements (Chow et al. 2013; Eberth et al. 2009; Jaiswal et al. 2011; Mitin et al. 2007; Moskwa et al. 2005; Rojas et al. 2007; Yohe et al. 2008). With a few exceptions (Cherfils and Zeghouf 2013; Mayer et al. 2013), it is conceptually still unclear how such autoregulatory mechanisms are operated. A better understanding of the specificity and the mode of action of these regulatory proteins is not only fundamentally important for many aspects of biology but is also a master key for the development of drugs against a variety of diseases caused by aberrant functions of Rho proteins.

References

- Adra CN, Manor D, Ko JL et al (1997) RhoGDI γ : a GDP-dissociation inhibitor for Rho proteins with preferential expression in brain and pancreas. *Proc Natl Acad Sci USA* 94:4279–4284
- Ahmadian MR, Mittal R, Hall A et al (1997) Aluminum fluoride associates with the small guanine nucleotide binding proteins. *FEBS Lett* 408:315–318
- Aittaleb M, Boguth CA, Tesmer JJ (2010) Structure and function of heterotrimeric G protein-regulated Rho guanine nucleotide exchange factors. *Mol Pharmacol* 77:111–125
- Bishop AL, Hall A (2000) Rho GTPases and their effector proteins. *Biochem J* 348(Pt 2):241–255
- Bos JL, Rehmann H, Wittinghofer A (2007) GEFs and GAPs: critical elements in the control of small G proteins. *Cell* 129:865–877
- Bouguet-Bonnet S, Buck M (2008) Compensatory and long-range changes in picosecond-nanosecond main-chain dynamics upon complex formation: 15N relaxation analysis of the free and bound states of the ubiquitin-like domain of human plexin-B1 and the small GTPase Rac1. *J Mol Biol* 377:1474–1487
- Boulter E, Garcia-Mata R (2010) RhoGDI: a rheostat for the Rho switch. *Small GTPases* 1:65–68
- Boureux A, Vignal E, Faure S et al (2007) Evolution of the Rho family of ras-like GTPases in eukaryotes. *Mol Biol Evol* 24:203–216
- Bulgin R, Raymond B, Garnett JA et al (2010) Bacterial guanine nucleotide exchange factors SopE-like and WxxxE effectors. *Infect Immun* 78:1417–1425
- Burridge K, Wennerberg K (2004) Rho and Rac take center stage. *Cell* 116:167–179
- Cherfils J, Chardin P (1999) GEFs: structural basis for their activation of small GTP-binding proteins. *Trends Biochem Sci* 24:306–311
- Cherfils J, Zeghouf M (2013) Regulation of small GTPases by GEFs, GAPs, and GDIs. *Physiol Rev* 93:269–309
- Chow CR, Suzuki N, Kawamura T et al (2013) Modification of p115RhoGEF Ser(330) regulates its RhoGEF activity. *Cell Signal* 25:2085–2092
- Chuang TH, Xu X, Knaus UG et al (1993) GDP dissociation inhibitor prevents intrinsic and GTPase activating protein-stimulated GTP hydrolysis by the Rac GTP-binding protein. *J Biol Chem* 268:775–778
- Cook DR, Rossman KL, Der CJ (2013) Rho guanine nucleotide exchange factors: regulators of Rho GTPase activity in development and disease. *Oncogene* 16:362

- DerMardirossian C, Bokoch GM (2005) GDIs: central regulatory molecules in Rho GTPase activation. *Trends Cell Biol* 15:356–363
- DerMardirossian C, Schnelzer A, Bokoch GM (2004) Phosphorylation of RhoGDI by Pak1 mediates dissociation of Rac GTPase. *Mol Cell* 15:117–127
- DerMardirossian C, Rocklin G, Seo JY et al (2006) Phosphorylation of RhoGDI by Src regulates Rho GTPase binding and cytosol-membrane cycling. *Mol Biol Cell* 17:4760–4768
- Dubash AD, Wennerberg K, Garcia-Mata R et al (2007) A novel role for Lsc/p115 RhoGEF and LARG in regulating RhoA activity downstream of adhesion to fibronectin. *J Cell Sci* 120:3989–3998
- Dvorsky R, Ahmadian MR (2004) Always look on the bright site of Rho: structural implications for a conserved intermolecular interface. *EMBO Rep* 5:1130–1136
- Eberth A, Dvorsky R, Becker CF et al (2005) Monitoring the real-time kinetics of the hydrolysis reaction of guanine nucleotide-binding proteins. *Biol Chem* 386:1105–1114
- Eberth A, Lundmark R, Gremer L et al (2009) A BAR domain-mediated autoinhibitory mechanism for RhoGAPs of the GRAF family. *Biochem J* 417:371–377
- Erickson JW, Cerione RA (2004) Structural elements, mechanism, and evolutionary convergence of Rho protein-guanine nucleotide exchange factor complexes. *Biochemistry* 43:837–842
- Etienne-Manneville S, Hall A (2002) Rho GTPases in cell biology. *Nature* 420:629–635
- Eva A, Vecchio G, Rao CD et al (1988) The predicted DBL oncogene product defines a distinct class of transforming proteins. *Proc Natl Acad Sci USA* 85:2061–2065
- Evdokimov AG, Tropea JE, Routzahn KM et al (2002) Crystal structure of the *Yersinia pestis* GTPase activator YopE. *Protein Sci* 11:401–408
- Fan L, Mellor H (2012) The small Rho GTPase Rif and actin cytoskeletal remodelling. *Biochem Soc Trans* 40:268–272
- Fidyk NJ, Cerione RA (2002) Understanding the catalytic mechanism of GTPase-activating proteins: demonstration of the importance of switch domain stabilization in the stimulation of GTP hydrolysis. *Biochemistry* 41:15644–15653
- Fiegen D, Blumenstein L, Stege P et al (2002) Crystal structure of Rnd3/RhoE: functional implications. *FEBS Lett* 525:100–104
- Fiegen D, Haeusler LC, Blumenstein L et al (2004) Alternative splicing of Rac1 generates Rac1b, a self-activating GTPase. *J Biol Chem* 279:4743–4749
- Fukumoto Y, Kaibuchi K, Hori Y et al (1990) Molecular-cloning and characterization of a novel type of regulatory protein (Gdi) for the Rho proteins, Ras P21-Like small Gtp-binding proteins. *Oncogene* 5:1321–1328
- Gad AK, Aspenstrom P (2010) Rif proteins take to the RhoD: Rho GTPases at the crossroads of actin dynamics and membrane trafficking. *Cell Signal* 22:183–189
- Garavini H, Riento K, Phelan JP et al (2002) Crystal structure of the core domain of RhoE/Rnd3: a constitutively activated small G protein. *Biochemistry* 41:6303–6310
- Garcia-Mata R, Boulter E, Burrige K (2011) The ‘invisible hand’: regulation of RHO GTPases by RHOGDIs. *Nat Rev Mol Cell Biol* 12:493–504
- Garrett MD, Self AJ, van Oers C et al (1989) Identification of distinct cytoplasmic targets for ras/R-ras and rho regulatory proteins. *J Biol Chem* 264:10–13
- Graham DL, Eccleston JF, Lowe PN (1999) The conserved arginine in rho-GTPase-activating protein is essential for efficient catalysis but not for complex formation with Rho.GDP and aluminum fluoride. *Biochemistry* 38:985–991
- Gu Y, Zheng Y, Williams DA (2005) RhoH GTPase: a key regulator of hematopoietic cell proliferation and apoptosis? *Cell Cycle* 4:201–202
- Guo Z, Ahmadian MR, Goody RS (2005) Guanine nucleotide exchange factors operate by a simple allosteric competitive mechanism. *Biochemistry* 44:15423–15429
- Haeusler LC, Hemsath L, Fiegen D et al (2006) Purification and biochemical properties of Rac1, 2, 3 and the splice variant Rac1b. *Methods Enzymol* 406:1–11
- Hall A, Lalli G (2010) Rho and Ras GTPases in axon growth, guidance, and branching. *Cold Spring Harb Perspect Biol* 2:a001818

14 Classical Rho Proteins: Biochemistry of Molecular Switch Function and Regulation 337

- Hancock JF, Hall A (1993) A novel role for RhoGDI as an inhibitor of GAP proteins. *EMBO J* 12:1915–1921
- Hart MJ, Eva A, Evans T et al (1991) Catalysis of guanine nucleotide exchange on the CDC42Hs protein by the *dbl* oncogene product. *Nature* 354:311–314
- Hart MJ, Maru Y, Leonard D et al (1992) A GDP dissociation inhibitor that serves as a GTPase inhibitor for the Ras-like protein CDC42Hs. *Science* 258:812–815
- Heasman SJ, Ridley AJ (2008) Mammalian Rho GTPases: new insights into their functions from *in vivo* studies. *Nat Rev Mol Cell Biol* 9:690–701
- Hiraoka K, Kaibuchi K, Ando S et al (1992) Both stimulatory and inhibitory GDP/GTP exchange proteins, smg GDS and rho GDI, are active on multiple small GTP-binding proteins. *Biochem Biophys Res Commun* 182:921–930
- Hoffman GR, Cerione RA (2002) Signaling to the Rho GTPases: networking with the DH domain. *FEBS Lett* 513:85–91
- Hutchinson JP, Eccleston JF (2000) Mechanism of nucleotide release from Rho by the GDP dissociation stimulator protein. *Biochemistry* 39:11348–11359
- Ismail SA, Vetter IR, Sot B et al (2010) The structure of an Arf-ArfGAP complex reveals a Ca²⁺ regulatory mechanism. *Cell* 141:812–821
- Jaiswal M, Gremer L, Dvorsky R et al (2011) Mechanistic insights into specificity, activity, and regulatory elements of the regulator of G-protein signaling (RGS)-containing Rho-specific guanine nucleotide exchange factors (GEFs) p115, PDZ-RhoGEF (PRG), and leukemia-associated RhoGEF (LARG). *J Biol Chem* 286:18202–18212
- Jaiswal M, Dubey BN, Koessmeier KT et al (2012) Biochemical assays to characterize Rho GTPases. *Methods Mol Biol* 827:37–58
- Jaiswal M, Dvorsky R, Ahmadian MR (2013a) Deciphering the molecular and functional basis of *Dbl* family proteins: a novel systematic approach toward classification of selective activation of the Rho family proteins. *J Biol Chem* 288:4486–4500
- Jaiswal M, Fansa EK, Dvorsky R et al (2013b) New insight into the molecular switch mechanism of human Rho family proteins: shifting a paradigm. *Biol Chem* 394:89–95
- Jaiswal M, Dvorsky R, Amin E et al (2014) Functional crosstalk between Ras and Rho pathways: p120RasGAP competitively inhibits the RhoGAP activity of Deleted in Liver Cancer (DLC) tumor suppressors by masking its catalytic arginine finger. *J Biol Chem* 289:6839–6849
- Joneson T, Bar-Sagi D (1997) Ras effectors and their role in mitogenesis and oncogenesis. *J Mol Med (Berl)* 75:587–593
- Jordan P, Brazao R, Boavida MG et al (1999) Cloning of a novel human Rac1b splice variant with increased expression in colorectal tumors. *Oncogene* 18:6835–6839
- Karnoub AE, Der CJ, Campbell SL (2001) The insert region of Rac1 is essential for membrane ruffling but not cellular transformation. *Mol Cell Biol* 21:2847–2857
- Klebe C, Prinz H, Wittinghofer A et al (1995) The kinetic mechanism of Ran–nucleotide exchange catalyzed by RCC1. *Biochemistry* 34:12543–12552
- Lammers M, Meyer S, Kuhlmann D et al (2008) Specificity of interactions between mDia isoforms and Rho proteins. *J Biol Chem* 283:35236–35246
- Lancaster CA, Taylor-Harris PM, Self AJ et al (1994) Characterization of rhoGAP. A GTPase-activating protein for rho-related small GTPases. *J Biol Chem* 269:1137–1142
- Leonard D, Hart MJ, Platko JV et al (1992) The identification and characterization of a GDP-dissociation inhibitor (GDI) for the CDC42Hs protein. *J Biol Chem* 267:22860–22868
- Li X, Bu X, Lu B et al (2002) The hematopoiesis-specific GTP-binding protein RhoH is GTPase deficient and modulates activities of other Rho GTPases by an inhibitory function. *Mol Cell Biol* 22:1158–1171
- Ligeti E, Dagher MC, Hernandez SE et al (2004) Phospholipids can switch the GTPase substrate preference of a GTPase-activating protein. *J Biol Chem* 279:5055–5058
- Loirand G, Scalbert E, Bril A et al (2008) Rho exchange factors in the cardiovascular system. *Curr Opin Pharmacol* 8:174–180

- Mayer S, Kumar R, Jaiswal M et al (2013) Collybistin activation by GTP-TC10 enhances postsynaptic gephyrin clustering and hippocampal GABAergic neurotransmission. *Proc Natl Acad Sci USA* 110:20795–20800
- Meller N, Merlot S, Guda C (2005) CZH proteins: a new family of Rho-GEFs. *J Cell Sci* 118:4937–4946
- Minoshima Y, Kawashima T, Hirose K et al (2003) Phosphorylation by aurora B converts MgcRacGAP to a RhoGAP during cytokinesis. *Dev Cell* 4:549–560
- Mitin N, Betts L, Yohe ME et al (2007) Release of autoinhibition of ASEF by APC leads to CDC42 activation and tumor suppression. *Nat Struct Mol Biol* 14:814–823
- Moon SY, Zheng Y (2003) Rho GTPase-activating proteins in cell regulation. *Trends Cell Biol* 13:13–22
- Moskwa P, Paclat MH, Dagher MC et al (2005) Autoinhibition of p50 Rho GTPase-activating protein (GAP) is released by prenylated small GTPases. *J Biol Chem* 280:6716–6720
- Mulinari S, Hacker U (2010) Rho-guanine nucleotide exchange factors during development: Force is nothing without control. *Small GTPases* 1:28–43
- Mulloy JC, Cancelas JA, Filippi MD et al (2010) Rho GTPases in hematopoiesis and hemopathies. *Blood* 115:936–947
- Nassar N, Hoffman GR, Manor D et al (1998) Structures of Cdc42 bound to the active and catalytically compromised forms of Cdc42GAP. *Nat Struct Biol* 5:1047–1052
- Nisimoto Y, Freeman JL, Motalebi SA et al (1997) Rac binding to p67(phox). Structural basis for interactions of the Rac1 effector region and insert region with components of the respiratory burst oxidase. *J Biol Chem* 272:18834–18841
- Ohga N, Kikuchi A, Ueda T et al (1989) Rabbit intestine contains a protein that inhibits the dissociation of GDP from and the subsequent binding of GTP to rhoB p20, a ras p21-like GTP-binding protein. *Biochem Biophys Res Commun* 163:1523–1533
- Pan X, Eathiraj S, Munson M et al (2006) TBC-domain GAPs for Rab GTPases accelerate GTP hydrolysis by a dual-finger mechanism. *Nature* 442:303–306
- Peck J, Douglas Gt WCH et al (2002) Human RhoGAP domain-containing proteins: structure, function and evolutionary relationships. *FEBS Lett* 528:27–34
- Pick E, Gorzalczyk Y, Engel S (1993) Role of the rac1 p21-GDP-dissociation inhibitor for rho heterodimer in the activation of the superoxide-forming NADPH oxidase of macrophages. *Eur J Biochem* 217:441–455
- Riou P, Villalonga P, Ridley AJ (2010) Rnd proteins: multifunctional regulators of the cytoskeleton and cell cycle progression. *Bioessays* 32:986–992
- Rittinger K (2009) Snapshots form a big picture of guanine nucleotide exchange. *Sci Signal* 2:pe63
- Rittinger K, Walker PA, Eccleston JF et al (1997) Structure at 1.65 Å of RhoA and its GTPase-activating protein in complex with a transition-state analogue. *Nature* 389:758–762
- Roberts PJ, Mitin N, Keller PJ et al (2008) Rho Family GTPase modification and dependence on CAAX motif-signaled posttranslational modification. *J Biol Chem* 283:25150–25163
- Rojas RJ, Yohe ME, Gershburg S et al (2007) Galphaq directly activates p63RhoGEF and Trio via a conserved extension of the Dbl homology-associated pleckstrin homology domain. *J Biol Chem* 282:29201–29210
- Rose R, Weyand M, Lammers M et al (2005) Structural and mechanistic insights into the interaction between Rho and mammalian Dia. *Nature* 435:513–518
- Rossmann KL, Worthylake DK, Snyder JT et al (2002) Functional analysis of cdc42 residues required for Guanine nucleotide exchange. *J Biol Chem* 277:50893–50898
- Rossmann KL, Der CJ, Sondek J (2005) GEF means go: turning on RHO GTPases with guanine nucleotide-exchange factors. *Nat Rev Mol Cell Biol* 6:167–180
- Rudolph MG, Weise C, Mirolid S et al (1999) Biochemical analysis of SopE from *Salmonella typhimurium*, a highly efficient guanosine nucleotide exchange factor for RhoGTPases. *J Biol Chem* 274:30501–30509
- Scheffzek K, Ahmadian MR (2005) GTPase activating proteins: structural and functional insights 18 years after discovery. *Cell Mol Life Sci* 62:3014–3038

14 Classical Rho Proteins: Biochemistry of Molecular Switch Function and Regulation 339

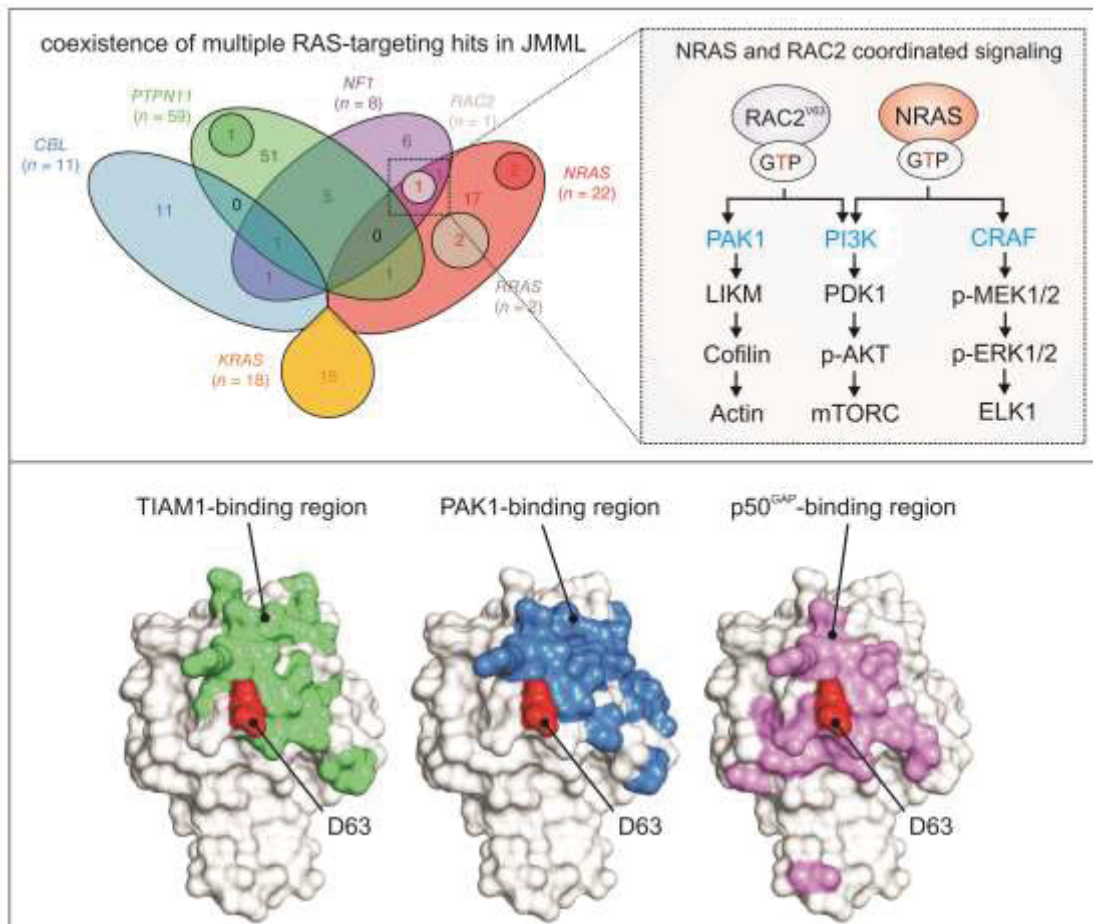
- Scheffzek K, Ahmadian MR, Kabsch W et al (1997) The Ras-RasGAP complex: structural basis for GTPase activation and its loss in oncogenic Ras mutants. *Science* 277:333–338
- Scherle P, Behrens T, Staudt LM (1993) Ly-GDI, a GDP-dissociation inhibitor of the RhoA GTP-binding protein, is expressed preferentially in lymphocytes. *Proc Natl Acad Sci USA* 90:7568–7572
- Schmidt A, Hall A (2002) Guanine nucleotide exchange factors for Rho GTPases: turning on the switch. *Genes Dev* 16:1587–1609
- Shutes A, Berzat AC, Chenette EJ et al (2006) Biochemical analyses of the Wrch atypical Rho family GTPases. *Methods Enzymol* 406:11–26
- Srivastava SK, Wheelock RH, Aaronson SA et al (1986) Identification of the protein encoded by the human diffuse B-cell lymphoma (dbl) oncogene. *Proc Natl Acad Sci USA* 83:8868–8872
- Stebbins CE, Galan JE (2000) Modulation of host signaling by a bacterial mimic: structure of the Salmonella effector SptP bound to Rac1. *Mol Cell* 6:1449–1460
- Takahashi K, Sasaki T, Mammoto A et al (1997) Direct interaction of the Rho GDP dissociation inhibitor with ezrin/radixin/moesin initiates the activation of the Rho small G protein. *J Biol Chem* 272:23371–23375
- Tcherkezian J, Lamarche-Vane N (2007) Current knowledge of the large RhoGAP family of proteins. *Biol Cell* 99:67–86
- Thapar R, Karnoub AE, Campbell SL (2002) Structural and biophysical insights into the role of the insert region in Rac1 function. *Biochemistry* 41:3875–3883
- Tnımov Z, Guo Z, Gambin Y et al (2012) Quantitative analysis of prenylated RhoA interaction with its chaperone, RhoGDI. *J Biol Chem* 287:26549–26562
- Troeger A, Chae HD, Senturk M et al (2013) A unique carboxyl-terminal insert domain in the hematopoietic-specific, GTPase-deficient Rho GTPase RhoH regulates post-translational processing. *J Biol Chem* 288:36451–36462
- Venter JC, Adams MD, Myers EW et al (2001) The sequence of the human genome. *Science* 291:1304–1351
- Viaud J, Gaits-Iacovoni F, Payrastre B (2012) Regulation of the DH-PH tandem of guanine nucleotide exchange factor for Rho GTPases by phosphoinositides. *Adv Biol Regul* 52:303–314
- Vigil D, Cherfils J, Rossman KL et al (2010) Ras superfamily GEFs and GAPs: validated and tractable targets for cancer therapy? *Nat Rev Cancer* 10:842–857
- Vlahou G, Rivero F (2006) Rho GTPase signaling in Dictyostelium discoideum: insights from the genome. *Eur J Cell Biol* 85:947–959
- Walker SJ, Brown HA (2002) Specificity of Rho insert-mediated activation of phospholipase D1. *J Biol Chem* 277:26260–26267
- Wennerberg K, Der CJ (2004) Rho-family GTPases: it's not only Rac and Rho (and I like it). *J Cell Sci* 117:1301–1312
- Wittinghofer A, Vetter IR (2011) Structure-function relationships of the G domain, a canonical switch motif. *Annu Rev Biochem* 80:943–971
- Wurtele M, Wolf E, Pederson KJ et al (2001) How the Pseudomonas aeruginosa ExoS toxin downregulates Rac. *Nat Struct Biol* 8:23–26
- Yamashita T, Tohyama M (2003) The p75 receptor acts as a displacement factor that releases Rho from Rho-GDI. *Nat Neurosci* 6:461–467
- Yang XY, Guan M, Vigil D et al (2009) p120Ras-GAP binds the DLC1 Rho-GAP tumor suppressor protein and inhibits its RhoA GTPase and growth-suppressing activities. *Oncogene* 28:1401–1409
- Yohe ME, Rossman K, Sondek J (2008) Role of the C-terminal SH3 domain and N-terminal tyrosine phosphorylation in regulation of Tim and related Dbl-family proteins. *Biochemistry* 47:6827–6839
- Zalcman G, Closson V, Camonis J et al (1996) RhoGDI-3 is a new GDP dissociation inhibitor (GDI). Identification of a non-cytosolic GDI protein interacting with the small GTP-binding proteins RhoB and RhoG. *J Biol Chem* 271:30366–30374

- Zhang B, Zheng Y (1998) Regulation of RhoA GTP hydrolysis by the GTPase-activating proteins p190, p50RhoGAP, Bcr, and 3BP-1. *Biochemistry* 37:5249–5257
- Zong H, Kaibuchi K, Quilliam LA (2001) The insert region of RhoA is essential for Rho kinase activation and cellular transformation. *Mol Cell Biol* 21:5287–5298

Chapter III

Juvenile myelomonocytic leukemia displays mutations in components of the RAS pathway and the PRC2 network

Graphical abstract



Status: Published in Nature Genetics, October 12, 2015

Impact factor: 29.35

Own Proportion to this work: 20 %

Cloning, expression and purification of RAC2 proteins, TIAM1, PAK1 and p50GAP

Preparing nucleotide-free RAC2 proteins

Generating mantGDP, mantGppNHp and tamraGTP bound RAC2 proteins

Fluorescence polarization measurement

GEF and GAP assay using stopped-flow apparatus

Evaluating the data and partially writing the manuscript

Juvenile myelomonocytic leukemia displays mutations in components of the RAS pathway and the PRC2 network

Aurélie Caye¹⁻³, Marion Strullu^{1,3}, Fabien Guidez¹, Bruno Cassinat^{1,4}, Steven Gazal^{5,6}, Odile Fenneteau⁷, Elodie Lainey^{1,2,7}, Kazem Nouri⁸, Saeideh Nakhaei-Rad⁸, Radovan Dvorsky⁸, Julie Lachenaud^{1,3}, Sabrina Pereira³, Jocelyne Vivent^{1,3}, Emmanuelle Verger^{1,4}, Dominique Vidaud^{9,10}, Claire Galambrun¹¹, Capucine Picard¹²⁻¹⁴, Arnaud Petit¹⁵, Audrey Contet¹⁶, Marilyne Poirée¹⁷, Nicolas Sirvent¹⁸, Françoise Méchinaud¹⁹, Dalila Adjaoud²⁰, Catherine Paillard²¹, Brigitte Nelken²², Yves Reguerre²³, Yves Bertrand²⁴, Dieter Häussinger²⁵, Jean-Hugues Dalle^{2,26}, Mohammad Reza Ahmadian⁸, André Baruchel^{2,26}, Christine Chomienne^{1,2,4} & Hélène Cavé¹⁻³

Juvenile myelomonocytic leukemia (JMML) is a rare and severe myelodysplastic and myeloproliferative neoplasm of early childhood initiated by germline or somatic RAS-activating mutations¹⁻³. Genetic profiling and whole-exome sequencing of a large JMML cohort (118 and 30 cases, respectively) uncovered additional genetic abnormalities in 56 cases (47%). Somatic events were rare (0.38 events/Mb/case) and restricted to sporadic (49/78; 63%) or neurofibromatosis type 1 (NF1)-associated (8/8; 100%) JMML cases. Multiple concomitant genetic hits targeting the RAS pathway were identified in 13 of 78 cases (17%), disproving the concept of mutually exclusive RAS pathway mutations and defining new pathways activated in JMML involving phosphoinositide 3-kinase (PI3K) and the mTORC2 complex through *RAC2* mutation. Furthermore, this study highlights PRC2 loss (26/78; 33% of sporadic JMML cases) that switches the methylation/acetylation status of lysine 27 of histone H3 in JMML cases with altered RAS and PRC2 pathways. Finally, the association between JMML outcome and mutational profile suggests a dose-dependent effect for RAS pathway activation, distinguishing very aggressive JMML rapidly progressing to acute myeloid leukemia.

JMML is considered a unique example of RAS-driven oncogenesis because it is thought to be initiated by mutations, usually described as mutually exclusive, in RAS genes (*NRAS* or *KRAS*) or RAS pathway regulators (*PTPN11*, *NF1* or *CBL*)¹. JMML can be sporadic or develop in patients displaying syndromic diseases with constitutional RAS overactivation such as Noonan syndrome, NF1 and CBL syndrome, which are caused by heterozygous germline mutations in *PTPN11*, *NF1* and *CBL*, respectively⁴.

We first explored the somatic mutation landscape of 30 patients with syndromic ($n = 8$) or sporadic ($n = 22$) JMML by combining genome-wide DNA array analysis, whole-exome sequencing and targeted sequencing in paired germline and tumoral samples

(Supplementary Table 1). In total, 85 somatically acquired genetic alterations were found in 25 of 30 (83%) patients in this subcohort (Supplementary Fig. 1 and Supplementary Tables 2 and 3). The low rate of somatic events (0.38 events/Mb/case versus 0.61 events/Mb/case on average in childhood cancer)⁵ confirms the paucity of oncogenic events required for JMML oncogenesis⁶.

Genes containing somatic variations detected by whole-exome sequencing or previously reported to be mutated in JMML (Supplementary Table 4) were then sequenced in the full cohort of 118 JMML cases (Supplementary Figs. 2 and 3). In total, 122 secondary clonal abnormalities in addition to initiating RAS pathway mutations were uncovered in 58 of the 118 (49%) patients (Fig. 1 and Supplementary Tables 2, 5 and 6). Interestingly, almost no additional mutations were detected in patients with CBL syndrome or Noonan syndrome. In line with phenotype-genotype correlations⁷⁻⁹, this observation supports an endogenous role for germline *PTPN11* and *CBL* mutations in the occurrence of myeloproliferative neoplasms and suggests that parameters other than additional somatic gene mutations, such as, for instance, a mutated hematopoietic microenvironment, might be involved in supporting leukemogenesis.

In contrast, at least one additional somatic hit was found in eight of eight (100%) NF1-associated JMML cases and 49 of 78 (63%) sporadic JMML cases. The percentage of sporadic JMML cases with secondary genetic alterations was similar in all subgroups, but the pattern of mutations varied substantially depending on the initiating lesion. JMML cases with an initiating *KRAS* lesion (KRAS-JMML) mostly displayed chromosomal abnormalities, including del7 or del7q in 56% of cases, unlike other genetic subgroups that mostly had point mutations (Supplementary Fig. 4 and Supplementary Table 5). Further studies are required to understand why RAS-driven oncogenesis proceeds through the acquisition of various patterns of secondary mutation that depend on the initiating lesion.

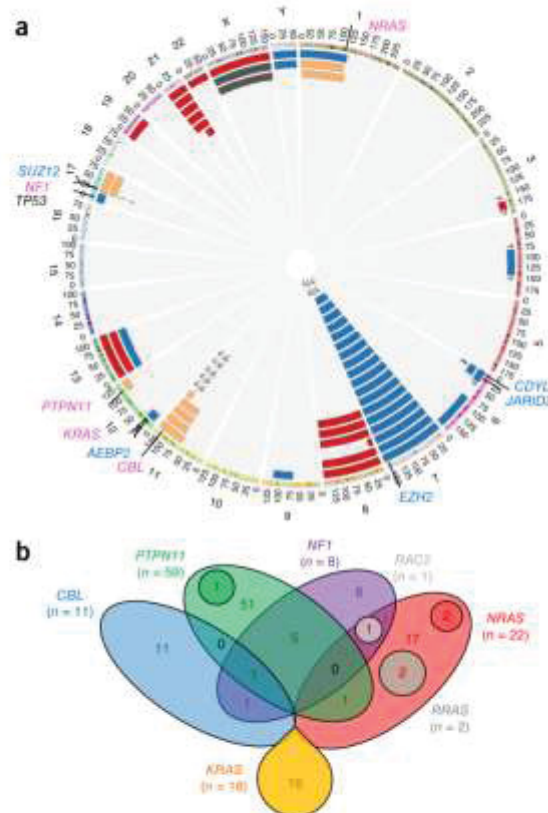
The secondary somatic mutations targeted genes known to be involved in myeloproliferative neoplasms, albeit with a much lower

A full list of author affiliations appears at the end of the paper.

Received 13 March; accepted 16 September; published online 12 October 2015; doi:10.1038/ng.3420

LETTERS

Figure 1 Combinations of multiple hits targeting the RAS pathway and PRC2 network. **(a)** Circos plot representing CNVs in 118 JMML cases. Copy number profiles are shown in red (somatic gain) or blue (somatic loss), aUPD regions are shown in orange and germline aneuploidies are shown in black. A question mark indicates undetermined boundaries. Relevant genes in the RAS pathway and PRC2 network are indicated in pink and blue, respectively. All aUPD events ($n = 16$) resulted in the duplication of oncogenic RAS-related variants. An aUPD region encompassed the second allele of *NFI* ($n = 3$) and *CBL* ($n = 10$) in patients with germline mutations of these genes or somatically acquired oncogenic *PTPN11* ($n = 1$) or *NRAS* ($n = 2$) mutations in sporadic JMML cases. Deletions targeted various PRC2 components. *EZH2* was haploinsufficient in patients with del17 or del7q. *AEBP2* was deleted in one patient with del12p. A 6p deletion encompassed *CDYL* (6p25.1) in three patients, with co-deletion of *JARID2* (6p22.3) in two of them. **(b)** Venn diagram showing the coexistence of multiple RAS-targeting hits in JMML. Both germline and somatically acquired mutations of canonical RAS pathway genes and orthologs are represented. Each colored segment corresponds to a different gene. In three cases (two *NRAS*-JMML and one *PTPN11*-JMML), represented by darker circles embedded in the segment of the altered gene, RAS double mutation corresponded to LOH of the oncogenic mutation. *RRAS* mutations are represented by a gray circle embedded in the *NRAS* segment, as the two *RRAS* mutations were found in patients with concomitant *NRAS* mutation.



prevalence than in adult diseases^{6,10} (Fig. 2). *SETBP1* was mutated in ten of the 118 (9%) cases, and the spliceosome gene *ZRSR2* was mutated in three cases. In contrast with a previous report, *JAK3* mutations were found in only four JMML cases⁶. The acquisition of *SETBP1*, *ASXL1*, *JAK3* and other somatic alterations, including monosomy 7, consistently appeared secondary to the RAS pathway mutation, usually following a linear pattern, except in two patients (Fig. 3). An active role for the variants in leukemogenesis is supported by the high proportion predicted to be deleterious (Supplementary Fig. 5) and, most notably, by their striking enrichment in RAS pathway and Polycomb repressive complex 2 (PRC2) network components (Fig. 1 and Supplementary Table 6).

Surprisingly, a second hit targeting the RAS pathway was observed in 13 of 78 (17%) sporadic JMML cases and two of eight (25%) *NFI*-associated JMML cases (Fig. 1b and Supplementary Table 5), hereafter termed 'RAS double mutants'. Duplication of the oncogenic mutation due to acquired uniparental disomy (aUPD) was observed in three patients. Various combinations of mutations activating the canonical RAS pathway were also found, with the most frequent being *NFI* haploinsufficiency in six sporadic JMML cases with an initiating lesion in *PTPN11* (*PTPN11*-JMML) (Supplementary Fig. 6).

Mutations in RAS regulators were also found. *PDE5A*, mutated in one *PTPN11*-JMML case, protects *RAF1* from inhibitory phosphorylation by protein kinase A (PKA), enhancing its activity¹¹. Two JMML cases with initiating lesions in *NRAS* (*NRAS*-JMML) had mutations in *RRAS*, an inducer of RAS-mitogen-activated protein kinase (MAPK) activation¹² and upstream regulator of RAC in hematopoietic stem cells¹³, and another had a mutation in the RHO GTPase *RAC2*. The coexistence of RAC and RAS-MAPK mutations in some tumors and cooperation between oncogenic *NRAS* and *RAC* has previously been demonstrated¹⁴. Investigations into the functional and structural properties of the Asp63Val *RAC2* mutant, which predominantly occurred in its active, GTP-loaded form, as compared to wild-type *RAC2* and the constitutively active Gly12Val *RAC2* variant demonstrated a drastic gain-of-function effect (Fig. 4). Interestingly, an analysis of signaling downstream of RAS showed that Asp63Val *RAC2* activated the PI3K-PDK1-AKT and mTORC2 pathways but did not have a significant effect on the RAF-MEK-ERK pathway (Fig. 4 and Supplementary Fig. 7). This finding is consistent with several

lines of evidence indicating a strong impact of the PI3K-PDK-AKT pathway on JMML¹⁵, and activating the catalytic p110 δ subunit of PI3K has recently been shown to promote the effects of Shp2 on granulocyte-macrophage colony-stimulating factor (GM-CSF) hypersensitivity¹⁶. Plexins catalyze *RRAS* inactivation via their GTPase-activating protein (GAP) domain¹⁷, and *PLXNB2* was mutated in one *PTPN11*-JMML case. Finally, *ABII*, belonging to a multimolecular complex required for SOS-mediated RAC activation^{18,19}, was mutated in one case. Together, these findings suggest that the *RRAS*-RAC pathway represents a meaningful mutated subnetwork in JMML.

Although no *KRAS*-JMML case was a RAS double mutant at diagnosis, loss of heterozygosity (LOH) for oncogenic *KRAS* during disease progression in one patient suggests that this could occur (Supplementary Fig. 8).

Sequencing of isolated myeloid colonies demonstrated the coexistence of multiple RAS hits in the same myeloid progenitors in three JMML cases tested (Supplementary Table 7). With the exception of *NFI* mutations, which were subclonal in four of six cases, consistent with their late acquisition (Supplementary Fig. 6), RAS mutations could not be temporally hierarchized at diagnosis, despite extensive colony screening. This suggests a role for mutational combinations in the early stages of the disease and a strong selective benefit for double mutants. Surprisingly, however, in one patient with both an *NRAS* and *RRAS* mutation at diagnosis, the *NRAS* mutation was lost after intensive chemotherapy whereas the *RRAS* mutation was still detected. This finding strongly suggests that *RRAS* mutations may initiate JMML (Fig. 3), a hypothesis consistent with the recent report of a myeloid

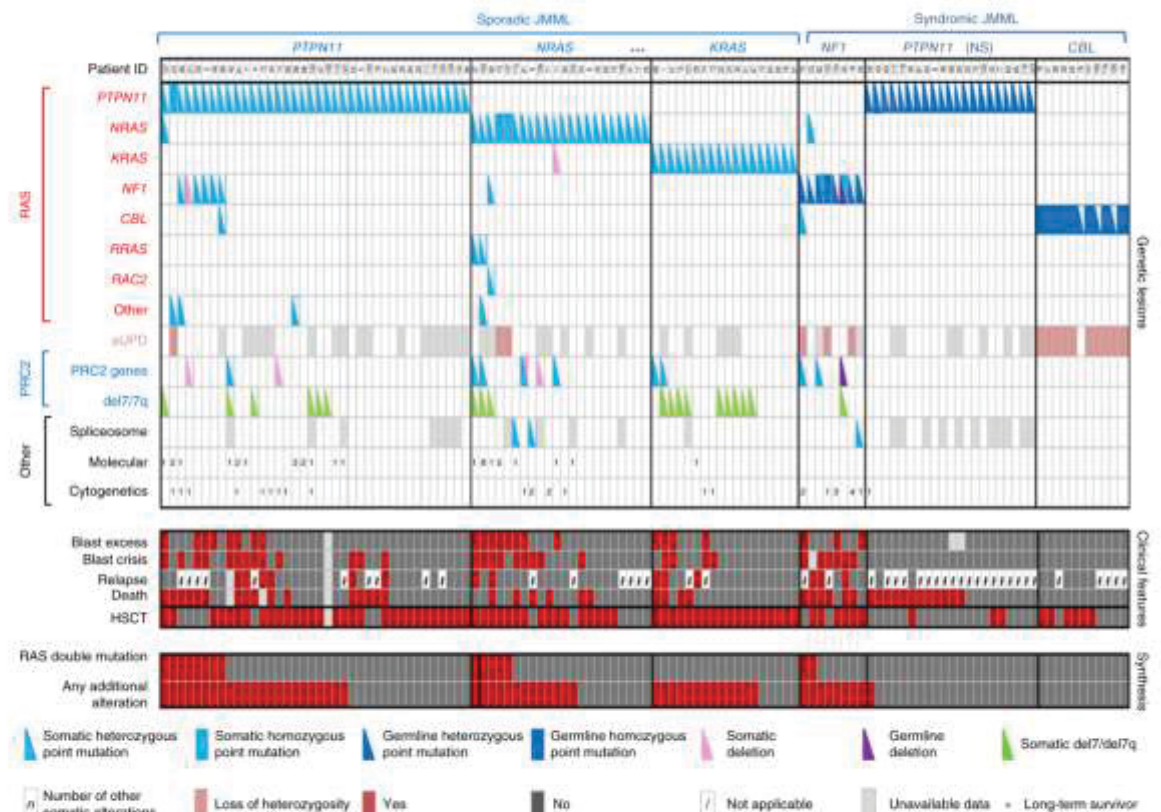


Figure 2 Alteration profiles in individual JMML cases. Germline and somatically acquired alterations with recurring hits in the RAS pathway and PRC2 network are shown for 118 patients with JMML who underwent detailed genetic analysis. Blast excess was defined as a blast count $\geq 10\%$ but $< 20\%$ of nucleated cells in the bone marrow at diagnosis. Blast crisis was defined as a blast count $\geq 20\%$ of nucleated cells in the bone marrow. NS, Noonan syndrome.

hemopathy in a patient harboring a germline *RRAS* mutation¹². Our findings challenge the dogma of the mutual exclusivity of RAS pathway mutations, supporting a dose-dependent effect for oncogenic RAS. The cooperative effects of RAS-activating events that were previously viewed as functionally equivalent have been evidenced in several mouse models^{20–22}. *Nf1* and *Kras* double-mutant mice have been shown to develop myeloid malignancies with reduced latency and increased severity in comparison to mice with only one of the two defects. More recently, the role of oncogene dosage has been demonstrated in the context of *Nras*-driven myeloid transformation^{21,22}. Our findings based on patient samples provide evidence that these models are fully relevant to human disease.

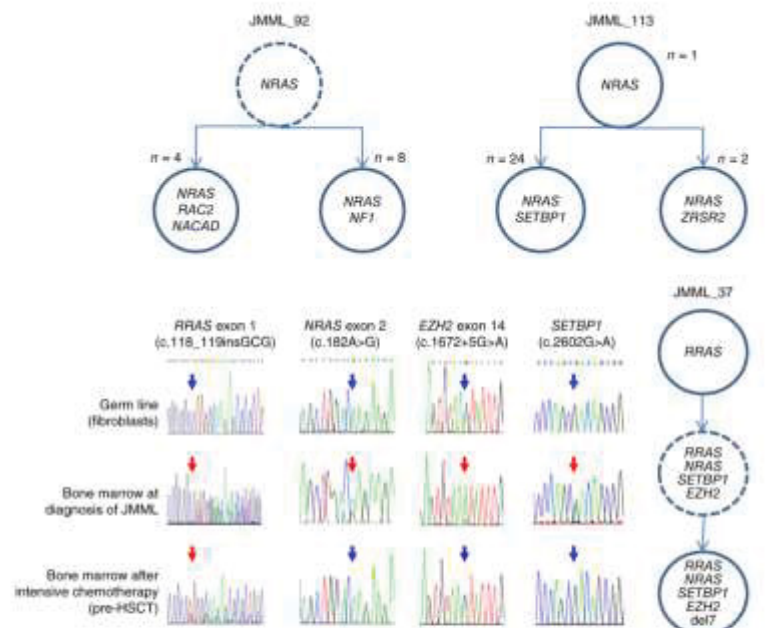
Another major group of genes targeted in JMML belonged to the PRC2 complex, involved in the transcriptional repression of target genes via methylation at lysine 27 of histone H3 (H3K27me3). In our cohort, copy number variations (CNVs) frequently resulted in haploinsufficiency for PRC2 core subunits (*SUZ12* or *EZH2*) or PRC2-associated factors necessary for optimal PRC2 activity (*AEBP2*, *CDYL* or *JARID2*) (Fig. 1a). In two patients, an *EZH2* point mutation became hemizygous by loss of the copy of chromosome 7 bearing the wild-type *EZH2* allele. *EZH2* haploinsufficiency induced by del7 or del7q reduces H3K27me3 levels at specific loci²³. *JARID2* is involved in the recruitment of the PRC2 complex to its target genes in hematopoietic stem cells^{24,25}, and *A2BP2* is an evolutionarily conserved PRC2 cofactor²⁶.

Hemizygous *JARID2* and *AEBP2* deletions have been described in the clonal evolution of myeloproliferative neoplasms²⁷. *CDYL*, for which three of our patients were haploinsufficient, encodes a transcriptional corepressor that recruits PRC2 to the chromatin substrate²⁸ but has not been demonstrated to undergo alteration in myeloid malignancies before now. Finally, inactivating mutations in the Polycomb-associated gene *ASXL1* were observed in eight of 118 (7%) JMML cases, all sporadic. *ASXL1* silencing reduces H3K27me3 levels through the inhibition of PRC2 recruitment to specific oncogenic target loci and collaborates with *NRAS* mutation encoding p.Gly12Asp *in vivo* to promote myeloid leukemogenesis^{29,30}. Thus, non-mutually exclusive genetic alterations impairing PRC2 function occurred in 26 of 78 (33%) sporadic JMML cases and five of eight (63%) *NF1*-associated JMML cases. Interestingly, hemizygous spliceosomal mutations similar to those found in three of our patients have recently been shown to induce nonsense-mediated decay of *EZH2*, reducing its expression to levels observed with hemizygous deletion³¹ and possibly further increasing the rate of PRC2 alterations in JMML.

Our findings extend a previous observation that components of epigenetic regulation are mutated at high frequencies in a subset of pediatric cancers³². Moreover, recent data show that haploinsufficiencies for multiple genes that regulate PRC2 function can cooperate in myeloid transformation^{33,33} and result in an antagonistic methylation-to-acetylation switch at H3K27, with the transcriptional activation of

LETTERS

Figure 3 Clonal evolution of JMML. Clonal architecture was investigated by sequencing isolated colonies (colony forming unit monocyte (CFU-M) or colony forming unit granulocyte-monocyte (CFU-GM)) obtained by culturing patient-derived myeloid progenitors *in vitro* and calculating the variant allele frequency (VAF) of each variant by next-generation sequencing (Supplementary Table 6). The clonal architecture of three NRAS-JMML cases, including the two cases displaying a nonlinear clonal architecture (JMML_92 and JMML_113), is represented. Each circle represents a clone. Dashed lines indicate clones whose presence was not directly assessed but was deduced from experimental data. At diagnosis, JMML_113 showed heterozygous mutations in *NRAS* and *SETBP1* and a subclonal frameshift mutation in *ZRSR2*. Sequencing of isolated myeloid colonies showed that both *SETBP1* and *ZRSR2* mutations were secondary and occurred in distinct *NRAS*-mutated clones. At diagnosis, JMML_92 had mutations in *NRAS* (VAF = 0.49), *RAC2* (VAF = 0.27), *NACAD* (VAF = 0.32) and *NF1* (VAF = 0.04). Colonies obtained at relapse confirmed that the *RAC2* and *NACAD* mutations were secondary to the *NRAS* mutation and showed that the *RAC2*-mutated clone was progressively outcompeted by another clone presenting biallelic *NF1* mutations. In JMML_37, the *NRAS* mutation was lost in a follow-up sample collected after intensive chemotherapy for blast crisis, whereas a subclonal *RRAS* mutation was still detected. This suggests that the *RRAS* and not the *NRAS* mutation initiated the JMML. The allelic imbalance of the *EZH2* mutation indicates that it preceded the loss of chromosome 7.



PRC2 target genes³⁴. Concordantly, using antibodies to H3K27me3 and H3K27ac, we found that primary JMML samples with decreased PRC2 activity due to *ASXL1* mutation or monosomy 7 showed a global

decrease in H3K27 trimethylation with a concomitant increase in acetylation (Fig. 5). The identification of recurrently affected biological pathways is a strong and powerful indication that mutations

Figure 4 The p.Asp63Val substitution in *RAC2* results in a gain-of-function effect associated with an increase in effector binding and a massive decrease in GAP function, leading to AKT activation via two distinct pathways. (a,b) Analysis of active, GTP-bound *RAC2* protein using a pull-down assay with glutathione S-transferase (GST) fused to the PAK1 GTPase-binding domain (GBD) (a) and densitometric quantification of three separate blots (b) showed, in contrast to wild-type (WT) *RAC2*, strong accumulation of active Asp63Val *RAC2* comparable to that seen with constitutively active Gly12Val *RAC2*. PD, pull-down; IB, immunoblot. (c,d) Immunoblot analysis of the phosphorylation levels of MEK1 and MEK2 (pMEK1/2), ERK1 and ERK2 (pERK1/2) and AKT (pAKT) (c) and densitometric quantification of three separate blots (d) showed clear activation of AKT but not MEK1/2 or ERK1/2, correlating with levels of the GTP-bound form of Asp63Val *RAC2* in regulating signaling cascades (PI3K-PDK1 and mTORC2) responsible for AKT activation (Supplementary Fig. 6). AKT, MEK1/2, ERK1/2 and α -actin were used as loading controls. (e-g) Biochemical analysis of Asp63Val *RAC2* *in vitro*. Wild-type *RAC2* and the Asp63Val mutant were analyzed for catalyzed nucleotide exchange by the RAC guanine nucleotide exchange factor (GEF) TIAM1 (e), interaction with the effector PAK1 (f) and stimulated GTP hydrolysis by the RACGAP p50^{GAP} (g) using purified proteins and fluorescently labeled nucleotides. K_{obs} is the observed rate constant, and K_D is the dissociation constant. (h) In the *RAC2* structure, Asp63 is located at the edge of the TIAM1- and PAK1-binding sites and rather central to the GAP-binding site, clarifying the reason for the robust decrease in GAP-accelerated GTP hydrolysis observed with alteration of this site.

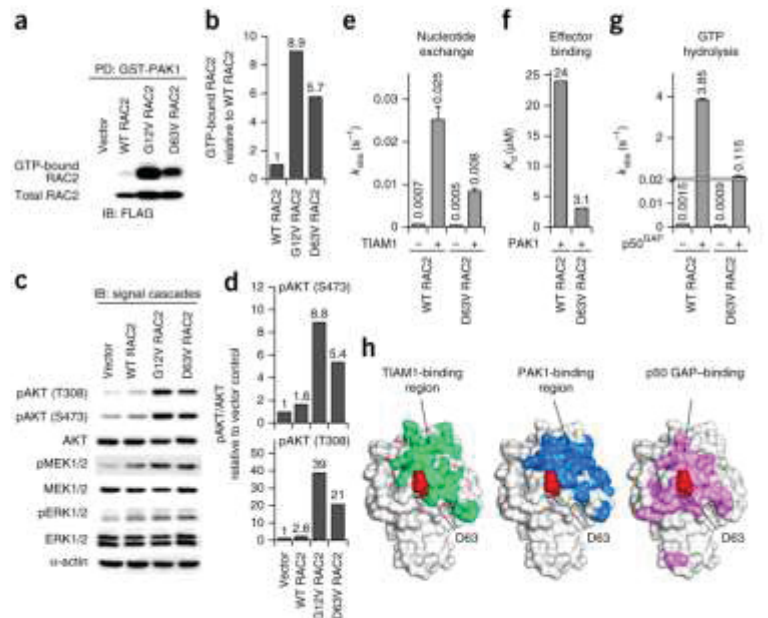
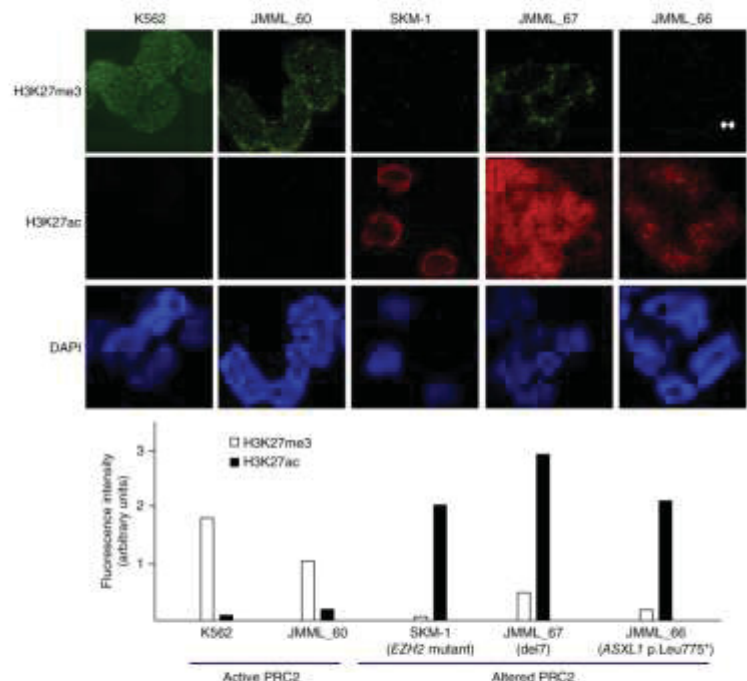


Figure 5 Reduced PRC2 dosage and histone H3 modifications. H3K27me3 and H3K27ac levels were detected by immunofluorescence in K562 cells (positive control for PRC2 activity), bone marrow mononuclear cells from patient JMML_60 without known PRC2 alterations, SKM-1 cells with a homozygous *EZH2* mutation, bone marrow mononuclear cells from patient JMML_67 with a PRC2 alteration (monosomy 7) and bone marrow mononuclear cells from patient JMML_66 with a PRC2 alteration (*ASXL1* mutation encoding p.Leu775*). Scale bar, 2 μ m. Immunofluorescence for H3K27me3 (white bars) and H3K27ac (black bars) was quantified in the cell lines and cells derived from patients with JMML with respect to PRC2 complex status. Mutations reducing PRC2 dosage resulted in reduced H3K27me3 levels and a concomitant increase in H3K27ac levels.



targeting these pathways drive the oncogenic process in JMML³⁵. The clonal architecture studies we performed by sequencing isolated colonies obtained by the *in vitro* culture of progenitors derived from patients with JMML consistently showed that RAS activation was the initiating oncogenic event, with PRC2 impairment being a secondary event. Our results suggest that neither PRC2 impairment nor any other genetic lesion can drive JMML in the absence of preexisting RAS pathway deregulation. Most interestingly, a cooperative effect from RAS activation and PRC2 impairment has recently been reported in NF1-associated cancers^{36–38}, where PRC2 component haploinsufficiency exerts a disproportionately suppressive effect on methylation at H3K27, augmenting acetylation and further elevating the transcription of RAS-regulated genes³⁸. Our data suggest that this molecular mechanism is also relevant in JMML.

Other additional mutations had unknown functions and/or affected single individuals. However, considering both our selective mutation filters, which included germline DNA screening, and the

extremely low frequency of clonal mosaicism in peripheral blood from normal children^{39–43}, most somatic variants detected in our patients are also likely to drive clonal selection.

Most JMML cases are severe, with the only curative treatment being hematopoietic stem cell transplantation (HSCT)^{2,3,43}. However, clinical evolution is heterogeneous, with transformation to acute myeloid leukemia (AML) in one of three cases and frequent relapses after HSCT, whereas some rare 'long-term survivors' experience spontaneous remission and survive without treatment^{3,44,45}. The management of patients with JMML urgently requires parameters to help in patient risk stratification. Unfortunately, the initiating RAS pathway lesion incompletely predicts outcome (Supplementary Fig. 9). We thus asked whether the newly identified alterations could improve the prediction of JMML outcome. Secondary alterations accumulated in a limited number of patients (Fig. 2 and Supplementary Table 5) and were associated with a poorer outcome, with a 3-year overall survival of 61% as compared with 85% in other patients ($P = 0.028$) (Fig. 6). Yet, it was possible to see that RAS double-mutant JMML had the most severe presentation, with an increase in the number of blasts in the bone marrow ($\geq 10\%$) in nine of 13 (69%) double-mutant cases versus

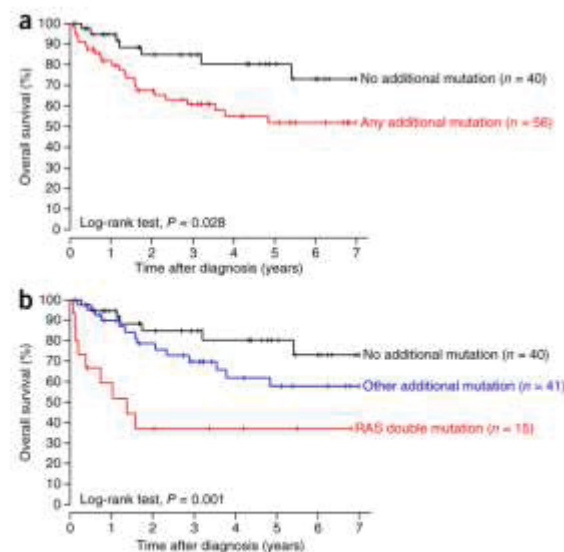


Figure 6 Overall survival of patients with sporadic JMML according to the presence and type of additional somatic mutations. Kaplan-Meier representations of overall survival are shown for 96 patients with JMML having clinical follow-up information available. Patients with Noonan syndrome were excluded from the analysis because non-hematological comorbidities may have jeopardized their survival⁷. As in Supplementary Table 5, additional somatic alterations were defined as somatically acquired mutations other than the somatic RAS pathway mutations assumed to be either the initiating event or part of the classical mechanism of leukemogenesis, such as hits targeting the wild-type *NF1* or *CBL* allele in germline-mutated patients^{8,9,48}. (a, b) The presence of any additional somatic alterations (a) together with RAS double mutations (b) allowed us to distinguish patients with a significantly poorer outcome.

LETTERS

11 of 64 (17%) other cases ($P < 0.001$) and rapid evolution to AML with myelodysplasia-related changes (AML-MRC), in line with previous single-case reports^{12,46,47} (Fig. 6). The outcome of RAS double-mutant cases was thus significantly poorer than that of other JMML cases, with a 3-year overall survival rate of 37% versus rates of 85% and 70% in patients with no or one other secondary alteration, respectively ($P = 0.001$) (Fig. 6). In NRAS-JMML cases, which display the greatest clinical diversity⁴⁴, three long-term survivors were observed; none of these patients had secondary abnormalities. In contrast, ten of 11 (91%) patients with aggressive disease, as assessed by blast excess at diagnosis or blast crisis before HSCT, had additional abnormalities, including double mutation of RAS pathway components in five cases. These findings suggest that oncogenic NRAS proteins require additional transforming hits to give rise to aggressive JMML and provide a useful prognostic tool to differentiate patients with NRAS-associated JMML who require HSCT from those who could benefit from a 'wait-and-see' approach.

In conclusion, our study shows for the first time, to our knowledge, that concomitant mutations in JMML target a small number of interacting networks, with a striking enrichment in components of the RAS and PRC2 networks. These findings extend and reinforce the notion that JMML is a RASopathy while showing that RAS activation is the major but not the only player in JMML. Such new information on the pathogenesis of JMML should provide functional guidance, prognostic markers and patient selection criteria for new therapeutic options in this very severe childhood leukemia.

URLs. UCSC Genome Browser, <http://www.genome.ucsc.edu/>; dbSNP137, <http://www.ncbi.nlm.nih.gov/projects/SNP/>; HapMap, <http://hapmap.ncbi.nlm.nih.gov/>; 1000 Genomes Project, <http://www.1000genomes.org/>; Catalogue of Somatic Mutations in Cancer (COSMIC), <http://cancer.sanger.ac.uk/cancergenome/projects/cosmic/>; SIFT, <http://sift.jcvi.org/>; PolyPhen-2, <http://genetics.bwh.harvard.edu/pph2/>; MutationTaster, <http://www.mutationtaster.org/>; Leiden Open Variation Database (LOVD), <http://www.lovd.nl/3.0/>; R-survival library, <http://CRAN.R-project.org/package=survival>; ArrayExpress database, <http://www.ebi.ac.uk/arrayexpress/>; European Genome-phenome Archive (EGA) database, <https://www.ebi.ac.uk/ega/>.

METHODS

Methods and any associated references are available in the online version of the paper.

Accession codes. SNP array data have been deposited in the ArrayExpress database under accessions E-MTAB-3399 and E-MTAB-3729. Targeted sequencing data have been deposited in the European Genome-phenome Archive (EGA), which is hosted by the European Bioinformatics Institute (EBI), under accession EGAS00001001324.

Note: Any Supplementary Information and Source Data files are available in the online version of the paper.

ACKNOWLEDGMENTS

We thank N. Roodur, M. Keita (Unité de Génétique Moléculaire, Hôpital Robert Debré) and L. Coste-Serguet (INSERM UMR 1131) for expert technical assistance. We thank E. Martin, J.-P. Sarava and M. Letexier (Integrigen) for advice and assistance in whole-exome sequencing analysis. SNP array analyses were performed by the Plateforme de Génomique Constitutionnelle-Nord (PIGC-Nord) (J. Soulier, S. Quentin and S. Drumat). We thank the technical team, and more particularly P. Aubin, from the Service de Biologie Cellulaire, Hôpital Saint Louis, for excellent technical help in the management of myeloid progenitor assays. We also thank S. Rasika for careful editing of the manuscript.

This work was supported by the Ligue contre le Cancer (LCC)-Île-de-France, by the Société Française de Lutte contre les Cancers et Leucémies de l'Enfant (SFCE), the Association pour la Recherche et pour les Études dans les Maladies Infantiles Graves (AREMIG, Nancy) and the German Research Foundation (Deutsche Forschungsgemeinschaft, DFG) through the Collaborative Research Center 974 (SFB 974) Communication and Systems Relevance during Liver Injury and Regeneration and the International Graduate School of Protein Science and Technology (iGRASP).

AUTHOR CONTRIBUTIONS

A. Caye collected subject samples, participated in the study design, performed laboratory assays, analyzed data and wrote the manuscript. M.S. and J.L. performed analyses and collected clinical data. F.G. performed epigenetic studies, and B.C. and E.V. performed colony assays. S.G. performed biostatistical analyses. O.F. and E.L. performed the cytological review. K.N., S.N.-R., R.D., D.H. and M.R.A. performed the functional and biochemical RAC2 studies. J.V. collected clinical data. S.P. performed laboratory assays. D.V. performed NF1 diagnosis. J.-H.D., A.B., C. Paillard, C. Picard, C.G., A.P., Y.R., F.M., B.N., Y.B., M.P., D.A., N.S. and A. Contet contributed subject samples and clinical data. M.S., A.B., C.C., B.C. and M.R.A. reviewed the manuscript. H.C. collected subject samples, designed and coordinated the study, analyzed data and wrote the manuscript.

COMPETING FINANCIAL INTERESTS

The authors declare no competing financial interests.

Reprints and permissions information is available online at <http://www.nature.com/reprints/index.html>.

- Chang, T.Y., Dvorak, C.C. & Loh, M.L. Bedside to bench in juvenile myelomonocytic leukemia: insights into leukemogenesis from a rare pediatric leukemia. *Blood* **124**, 2487–2497 (2014).
- Niemeyer, C.M. et al. Chronic myelomonocytic leukemia in childhood: a retrospective analysis of 110 cases. European Working Group on Myelodysplastic Syndromes in Childhood (EWOG-MDS). *Blood* **89**, 3534–3543 (1997).
- Locatelli, F. & Niemeyer, C.M. How I treat juvenile myelomonocytic leukemia. *Blood* **125**, 1083–1090 (2015).
- Niemeyer, C.M. RAS diseases in children. *Haematologica* **99**, 1653–1662 (2014).
- Shlien, A. et al. Combined hereditary and somatic mutations of replication error repair genes result in rapid onset of ultra-hypermutated cancers. *Nat. Genet.* **47**, 257–262 (2015).
- Sakaguchi, H. et al. Exome sequencing identifies secondary mutations of *SETBP1* and *JAK3* in juvenile myelomonocytic leukemia. *Nat. Genet.* **45**, 937–941 (2013).
- Strullu, M. et al. Juvenile myelomonocytic leukaemia and Noonan syndrome. *J. Med. Genet.* **51**, 689–697 (2014).
- Niemeyer, C.M. et al. Germline *CBL* mutations cause developmental abnormalities and predispose to juvenile myelomonocytic leukemia. *Nat. Genet.* **42**, 794–800 (2010).
- Perez, B. et al. Germline mutations of the *CBL* gene define a new genetic syndrome with predisposition to juvenile myelomonocytic leukaemia. *J. Med. Genet.* **47**, 686–691 (2010).
- Makishima, H. et al. Somatic *SETBP1* mutations in myeloid malignancies. *Nat. Genet.* **45**, 942–946 (2013).
- Brown, K.M. et al. Phosphodiesterase-8A binds to and regulates Raf-1 kinase. *Proc. Natl. Acad. Sci. USA* **110**, E1533–E1542 (2013).
- Flex, E. et al. Activating mutations in *RRAS* underlie a phenotype within the RASopathy spectrum and contribute to leukemogenesis. *Hum. Mol. Genet.* **23**, 4315–4327 (2014).
- Shang, X. et al. R-Ras and Rac GTPase cross-talk regulates hematopoietic progenitor cell migration, homing, and mobilization. *J. Biol. Chem.* **286**, 24068–24078 (2011).
- Kawazu, M. et al. Transforming mutations of RAC guanosine triphosphatases in human cancers. *Proc. Natl. Acad. Sci. USA* **110**, 3029–3034 (2013).
- Emanuel, P.D. Highway gossip between Ras and PI3K pathways. *Blood* **123**, 2751–2753 (2014).
- Goodwin, C.B. et al. PI3K p110 δ uniquely promotes gain-of-function Shp2-induced GM-CSF hypersensitivity in a model of JMML. *Blood* **123**, 2838–2842 (2014).
- Worfeld, T. et al. Genetic dissection of plexin signaling in vivo. *Proc. Natl. Acad. Sci. USA* **111**, 2194–2199 (2014).
- Innocenti, M. et al. Phosphoinositide 3-kinase activates Rac by entering in a complex with Eps8, Abi1, and Sos-1. *J. Cell Biol.* **160**, 17–23 (2003).
- Offenhäuser, N. et al. The eps8 family of proteins links growth factor stimulation to actin reorganization generating functional redundancy in the Ras/Rac pathway. *Mol. Biol. Cell* **15**, 91–98 (2004).
- Cutts, B.A. et al. *Nf1* deficiency cooperates with oncogenic K-RAS to induce acute myeloid leukemia in mice. *Blood* **114**, 3629–3632 (2009).



21. Xu, J. *et al.* Dominant role of oncogene dosage and absence of tumor suppressor activity in *Nras*-driven hematopoietic transformation. *Cancer Discov.* **3**, 993–1001 (2013).
22. Wang, J. *et al.* Endogenous oncogenic *Nras* mutation initiates hematopoietic malignancies in a dose- and cell type-dependent manner. *Blood* **118**, 368–379 (2011).
23. Khan, S.N. *et al.* Multiple mechanisms deregulate EZH2 and histone H3 lysine 27 epigenetic changes in myeloid malignancies. *Leukemia* **27**, 1301–1309 (2013).
24. Son, J., Shen, S.S., Margueron, R. & Reinberg, D. Nucleosome-binding activities within JARID2 and EZH1 regulate the function of PRC2 on chromatin. *Genes Dev.* **27**, 2663–2677 (2013).
25. Kinkel, S.A. *et al.* *Jarid2* regulates hematopoietic stem cell function by acting with Polycomb repressive complex 2. *Blood* **125**, 1890–1900 (2015).
26. Ciferri, C. *et al.* Molecular architecture of human Polycomb repressive complex 2. *eLife* **1**, e03005 (2012).
27. Pada, A. *et al.* Frequent deletions of *JARID2* in leukemic transformation of chronic myeloid malignancies. *Am. J. Hematol.* **87**, 245–250 (2012).
28. Zhang, Y. *et al.* Corepressor protein CDYL functions as a molecular bridge between Polycomb repressor complex 2 and repressive chromatin mark trimethylated histone lysine 27. *J. Biol. Chem.* **286**, 42414–42425 (2011).
29. Abdel-Wahab, O. *et al.* *ASXL1* mutations promote myeloid transformation through loss of PRC2-mediated gene repression. *Cancer Cell* **22**, 180–193 (2012).
30. Abdel-Wahab, O. & Levine, R.L. Mutations in epigenetic modifiers in the pathogenesis and therapy of acute myeloid leukemia. *Blood* **121**, 3563–3572 (2013).
31. Kim, E. *et al.* *SRSF2* mutations contribute to myelodysplasia by mutant-specific effects on exon recognition. *Cancer Cell* **27**, 617–630 (2015).
32. Huether, R. *et al.* The landscape of somatic mutations in epigenetic regulators across 1,000 paediatric cancer genomes. *Nat. Commun.* **5**, 3630 (2014).
33. Yang, F. PRC2 dysfunction through multiple mechanisms in myeloid malignancies. *Epigenomics* **5**, 481 (2013).
34. Pasini, D. *et al.* Characterization of an antagonistic switch between histone H3 lysine 27 methylation and acetylation in the transcriptional regulation of Polycomb group target genes. *Nucleic Acids Res.* **38**, 4958–4969 (2010).
35. Leiserson, M.D. *et al.* Pan-cancer network analysis identifies combinations of rare somatic mutations across pathways and protein complexes. *Nat. Genet.* **47**, 106–114 (2015).
36. Lee, W. *et al.* PRC2 is recurrently inactivated through EED or SUZ12 loss in malignant peripheral nerve sheath tumors. *Nat. Genet.* **46**, 1227–1232 (2014).
37. Zhang, M. *et al.* Somatic mutations of *SUZ12* in malignant peripheral nerve sheath tumors. *Nat. Genet.* **46**, 1170–1172 (2014).
38. De Raedt, T. *et al.* PRC2 loss amplifies Ras-driven transcription and confers sensitivity to BRD4-based therapies. *Nature* **514**, 247–251 (2014).
39. Jaiswal, S. *et al.* Age-related clonal hematopoiesis associated with adverse outcomes. *N. Engl. J. Med.* **371**, 2488–2498 (2014).
40. Genovese, G. *et al.* Clonal hematopoiesis and blood-cancer risk inferred from blood DNA sequence. *N. Engl. J. Med.* **371**, 2477–2487 (2014).
41. Jacobs, K.B. *et al.* Detectable clonal mosaicism and its relationship to aging and cancer. *Nat. Genet.* **44**, 651–658 (2012).
42. Laurie, C.C. *et al.* Detectable clonal mosaicism from birth to old age and its relationship to cancer. *Nat. Genet.* **44**, 642–650 (2012).
43. Locatelli, F. *et al.* Hematopoietic stem cell transplantation (HSCT) in children with juvenile myelomonocytic leukemia (JMML): results of the EWOG-MDS/EBMT trial. *Blood* **105**, 410–419 (2005).
44. Takagi, M. *et al.* Autoimmunity and persistent RAS-mutated clones long after the spontaneous regression of JMML. *Leukemia* **27**, 1926–1928 (2013).
45. Matsuda, K. *et al.* Spontaneous improvement of hematologic abnormalities in patients having juvenile myelomonocytic leukemia with specific RAS mutations. *Blood* **109**, 5477–5480 (2007).
46. Matsuda, K. *et al.* Acquisition of loss of the wild-type *NRAS* locus with aggressive disease progression in a patient with juvenile myelomonocytic leukemia and a heterozygous *NRAS* mutation. *Haematologica* **92**, 1576–1578 (2007).
47. Kato, M. *et al.* Aggressive transformation of juvenile myelomonocytic leukemia associated with duplication of oncogenic *NRAS* due to acquired uniparental disomy. *J. Pediatr.* **162**, 1285–1288 (2013).
48. Kalra, R., Paderanga, D.C., Olson, K. & Shannon, K.M. Genetic analysis is consistent with the hypothesis that NF1 limits myeloid cell growth through p21ras. *Blood* **84**, 3435–3439 (1994).

¹INSERM UMR 1131, Institut Universitaire d'Hématologie, Paris, France. ²Université Paris Diderot, Paris Sorbonne Cité, Paris, France. ³Assistance Publique des Hôpitaux de Paris (AP-HP), Hôpital Robert Debré, Département de Génétique, Paris, France. ⁴Assistance Publique des Hôpitaux de Paris (AP-HP), Hôpital Saint Louis, Service de Biologie Cellulaire, Paris, France. ⁵Assistance Publique des Hôpitaux de Paris (AP-HP), Plateforme de Génétique Constitutionnelle-Nord (PFGC-Nord), Paris, France. ⁶INSERM UMR 1137, Infection Antimicrobienne Modelling and Evolution (IAME) Laboratory, Paris, France. ⁷Assistance Publique des Hôpitaux de Paris (AP-HP), Hôpital Robert Debré, Service d'Hématologie Biologique, Paris, France. ⁸Institute of Biochemistry and Molecular Biology II, Medical Faculty of the Heinrich Heine University, Düsseldorf, Germany. ⁹Equipe d'Accueil 7331, Université Paris Descartes, Sorbonne Paris Cité, Faculté de Pharmacie de Paris, Paris, France. ¹⁰Assistance Publique des Hôpitaux de Paris (AP-HP), Hôpital Cochin, Service de Biochimie Génétique, Paris, France. ¹¹Assistance Publique des Hôpitaux de Marseille (AP-HM), Hôpital de la Timone, Service d'Hématologie Pédiatrique, Marseille, France. ¹²Assistance Publique des Hôpitaux de Paris (AP-HP), Hôpital Necker-Enfants Malades Paris, Centre d'Etudes des Déficiences Immunitaires, Immuno-Hematology Unit, Paris, France. ¹³Université Paris Descartes, Paris Sorbonne Cité, Paris, France. ¹⁴INSERM UMR 1163, Institut Imagine, Laboratory of Human Genetics of Infectious Diseases, Paris, France. ¹⁵Assistance Publique des Hôpitaux de Paris (AP-HP), Hôpital Armand Trousseau, Service d'Hématologie Oncologie Pédiatrique, Paris, France. ¹⁶Hôpital d'Enfants de Brabois, Service d'Onco-Hématologie Pédiatrique, Vandœuvre lès Nancy, France. ¹⁷Hôpital l'Archet, Service d'Onco-Hématologie Pédiatrique, Nice, France. ¹⁸Centre Hospitalier Universitaire (CHU) de Montpellier, Service d'Onco-Hématologie Pédiatrique, Montpellier, France. ¹⁹CHU de Nantes, Service d'Onco-Hématologie Pédiatrique, Nantes, France. ²⁰CHU de Grenoble, Service d'Onco-Hématologie Pédiatrique, Grenoble, France. ²¹Hôpital de Hautepierre, Service de Pédiatrie, Strasbourg, France. ²²CHU de Lille, Unité d'Hématologie Pédiatrique, Lille, France. ²³Centre Hospitalier Félix Guyon, Saint-Denis, La Réunion, France. ²⁴Institut d'Hémo-Oncologie Pédiatrique (IHOP), Département d'Immunologie et Hématologie Pédiatrique, Lyon, France. ²⁵Clinic of Gastroenterology, Hepatology and Infectious Diseases, Medical Faculty of the Heinrich Heine University, Düsseldorf, Germany. ²⁶Assistance Publique des Hôpitaux de Paris (AP-HP), Hôpital Robert Debré, Service d'Hématologie Pédiatrique, Paris, France. Correspondence should be addressed to H.C. (helene.cavs@rdp.aphp.fr).

ONLINE METHODS

Patients. The study included 118 patients with JMML consecutively referred to our laboratory between 1995 and 2014, for whom a RAS-activating mutation was identified as part of the routine diagnostic workup (Supplementary Note).

All patients fulfilled the consensus JMML criteria reported recently by Chan *et al.*⁴⁹. Centralized cytomorphological review was performed on bone marrow and blood samples. Measurement of fetal hemoglobin (HbF) dosage and karyotyping were systematically performed using standard procedures.

Diagnosis with JMML was based on clinical and hematological findings, cytomorphological examination of blood and bone marrow smears, *in vitro* growth of myeloid progenitors and mutation screening of DNA obtained from the leukemia sample.

A somatically acquired RAS-activating mutation was identified at diagnosis in 78 of 118 (66%) patients in the following genes: *PTPN11* ($n = 38$), *KRAS* ($n = 18$) and *NRAS* ($n = 22$). JMML cases were classified according to these initial lesions as *PTPN11*-JMML, *KRAS*-JMML and *NRAS*-JMML, respectively. In 40 of 118 (34%) cases, JMML was syndromic with a germline *PTPN11* mutation consistent with Noonan syndrome features ($n = 22$), a germline *CBL* mutation consistent with CBL syndrome ($n = 11$) or molecularly confirmed *NFI* ($n = 8$) (Supplementary Fig. 3 and Supplementary Table 5). The sex ratio (males/females) was 2.1. The median age at diagnosis was 18 months. Seventy-eight of 118 (66%) patients received bone marrow transplantation. Blast excess was defined as a blast count $\geq 10\%$ but $< 20\%$ in the bone marrow at diagnosis. Blast crisis was defined as a blast count $\geq 20\%$ in the bone marrow. Two patients with sporadic JMML were lost to follow-up.

Samples. Peripheral blood and/or bone marrow aspirates were collected on EDTA at diagnosis. Non-hematopoietic tissues (fibroblasts, nails or hair follicles) were also collected. Genomic DNA was extracted using a Qiagen Mini or Midi kit.

To use minimal amounts of native DNA, all diagnostic DNA samples underwent whole-genome amplification using the RepliG Midi kit (Qiagen) according to the manufacturer's instructions.

Diagnostic workup. Mutational screening using bidirectional Sanger sequencing of exons and their flanking intron-exon boundaries was performed on genomic DNA as part of the classic diagnostic workup for JMML and included analysis of *NRAS* exons 2 and 3 (NM_002524.4), *KRAS* exons 2 and 3 (NM_033360.3), *PTPN11* exons 3 and 13 (NM_002834.3) and *CBL* exons 8 and 9 (NM_005188.3). Genes recently shown to be involved in JMML (*ASXL1* exon 14 (NM_015338.5) and the *SETBP1* sequence in exon 6 encoding the SKI-homologous region (NM_015559.2)) were also systematically screened by Sanger sequencing as previously described⁵⁰. The germline origin of mutations was tested using constitutional DNA. Microsatellite analysis of the 17p region encompassing *NFI* was performed as previously described⁵⁰. Primer sequences are given in Supplementary Table 8.

Genome-wide DNA array analysis. Genomic DNA from 78 leukemia samples was analyzed by SNP array technologies using the Genome-Wide GeneChip Human SNP Array 6.0 (Affymetrix) ($n = 63$) and/or by high-density array comparative genomic hybridization (CGH) technologies using the 4×180M Microarray SurePrint G3 Catalog (Agilent Technologies) ($n = 16$), according to the manufacturers' recommendations. Analyses were performed using CytoGenomics (Agilent Technologies) for array CGH data and Genomic Suite 6.5 software (Partek) and the hidden Markov model and segmentation algorithms for the analysis of both CNVs and LOH. The final abnormalities retained were validated by visual analysis, considering the sizes and \log_2 (ratios) of the abnormalities with respect to the individual background noise of each array at each particular chromosomal location. Polymorphic CNVs were excluded using the Database of Genomic Variants track in the UCSC Genome Browser in Cartagenia Bench Lab CNV software. Human genome assembly GRCh37/hg19 was used as a reference. Final validated data are provided in Supplementary Table 3.

Whole-exome sequencing. Targeted enrichment and massively parallel sequencing were performed on paired genomic DNA samples from leukocytes and fibroblasts. Exome capture was carried out using SureSelect Human All

Exon v4+UTRs (Agilent Technologies), and sequencing was performed with a HiSeq 2000 instrument (Illumina). Image analysis and base calling were performed using the Real-Time Analysis (RTA) pipeline, v. 1.14 (Illumina). Alignment of paired-end reads to the reference human genome (UCSC GRCh37/hg19), variant calling and generation of quality scores for variants were carried out using the CASAVA v.1.8 pipeline (Illumina).

Variant annotation, SNP filtering and patient-matched germline variant filtering were achieved using an in-house pipeline by IntegraGen. Gene and transcript names, strand and position (intron, 5' UTR, 3' UTR, etc.) were reported for each variant. Nucleotide, codon and amino acid changes as well as functional class (synonymous, missense, nonsense, splice site, etc.) were reported for coding variants. Annotation content was compiled from several sources: 1000 Genomes Project, dbSNP rsID and frequencies from the IntegraGen Exome Database, which comprises 200 reference exomes. Finally, germline and tumoral genotypes were compared to determine the somatic nature of each variant. Only positions that were present in both files and met the minimum coverage requirement ($\geq 6\times$) were compared. The significance of the allele frequency difference (as a P value) was calculated by Fisher's exact test for each variant, taking into account the counts of the mutated allele in both samples. A somatic score was calculated for each variant (from 1 to 30, with 30 indicating the highest confidence). The somatic variant caller handled indels similarly, determining the number of alignments covering a given position that included a particular indel (variant count) versus the overall coverage at that position. Yield per exome ranged between 3.64 and 7.17 Mb (mean of 4.78 Mb). Mean coverage per sample is given in Supplementary Figure 10.

Known polymorphisms reported at a frequency $> 0.1\%$ in at least one of the above-mentioned databases, low-coverage variants (< 10 reads in germline and/or tumoral samples) and low-quality variants (Q variant score from IntegraGen ≤ 30) were systematically excluded. Only variants with a probable impact at the protein level (nonsynonymous exonic variants and abnormalities located at intron-exon junctions) were considered for further analysis. All putative somatic events (absent in the germline sample but acquired in tumoral DNA or heterozygous in the germline sample but homozygous in the tumoral sample) were verified by conventional Sanger sequencing and searched for in constitutional DNA, when available.

The previous involvement of confirmed somatic variants in cancer was verified by consulting the Catalogue of Somatic Mutations in Cancer (COSMIC). Prediction of the effects of amino acid substitutions on the function and structure of proteins was achieved using dedicated prediction software: Scale-Invariant Feature Transform (SIFT), MutationTaster and PolyPhen-2. Final validated data are provided in Supplementary Table 2.

High-throughput targeted sequencing. High-throughput targeted sequencing by multiplex PCR was performed on whole genome-amplified tumoral DNA diluted 1:5. The coding regions of 38 genes were targeted. The complete list of targeted genes and their corresponding sequencing performance are available in Supplementary Figure 11 and Supplementary Table 4. Primer pairs were designed with the IntegraGen internal pipeline (Supplementary Table 8). DNA samples were amplified on an Access Array system (Fluidigm) and subjected to six additional PCR cycles to add specific barcodes and P5 and P7 adaptors. An equimolar pool of all PCR products was sequenced on the MiSeq instrument (Illumina), with MiSeq Reagent Kit V2 cycles and paired-end 2×150 bases. Image analysis and base calling, alignment of reads to the reference human genome, variant calling, variant annotation and subsequent mutational analysis were performed as for whole-exome sequencing. All identified variants were verified in native tumoral DNA and searched for by Sanger sequencing in constitutional DNA, when available.

Sanger sequencing. PCR was performed using the GoTaq DNA Polymerase kit (Promega) or the FastStart Taq DNA Polymerase kit (Roche) according to the manufacturer's instructions. Primer sequences for Sanger sequencing performed in the whole JMML cohort are provided in Supplementary Table 8. Primer sequences used for control variants found by whole-exome sequencing and high-throughput targeted sequencing are available on request. PCR products were purified using the Illustra ExoStar 1-Step kit (GE Healthcare, Life Sciences), and direct sequencing was performed using the BigDye Terminator Ready Reaction Cycle Sequencing kit (Applied Biosystems). Reaction products

were run on an automated capillary sequencer (ABI 3130 Genetic Analyzer, Applied Biosystems). Sequences were aligned using Seqscape analysis software (Applied Biosystems) or visualized on Chromas software (Technelysium) and were compared with the reference sequences for genomic DNA.

Myeloid progenitor cell growth and genetic testing. *In vitro* growth assays of myeloid progenitors were performed by plating bone marrow and/or peripheral blood mononucleated cells in semisolid methylcellulose with or without leukocyte-conditioned medium (cytokine medium, LCM, Stemcell Technologies), as previously described⁵⁰. Colonies (aggregates containing >50 cells) were scored on days 11 and 14 after plating.

Targeted sequencing of isolated colonies. Colonies obtained from the *in vitro* growth of myeloid progenitors were picked and resuspended in 100 μ l of sterile water. Isolated colonies were lysed with proteinase K (10 μ g) in 50 μ l of lysis buffer (50 mM KCl, 10 mM Tris-HCl, pH 8, 2.5 mM MgCl₂, 0.45% NP-40 and 0.45% Tween-20). Sanger direct sequencing was performed as described above. Genetic screening was restricted to colonies obtained from JMML cases displaying at least two somatically acquired genetic lesions ($n = 6$, with 8–93 colonies successfully screened per patient).

RAC2 constructs. Different variants of the pGEX vector (pGEX2T and pGEX4T-1) encoding N-terminal GST were used for the overexpression of wild-type RAC2, Asp63Val RAC2, the GBD of PAK1 (amino acids 57–141), the catalytic domains of TIAM1 (DH-PH; amino acids 1033–1404) and p50^{GAP} (a GAP; amino acids 198–439). To generate RAC2 constructs with mutation, wild-type RAC2 in pGEX4T-1 and pcDNA3.1 vectors was used as the template and the mutation encoding p.Asp63Val was generated by PCR-based site-directed mutagenesis as described⁵¹.

Proteins. All proteins were purified as GST fusion proteins from *Escherichia coli* as previously described^{52–56}. The GST tag was cleaved off with purified tobacco etch virus (Tev) protease and removed by reverse glutathione affinity purification in the case of the RAC2 proteins. Nucleotide-free RAC2 proteins were prepared using alkaline phosphatase (Roche) and phosphodiesterase (Sigma-Aldrich) at 4 °C, as described⁵⁴. Fluorescent methylantraniloyl (mant) and tetramethylrhodamine (tamra) were used to generate fluorescent mantGDP-, mantGppNHP- and tamraGTP-bound RAC2 proteins.

Fluorescence polarization. Experiments were performed in a Fluoromax 4 fluorometer in polarization mode as previously described⁵⁷. Briefly, an increasing amount of GST-PAK GBD was titrated into mantGppNHP-bound wild-type and Asp63Val RAC2 (1 μ M) in a buffer containing 30 mM Tris-HCl, pH 7.5, 150 mM NaCl, 5 mM MgCl₂ and 1 mM Tris-(2-carboxyethyl) phosphine (TCEP) in a total volume of 200 μ l at 25 °C. The dissociation constant (K_d) was calculated by fitting the concentration-dependent binding curve using a quadratic ligand-binding equation.

Fluorescence measurements. Kinetic measurements of intrinsic and GEF-catalyzed nucleotide exchange and of intrinsic and GAP-stimulated GTP hydrolysis for wild-type and Asp63Val RAC2 were monitored by stopped-flow apparatus (Hi-Tech Scientific SF-61 with a mercury xenon light source and TgK Scientific Kinetic Studio software) and performed as described^{52–54}. The observed rate constants (K_{obs}) were fitted single exponentially using the GrafFit program (Erithacus software)⁵².

Pulldown assays and immunoblotting. Sequences encoding human wild-type, Gly12Val and Asp63Val RAC2, Gly12Val NRAS, Gly12Val HRAS and Gly12Val KRAS were cloned into pcDNA3.1, and constructs were overexpressed in COS-7 cells (ACC-60, Deutsche Sammlung von Mikroorganismen und Zellkulturen (DSMZ); cells were tested for mycoplasma by the DSMZ and used freshly) for 48 h. Cells were lysed with fish buffer (50 mM Tris-HCl, pH 7.5, 100 mM NaCl, 2 mM MgCl₂, 1% Igepal CA-630, 10% glycerol, 20 mM β -glycerophosphate, 1 mM sodium orthovanadate and one EDTA-free inhibitor tablet). GST-fused PAK1 GBD (amino acids 57–141) was expressed in *E. coli* for 4 h at 37 °C, and total bacterial proteins were released by sonication.

The bacterial lysates were incubated with glutathione-conjugated beads for 30 min, and beads were washed three times with fish buffer. The total cell lysates from COS-7 cells were divided into two parts. One part was added to the GST-PAK1 GBD/glutathione-conjugated bead complex for 30 min, and beads were washed three times with fish buffer. The second part was used to check the activity of the PI3K-AKT-mTORC and RAF-MEK1/2-ERK1/2 cascades in transfected cells by immunoblotting. Immunoblotting was carried out using rabbit antibody to FLAG (F7425, Sigma-Aldrich), mouse antibody to α -actin (MAB1510), and rabbit antibodies to MEK1/2 (9126), phosphorylated MEK1/2 (Ser217/Ser221, 9154), ERK1/2 (9102), phosphorylated ERK1/2 (Thr202/Thr204, 9106), AKT (9272) and phosphorylated AKT (Ser473, 4060 and Thr308, 2965) from Cell Signaling Technology as described⁵⁸.

Structural analysis. Interaction interfaces for RAC GTPases were analyzed on base RAC1 structures for RAC1 in complex with TIAM1 (ref. 59; Protein Data Bank (PDB) 1FOE) and with PAK1 (ref. 60). As there is no complex structure for any RAC GTPase interacting with a GAP, the corresponding interaction interface was deduced from the structure of Cdc42 in complex with Cdc42GAP⁶¹. Interacting residues were considered to be amino acids from GTPases that had at least one atom within 4.0 Å of the interacting protein. Individual as well as overlapping interaction surfaces were finally projected onto the molecular surface of RAC1 in the active, GTP-bound state using the program PyMOL (PyMOL Molecular Graphics System, version 1.7.4, Schrödinger).

Immunofluorescence and confocal microscopy. Cells were cytospun onto polylysine-coated slides, fixed in 4% paraformaldehyde for 15 min at room temperature and permeabilized with 0.3% Triton in PBS for 15 min at room temperature, washed twice for 5 min each wash in PBS and incubated in blocking buffer (1% BSA in PBS) for 1 h at room temperature. Cells were then incubated with mouse monoclonal antibody to histone H3 (H3K27me3, Abcam, 6002; following the manufacturer's instructions) for 1 h at room temperature, followed by three 5-min washes in PBS. Secondary Alexa Fluor 488-conjugated goat anti-mouse IgG (Life Technologies, A11001) was then applied for 1 h. The second incubation was identical to the first one, using as primary antibody rabbit polyclonal antibody to histone H3 (H3K27ac, Abcam, Ab4729) and as secondary antibody Alexa Fluor 594-conjugated goat anti-rabbit IgG (Life Technologies, A11012). Cells were subsequently washed three times for 5 min each wash in PBS and were then mounted in SlowFade Gold Antifade Reagent with DAPI (Life Technologies, S36939), coverslips were sealed with nail varnish and slides were visualized using the Zeiss LSM 510 confocal system. The SKM-1 and K562 myeloid cell lines were purchased from DSMZ and the American Type Culture Collection (ATCC), respectively. The presence of an *EZH2* mutation encoding p.Tyr646Cys (COSMIC, 37032) was checked, with the mutation found to be homozygous, by Sanger sequencing (data not shown).

Statistical methods. Statistical analyses were performed with R version 3.1.2. Fisher's exact test was used to determine whether different groups of cases were significantly different with respect to the number of individuals with somatic alterations. Overall survival was calculated from the date of diagnosis to the date of death. Distribution of overall survival in the different groups of cases was estimated by the Kaplan-Meier technique implemented in the survival library of R. Tabular data for survival curves are given in **Supplementary Table 9**.

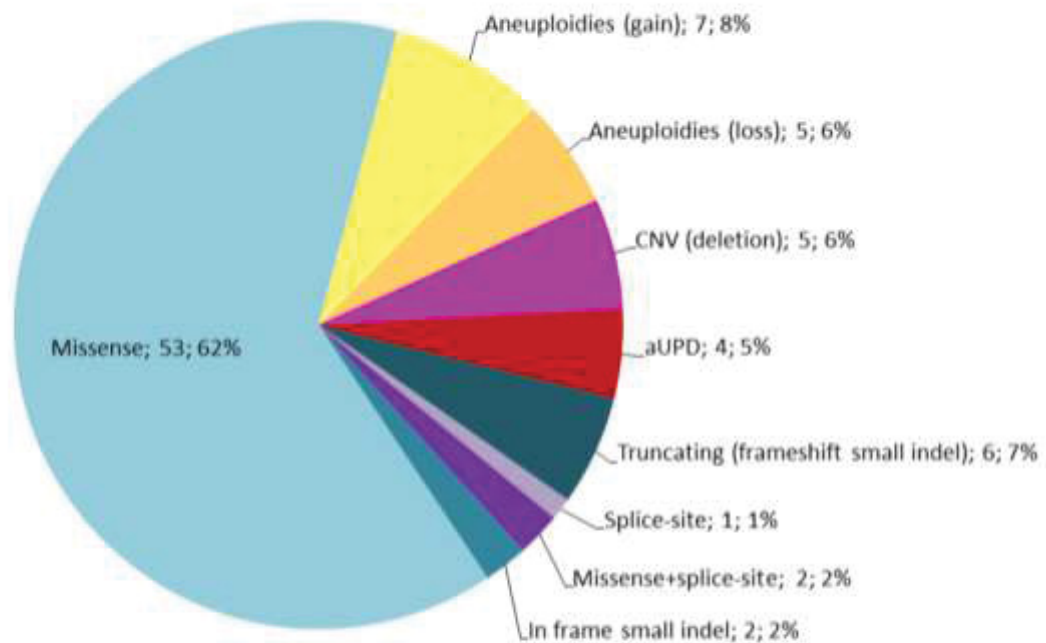
The differences between the Kaplan-Meier curves for different groups of cases were tested using the two-tailed Mantel-Haenszel log-rank test.

49. Chan, R.J., Cooper, T., Kratz, C.P., Weiss, B. & Loh, M.L. Juvenile myelomonocytic leukemia: a report from the 2nd International JMML Symposium. *Leuk. Res.* **33**, 355–362 (2009).

50. Pérez, B. et al. Genetic typing of *CBL*, *ASXL1*, *RUNX1*, *TET2* and *JAK2* in juvenile myelomonocytic leukaemia reveals a genetic profile distinct from chronic myelomonocytic leukaemia. *Br. J. Haematol.* **151**, 460–468 (2010).

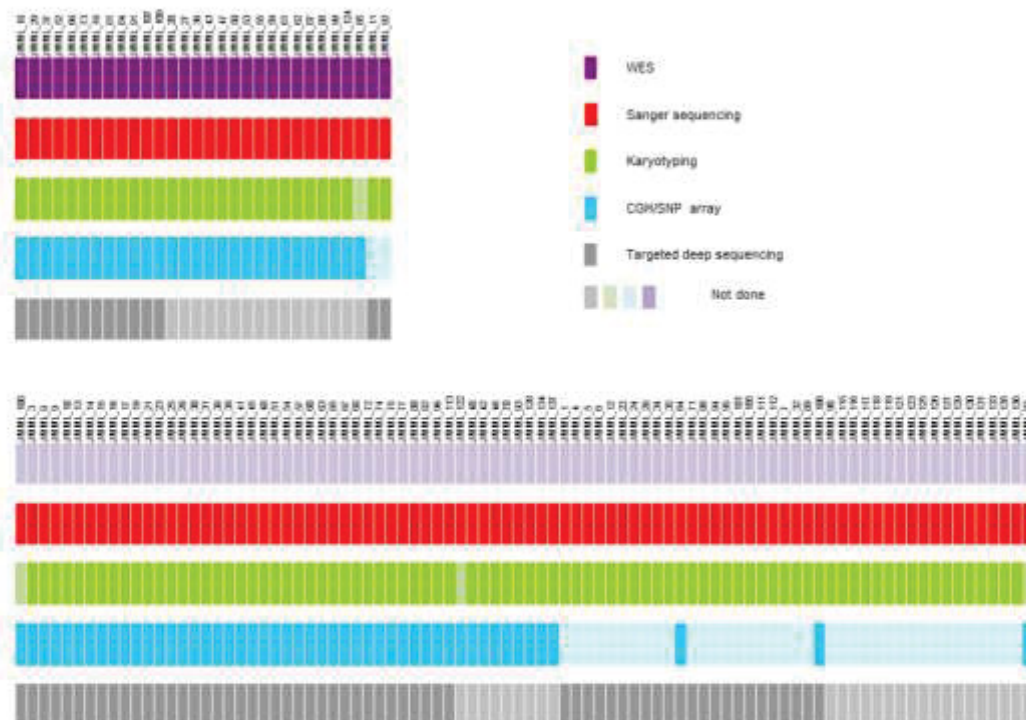
51. Ahmadian, M.R., Stege, P., Scheffzek, K. & Wittinghofer, A. Confirmation of the arginine-finger hypothesis for the GAP-stimulated GTP-hydrolysis reaction of Ras. *Nat. Struct. Biol.* **4**, 686–689 (1997).

52. Hensath, L. & Ahmadian, M.R. Fluorescence approaches for monitoring interactions of Rho GTPases with nucleotides, regulators, and effectors. *Methods* **37**, 173–182 (2005).
53. Eberth, A. & Ahmadian, M.R. *in vitro* GEF and GAP assays. *Curr. Protoc. Cell Biol.* Chapter 14, Unit 14.9 (2009).
54. Jaiswal, M., Dubey, B.N., Koessmeier, K.T., Gremer, L. & Ahmadian, M.R. Biochemical assays to characterize Rho GTPases. *Methods Mol. Biol.* **827**, 37–58 (2012).
55. Eberth, A. et al. A BAR domain-mediated autoinhibitory mechanism for RhoGAPs of the GRAF family. *Biochem. J.* **417**, 371–377 (2009).
56. Jaiswal, M., Dubey, B.N., Koessmeier, K.T., Gremer, L. & Ahmadian, M.R. Biochemical assays to characterize Rho GTPases. *Methods Mol. Biol.* **827**, 37–58 (2012).
57. Gremer, L. et al. Germline *KRAS* mutations cause aberrant biochemical and physical properties leading to developmental disorders. *Hum. Mutat.* **32**, 33–43 (2011).
58. Nakhaei-Rad, S. et al. The function of embryonic stem cell-expressed RAS (E-RAS), a unique RAS family member, correlates with its additional motifs and its structural properties. *J. Biol. Chem.* **290**, 15892–15903 (2015).
59. Worthylake, D.K., Rossman, K.L. & Sondek, J. Crystal structure of Rac1 in complex with the guanine nucleotide exchange region of Tiam1. *Nature* **408**, 682–688 (2000).
60. Morreale, A. et al. Structure of Cdc42 bound to the GTPase binding domain of PAK. *Nat. Struct. Mol. Biol.* **7**, 384–388 (2000).
61. Nassar, N., Hoffman, G.R., Manor, D., Clardy, J.C. & Cerione, R.A. Structures of Cdc42 bound to the active and catalytically compromised forms of Cdc42GAP. *Nat. Struct. Biol.* **5**, 1047–1052 (1998).

**Supplementary Figure 1**

Spectrum of somatically acquired mutations identified by combining WES and genome-wide DNA array analysis in the discovery cohort of 30 JMML cases.

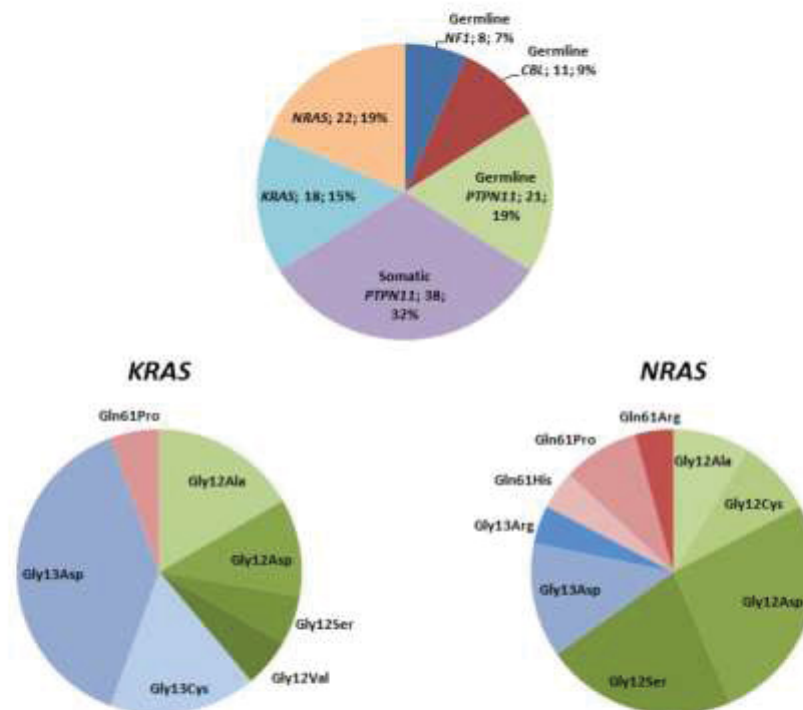
A total of 85 somatically acquired alterations were found, including 64 nonsynonymous point mutations or small insertion-deletions (indels) identified in the coding regions of these tumors by WES and 21 somatic cytogenetic alterations evidenced by SNP/CGH array, WES and/or metaphase cytogenetics.



Supplementary Figure 2

Graphical representation of the type of data obtained by sample in a cohort of 118 patients with JMML.

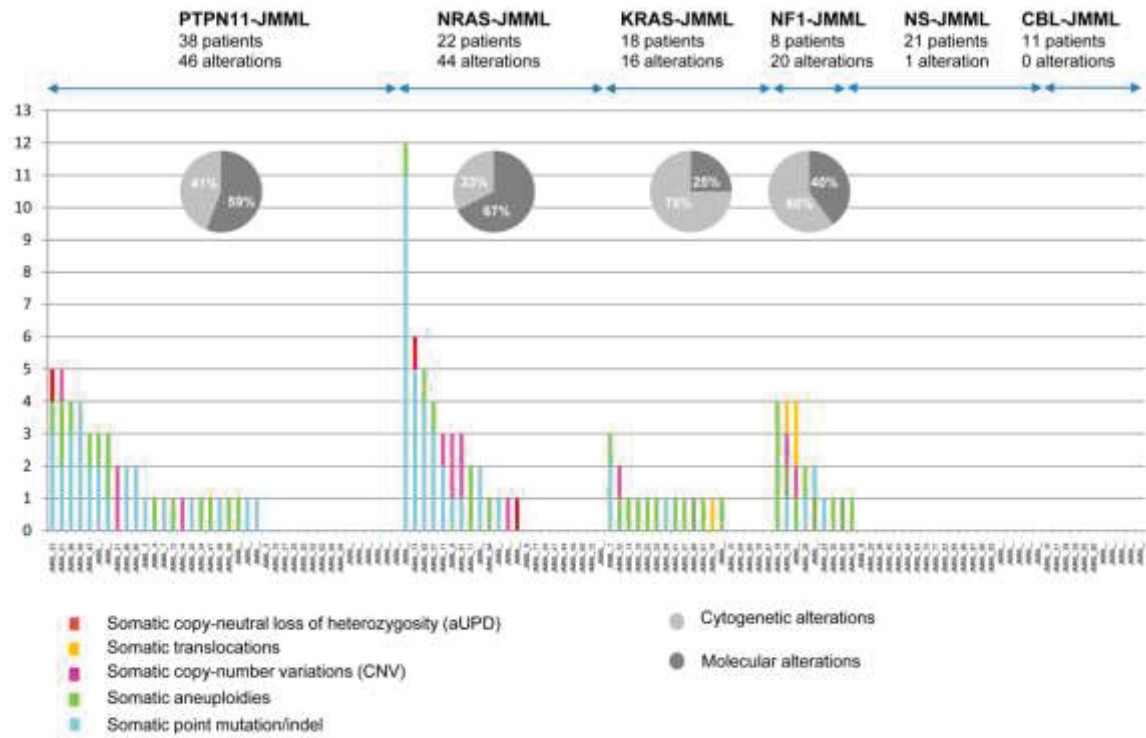
Both the discovery cohort (top; n = 30) and validation cohort (bottom; n = 88) are represented.



Supplementary Figure 3

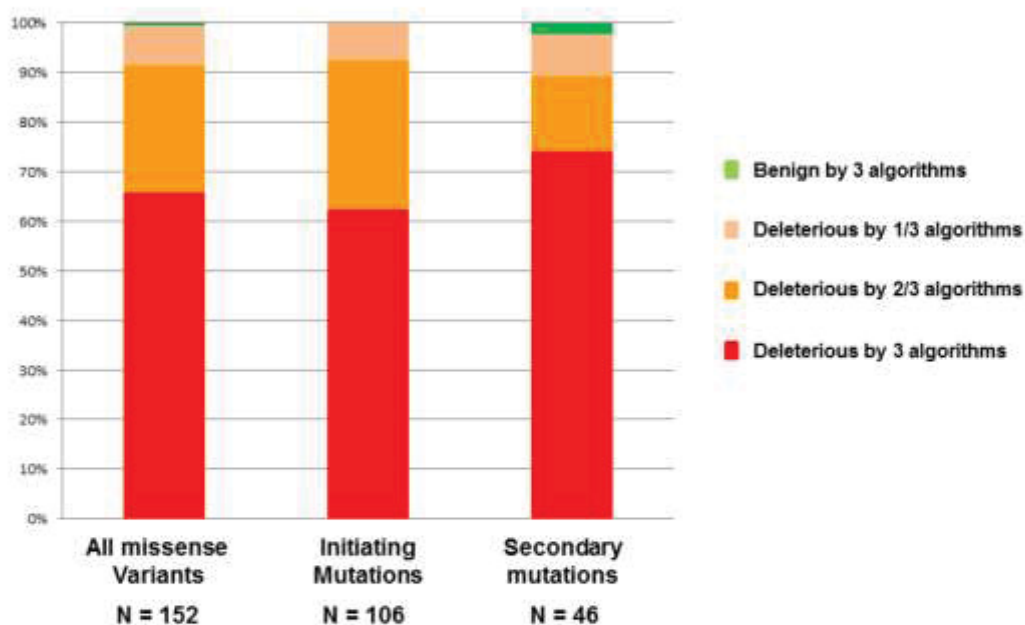
Distribution of RAS-related mutations in a cohort of 118 patients with JMML as detected by routine workup.

Distribution of RAS-related mutations in 118 consecutively diagnosed JMML cases as detected by routine workup and detailed spectrum of *KRAS* ($n = 18$) and *NRAS* ($n = 22$) mutations.



Supplementary Figure 4

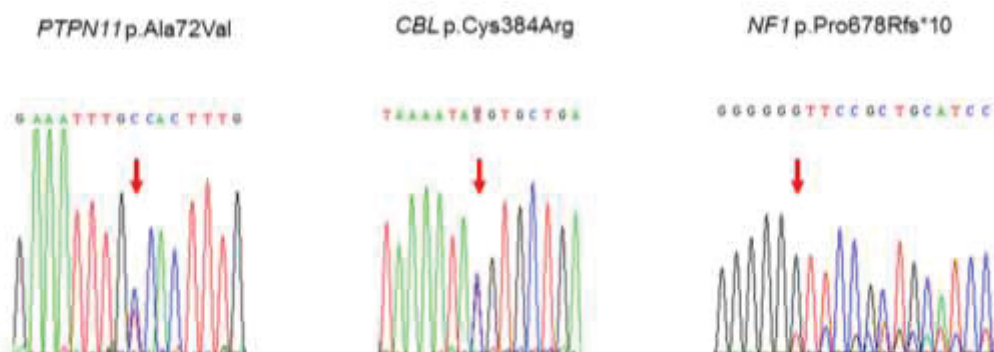
Histogram showing the type and number of additional somatic mutations per patient with JMML, according to genetic subgroup.



Supplementary Figure 5

Proportion of mutations predicted to be deleterious versus non-pathogenic substitutions.

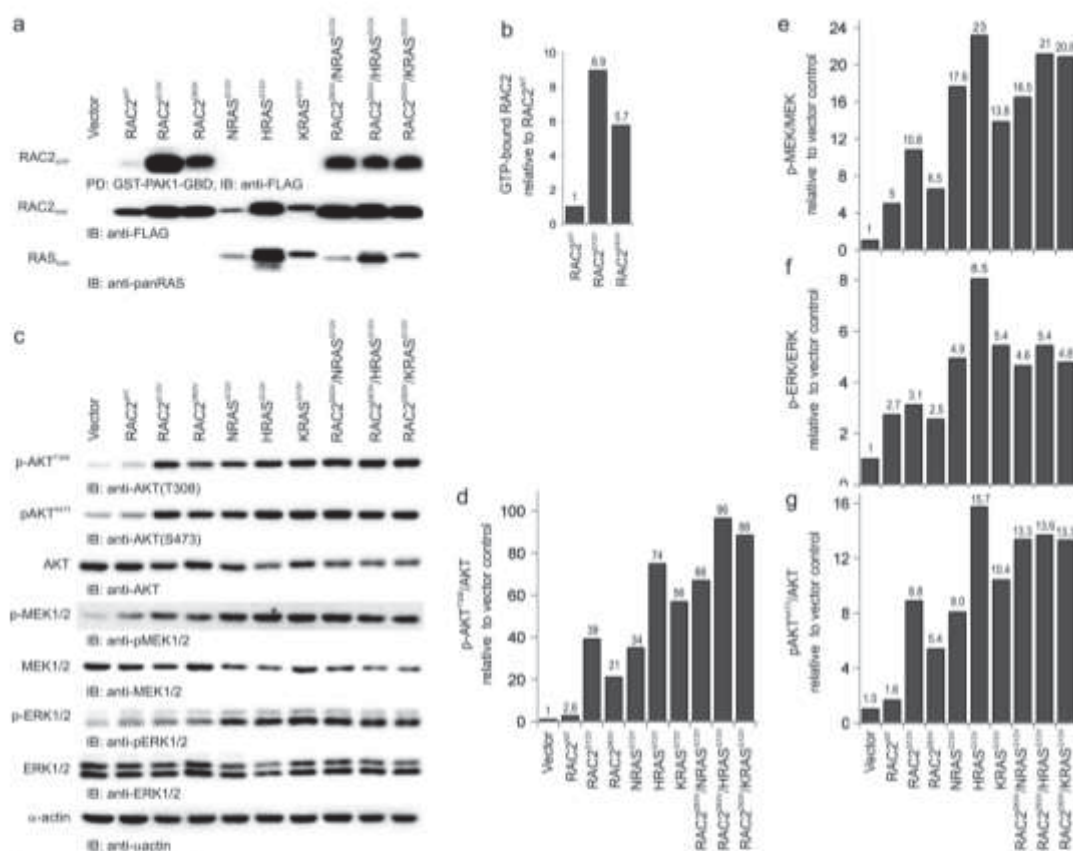
The pathogenicity of somatic nonsynonymous exonic missense variants with respect to gene function was predicted using the SIFT, PolyPhen-2 and MutationTaster algorithms (**Supplementary Table 6**). A total of 91% of all missense mutations were predicted to result in functionally relevant alterations by at least two of the three methods used for functional prediction. This percentage was similar when considering only initiating mutations, known to be deleterious in all cases (92%), as well as secondary mutations (89%).



Supplementary Figure 6

Sequence electrophoregram showing the presence of three concomitant mutations targeting the RAS pathway at diagnosis of JMML_89.

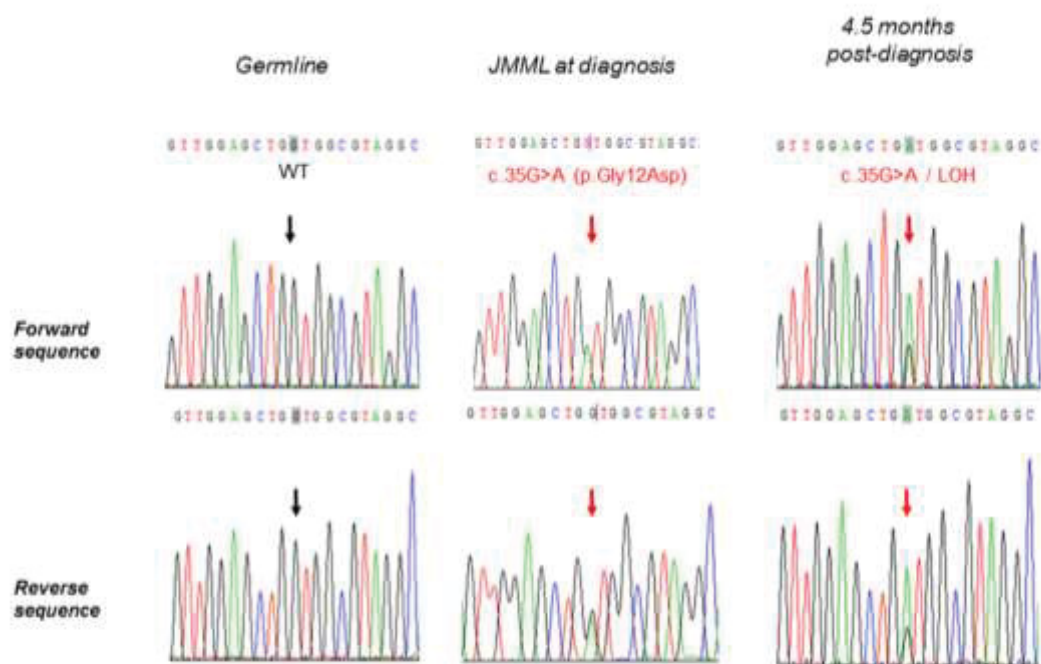
Mutated nucleotides are indicated by a red arrow. The subclonal pattern of *NF1* mutation is consistent with late acquisition. *NF1* haploinsufficiency was due to a recurrent c.2033delG mutation of a G homopolymer within the *NF1* coding region (exon 18). The frequency of this mutation appeared strikingly higher among somatic variants (5/6 cases with a secondary *NF1* mutation) than among germline variants (Leiden Open Variation Database, LOVD).



Supplementary Figure 7

Hyperactive RAC2 Asp63Val contributes to AKT activation via both the PI3K-PDK1 and mTORC2 cascades.

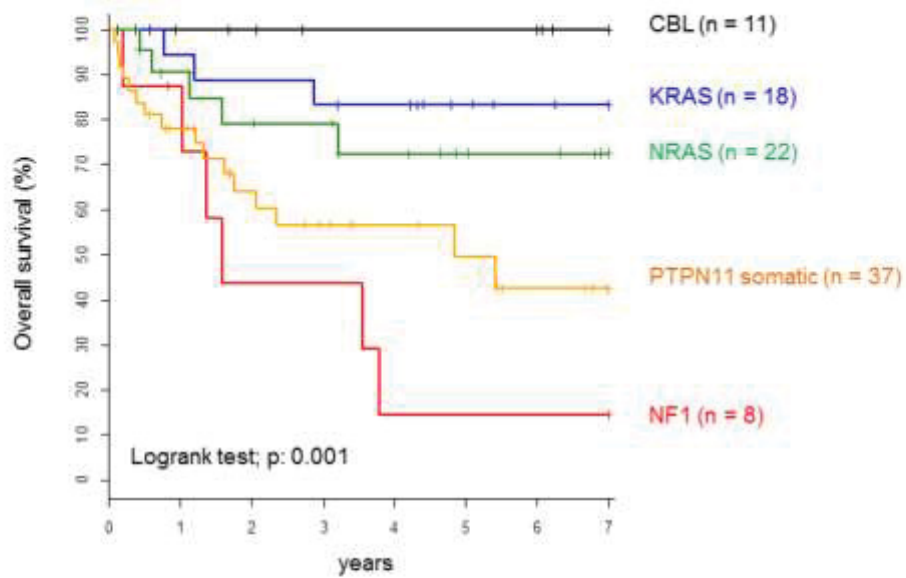
Pull-down experiments (a,b) and immunoblot (IB) analysis were conducted using total cell lysates (c-g) derived from transfected COS-7 cells with FLAG-tagged RAC2 and RAS variants. The GTPase-binding domain (GBD) of the RAC effector PAK1 was used as a GST fusion protein for the pull-down experiment. All experiments were performed three times. (a) Pull-down analysis showed that RAC2 Asp63Val largely exists in an active, GTP-bound state as compared to wild-type RAC2 (RAC2 WT), but activation is not as strong as for constitutively active RAC2 Gly12Val. Total RAC2 and RAS proteins were detected using antibody to FLAG and pan-RAS antibody to show the total amounts of the transfected FLAG-tagged RAC2 and RAS variants. (b) The RAC2 protein bands in a were densitometrically quantified (depicted as numbers and bars) as the amount of the GTP-bound RAC2 protein relative to wild-type RAC2. Coexpression of constitutively active NRAS Gly12Val, HRAS Gly12Val and KRAS Gly12Val did not change the level of GTP-bound RAC2 Asp63Val. (c) Total cell lysates were analyzed for the phosphorylation levels of AKT (pAKT 308 and pAKT 473), MEK1/2 (pMEK1/2) and ERK1/2 (pERK1/2). Total amounts of these kinases were used as loading controls. AKT is phosphorylated at Thr308 by the PI3K-PDK1 pathway, whereas the mTORC2 complex phosphorylates AKT at Ser473. (d-g) The protein bands in c were densitometrically quantified (depicted as numbers and bars), clearly showing that the presence of RAC2 Asp63Val resulted in strong AKT phosphorylation and slight MEK phosphorylation but no ERK phosphorylation. Interestingly, a comparison of RAC2 Asp63Val and RAC2 Gly12Val showed that the relative amount of phosphorylated protein was proportional to the amount of the GTP-bound protein.



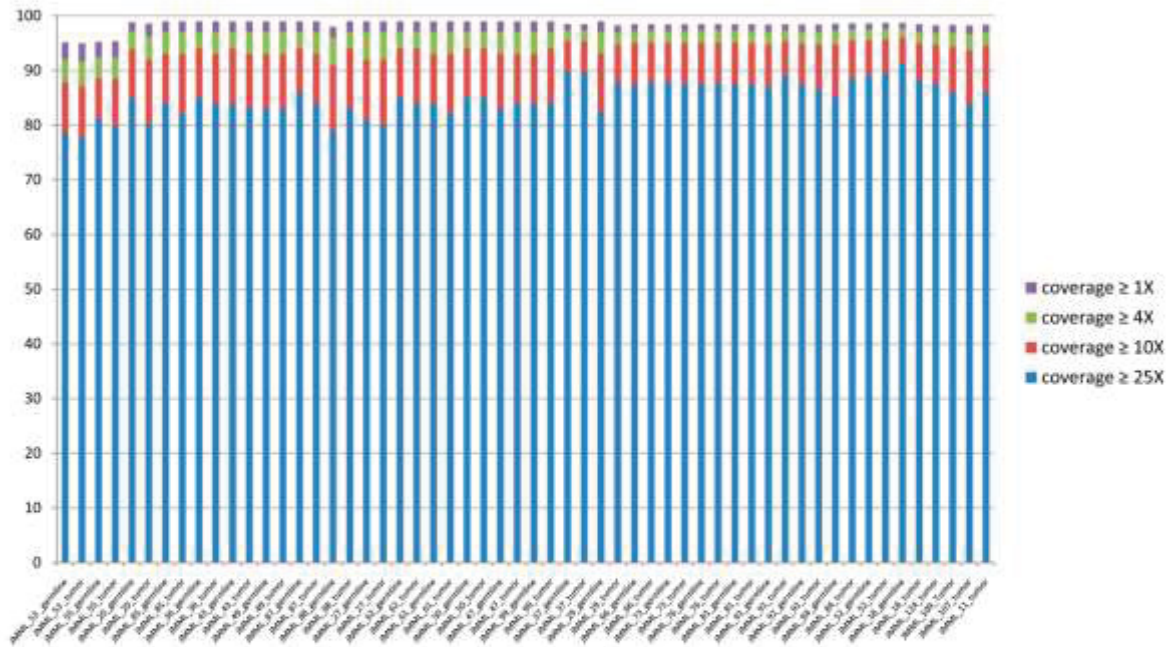
Supplementary Figure 8

Sequence electropherogram showing progressive LOH of the *KRAS* locus with an allelic imbalance in favor of the oncogenic allele in JMML_24.

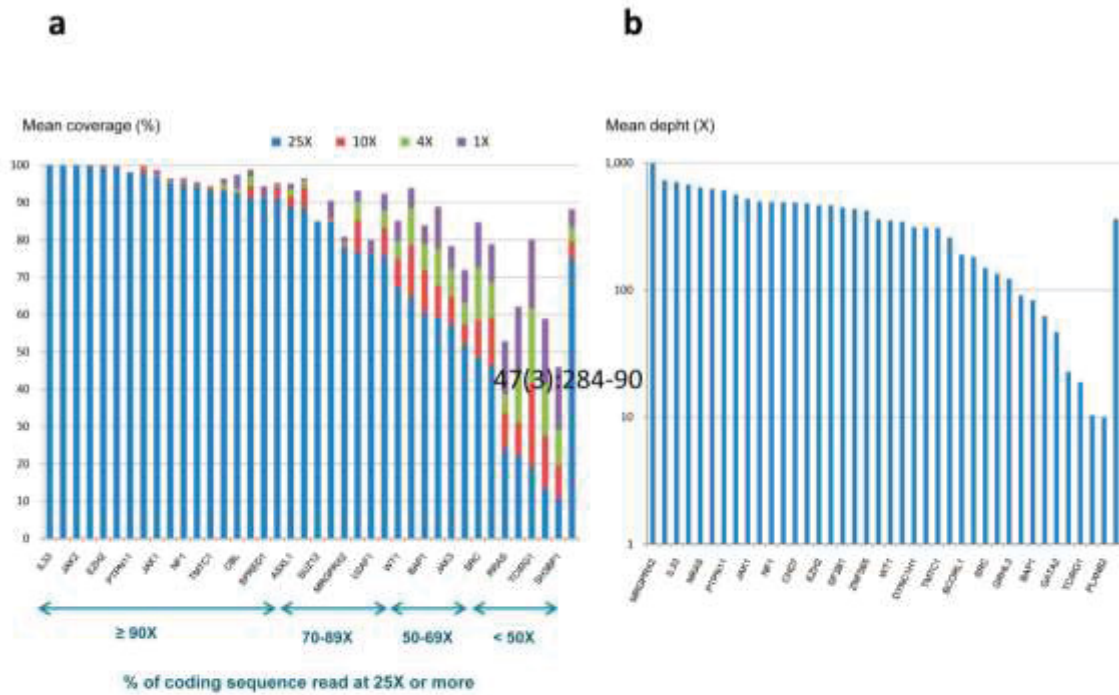
Wild-type (WT) and mutated nucleotides are indicated by black and red arrows, respectively.

**Supplementary Figure 9****Overall survival in sporadic JMML according to initiating RAS-activating lesion.**

Kaplan-Meier representation of the overall survival (%) in 96 patients with JMML evaluable for follow-up. Patients with Noonan syndrome were excluded from the analysis.

**Supplementary Figure 10**

Mean coverage of whole-exome sequencing in 30 paired JMML and germline DNA samples.



Supplementary Figure 11

Performances of PCR-based targeted deep sequencing in 75 JMML samples.

(a) The mean coverage of the coding regions is plotted for each gene by 25× descending order. (b) The mean depth of sequencing is plotted for each gene on a logarithmic scale, by descending order.

Supplementary Table 1: Characteristics of 30 patients with JMML subjected to whole exome sequencing

	Gender	Age at onset (yrs)	Underlying genetic condition	PB blasts (%)	BM blasts (%)	Karyotype	RAS pathway mutation	ASXL1	SETBP1	Leukemia sample	Germine control sample	
JMML_11	M	7.2	-	0.5	7	46,XY,del(12)(p113)(11)46,XY[9]	NRAS (p.G13D)	Somatic	p.G645Vfs*58	p.G870S	BM	Hair follicles
JMML_18	M	0.3	NF1	3	16	46,XY[20]	NRAS (p.R124I)	Germine/somatic	-	-	BM	Fibroblasts
JMML_20	F	0.0	NS	2	8	46,XX[20]	PTPN11 (p.G503R)	Germine	-	-	PB	Fibroblasts
JMML_27	F	0.9	-	0	8	46,XY[20]	PTPN11 (p.E76A)	Somatic	-	-	BM	Fibroblasts
JMML_29	F	1.1	-	0	9	46,XX[20]	NRAS (p.G13C)	Somatic	-	-	BM	Fibroblasts
JMML_36	M	0.7	NS	4	7	46,XY[20]	PTPN11 (p.G503R)	Germine	-	-	BM	Fibroblasts
JMML_37	F	9.8	-	4	14	45,XX,-7[20]46,XX[1]	NRAS (p.Q61R)	Somatic	-	p.D500N	BM	Fibroblasts
JMML_43	M	0.0	NS	4	8	46,XY[22]	PTPN11 (p.D61H)	Germine	-	-	PB	Fibroblasts
JMML_47	M	0.5	-	3	5.5	45,XY,-7[19]46,XY[1]	PTPN11 (p.D61Y)	Somatic	-	-	BM	Fibroblasts
JMML_50	F	0.7	-	1.5	8	46,XX[20]	PTPN11 (p.D61V)	Somatic	-	-	BM	Fibroblasts
JMML_62	M	2.2	-	2	0	46,XY[20]	PTPN11 (p.E76K)	Somatic	-	-	BM	Fibroblasts
JMML_53	M	2.2	-	2	8	46,XY[19]45,X,-Y[12]	PTPN11 (p.G503A)	Somatic	-	-	BM	Fibroblasts
JMML_55	F	1.1	CBL5	0.5	8.5	46,XX[20]	CBL (p.Y371H)	Germine/somatic	-	-	PB	Fibroblasts
JMML_58	M	0.1	NS	1	2	46,XY[20]	PTPN11 (p.D61H)	Germine	-	-	BM	Fibroblasts
JMML_61	M	2.2	-	27	32	46,XY,del(q21q32)(10q48;del.+(21,+22)(1)-46,XY,+21,+22[3]/46,XY[16]	PTPN11 (p.E76D)	Somatic	-	p.D660N	BM	Fibroblasts
JMML_62	F	0.7	-	3	3	46,XX[20]	PTPN11 (p.D61V)	Somatic	-	-	BM	Fibroblasts
JMML_66	F	3.1	-	2	10	46,XX[25]	NRAS (p.Q61P)	Somatic	p.L775K	-	BM	Fibroblasts
JMML_73	M	4.2	-	2	35	46,XY[20]	NRAS (p.G12D)	Somatic	-	-	BM	Fibroblasts
JMML_76	M	9.3	-	0	4	46,XY[20]	NRAS (p.G13C)	Somatic	-	-	BM	Fibroblasts
JMML_81	M	0.3	-	4	6	46,XY[20]	NRAS (p.G13D)	Somatic	-	-	BM	Fibroblasts
JMML_84	M	0.1	-	8	8	46,XY[25]	PTPN11 (p.E76K)	Somatic	-	-	PB	Normal HC
JMML_85	M	0.6	NS	0.7	2	Female	PTPN11 (p.A72D)	Germine	-	-	BM	Fibroblasts
JMML_87	M	0.0	NS	ND	<5%	47,XXY,(13)46,XY[7]	PTPN11 (p.A72D)	Germine	-	-	PB	Fibroblasts
JMML_88	M	2.8	-	2	5.5	46,XY[20]	PTPN11 (p.E76V)	Somatic	-	-	BM	Fibroblasts
JMML_91	F	2.9	-	21	37	46,XX,del(22)(p11.2)	NRAS (p.Arg64_Nle66del)	Somatic	p.E630Rfs*13	-	BM	Fibroblasts
JMML_92	F	4.5	-	1	15	46,XX,del(7)(q37)q37[6](3)46,XX[17]	NRAS (p.G12D)	Somatic	-	-	BM	Fibroblasts
JMML_98	M	2.5	-	3	5	46,XY[20]	PTPN11 (p.D61V)	Somatic	-	p.G870S	PB	Fibroblasts
JMML_107	F	3.7	-	13	30	45,XX,-7[24]	PTPN11 (p.G60R)	Somatic	-	-	BM	Fibroblasts
JMML_108	F	13.3	-	10.5	19	45,XX,-7[20]	NRAS (p.G12D)	Somatic	p.G848Wfs*12	p.E645K p.D660N	PB	Skin Biopsy
JMML_124	M	1.5	-	1	2	46,XY[20]	NRAS (p.G12A)	Somatic	-	p.D660N	BM	Fibroblasts

M: male; F: female; BM: bone marrow; PB: peripheral blood; yrs: years; NS: Noonan syndrome; CBL5: CBL syndrome; NF1: type 1 neurofibromatosis; HC: hematopoietic cells.

Supplementary Table 4: Gene panel for targeted sequencing and NGS performances

gene symbol	method	Target region	(bp)	Mean depth (X)	Rational for sequencing
ASXL1	NGS	whole coding region	5 067	626	Mutations reported in JMML
ASXL2	NGS	whole coding region	4 676	565	ASXL1-related
ASXL3	NGS	whole coding region	7 239	345	ASXL1-related
BAP1	NGS	whole coding region	2 887	83	ASXL1-related
BCORL1	NGS	whole coding region	5 628	190	Mutations reported in JMML
CBL	NGS	whole coding region	3 377	499	Mutations reported in JMML
CHD7	NGS	whole coding region	10 511	491	Mutated in a NS-AML with RRAS germline mutation
DYNC1H1	NGS	whole coding region	17 139	314	Mutation(s) found by WES in our cohort of JMML
EZH2	NGS	whole coding region	3 035	466	PRC2-related
GATA2	NGS	whole coding region	1 648	47	Mutated in a NS-AMLwith RRAS germline mutation
GATA3	NGS	whole coding region	1 540	183	GATA2-related
GRHL3	NGS	whole coding region	2 766	123	Mutated in a NS-AML with RRAS germline mutation
IL33	NGS	whole coding region	1 100	710	Mutation(s) found by WES in our cohort of JMML
ITPR3	NGS	whole coding region	10 394	62	Mutation(s) found by WES in our cohort of JMML
JAK1	NGS	whole coding region	4 449	524	JAK3-related
JAK2	NGS	whole coding region	4 342	677	JAK3-related
JAK3	NGS	whole coding region	4 318	91	Mutations reported in JMML
KRAS	NGS	whole coding region	892	466	Mutations reported in JMML
KRT1	NGS	whole coding region	2 304	484	Mutation(s) found by WES in our cohort of JMML
MRGPRX2	NGS	whole coding region	1 034	1 028	Mutation(s) found by WES in our cohort of JMML
NF1	NGS	whole coding region	10 524	496	Mutations reported in JMML
NRAS	NGS	whole coding region	734	642	Mutations reported in JMML
PDE8A	NGS	whole coding region	3 392	495	Mutation(s) found by WES in our cohort of JMML
PLXNB2	NGS	whole coding region	6 952	10	Mutation(s) found by WES in our cohort of JMML
PTPN11	NGS	whole coding region	2 401	612	Mutations reported in JMML
RRAS	NGS	whole coding region	903	23	RAS-related
SETBP1	NGS	whole coding region	5 226	435	Mutations reported in JMML
SF3B1	NGS	whole coding region	5 001	446	Mutations reported in JMML
SH3BP1	NGS	whole coding region	2 844	10	Mutations reported in JMML
SPRED1	NGS	whole coding region	1 622	734	related to NF1
SRC	NGS	whole coding region	1 771	149	RAS-related
SRSF2	NGS	whole coding region	748	135	Mutations reported in JMML (spliceosome)
SUZ12	NGS	whole coding region	2 182	361	PRC2 component
TCIRG1	NGS	whole coding region	3 272	19	Osteopetrosis-related
TMTC1	NGS	whole coding region	3 387	310	Mutation(s) found by WES in our cohort of JMML
U2AF1	NGS	whole coding region	1 159	259	Mutations reported in JMML (spliceosome)
WT1	NGS	whole coding region	2 015	352	Mutated in a NS-AML with RRAS germline mutation
ZNF565	NGS	whole coding region	1 664	423	Mutated in a NS-AML with RRAS germline mutation
ZRSR2	NGS	whole coding region	1 900	313	Spliceosome-related
CDYL	Sanger	NM_004824.3 (ex 7b-12)	NA	NA	Deletion found in our cohort of JMML
RRAS	Sanger	NM_006270.3 (ex 1-6)	NA	NA	RAS-related
RAC2	Sanger	NM_002872.4 (1-3)	NA	NA	RAS-related
NF1	Sanger	NM_001042492.2 (ex 18)	NA	NA	RAS-related
JAK3	Sanger	NM_000215.3 (ex 15)	NA	NA	Mutations reported in JMML
SH3BP1	Sanger	NM_018957.3 (ex 10; 11)	NA	NA	Mutations reported in JMML
GATA2	Sanger	NM_032638.4 (ex 2-6)	NA	NA	Mutations reported in JMML
SETBP1	Sanger	NM_015559.2 (ex 6 part)	NA	NA	Diagnostic workup
ASXL1	Sanger	NM_015338.5 (ex 14)	NA	NA	Diagnostic workup
PTPN11	Sanger	NM_002834.3 (ex 3;13)	NA	NA	Diagnostic workup
CBL	Sanger	NM_005188.3 (ex 7;8;9)	NA	NA	Diagnostic workup
KRAS	Sanger	NM_033360.3 (ex 2; 3)	NA	NA	Diagnostic workup
NRAS	Sanger	NM_002524.4 (ex 2; 3)	NA	NA	Diagnostic workup

bp: base pairs; NA: not applicable

Supplementary Table 5: General features of 118 JMML cases, additional somatic mutations and outcome according to genetic status. The number of additional somatic alterations was evaluated by disregarding somatic RAS-pathway mutations assumed to be either the initiating event or part of the classic mechanism of leukemogenesis, such as hits targeting the wild-type *NF1* or *CBL* allele in germline-mutated patients^{3,5,46}. Despite a trend toward more cytogenetic alterations and fewer point mutations in the KRAS-JMML group, no significant difference was found in the total number of additional somatic alterations ($p = 0.683$), cytogenetic alterations ($p = 0.103$) or point mutations ($p = 0.242$) between genetically-defined sporadic JMML groups. However, del(7)7q was significantly more frequent in KRAS-JMML ($p = 0.004$), whereas no difference was observed for aUPD ($p = 0.433$), CNV (0.431) and other aneuploidies (0.134) between groups.⁶

Genetic group	SOMATIC (sporadic JMML)				GERMLINE (syndromic JMML)			TOTAL
	PTPN11	NRAS	KRAS	Total	NF1	PTPN11	CBL	
Number of cases	38	22	18	78	8	21	11	118
M:F sex ratio	30/8 (3.7)	12/10 (1.2)	12/6 (2.0)	54/25 (2.2)	5/0	14/7 (2.0)	4/7 (0.6)	79/38 (2.1)
Median age at onset (yrs)	2.7 [0.1 – 8.1]	2.7 [0.2 – 13.3]	1.1 [0.3 – 3.0]	2.2 [0.1 – 13.3]	3.0 [0.3 – 15.7]	0.1 [0 – 0.8]	1.3 [0.2 – 5.1]	1.6 [0 – 13.3]
WBC counts, median [IQ], $\times 10^9/L$	24.4 [1.7 – 106.0]	26.8 [7.4 – 96.7]	20.8 [4.0 – 107.8]	24.7 [1.7 – 167.8]	29.6 [11.6 – 83.0]	37.5 [9.2 – 70.0]	26.7 [9.4 – 79.0]	28.3 [1.7 – 167.8]
Platelet counts, median [IQ], $\times 10^9/L$	33.0 [3.0 – 292.0]	129.5 [23.0 – 238.0]	88.0 [3.0 – 153.0]	54.5 [3.0 – 292.0]	146.5 [15.0 – 302.0]	68.0 [4.0 – 281.0]	130.0 [6.0 – 266.0]	86.5 [3.0 – 302.0]
Myeloid precursors in peripheral blood, no. of patients (%)	35 (92)	20 (91)	17 (94)	72 (92)	7 (88)	20 (95)	9 (82)	108 (91)
Circulating blasts $\geq 10\%$, no. of patients (%)	7 (18)	6 (27)	3 (17)	16 (21)	3 (37)	0 (0)	0 (0)	19 (16)
Myelodysplastic features, no. of patients (%)	24 (63)	11 (50)	14 (78)	49 (63)	6 (75)	11 (52)	6 (56)	72 (61)
HbF elevated for age, no. of patients (%) ⁶	21/35 (60)	5/19 (26)	3/15 (20)	29/69 (42)	5/8 (62)	1/14 (7)	2/10 (20%)	37/101 (37)
Additional somatic alterations⁶								
No. of patients with ≥ 1 additional somatic alteration [Max. no. of alterations per patient]	23 (60) [0]	13 (59) [12]	13 (72) [3]	49 (63) [12]	8 (100) [4]	1 (5) [1]	0 (0) -	58 (49) [12]
No. of additional somatic alterations	45	43	16	104	19	1	0	124
No. of patients with ≥ 1 cytogenetic alteration [Max. no. of alterations per patient]	14 (37) [3]	11 (50) [2]	11 (61) [2]	36 (46) [3]	5 (63) [4]	1 (5) [1]	0 (0) [0]	42 (36) [4]
No. of cytogenetic alterations	19	14	12	45	12 ^d	1	0 ^d	58
Translocation, no. of patients (%)	-	-	1	1	2	-	-	3
Del(7)7q, no. of patients (%)	6 (16)	3 (14)	10 (56)	19 (25)	1 (13)	-	-	20 (17)
Other aneuploidies, no. of patients (%)	7 (18)	2 (9)	-	9 (12)	3 (38)	1 (5)	-	12 (10)
CNV, no. of patients (%)	3 (8)	4 (18)	1 (6)	8 (10)	2 ^d (25)	-	-	10 (8)
aUPD, no. of patients (%)	1 (3)	2 (9)	0 (0)	3 (4)	0 ^d (0)	-	-	3 (3)
No. of patients with ≥ 1 point mutation [Max. no. of alterations per patient]	14 (37) [4]	9 (41) [11]	3 (16) [2]	26 (33) [11]	4 (50) [2]	-	-	30 (25) [11]
No. of point mutations	27	29	4	60	7	-	-	67

etlcs: doi:10.1038/ng.3420

Genetic group	SOMATIC (sporadic JMML)				GERMLINE (syndromic JMML)			TOTAL
	PTPN11	NRAS	KRAS	Total	NF1	PTPN11	CBL	
Additional RAS-related mutations, no. of patients (%) [Max. no. of alterations per patient]	6 (21) [2]	5 (23) [1]	0 (0)	13 (18) [2]	2 (25) [1]	-	-	15 (13) [2]
PRC2-related mutations, no. of patients (%) without del(7)q [Max. no. of alterations per patient]	3 (8) [2]	7 (32) [3]	2 (11) [2]	12 (15) [3]	5 (53) [1]	-	-	18 (15) [3]
PRC2-related mutations, no. of patients (%) including del(7)q [Max. no. of alterations per patient]	6 (21) [2]	8 (36) [3]	10 (56) [3]	26 (33) [3]	5 (53) [2]	-	-	31 (26) [3]
Outcome								
Blast crisis before HSCT, no. of patients (%)	13 (34)	9 (41)	4 (22)	26 (33)	5 (52)	1 (5)	0 (0)	32 (27)
HSCT, no. of patients (%)	29 (76)	15 (68)	18 (100)	62 (79)	5 (52)	3 (14)	6 (55)	76 (64)
Autologous reconstitution, no. of patients (% of HSCT)	1 (3)	2 (13)	3 (17)	6 (10)	0 (0)	0 (0)	3 (50)	9 (12)
Relapse / disease progression, no. of patients (% HSCT)	6 (21)	2 (13)	3 (17)	11 (18)	2 (40)	0 (0)	0 (0)	13 (17)
Death, no. of patients (%)	16 (42)	6 (27)	4 (22)	26 (33)	6 (75)	12 (57)	0 (0)	44 (37)

[IQ] : Interquartile range; CNV: copy-number variations; aUPD: acquired uniparental disomy; HSCT: hematopoietic stem cell transplantation.

¹ the number of patients who were evaluated is indicated.

² In patients with NF1 and CBL syndrome, events targeting the second allele of NF1 and CBL were not considered as additional events since the loss of the wild-type allele is part of the classic mechanism of leukemogenesis in these settings. 10/11 patients with germline CBL mutations had an aUPD encompassing CBL whereas 5/8 patients with neurofibromatosis had a somatically acquired event targeting NF1 (including 3 aUPDs).

³ One patient had a germline codon deletion of SUZ12.

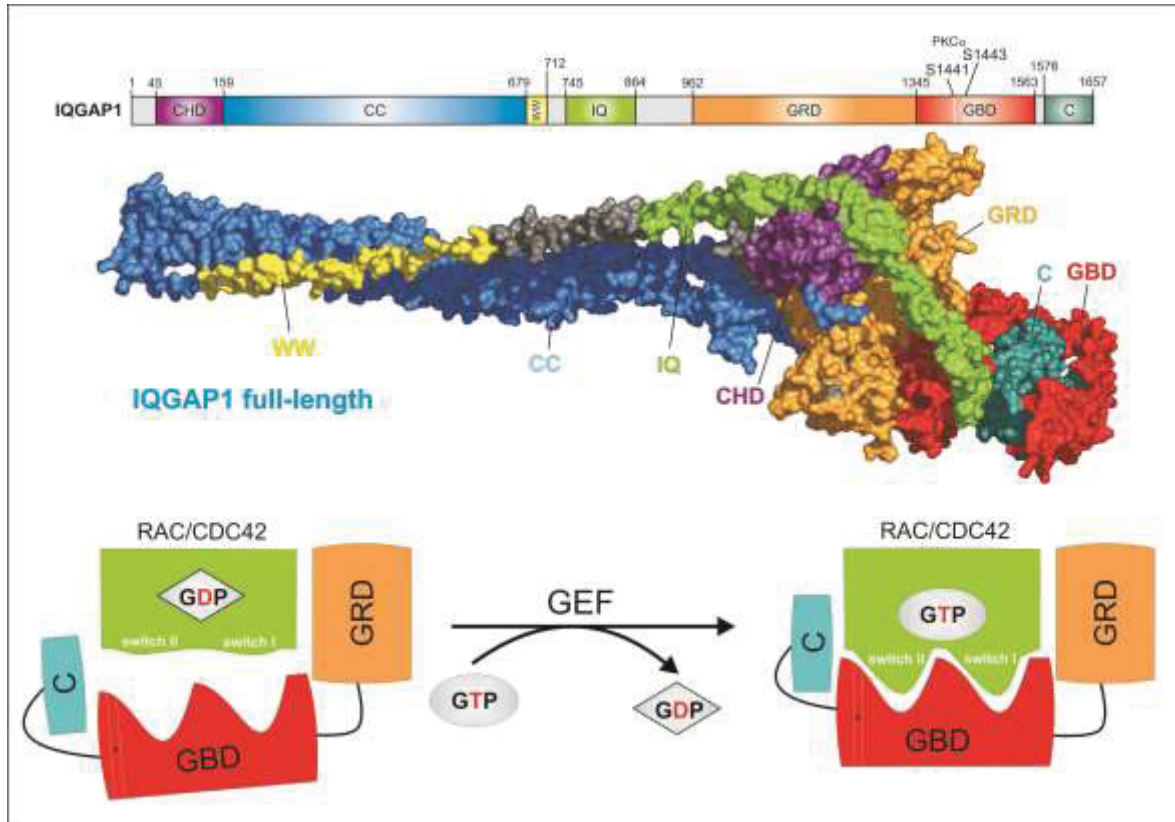
Supplementary Note**Leukemia samples**

JMML patient samples were collected in a diagnostic setting. All patients' parents have given their written informed consent before sample collection. This study was approved by the ethical evaluation committee of the French Institute of Medical Research and Health (INSERM) (IORG0003254) in accordance with the declaration of Helsinki.

Chapter IV

IQGAP1 interaction with RHO family proteins revisited: kinetic and equilibrium evidence for two distinct binding sites

Graphical abstract



Status: In preparation

Impact factor:

Own Proportion to this work: 70 %

Cloning, expression and purification of RHO, IQGAPs, and RAC partners proteins

Preparing RHO proteins in nucleotide-free form

Generating mantGDP, mantGppNHp and tamraGTP bound RHO proteins

Fluorescence polarization measurements

Stopped-flow measurements

Designing and performing the experiments

ABSTRACT

The scaffolding IQ motif-containing GTPase activating protein 1 (IQGAP1) plays a central role in the physical assembly of relevant signaling networks that are responsible for various cellular processes, including cell adhesion, polarity and transmigration. Amongst various proteins, RAC1 and CDC42, have been also proposed to interact with the GAP-related domain (GRD) of IQGAP1, however, the exact nature of this interaction process has remained obscure. Here, we demonstrate that (i) IQGAP1 associates with six different RAC- and CDC42-related proteins but not with other members of the RHO family, including the RHO-and RND-proteins, and (ii) unlike published models, IQGAP1 interaction with RAC- and CDC42-related proteins underlies a two-step binding mechanism, first a low-affinity, largely nucleotide-independent binding of GRD outside the switch regions, and second a high-affinity, GTP-dependent binding of the RHO GTPase binding domain (GBD) to the switch region. These data were confirmed by phosphomimetic mutations of S1443 in GBD, which resulted in complete abolishment of the IQGAP1 interaction with RAC1 and CDC42, clearly indicating that S1443 phosphorylation by protein kinase C is critical for these interactions. Taken together, these results provide the field with new insights into interaction characteristics of IQGAP1 and highlight the complementary importance of kinetic and equilibrium analyses. Therefore, herein, we challenge the paradigm that the ability of IQGAP1 to interact with RAC/CDC42 proteins is based on a two-step binding process which is a prerequisite for IQGAP1 activation and a critical mechanism in temporal regulation and integration of IQGAP1-mediated cellular responses.

Key words: CDC42, GBD, GRD, stopped-flow, fluorescence, polarization, anisotropy, interaction, IQGAPs, RAC1, RHOA, RHO family

INTRODUCTION

The RHO family proteins are known to play an important role in diverse cellular processes and progression of different diseases, such as cardiovascular diseases, developmental and neurological disorders, tumor invasion and metastasis as well as regulating liver regeneration [1-3]. RHO proteins share two common functional characteristics, membrane anchorage and an on/off switch cycle [4]. Subcellular localization of RHO proteins to different cellular membranes is known to be critical for their biological activity. This is achieved by a hyper variable region (HVR) [5] and a lipid anchor in their C-terminal tail at a distinct cysteine residue in the CAAX motif (C is cysteine, A is any aliphatic amino acid, and X is any amino acid) [6]. RHO protein function is dependent on the guanine nucleotide-binding (G) domain that contains the principle binding center for GDP and GTP and presents depending on its nucleotide-bound state various contact sites for regulators and effectors [4]. Thus, membrane-associated RHO proteins act, with some exceptions [7], as molecular switches by cycling between an inactive GDP-bound state and an active GTP-bound state. This cycle underlies two critical intrinsic functions, the GDP-GTP exchange and GTP hydrolysis [7] and is controlled at least three classes of regulatory proteins [4]: (i) Guanine nucleotide exchange factors (GEFs) catalyze the exchange of GDP to GTP and activate the RHO protein [8,9]; ii) GTPase activating proteins (GAPs) stimulate the GTP hydrolysis and convey the RHO protein in its inactive conformation [10,11]; (iii) Guanine nucleotide dissociation inhibitors (GDIs) bind to prenylated RHO proteins and extract them from the membranes into the cytoplasm [12-15]. The formation of the active GTP-bound state of RHO proteins is accompanied by a conformational change in two regions, known as switch I and II [4], which provide a platform for the selective interaction with structurally and functionally diverse effectors, *e.g.* p21-activated kinase 1 (PAK1) [16], p67^{phox} a member of the NSDPH oxidase [17], semaphorin receptor Plexin B1 [18,19] as well as the IQ motif-containing GTPase activating proteins (IQGAPs) [20,21].

In mammals, three isoforms of IQGAPs are expressed: IQGAP1, IQGAP2 and IQGAP3. These homologues have similar domain compositions but different subcellular localization, tissue expression and functions [20,22]. This class of proteins activates a wide variety of downstream signaling cascades [22-25], thereby regulating many important physiological and pathophysiological processes in eukaryotic cells [20,26,27]. Among IQGAP isoforms, IQGAP1 is ubiquitously expressed and is the most investigated member of IQGAP family, and our understanding mainly relies on the evidences from IQGAP1. IQGAP1 is involved in wide spectrum of cellular processes, such as adhesion, cell polarity and directional migration [24] and also cancer progression [22,28] *via* binding to RHO protein. The domain organization of IQGAP1 is highly conserved in IQGAP family consisting of an N-terminal calponin homology domain (CHD), a coiled-coil repeat region (CC), a tryptophan-containing proline-rich motif-binding region (WW), four isoleucine/glutamine-containing motifs (IQ), a RASGAP-related domain (GRD), an originally called RASGAP C-terminal domain (RGTC) [24], which we called a GTPase-binding domain (GBD) in this study, and a C-terminal domain (C).

IQGAP2 and IQGAP3 are also able to bind RHO proteins [29-32]. IQGAP2 has 62% sequence identity to IQGAP1 and is expressed predominantly in the liver, but can be detected in stomach, prostate, thyroid, testis, kidney, platelets and salivary glands [20,30,31,33,34]. IQGAP3 is enriched in brain, testis, lung, small intestine, and colon [31-33,35-37]. Recent differential gene expression analysis revealed a reciprocal expression of IQGAPs in Hepatocellular carcinoma (HCC) and subsequently opposing functions [38]. Given that IQGAP proteins share a domain structure and

have sequence homology, such a paradoxical phenomenon may be due to their protein binding partners, subcellular localization and diverse tissue expression.

Furthermore, in hepatic stellate cells (HSCs) has been shown that *Iqgap1* deficiency promotes myofibroblast activation, tumor implantation, and metastatic growth in mice *via* upregulation of paracrine signaling molecules [39]. In spite of having RASGAP homology domain, none of these three isoforms have GTPase-activating protein (GAP) activity. GAPs increase the intrinsic activity of RHO proteins and inactivate them. By contrast, IQGAP proteins exhibit an inhibitory effect on the intrinsic GTPase activity of the RHO family members CDC42 and RAC1, thereby stabilize them in their active GTP-bound form [30,40,41]. Apart from RAC1 and CDC42, a multitude of IQGAP interacting partners have been reported to date [20,24,25,27,42-44]. From IQGAP family, IQGAP1 has been implicated as a drug target although the molecular mechanism of the IQGAP1 functions is unclear. A prerequisite to achieve these functions is the dissection of its distinct domains and the analysis of their interactions with desired protein partners.

Work from several laboratories has shown that the C-terminal half of IQGAP1 (amino acids 863-1657), encompassing GRD (amino acids 1025-1238) and RGTC (called GBD in this study; amino acids 1451-1583), binds physically to active, GTP-bound forms of CDC42 and RAC1 [29,45-47]. IQGAP1 GRD, which is structurally a homologous but functionally an inactive RASGAP [48], also undergoes interaction with RAC1 and CDC42, although with a lower affinity than the larger protein fragment, containing GRD and RGCT [47,48]. These works together with homology modeling, based on the RHOGAP in complex with RHOA [49] and CDC42 [50], and RASGAP in complex with HRAS [51], provided a structural model of IQGAP1 GRD that contacts the switch regions of the GTP-bound CDC42 [47,48,52]. In contrast, another study has shown phosphomimetic variants of IQGAP1 at position S1441 and S1443 were significantly impaired in interacting with active CDC42 [46]. This strongly indicates that regions downstream of GRD, may also be critical in the interaction with RAC1 and CDC42. In an attempt to resolve this controversy, we set out to investigate comprehensively the structure-function relationship of IQGAP1 interaction with the RHO proteins. Detailed characterization of the IQGAP1 interaction with the RHO family members, using time-resolved fluorescence spectroscopy, provided unprecedented insights into the structure, function, and mechanistic properties of IQGAP1, especially regarding its interaction with RAC- and CDC42-like proteins. Obtained data showed that GRD-C associated with the RAC- and CDC42-like proteins (RAC1, RAC2, RAC3, RHOG, CDC42, and TC10), but not with RHOA, RHOB, RHOC, RHOD, TCL, RND and RIF. Furthermore, GRD1 and GRD2 do not associate with RAC1 under this experimental condition. We next investigated the effect of the last 99 amino acids of IQGAP1 on RAC1 and CDC42 binding and our results clearly suggest that the very C-terminal region of IQGAP1 may negatively regulate GBD-RAC1/CDC42 interaction. Moreover, we found that point mutations of the PKC α phosphorylation sites (S1441 and S1443) differently affect GRD-GBD association with RAC1/CDC42-mantGppNHp. Additionally, equilibrium measurement using fluorescence polarization experiments showed that IQGAP1GRD2 also interacts with RAC1 and CDC42 but with a much lower affinity and in a largely nucleotide-independent manner as compared with IQGAP1GRD-C. Results described here clearly suggest that IQGAP1 binds RAC1- and CDC42-like proteins at least at two sites by utilizing the GBD domain rather than the GRD domain to contact the switch regions.

MATERIALS AND METHODS

Constructs. Different variants of pGEX vectors (pGEX2T, pGEX4T-1, pGEX3) encoding an N-terminal glutathione S-transferase (GST) fusion protein were used for the overexpression of various human IQGAP1 (Acc. no. P46940) variants (aa 863-1345, 962-1345, and 863-1657, 877-1558, 877-1558 S1443E and S1443A), human Plexin-B1 (Acc. no. O43157) (aa 1724-1903), human p67^{phox} (Acc. no. P19878) (aa 1-203), human PAK1 (Acc. No. Q13153) (aa 57-141), murine TIAM1 DH-PH (Acc. no. Q60610) (aa 1033–1404), human TrioN DH-PH (Acc. no. O75962) (aa 1226–1535), and human RHOGDI α (Acc. no. P52565) as well as human RHO-related genes, i.e. RAC1 (Acc. no. P63000) (aa 1-179), RAC2 (Acc. no. P15153) (aa 1-192), RAC3 (Acc. no. P60763) (aa 1-192), RHOG (Acc. no. P84095) (aa 1-178), RHOA (Acc. no. P61586) (aa 1-181), RHOB (Acc. no. P62745) (aa 1-181), RHOC (Acc. no. P08134) (aa 1-181), CDC42 (Acc. no. P60953) (aa 1-178), TC10 (Acc. no. P17081) (aa 2-193), TCL (Acc. no. Q9H4E5) (aa 2 – 197), RND1 (Acc. no. Q92730) (aa 1-232), RND2 (Acc. no. P52198) (aa 26-184), RND3 (Acc. no. P61587) (aa, 1-244), RIF (Acc. no. Q9HBH0) (aa 1-195), and mouse RHOD (Acc. no. P97348) (aa 2-193). pET46 EkLIC vector (Merck, Nottingham, United Kingdom) was used for the overexpression of IQGAP1 877-1558 S1441E, S1143D, S1441A/S1443A, and S1441E/S1443D mutants as a his tag protein. The Kazusa cDNA clone KIAA0051 [53] was used as a template for making mutants.

Proteins. All proteins were purified according to the protocols described [7,54,55]. Nucleotide-free RHO proteins were prepared using alkaline phosphatase (Roche) and phosphodiesterase (Sigma Aldrich) at 4°C as described [56]. Fluorescent methylantraniloyl (mant) was used to generate mantGDP and mantGppNHp bound RHO proteins, where GppNHp is non hydrolyzable analog of GTP. Quality and concentrations of labeled proteins were determined as described [56].

Fluorescence measurements. Kinetics measurements were monitored by stopped-flow apparatus (Hi-Tech Scientific SF-61 with a mercury xenon light source and TgK Scientific Kinetic Studio software), and performed as described [55]. The observed rate constants were fitted single exponentially using the GraFit program (Erithacus software).

Fluorescence polarization. Experiments were performed in a Fluoromax 4 fluorimeter in polarization mode as described [57]. The dissociation constant (K_d) were calculated by fitting the concentration dependent binding curve using a quadratic ligand binding equation.

Cell isolation and culture. Livers from male Wistar rats (local animal facility of the Heinrich Heine University) were enzymatically digested with collagenase H (Roche, Germany) and protease E (Merck, Germany). Primary hepatic stellate cell (HSC) isolation was followed by density gradient centrifugation. HSCs were feeded with Dulbecco's Modified Eagle Medium (DMEM) supplemented with 15% fetal calf serum and 50 units of penicillin/streptomycin (Gibco® Life Technologies).

Reverse transcriptase polymerase chain reaction. To isolated RNA, cells were lysed by QIAzol lysis reagent (QIAGEN, Germany) and proceed with RNeasy plus kit (Qiagen, Germany). To eliminate any possible genomic DNA contaminations, isolated RNAs were subjected to DNase with the DNA-free™ DNA Removal Kit (Ambion, Life Technologies, Germany). Transcription of the RNA to first strand complementary DNA (cDNA) was followed by using the ImProm-II™ reverse transcription system (Promega, Germany). Quantitative polymerase chain reaction (qPCR) was

performed using the SYBR Green reagent (Life Technologies, Germany). Primers are listed in Table S1. $2^{-\Delta Ct}$ method was used to calculate the mRNA levels according to relative endogenous levels of the HPRT1.

Immunoblotting. Cell membranes and nuclei were disturbed with lysis buffer (50 mM Tris-HCl pH 7.5, 100 mM NaCl, 2 mM MgCl₂, 1% Igepal CA-630, 10% glycerol, 20 mM beta-glycerolphosphate, 1 mM Ortho-Na₃VO₄, 1 EDTA-free inhibitor tablet). To normalize the amount of the total proteins, the Bradford assay applied to measure the protein concentration (Bio-Rad). Primary antibodies to mouse γ -tubulin (# T5326) Sigma-Aldrich; mouse RAC1 (05-389) millipore; rabbit CDC42 (2462) cell signaling; mouse IQGAP1 (ab56529) and rabbit IQGAP2 (ab181127) abcam were diluted in 5% non-fat milk (Merck, Germany)/TBST (Tris-buffered saline, 0.05% Tween 20), and incubated overnight in 4°C. After washing steps, membranes were incubated with horseradish peroxidase-coupled secondary antibodies for 1 h and signals were visualized by the ECL detection system (GE Healthcare) and images were collected using the ChemoCam Imager ECL (INTAS science imaging, Germany).

RESULTS

IQGAP1^{GRD-C} selectively associates with various RAC- and CDC42-like proteins

Kinetics of IQGAP1^{GRD-C} (IQGAP1⁸⁶³⁻¹⁶⁵⁷; **Fig. 1**) association with different RHO proteins was monitored using stopped-flow fluorescence spectroscopic methods established previously [58]. MantGppNHp (**Fig. 2A**) is a fluorescent, non-hydrolysable GTP analog and stopped-flow fluorescence is a direct way to monitor the association between two proteins in real-time [56]. Rapid mixing of GRD-C with active, mantGppNHp bound RAC1 and CDC42 resulted in change in fluorescence (**Figs. 2B and 2F green trace**), which represents the RAC1/CDC42-IQGAP1 association reaction. Under the same conditions, most remarkably, we did not observe any fluorescence change when mixing RAC1/CDC42-mantGppNHp with GRD itself (IQGAP1⁹⁶²⁻¹³⁴⁵) (**Figs. 2B and 2F red trace**). This was unexpected because GRD has been generally accepted as the RAC1- and CDC42-binding domain of IQGAP1 to date [40,41,46-48,52,59]. Under the same conditions we measured kinetics for other members of the RHO family and evaluated the data by single exponential fitting to obtain the respective observed rate constants (k_{obs}). Data presented in **figure 2B-G** show that GRD-C associated with various RAC- and CDC42-like proteins (RAC1, RAC2, RAC3, RHOG, CDC42 and TC10), but not with RHOA, RHOB, RHOC, RHOD, TCL and RIF. Mixing of mantGppNHp-bound form of the latter did not result in a fluorescence change (**Fig. 2H**). Due to instability, fluorescently labeled RND proteins could not be prepared. Therefore, their association with GRD-C was measured indirectly by premixing excess amounts of GTP-bound RND proteins with GRD-C before measuring its association with RAC1-mantGppNHp. RND1, RND2 and RND3 did not interfere with the RAC1-IQGAP1 interaction (**Fig. 2I**), indicating that IQGAP1 does also not associate with RND proteins under these conditions, while **Figure 2J** shows association competition of mantGppNHp-RAC1 with IQGAP1^{GRD-C} in the presence of excess amount of CDC42, or *vice versa*.

RAC2 showed highest affinity for IQGAP1^{GRD-C}

In some studies was previously shown that the binding affinity of CDC42 for IQGAP1 was considerably higher than that of RAC1 for IQGAP1 (see **Table 1**) [29,45,60]. Later *Owen et al.* reported that, IQGAP1 has similar affinities for both RAC1 and CDC42 (see **Table 1**) [47]. Here

individual kinetic parameters were determined for the interaction of IQGAP1^{GRD-C} with RAC- and CDC42-like proteins under conditions described previously [55]. An incremental increase in fluorescence was observed when increasing the concentrations of GRD-C were rapidly mixed with RAC1-mantGppNHp (**Fig. 3A**). Increase in fluorescence was also observed for other RAC- and CDC42-like proteins except for CDC42 that the mode of interaction was different and we observed decrease in fluorescence (**Fig. S3**). Association kinetics was then performed for all other RAC- and CDC42-like proteins. k_{obs} values obtained by a single exponential fitting were evaluated in a linear fashion as a function of the GRD-C concentration (**Fig. 3B**), which yielded the respective association rate constants (k_{on}). The dissociation of GRD-C from its complex with RAC1-mantGppNHp was measured in a displacement experiment when excess amounts of RAC1-GppNHp were rapidly mixed with the complex. This led expectedly to fast decrease (for CDC42; increase) in fluorescence (**Figs. S2 and S4**), which was also observed for other RAC- and CDC42-like proteins (data not shown). Exponential fitting of the curves yielded the dissociation rate constants (k_{off}). The dissociation constants (K_d) (**Fig. 3D**, Green bars), which is the binding affinity and defined as the strength of IQGAP-RHO protein interactions was ultimately calculated from the ratio of the k_{off} values (**Fig. 3D**, Orange bars) divided by the k_{on} values (**Fig. 3D**, Blue bars). Accordingly, RAC2 turned out to possess the highest affinity for GRD-C that was between 16- and 75-fold higher than that of the other RHO proteins (**Fig. 4D**, Green bars). All individual data are summarized in **Table 1**.

GBD but not GRD appears to be critical for the IQGAP1 interaction with RAC1 and CDC42

To further prove the critical role of the more C-terminal domains of IQGAP1 beyond GRD we generated various deletion and point mutations of IQGAP1 (**Fig. 1**). **Figures 4A, S1, and S3** clearly show that GRD1 and GRD2 do not associate with RAC1 and CDC42 under this experimental condition. We next measured the effect of the last 99 amino acids of IQGAP1 on RAC1 and CDC42 binding and found that GRD-GBD (IQGAP1⁸⁷⁷⁻¹⁵⁵⁸), which lacks this region associated 3-fold faster with RAC1 as compared to GRD-C. Moreover, we found that point mutations of the PKC α phosphorylation sites (S1441 and S1443; **Fig. 1**) differently affect GRD-GBD association with RAC1-mantGppNHp. In contrast to GRD-GBD^{SE} (Ser1441 substituted by Glu), GRD-GBD^{SD} (Ser1443 substituted by Asp), and the double mutations GRD-GBD SE/SD (phosphomimetic substitutions) and GRD-GBD SA/SA (neutral substitutions to Ala) completely abolished GRD-GBD association with RAC1 and CDC42 (**Fig. 4A**).

As it is shown in **Figures 4B and 4C**, association kinetics were performed for the interaction of GRD-C, GRD-GBD, and GRD-GBD^{SE} with RAC1 and CDC42. k_{obs} values gained by a single exponential fitting were evaluated in a linear fashion as a function of the GRD-C, GRD-GBD, and GRD-GBD^{SE} concentrations, which yielded the respective association rate constants (k_{on}). The k_{on} for all three variants was almost similar and the same pattern was observed for RAC1 and CDC42 (**Figs. 4B and 4C**). The dissociation of all three proteins from their complex with RAC1-/CDC42-mantGppNHp was measured in a displacement experiment in the presence of excess amounts of RAC1- and CDC42-GppNHp mixed with the complex (**Figs. S2 and S4**). Exponential fitting of the curves yielded the dissociation rate constants (k_{off}) (**Figs. 4B and 4C**). The binding affinity (K_d) as the strength of IQGAP1-RAC1/CDC42 interactions was calculated from the ratio of the k_{off} values divided by the k_{on} values. Our results showed 2 folds lower K_d of GRD-GBD^{SE} compared to GRD-GBD in the case of RAC1, and K_d for CDC42 was not significantly changed (**Figs. 4B and C**, Green bars).

IQGAP1 possesses at least two RAC/CDC42-binding domains

To further shed light on the potent interaction of GRD-C versus GRD alone we used a different method, fluorescence polarization, that measures the binding affinity of two proteins and provide an equilibrium dissociation constant (K_d) of their interaction. As shown in figures 5A-5C, both IQGAP1 variants, GRD-C and GRD do in fact interact with mantGppNHp-bound RAC1 and CDC42 but as expected not with RHOA using fluorescence polarization (equilibrium mode). Evaluated K_d values obtained from the measurements showed that GRD-C is a high affinity binder as compared to GRD with 10-15-fold lower affinity for mantGppNHp-bound RAC1 and CDC42 (Fig. 5C; Table 1). This was not observed using Stopped-flow fluorescence, measuring the kinetics of the association in real-time, as is shown in figures 2 and 4A. Furthermore, for GRD-GBD and GRD-GBD^{SE} with mantGppNHp-bound RAC1 comparable affinity to GRD-C was observed but GRD-GBD^{SD} showed 5-8 folds lower affinity (Figs. 5E and 5F; Table 1). The explanation for our observations regarding binding of RAC1 to GRD is simple; in direct mode only a change in fluorescence can be observed when the associating protein (IQGAP1) binds to close vicinity of the fluorophore (mant group of the bound GppNHp) on the surface of RAC1 and CDC42 (Fig. 2). This surface covers the switch regions that changes their conformation upon a GDP/GTP exchange [4]. This is of fundamental importance because binding effectors (such as IQGAP1) to the switch regions determines the specificity of the signal transduction [4,58]. To prove this idea we repeated the measurements by using inactive RHO proteins bound to mantGDP. Both GRD-C and GRD were able to interact with CDC42-mantGDP although with very low affinities (Fig. 5G-H). This strongly suggests that IQGAP1 consists of two distinct binding domains, with GBD binding to the switch regions and with GRD that binds to other regions of CDC42 beyond the switch regions in a largely nucleotide-independent manner.

Differential expression analysis of IQGAPs in hepatic stellate cells

Each IQGAP isoform possess its specific binding partners and therefore contribute to different cellular processes. For instance, IQGAP1 is known as an oncogene where IQGAP2 is a tumor suppressor [22,38]. IQGAP2 is shown to express predominantly in liver. We asked the questions, is there any isoform preference for IQGAPs in the specific liver cell types called hepatic stellate cells and how they could scaffold the RHO proteins in these cells? Hepatic stellate cells (HSCs) reside in the Disse space of the liver and during chronic liver injuries become activated and contribute in either liver repair or fibrosis [61,62]. It is reported that the IQGAP1 play a role in HSC activation by binding to TGF- β receptor II and suppress HSC activation [39]. To investigate the biological function of IQGAP isoforms and their responsive target proteins (RAC and CDC42), freshly isolated HSCs were cultivated for 8 days that induce spontaneous activation of these cells. Quantitative RNA analysis revealed that IQGAP1 and 3 were upregulated during the activation process of HSCs where the IQGAP2 was downregulated. RAC2 exhibits the drastic increased in HSC d8, however, other RAC isoforms (RAC1 and 3) did not altered. To further investigate the correlation between the IQGAP1 regulation of RAC1 and CDC42 mechanisms in HSCs, the protein levels of IQGAP1, 2, RAC1, and CDC42 were detected. Consistent with qPCR data, obtained data showed IQGAP1 increase at proteins levels, where IQGAP2 is downregulated. The RAC1 and CDC42 exist at higher levels in activated HSCs (Fig. 6).

DISCUSSION

The interaction with the active, GTP-bound form of RAC1 and CDC42 identified IQGAP1 as a putative downstream effector [29,40,45-48,52,63-69]. Subsequent studies have shown that the interaction between IQGAP1 and the RHO proteins has significance on variety of biological functions. Accumulating evidence supports diverse roles for IQGAP-RHO protein interaction in vertebrates. However, the nature of such a protein-protein recognition process has remained obscure. While modulation of the cytoskeletal architecture was initially thought to be the primary function of the interaction of IQGAP1 with RHO proteins, it is now clear that they have some critical physiological roles beyond the cytoskeleton. CDC42 promotes the interaction of PTP1 with IQGAP1 to stimulate actin remodeling and, eventually, neurite outgrowth [70], and also complex of active CDC42, Lis1, and CLIP-170 with IQGAP1 seems to be crucial for cerebellar neuronal motility [66]. Another example is in the pancreatic β -cells. Analysis of the insulin secretory pathway has shown that IQGAP1 scaffolds CDC42, RAB27A, and coronin-3 and this complex controls endocytosis of insulin secretory membranes [71].

Of the RHO family proteins, RAC1, RHOA, and CDC42 have been most extensively studied and characterized [72]. In this study, a comprehensive interaction study of RHO proteins and C-terminal domain of IQGAP1⁸⁶³⁻¹⁶⁵⁷ (here called GRD-C) was conducted. Kinetics of GRD-C association with different RHO proteins was monitored using stopped-flow fluorescence spectroscopic methods (**Fig. 2**). The results clearly indicate that IQGAP1 binds among RHO proteins selectively to RAC- and CDC42-like proteins in the active form and that GRD-C most obviously recognizes and binds to the switch regions but however not, as previously proposed by several groups [47,48,52], the GRD alone. In contrast to our data, Casteel *et al.* have shown that GRD-C interacts with the active, G14V variant of RHOA and RHOC but not with that of RHOB, which were overexpressed in, and immunoprecipitated from human embryonic kidney 293T cell lysates [73]. In addition, recent immunoprecipitation studies have shown that IQGAP1 binds to both RHOA and p190A-RHOGAP to inactivate RHOA, and to modulate contractility of airway smooth muscle cells [74]. *Wu et al.* have also found RHOC and IQGAP1 in immunoprecipitates. This study has shown that an isoform-specific interaction of RHO proteins with IQGAP1 regulates cancer cell proliferation, and has been proposed that IQGAP1 is a downstream effector of RHOC in the regulation of gastric cancer cell migration [75,76]. In contrast, our study showed no physical interaction between GRD-C and the RHO isoforms, including RHOA or RHOC, under cell-free conditions using purified proteins. In this context, we think that observed interactions of GRD-C with RHOA and RHOC most likely are indirect, mediated by other proteins co-immunoprecipitated from cells expressing tagged RHO protein. We also exclude an interaction with other regions of RHOA outside switch regions evident from our fluorescence polarization data (**Figs. 5A-5C**).

Another striking observation was an increase in fluorescence upon association of GRD-C with RAC1, RAC2, RAC3, RHOG, and TC10 but a decrease in fluorescence with CDC42 (**Figs. 2, S1 and S3**). In contrast, we have monitored in an earlier study a fluorescence decrease for the association of the CDC42/RAC-interacting binding (CRIB) motif of the Wiskott-Aldrich syndrome protein (WASP) with the CDC42, RAC1 and TC10, respectively [58]. This observation indicates that (i) the binding mode of CDC42 interaction with IQGAP1 is different from that of TC10 and the RAC-like proteins, and (ii) the binding mode of IQGAP1 interaction with these RHO proteins differs from that of WASP. *Owen et al.* have studied GRD-C interaction with a large panel of RAC1 and CDC42

variants and have suggested, despite their 71% identity, RAC1 and CDC42 appear to have only partially overlapping binding sites on IQGAP1, and each uses different determinants to achieve high affinity binding [47]. However, our competition experiment has shown in **figure 2J** clearly indicated that GRD-C competitively associates with an overlapping binding region of RAC1 and CDC42.

The determination of individual kinetics parameters for the interaction of GRD-C with RAC- and CDC42-like proteins indicates that GRD-C may utilize a homologous set of associating residues of various CDC42-/RAC-like proteins, in spite of differences in the reaction rates (**Fig. 3D; Table 1**). The fact that six members of the RHO family and probably also WRCH1 and Chp/WRCH2 (not analyzed in this study), associate with IQGAP1 raises the question of how an interaction specificity is achieved in cells. RHOG is due to its high sequence similarity with the RAC proteins classified as a RAC-related protein, although it shares with RAC1 overlapping signal transduction pathways [77]. TC10 and RHOG interaction with IQGAP1 and IQGAP2, respectively, has been previously reported [78,79]. RHOG has been reported that do not bind to effectors such as PAK1, PAK5, PAK6, PAR6, IRSp53, WASP, or POSH, but on the other hand it binds in an activated GTP bound form to the RAC/CDC42-specific effectors MLK3, PLD1, and IQGAP2 which in turn, stimulates some downstream signaling targets of activated RAC1 and CDC42 such as JNK and Akt [78]. Although the consequence of TC10-IQGAP1 interaction is not defined, it seems to play a role in exocytosis and cell polarity. EXO70, a component of the exocyst complex, has been shown to bind to the N-terminal IQGAP1, most likely to the WW motif [77] but probably not to the IQ region because Exo70 was not found as binding partner of this region [21]. In mammals, RALA, a member of the RAS family, and TC10 have been shown to bind the exocyst [80]. TC10-EXO70 interaction is implicated in the tethering of GLUT4 vesicles to the plasma membrane in response to insulin [80-82], and in promoting neurite outgrowth [83-85]. IQGAP proteins has been shown to be involved in both processes [21,31,86]. Data presented in this study, revealed that TC10 has the fastest dissociation rate from GRD-C (**Fig. 3D**), suggesting that the IQGAP-TC10 complex requires stabilization by additional binding proteins, for example EXO70. Investigating the protein interaction network of the IQGAPs, modulating their function in space and time, remains an open and very interesting issue for future studies.

The highest affinity of RAC2 for GRD-C can most likely be attributed to distinct amino acid sequence deviations. The high affinity of RAC2 for IQGAP1 cannot be explained by comparing potential residues that may undergo direct interacting contacts in spite of high amino acid sequence identity of RAC isoforms. An aspect to be considered is the overall dynamics of the protein parts originated from few different amino acids all over the molecule. The lower flexibility of the switch I region of RAC2 in comparison to RAC1 and RAC3 may explain the functional differences of these proteins as it has been previously proposed to contribute to a higher TIAM1 activity on RAC2 compared to RAC1 and RAC3 [87].

Previous studies by other groups have shown that shorter IQGAP1 fragments, encompassing the GRD domain, are responsible for the RAC1 and CDC42 interactions. For the first time, *Zhang and coworkers* have shown that activated form of CDC42 is able to bound IQGAP1 GRD-C (aa 864-1657) [60]. One year later the same group reported that not only CDC42 but also RAC1, although with lower affinity, could interact to GRD-C [45]. Afterwards, *Nomanbhoy and Cerione*, have shown that GRD-C interacts tightly to CDC42-mantGTP using fluorescence assay [88]. *Owen et al.* have also reported that a GRD protein (aa 950-1407) was able to tightly bind CDC42(Q61L) with a

K_d value of 140 nM but failed to bind RAC1(Q61L) using scintillation proximity assay [47]. In this study, GRD-C (aa 864-1657) has shown a much higher affinity for the Q61L mutant of not only CDC42 but also RAC1, and yet the GRD was proposed to be the binding domain of IQGAP1 that associates with the switch regions of CDC42. Correspondingly, *Kurella et al.* have reported that GRD2 (aa 62-1345) binds CDC42 in a GTP-dependent manner with an affinity of 1300 nM using isothermal titration calorimetry [48]. These biochemical data (summarized in **Table 1**) along with homology modeling, based on the RAS-RASGAP structure [51], provided up to date a structural model of IQGAP1 GRD contacting the switch regions of the CDC42 which is generally accepted [40,41,46-48,52,59]. Contrary to the existing model, we observed a low-affinity, largely nucleotide-independent binding of GRD that associates with RAC- and CDC42-like proteins outside the switch regions. This was evidenced by kinetic measurements of GRD-GBD and GRD-C association, but not GDR, with RAC1 and CDC42 proteins (**Figs. 2 and 4**; no changes in fluorescence were observed with GRD). Conducted equilibrium measurements using fluorescence polarization not only substantiated the essential role of IQGAP1 GBD in a GTP-dependent interaction with RAC1 and CDC42 in support with our kinetic analysis but also provided striking insights into the main feature of IQGAP1 GRD. Our quantitative analysis under equilibrium conditions clearly revealed that GRD indeed undergoes a low-affinity, largely nucleotide-independent interaction with CDC42 and also RAC1 but in contrast to GBD its binding site resides outside the critical switch regions (**Fig. 5**). The significance of GBD (previously called RGTC) as a GTP-dependent interacting domain for RAC- and CDC42-like proteins was proved using single point mutants of GRD-GBD (e.g. Ser1443 substituted by Asp and Ala but not Ser1441 to Glu and Ala, two PKC α phosphorylation sites), which led to the abolishment of a GTP-dependent interaction of GRD-GBD while nucleotide-independent association through the GRD was unchanged. *Grohmanova and coworkers* previously have shown *via* GST pull down experiments and using MCF10A cell lysate, that in the presence of phosphatase inhibitor there is a significant reduction in the interaction between IQGAP1 and CDC42-GTP bound in contrast to CDC42 nucleotide depleted which bound to phosphorylated IQGAP1 much stronger [89]. In addition, our data have clearly demonstrated that the region upstream of GRD2 (aa 863-961) is dispensable for the RAC1 and CDC42 interaction. Another interesting issue was the inhibitory effect of the very C-terminal 99 amino acids (C domain) on the GBD determined through a 3-fold faster association of GRD-GBD (lacking the C domain) with RAC1 and CDC42 as compared to GRD-C. This is consistent with observations regarding the interaction of GRD and GBD-C domains with each other, favoring GTP-dependent binding to CDC42 [89,90].

Upon HSCs activation, quiescent HSCs develop into the cells that are able to contract and migrate. It is reported that IQGAP1 plays a role in HSC activation by binding to TGF- β receptor II and suppress HSC activation [39]. These observations raised the questions, which IQGAP isoforms are present in HSCs and is there any evidence that IQGAPs actively scaffolds RHO proteins in HSCs? To address these questions, first we investigated the expression pattern of IQGAP1, 2, 3, RAC1, 2, 3, and CDC42 in quiescent vs. activated HSCs. Our quantitative RNA analysis revealed that *IQGAP1* and *3* isoforms get upregulated during the activation process of HSCs while *IQGAP2* is down-regulated. At protein levels, we were able to detect IQGAP2 isoform only in quiescent HSCs while IQGAP1 was presented in both states of HSCs, and became upregulated during HSC activation. These results are in consistent with what *Schmidt and colleagues*, have reported regarding the reciprocal expression of IQGAP1 and 2 in human hepatocellular carcinomas, where

IQGAP1 increased and IQGAP2 decreased [91]. In quiescent HSCs, we speculate that IQGAP2 exerts its specific functions by scaffolding the distinct signaling components in different protein complexes than IQGAP1. Canonical Wnt signaling is very dynamic in quiescent HSCs and it is shown in other cells that IQGAP2 can interact with Dishevelled/ β -catenin, therefore in qHSCs IQGAP2 may modulate Wnt- β -catenin signaling and stimulate GFAP synthesis and cell-cycle arrest [92,93]. Another possibility would be, IQGAP2 competes with other scaffolding proteins to recruits RHO proteins and may interfere with RHO-dependent cell migration. The functions and specific binding partners of IQGAP2 in qHSCs remain to be investigated. aHSCs display the elevated levels of PDGF signaling and focal adhesion kinase (FAK), acts downstream of PDGF [94]. PDGF induces the IQGAP1-dependent complex formation of focal adhesion proteins (paxillin and vinculin) and PDGF receptor β [95]. IQGAP1 also binds to FAK [96], therefore, PDGF-IQGAP1 may regulate the focal adhesion assembly in aHSCs that is important for cell motility and migration.

Elevated levels of the RAC1 and CDC42 correlate with high amount of IQGAP1 in activated HSCs; we detected higher levels of RAC1, RAC2 and CDC42 in aHSCs than qHSCs. On the other hand, our biochemical studies demonstrated that RAC1 and CDC42 interact in GTP-bound forms with IQGAP1. Therefore, we suggest that IQGAP1 scaffolds RAC1 and CDC42 to regulate cell-adhesion and migration in these cells. However, the role of IQGAP1 in aHSCs needs to be investigated.

Taken together, our kinetic and equilibrium measurements clearly challenge the paradigm that the ability of IQGAP1 to interact with RAC/CDC42 proteins is mainly attributed to its GRD. On the contrary, we propose that the C-terminal half of IQGAP1 utilize at least three functionally distinct units, including GRD, GBD and C, to achieve the interaction with RAC1- and CDC42-like proteins. Keeping this in mind, the switch regions of the RHO family proteins have been previously proposed as the first binding site for the downstream effectors and if this first contact is achieved then additional contacts outside the switch regions will be required to guarantee effector activation [4]. Remarkably, IQGAP1 seems to employ a different strategy to interact with RAC1 and CDC42 proteins as schematically illustrated in **Figure 7**: (i) GRD undergoes a low-affinity, GDP-/GTP-independent complex with RAC1 and CDC42 proteins outside their switch regions in a way that is independent of the upstream signals, providing it is structurally accessible and available for interactions; (ii) GBD only binds to the RAC1 and CDC42 proteins if they are active and exist in the GTP-bound forms; (iii) the C-terminal region of IQGAP1 may potentiate the IQGAP1 interaction with RAC1 and CDC42 proteins by probably extending the resident time of the respective proteins complexes. Such a sequential association with the RAC1 and CDC42 proteins most likely leads to activation of IQGAP1, can be envisaged as conformational changes allowing further IQGAP1 interaction with its downstream targets depending on both the cell types and the upstream signals. We further propose that this is a conserved control mechanism also for IQGAP2 and probably also IQGAP3 due to high sequence homology.

CONFLICT OF INTEREST

The authors declare no conflict of interest.

ACKNOWLEDGEMENTS

This work was supported in part by the German Research Foundation (Deutsche Forschungsgemeinschaft or DFG) through both the Collaborative Research Center 974 (SFB 974) “Communication and Systems Relevance during Liver Injury and Regeneration” and the International Research Training Group 1902 (IRTG 1902) “Intra- and interorgan communication of the cardiovascular system”, and by the International Graduate School of Protein Science and Technology (iGRASP), and the Research committee of the Medical Faculty of the Heinrich-Heine University Düsseldorf (Grant Number 9772617).

REFERENCES

1. Yuan H, Zhang H, Wu X, Zhang Z, Du D, et al. (2009) Hepatocyte-specific deletion of Cdc42 results in delayed liver regeneration after partial hepatectomy in mice. *Hepatology* 49: 240-249.
2. Fukata M, Nakagawa M, Kaibuchi K (2003) Roles of Rho-family GTPases in cell polarisation and directional migration. *Curr Opin Cell Biol* 15: 590-597.
3. Hall A (2012) Rho family GTPases. *Biochem Soc Trans* 40: 1378-1382.
4. Dvorsky R, Ahmadian MR (2004) Always look on the bright site of Rho: structural implications for a conserved intermolecular interface. *EMBO Rep* 5: 1130-1136.
5. Lam BD, Hordijk PL (2013) The Rac1 hypervariable region in targeting and signaling: a tail of many stories. *Small GTPases* 4: 78-89.
6. Wennerberg K, Der CJ (2004) Rho-family GTPases: it's not only Rac and Rho (and I like it). *J Cell Sci* 117: 1301-1312.
7. Jaiswal M, Fansa EK, Dvorsky R, Ahmadian MR (2013) New insight into the molecular switch mechanism of human Rho family proteins: shifting a paradigm. *Biol Chem* 394: 89-95.
8. Jaiswal M, Dvorsky R, Ahmadian MR (2013) Deciphering the molecular and functional basis of Dbl family proteins: a novel systematic approach toward classification of selective activation of the Rho family proteins. *J Biol Chem* 288: 4486-4500.
9. Rossman KL, Der CJ, Sondek J (2005) GEF means go: turning on RHO GTPases with guanine nucleotide-exchange factors. *Nature reviews Molecular cell biology* 6: 167-180.
10. Tcherkezian J, Lamarche-Vane N (2007) Current knowledge of the large RhoGAP family of proteins. *Biology of the Cell* 99: 67-86.
11. Jaiswal M, Dvorsky R, Amin E, Risse SL, Fansa EK, et al. (2014) Functional cross-talk between ras and rho pathways: a Ras-specific GTPase-activating protein (p120RasGAP) competitively inhibits the RhoGAP activity of deleted in liver cancer (DLC) tumor suppressor by masking the catalytic arginine finger. *J Biol Chem* 289: 6839-6849.
12. DerMardirossian C, Bokoch GM (2005) GDIs: central regulatory molecules in Rho GTPase activation. *Trends Cell Biol* 15: 356-363.
13. Garcia-Mata R, Boulter E, BurrIDGE K (2011) The 'invisible hand': regulation of RHO GTPases by RHOGDIs. *Nature reviews Molecular cell biology* 12: 493-504.
14. Tnimov Z, Guo Z, Gambin Y, Nguyen UT, Wu YW, et al. (2012) Quantitative analysis of prenylated RhoA interaction with its chaperone, RhoGDI. *J Biol Chem* 287: 26549-26562.
15. Zhang SC, Gremer L, Heise H, Janning P, Shymanets A, et al. (2014) Liposome Reconstitution and Modulation of Recombinant Prenylated Human Rac1 by GEFs, GDI1 and Pak1. *PLoS ONE* 9: e102425.
16. Lei M, Lu W, Meng W, Parrini MC, Eck MJ, et al. (2000) Structure of PAK1 in an autoinhibited conformation reveals a multistage activation switch. *Cell* 102: 387-397.
17. Lapouge K, Smith SJ, Walker PA, Gamblin SJ, Smerdon SJ, et al. (2000) Structure of the TPR domain of p67phox in complex with Rac.GTP. *Mol Cell* 6: 899-907.
18. Fansa EK, Dvorsky R, Zhang SC, Fiegen D, Ahmadian MR (2013) Interaction characteristics of Plexin-B1 with Rho family proteins. *Biochem Biophys Res Commun* 434: 785-790.
19. Hota PK, Buck M (2012) Plexin structures are coming: opportunities for multilevel investigations of semaphorin guidance receptors, their cell signaling mechanisms, and functions. *Cell Mol Life Sci* 69: 3765-3805.
20. Watanabe T, Wang S, Kaibuchi K (2015) IQGAPs as Key Regulators of Actin-cytoskeleton Dynamics. *Cell Struct Funct* 40: 69-77.
21. Hedman AC, Smith JM, Sacks DB (2015) The biology of IQGAP proteins: beyond the cytoskeleton. *EMBO reports* 16: 427-446.
22. White CD, Brown MD, Sacks DB (2009) IQGAPs in cancer: a family of scaffold proteins underlying tumorigenesis. *FEBS Lett* 583: 1817-1824.
23. Bishop AL, Hall A (2000) Rho GTPases and their effector proteins. *Biochem J* 348 Pt 2: 241-255.
24. White CD, Erdemir HH, Sacks DB (2012) IQGAP1 and its binding proteins control diverse biological functions. *Cell Signal* 24: 826-834.
25. Abel AM, Schuldt KM, Rajasekaran K, Hwang D, Riese MJ, et al. (2015) IQGAP1: insights into the function of a molecular puppeteer. *Mol Immunol* 65: 336-349.

26. Heasman SJ, Ridley AJ (2008) Mammalian Rho GTPases: new insights into their functions from in vivo studies. *Nature reviews Molecular cell biology* 9: 690-701.
27. Smith JM, Hedman AC, Sacks DB (2015) IQGAPs choreograph cellular signaling from the membrane to the nucleus. *Trends Cell Biol* 25: 171-184.
28. Johnson M, Sharma M, Henderson BR (2009) IQGAP1 regulation and roles in cancer. *Cell Signal* 21: 1471-1478.
29. McCallum SJ, Wu WJ, Cerione RA (1996) Identification of a putative effector for Cdc42Hs with high sequence similarity to the RasGAP-related protein IQGAP1 and a Cdc42Hs binding partner with similarity to IQGAP2. *J Biol Chem* 271: 21732-21737.
30. Brill S, Li S, Lyman CW, Church DM, Wasmuth JJ, et al. (1996) The Ras GTPase-activating-protein-related human protein IQGAP2 harbors a potential actin binding domain and interacts with calmodulin and Rho family GTPases. *Mol Cell Biol* 16: 4869-4878.
31. Wang S, Watanabe T, Noritake J, Fukata M, Yoshimura T, et al. (2007) IQGAP3, a novel effector of Rac1 and Cdc42, regulates neurite outgrowth. *J Cell Sci* 120: 567-577.
32. Nojima H, Adachi M, Matsui T, Okawa K, Tsukita S (2008) IQGAP3 regulates cell proliferation through the Ras/ERK signalling cascade. *Nat Cell Biol* 10: 971-978.
33. Schmidt VA, Scudder L, Devoe CE, Bernardis A, Cupit LD, et al. (2003) IQGAP2 functions as a GTP-dependent effector protein in thrombin-induced platelet cytoskeletal reorganization. *Blood* 101: 3021-3028.
34. Cupit LD, Schmidt VA, Miller F, Bahou WF (2004) Distinct PAR/IQGAP expression patterns during murine development: implications for thrombin-associated cytoskeletal reorganization. *Mamm Genome* 15: 618-629.
35. Mateer SC, Wang N, Bloom GS (2003) IQGAPs: integrators of the cytoskeleton, cell adhesion machinery, and signaling networks. *Cell Motil Cytoskeleton* 55: 147-155.
36. Brandt DT, Grosse R (2007) Get to grips: steering local actin dynamics with IQGAPs. *EMBO Rep* 8: 1019-1023.
37. Smith JM, Hedman AC, Sacks DB (2015) IQGAPs choreograph cellular signaling from the membrane to the nucleus. *Trends Cell Biol*.
38. White CD, Khurana H, Gnatenko DV, Li Z, Odze RD, et al. (2010) IQGAP1 and IQGAP2 are reciprocally altered in hepatocellular carcinoma. *BMC Gastroenterol* 10: 125.
39. Liu C, Billadeau DD, Abdelhakim H, Leof E, Kaibuchi K, et al. (2013) IQGAP1 suppresses TbetarII-mediated myofibroblastic activation and metastatic growth in liver. *J Clin Invest* 123: 1138-1156.
40. Hart MJ, Callow MG, Souza B, Polakis P (1996) IQGAP1, a calmodulin-binding protein with a rasGAP-related domain, is a potential effector for cdc42Hs. *Embo J* 15: 2997-3005.
41. Ho YD, Joyal JL, Li Z, Sacks DB (1999) IQGAP1 integrates Ca²⁺/calmodulin and Cdc42 signaling. *J Biol Chem* 274: 464-470.
42. Malarkannan S, Awasthi A, Rajasekaran K, Kumar P, Schuldt KM, et al. (2012) IQGAP1: a regulator of intracellular spacetime relativity. *J Immunol* 188: 2057-2063.
43. Liu J, Guidry JJ, Worthylake DK (2014) Conserved sequence repeats of IQGAP1 mediate binding to Ezrin. *J Proteome Res* 13: 1156-1166.
44. Pathmanathan S, Hamilton E, Atcheson E, Timson DJ (2011) The interaction of IQGAPs with calmodulin-like proteins. *Biochem Soc Trans* 39: 694-699.
45. Zhang B, Chernoff J, Zheng Y (1998) Interaction of Rac1 with GTPase-activating proteins and putative effectors. A comparison with Cdc42 and RhoA. *J Biol Chem* 273: 8776-8782.
46. Elliott SF, Allen G, Timson DJ (2012) Biochemical analysis of the interactions of IQGAP1 C-terminal domain with CDC42. *World J Biol Chem* 3: 53-60.
47. Owen D, Campbell LJ, Littlefield K, Evetts KA, Li Z, et al. (2008) The IQGAP1-Rac1 and IQGAP1-Cdc42 interactions: interfaces differ between the complexes. *J Biol Chem* 283: 1692-1704.
48. Kurella VB, Richard JM, Parke CL, Lecour LF, Jr., Bellamy HD, et al. (2009) Crystal structure of the GTPase-activating protein-related domain from IQGAP1. *J Biol Chem* 284: 14857-14865.
49. Rittinger K, Walker PA, Eccleston JF, Nurmahomed K, Owen D, et al. (1997) Crystal structure of a small G protein in complex with the GTPase-activating protein rhoGAP. *Nature* 388: 693-697.
50. Nassar N, Hoffman GR, Manor D, Clardy JC, Cerione RA (1998) Structures of Cdc42 bound to the active and catalytically compromised forms of Cdc42GAP. *Nat Struct Biol* 5: 1047-1052.
51. Scheffzek K, Ahmadian MR, Kabsch W, Wiesmuller L, Lautwein A, et al. (1997) The Ras-RasGAP complex: structural basis for GTPase activation and its loss in oncogenic Ras mutants. *Science* 277: 333-338.

52. Mataraza JM, Briggs MW, Li Z, Frank R, Sacks DB (2003) Identification and characterization of the Cdc42-binding site of IQGAP1. *Biochem Biophys Res Commun* 305: 315-321.
53. Suyama M, Nagase T, Ohara O (1999) HUGE: a database for human large proteins identified by Kazusa cDNA sequencing project. *Nucleic Acids Res* 27: 338-339.
54. Fiegen D, Blumenstein L, Stege P, Vetter IR, Ahmadian MR (2002) Crystal structure of Rnd3/RhoE: functional implications. *FEBS letters* 525: 100-104.
55. Hemsath L, Ahmadian MR (2005) Fluorescence approaches for monitoring interactions of Rho GTPases with nucleotides, regulators, and effectors. *Methods* 37: 173-182.
56. Jaiswal M, Dubey BN, Koessmeier KT, Gremer L, Ahmadian MR (2012) Biochemical assays to characterize Rho GTPases. *Methods in molecular biology* 827: 37-58.
57. Nouri K, J. MM, Milroy LG, Hain A, Dvorsky R, et al. (2015) Biophysical Characterization of Nucleophosmin Interactions with Human Immunodeficiency Virus Rev and Herpes Simplex Virus US11. *PLoS ONE*.
58. Hemsath L, Dvorsky R, Fiegen D, Carlier MF, Ahmadian MR (2005) An electrostatic steering mechanism of Cdc42 recognition by Wiskott-Aldrich syndrome proteins. *Mol Cell* 20: 313-324.
59. Kuroda S, Fukata M, Nakagawa M, Fujii K, Nakamura T, et al. (1998) Role of IQGAP1, a target of the small GTPases Cdc42 and Rac1, in regulation of E-cadherin-mediated cell-cell adhesion. *Science* 281: 832-835.
60. Zhang B, Wang ZX, Zheng Y (1997) Characterization of the interactions between the small GTPase Cdc42 and its GTPase-activating proteins and putative effectors. Comparison of kinetic properties of Cdc42 binding to the Cdc42-interactive domains. *J Biol Chem* 272: 21999-22007.
61. Kordes C, Häussinger D (2013) Hepatic stem cell niches. *Journal of Clinical Investigation* 123: 1874-1880.
62. Yin C, Evason KJ, Asahina K, Stainier DYS (2013) Hepatic stellate cells in liver development, regeneration, and cancer. *Journal of Clinical Investigation* 123: 1902-1910.
63. Kuroda S, Fukata M, Nakagawa M, Kaibuchi K (1999) Cdc42, Rac1, and their effector IQGAP1 as molecular switches for cadherin-mediated cell-cell adhesion. *Biochem Biophys Res Commun* 262: 1-6.
64. Izumi G, Sakisaka T, Baba T, Tanaka S, Morimoto K, et al. (2004) Endocytosis of E-cadherin regulated by Rac and Cdc42 small G proteins through IQGAP1 and actin filaments. *J Cell Biol* 166: 237-248.
65. Watanabe T, Wang S, Noritake J, Sato K, Fukata M, et al. (2004) Interaction with IQGAP1 links APC to Rac1, Cdc42, and actin filaments during cell polarization and migration. *Dev Cell* 7: 871-883.
66. Kholmanskikh SS, Koeller HB, Wynshaw-Boris A, Gomez T, Letourneau PC, et al. (2006) Calcium-dependent interaction of Lis1 with IQGAP1 and Cdc42 promotes neuronal motility. *Nat Neurosci* 9: 50-57.
67. Brown MD, Bry L, Li Z, Sacks DB (2007) IQGAP1 regulates Salmonella invasion through interactions with actin, Rac1, and Cdc42. *J Biol Chem* 282: 30265-30272.
68. Sakurai-Yageta M, Recchi C, Le Dez G, Sibarita JB, Daviet L, et al. (2008) The interaction of IQGAP1 with the exocyst complex is required for tumor cell invasion downstream of Cdc42 and RhoA. *J Cell Biol* 181: 985-998.
69. Noritake J, Watanabe T, Sato K, Wang S, Kaibuchi K (2005) IQGAP1: a key regulator of adhesion and migration. *J Cell Sci* 118: 2085-2092.
70. Li Z, McNulty DE, Marler KJ, Lim L, Hall C, et al. (2005) IQGAP1 promotes neurite outgrowth in a phosphorylation-dependent manner. *J Biol Chem* 280: 13871-13878.
71. Kimura T, Yamaoka M, Taniguchi S, Okamoto M, Takei M, et al. (2013) Activated Cdc42-bound IQGAP1 determines the cellular endocytic site. *Mol Cell Biol* 33: 4834-4843.
72. Etienne-Manneville S, Hall A (2002) Rho GTPases in cell biology. *Nature* 420: 629-635.
73. Casteel DE, Turner S, Schwappacher R, Rangaswami H, Su-Yuo J, et al. (2012) Rho isoform-specific interaction with IQGAP1 promotes breast cancer cell proliferation and migration. *The Journal of biological chemistry* 287: 38367-38378.
74. Bhattacharya M, Sundaram A, Kudo M, Farmer J, Ganesan P, et al. (2014) IQGAP1-dependent scaffold suppresses RhoA and inhibits airway smooth muscle contraction. *J Clin Invest* 124: 4895-4898.
75. Wu Y, Tao Y, Chen Y, Xu W (2012) RhoC regulates the proliferation of gastric cancer cells through interaction with IQGAP1. *PLoS ONE* 7: 7.
76. Clark EA, Golub TR, Lander ES, Hynes RO (2000) Genomic analysis of metastasis reveals an essential role for RhoC. *Nature* 406: 532-535.

77. Prieto-Sanchez RM, Bustelo XR (2003) Structural basis for the signaling specificity of RhoG and Rac1 GTPases. *J Biol Chem* 278: 37916-37925.
78. Wennerberg K, Ellerbroek SM, Liu RY, Karnoub AE, Burridge K, et al. (2002) RhoG signals in parallel with Rac1 and Cdc42. *J Biol Chem* 277: 47810-47817.
79. Neudauer CL, Joberty G, Tatis N, Macara IG (1998) Distinct cellular effects and interactions of the Rho-family GTPase TC10. *Curr Biol* 8: 1151-1160.
80. Inoue M, Chang L, Hwang J, Chiang SH, Saltiel AR (2003) The exocyst complex is required for targeting of Glut4 to the plasma membrane by insulin. *Nature* 422: 629-633.
81. Inoue M, Chiang SH, Chang L, Chen XW, Saltiel AR (2006) Compartmentalization of the exocyst complex in lipid rafts controls Glut4 vesicle tethering. *Mol Biol Cell* 17: 2303-2311.
82. Chiang SH, Chang L, Saltiel AR (2006) TC10 and insulin-stimulated glucose transport. *Methods Enzymol* 406: 701-714.
83. Pommereit D, Wouters FS (2007) An NGF-induced Exo70-TC10 complex locally antagonises Cdc42-mediated activation of N-WASP to modulate neurite outgrowth. *J Cell Sci* 120: 2694-2705.
84. Dupraz S, Grassi D, Bernis ME, Sosa L, Bisbal M, et al. (2009) The TC10-Exo70 complex is essential for membrane expansion and axonal specification in developing neurons. *J Neurosci* 29: 13292-13301.
85. Fujita A, Koinuma S, Yasuda S, Nagai H, Kamiguchi H, et al. (2013) GTP hydrolysis of TC10 promotes neurite outgrowth through exocytic fusion of Rab11- and L1-containing vesicles by releasing exocyst component Exo70. *PLoS ONE* 8.
86. Ory S, Gasman S (2011) Rho GTPases and exocytosis: what are the molecular links? *Semin Cell Dev Biol* 22: 27-32.
87. Haeusler LC, Blumenstein L, Stege P, Dvorsky R, Ahmadian MR (2003) Comparative functional analysis of the Rac GTPases. *FEBS letters* 555: 556-560.
88. Nomanbhoy T, Cerione RA (1999) Fluorescence assays of Cdc42 interactions with target/effector proteins. *Biochemistry* 38: 15878-15884.
89. Grohmanova K, Schlaepfer D, Hess D, Gutierrez P, Beck M, et al. (2004) Phosphorylation of IQGAP1 modulates its binding to Cdc42, revealing a new type of rho-GTPase regulator. *J Biol Chem* 279: 48495-48504.
90. Le Clairche C, Schlaepfer D, Ferrari A, Klingauf M, Grohmanova K, et al. (2007) IQGAP1 stimulates actin assembly through the N-WASP-Arp2/3 pathway. *J Biol Chem* 282: 426-435.
91. White CD, Khurana H, Gnatenko DV, Li Z, Odze RD, et al. (2010) IQGAP1 and IQGAP2 are Reciprocally Altered in Hepatocellular Carcinoma. *BMC Gastroenterology* 10: 125.
92. Kordes C, Sawitza I, Häussinger D (2008) Canonical Wnt signaling maintains the quiescent stage of hepatic stellate cells. *Biochemical and Biophysical Research Communications* 367: 116-123.
93. Schmidt VA, Chiariello CS, Capilla E, Miller F, Bahou WF (2008) Development of hepatocellular carcinoma in Iqgap2-deficient mice is IQGAP1 dependent. *Mol Cell Biol* 28: 1489-1502.
94. Carloni V, Pinzani M, Giusti S, Romanelli RG, Parola M, et al. (2000) Tyrosine phosphorylation of focal adhesion kinase by PDGF is dependent on ras in human hepatic stellate cells. *Hepatology* 31: 131-140.
95. Kohno T, Urao N, Ashino T, Sudhakar V, Inomata H, et al. (2013) IQGAP1 links PDGF receptor-beta signal to focal adhesions involved in vascular smooth muscle cell migration: role in neointimal formation after vascular injury. *Am J Physiol Cell Physiol* 305: C591-600.
96. Cheung KL, Lee JH, Shu L, Kim JH, Sacks DB, et al. (2013) The Ras GTPase-activating-like protein IQGAP1 mediates Nrf2 protein activation via the mitogen-activated protein kinase/extracellular signal-regulated kinase (ERK) kinase (MEK)-ERK pathway. *J Biol Chem* 288: 22378-22386.

Table 1. Data summary for the interaction of RHO proteins with IQGAP variants

Proteins ^a	K_d (nM) ^{b1}	Method ^c	Reference
IQGAP1 ⁸⁶³⁻¹³⁴⁵ /RAC1-mantGppNHp	no binding	FM	this study
IQGAP1 ⁸⁶³⁻¹³⁴⁵ /CDC42-mantGppNHp	no binding	FM	this study
IQGAP1 ⁹⁶²⁻¹³⁴⁵ /RAC1-mantGppNHp	no binding	FM	this study
IQGAP1 ⁹⁶²⁻¹³⁴⁵ /CDC42-mantGppNHp	no binding	FM	this study
IQGAP1 ⁸⁶³⁻¹⁶⁵⁷ /RAC1-mantGppNHp	1,420	FM	this study
IQGAP1 ⁸⁶³⁻¹⁶⁵⁷ /CDC42-mantGppNHp	2,000	FM	this study
IQGAP1 ⁸⁶³⁻¹⁶⁵⁷ /RAC2-mantGppNHp	27	FM	this study
IQGAP1 ⁸⁶³⁻¹⁶⁵⁷ /RAC3-mantGppNHp	450	FM	this study
IQGAP1 ⁸⁶³⁻¹⁶⁵⁷ /RHOG-mantGppNHp	490	FM	this study
IQGAP1 ⁸⁶³⁻¹⁶⁵⁷ /TC10-mantGppNHp	1,530	FM	this study
IQGAP1 ⁸⁷⁷⁻¹⁵⁵⁸ /RAC1-mantGppNHp	4,110	FM	this study
IQGAP1 ⁸⁷⁷⁻¹⁵⁵⁸ /CDC42-mantGppNHp	4,200	FM	this study
IQGAP1 ^{877-1558(S1441E)} /RAC1-mantGppNHp	9,960	FM	this study
IQGAP1 ^{877-1558(S1441E)} /CDC42-mantGppNHp	6,060	FM	this study
IQGAP1 ^{877-1558(S1443D)} /RAC1-mantGppNHp	no binding	FM	this study
IQGAP1 ^{877-1558(S1443D)} /CDC42-mantGppNHp	no binding	FM	this study
IQGAP1 ^{877-1558(SS/AA)} /RAC1-mantGppNHp	no binding	FM	this study
IQGAP1 ^{877-1558(SS/AA)} /CDC42-mantGppNHp	no binding	FM	this study
IQGAP1 ^{877-1558(SS/ED)} /RAC1-mantGppNHp	no binding	FM	this study
IQGAP1 ^{877-1558(SS/ED)} /CDC42-mantGppNHp	no binding	FM	this study
IQGAP1 ⁸⁷⁷⁻¹⁵⁵⁸ /CDC42-GTP	1,300	SPR	[46]
IQGAP1 ^{877-1558(S1441E)} /CDC42-GTP	220,000	SPR	[46]
Proteins ^a	eK_d (nM) ^{b2}	Method ^c	Reference
IQGAP ⁹⁶²⁻¹³⁴⁵ /RAC1-mantGppNHp	8,145	FP	this study
IQGAP ⁹⁶²⁻¹³⁴⁵ /CDC42-mantGDP	184,700	FP	this study
IQGAP ⁸⁶³⁻¹⁶⁵⁷ /RAC1-mantGppNHp	5,530	FP	this study
IQGAP ⁸⁶³⁻¹⁶⁵⁷ /CDC42-mantGDP	95,100	FP	this study
IQGAP ⁹⁶²⁻¹³⁴⁵ /CDC42-mantGppNHp	30,200	FP	this study
IQGAP ⁸⁶³⁻¹⁶⁵⁷ /CDC42-mantGppNHp	3,400	FP	this study
IQGAP ⁹⁶²⁻¹³⁴⁵ /RHOA-mantGppNHp	no binding	FP	this study
IQGAP ⁸⁶³⁻¹⁶⁵⁷ /RHOA-mantGppNHp	no binding	FP	this study
IQGAP1 ⁸⁷⁷⁻¹⁵⁵⁸ /RAC1-mantGppNHp	4,570	FP	this study
IQGAP1 ^{877-1558(S1441E)} /RAC1-mantGppNHp	6,680	FP	this study
IQGAP1 ^{877-1558(S1443D)} /RAC1-mantGppNHp	288,300	FP	this study
IQGAP1 ⁸⁶⁴⁻¹⁶⁵⁷ /CDC42-mantdGTP	28	FA	[88]
IQGAP1 ⁸⁶⁴⁻¹⁶⁵⁷ /RAC1 ^{Q61L} -[³ H]GTP	18	SPA	[47]
IQGAP1 ⁹⁵⁰⁻¹⁴⁰⁷ /RAC1 ^{Q61L} -[³ H]GTP	no binding	SPA	[47]
IQGAP1 ⁸⁶⁴⁻¹⁶⁵⁷ /CDC42 ^{Q61L} -[³ H]GTP	24	SPA	[47]
IQGAP1 ⁹⁵⁰⁻¹⁴⁰⁷ /CDC42 ^{Q61L} -[³ H]GTP	140	SPA	[47]
IQGAP1 ⁹⁶²⁻¹³⁴⁵ /CDC42-GTP	1,300	ITC	[48]
IQGAP1 ⁹⁶²⁻¹³⁴⁵ /CDC42-GDP	no binding	ITC	[48]
Proteins ^a	K_i (nM) ^{b3}	Method ^c	Reference
IQGAP1 ⁸⁶⁴⁻¹⁶⁵⁷ /CDC42-GTP	82	PRA	[60]
IQGAP1 ⁸⁶⁴⁻¹⁶⁵⁷ /CDC42-GTP	390	PRA	[45]
IQGAP1 ⁸⁶⁴⁻¹⁶⁵⁷ /RAC1-GTP	2,130	PRA	[45]

^aIQGAP1 proteins; ^{b1}the binding affinity of the IQGAP proteins for various RHO proteins has been analyze in different ways: ^{b1}under kinetic condition that provides the individual association and dissociation rate constant (k_{on} and k_{off}) and determines the dissociation constants (K_d) or ^{b2}under equilibrium conditions by determining the equilibrium dissociation constants (eK_d) or ^{b3}under competitive reaction conditions, for example inhibition the intrinsic GTP-hydrolysis reaction the RHO proteins that determines the equilibrium inhibition constant (K_i); ^c FM, fluorescence measurement by stopped flow, FA, fluorescence assay; FP, fluorescence polarization; ITC, isothermal titration calorimetry; PRA, Phosphate-release assay; SPA, scintillation proximity assay; SPR, surface plasmon resonance.

FIGURE LEGENDS

Figure 1. Schematic representation of domain organization and various constructs and proteins of IQGAP1. (A) Domain organization (color coded) along with the PKC α phosphorylation sites and constructs relevant to this project. (B) Coomassie brilliant blue (CBB) stained SDS-PAGE of purified IQGAP1 used in this study.

Figure 2. GRD-C selectively associates with various RAC- and CDC42-like proteins. (A) Chemical structure of mantGppNHp, a fluorescently labelled, non-hydrolyzable GTP analog. (B-H) Association of GRD-C (2 μ M) with mantGppNHp-bound RHO proteins (0.2 μ M). B and F also show the association of RAC1 and CDC42 with GRD-C (green), but not with GRD (red). (I) Association of mantGppNHp-RAC1 (0.2 μ M) with IQGAP1^{GRD-C} (2 μ M) in the presence of excess amount of RND1, RND2 or RND3 (10 μ M). (J) Association of RAC1-mantGppNHp (0.2 μ M) with IQGAP1GRD-C (2 μ M) in the presence of excess amount of CDC42-GppNHp (10 μ M), and *vice versa*.

Figure 3. Kinetic measurements of GRD-C with RAC- and CDC42-like proteins. (A) Association of RAC1-mantGppNHp (0.2 μ M) with increasing GRD-C concentrations (0.25-8 μ M). (B) Association rates (k_{on}) of GRD-C binding RHO proteins. (C) Dissociation of GRD-C (2 μ M) from RAC1-mantGppNHp (0.2 μ M) in the presence of unlabeled RAC1-GppNHp (10 μ M). (D) Association rates (k_{on}), dissociation rates (k_{off}) and dissociation constants (k_d) of GRD-C binding RHO proteins.

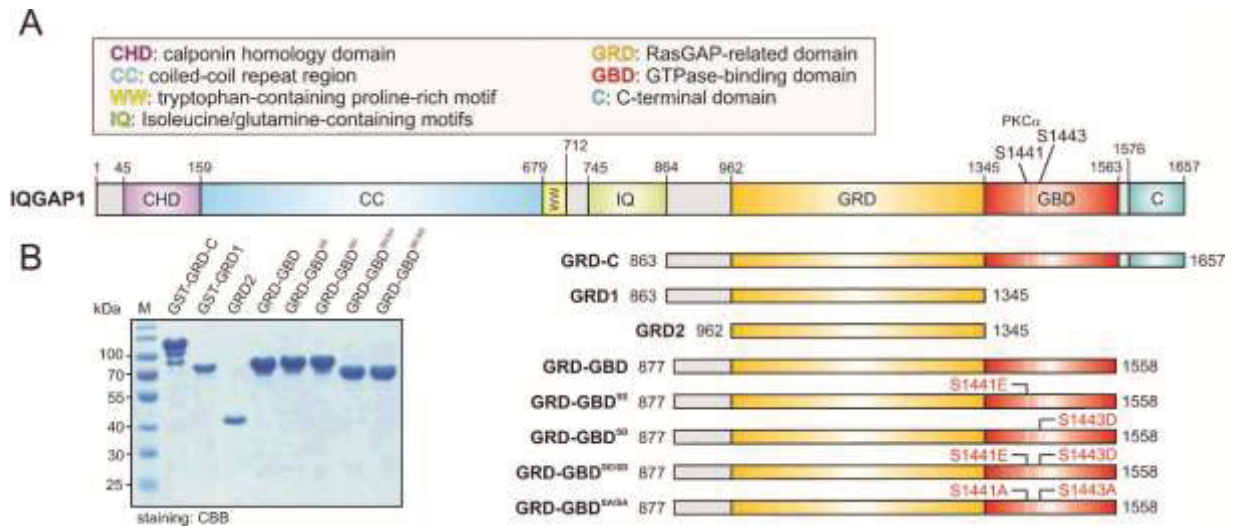
Figure 4. Interaction of different C-terminal variants and phosphomimicking mutants of IQGAP1 with RAC1 and CDC42. (A) Association of different IQGAP1 variants with RAC1/CDC42-mantGppNHp (0.2 μ M) was measured and the observed rate constants (k_{obs}) were plotted against the investigated IQGAP1 C-terminal domains. In contrast to GRD-C, GDR-GBD and GRD-GBR^{SD} of IQGAP1, which efficiently interact with RAC1 and CDC42, GRD1, GRD2, and GDR-GBD variants (SD, SE/SD and SA/SA) were disabled to associate RAC1 and CDC42. (B, C) Kinetic measurements were performed to obtain the k_{on} and the k_{off} values, and to calculate the K_d values for the interaction of GRD-C, GRD-GBD, and GRD-GBD^{SE} with RAC1 (B) and CDC42 (C). Obtained data show the comparable results for RAC1 and CDC42.

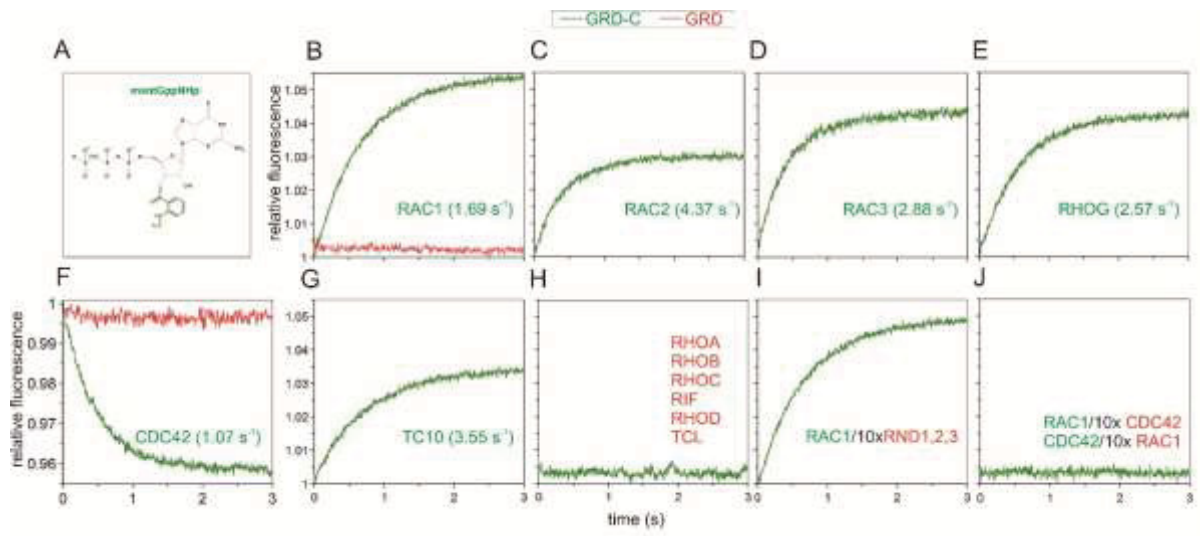
Figure 5. GRD binds RAC-/CDC42 like proteins but outside the switch regions. (A-C) Fluorescence polarization experiments were conducted to measure the interaction of mantGppNHp-bound RAC1, CDC42 and RHOA (1 μ M, respectively) with increasing concentrations of GRD-C (0-20 μ M) (A), and GRD (0-120 μ M) (B). (C) Evaluated data and obtained dissociation constant (K_d) shown in the bars illustrates a significant difference in the binding affinities of these two IQGAP1 proteins. (D) Binding of mantGppNHp-bound RAC1 protein (1 μ M) with increasing concentrations (0-45 μ M) of GRD-GBD, GRD-GBD^{SE} and GRD-GBD^{SD}. (E) Calculated dissociation constants (k_d) shown in the bars reveal a significant decrease in the affinities of GRD-GBD^{SD} compared to GRD-GBD and GRD-GBD^{SE}. (F-G) Fluorescence polarization experiments were conducted under the same conditions as in A and B, the only different was that inactive mantGDP-bound CDC42 was used. Calculated K_d values were 95 μ M for GRD-C and 184 μ M for GRD, respectively.

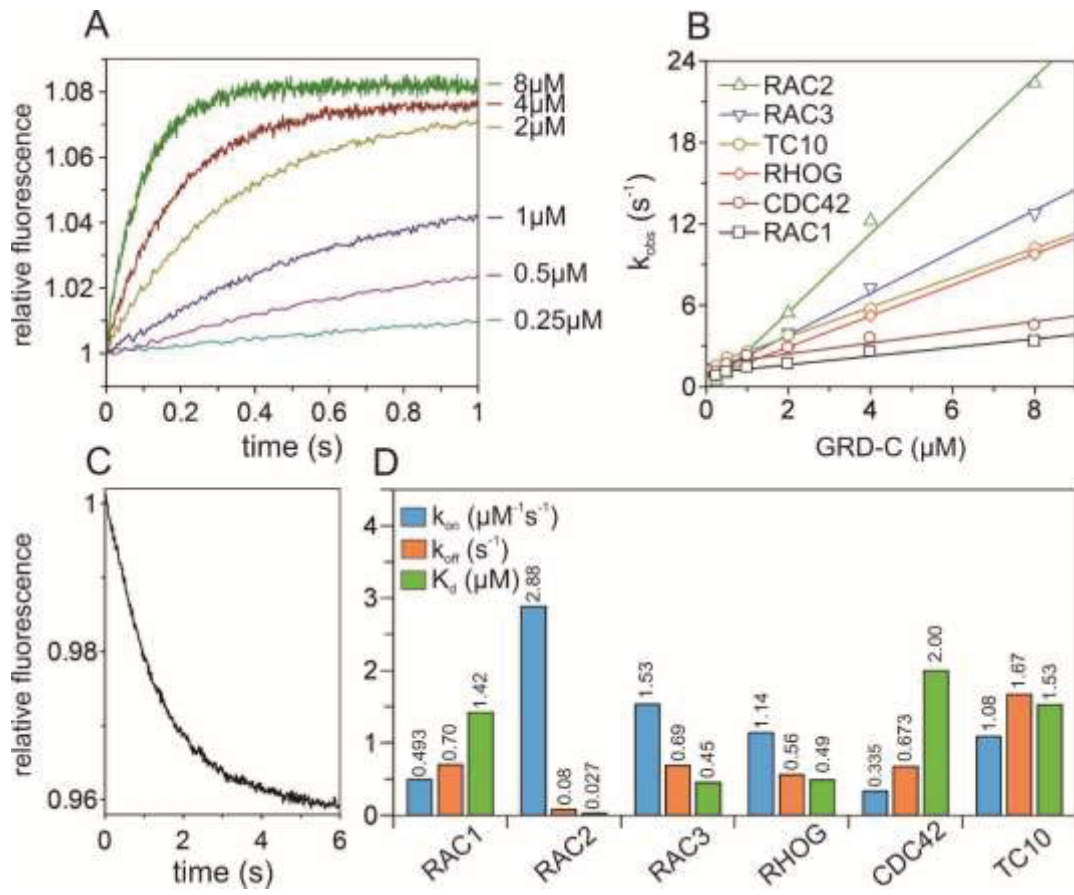
Figure 6. Reciprocal expression of IQGAP isoforms and RHO proteins in hepatic stellate cells. (A) qPCR analysis of IQGAP1, 2, 3, RAC1, 2, 3, and CDC42 in freshly isolated (quiescent, d0) and activated HSCs (day 8) revealed that IQGAP1, 3 and RAC2 preferentially expressed in aHSCs where IQGAP2 is downregulated. (B) Western blot analysis of RAC1, CDC42, IQGAP1 and 2 were

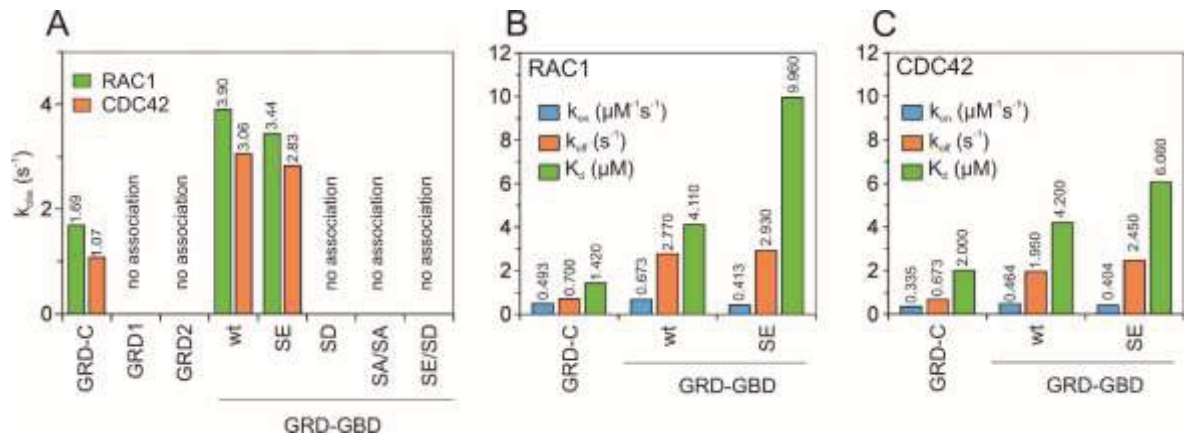
performed at different time points after HSC isolation (d0, d1, d4 and d8). On contrary to IQGAP2 which was expressed more in qHSCs and lesser in aHSCs, IQGAP1, RAC1, and CDC42 had higher levels of expression in aHSCs. γ -tubulin was applied as a internal control for western blotting.

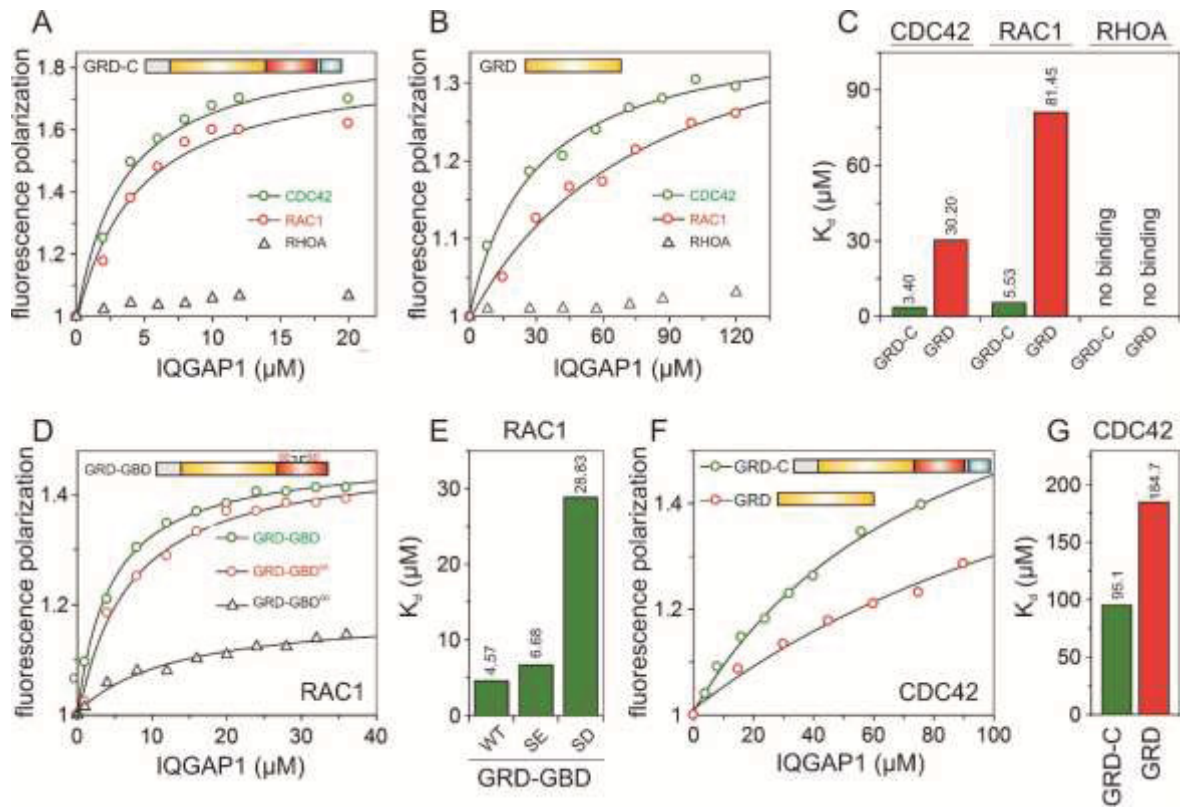
Figure 7. A proposed multi-stage mechanistic model of IQGAP interaction with IQGAP1. Low-affinity, GDP-/GTP-independent interaction of GRD with RAC1 and CDC42 proteins outside their switch regions occurs in a way that is independent of the upstream signals, providing it is structurally accessible and available for interactions. GBD only binds to the RAC1 and CDC42 proteins after GEFs catalyze the exchange of GDP to GTP, and they exist in an active GTP-bound forms. The C-terminal domain of IQGAP1 may potentiate the IQGAP1 interaction with RAC1 and CDC42 proteins by probably extending the resident time of the respective proteins complexes.

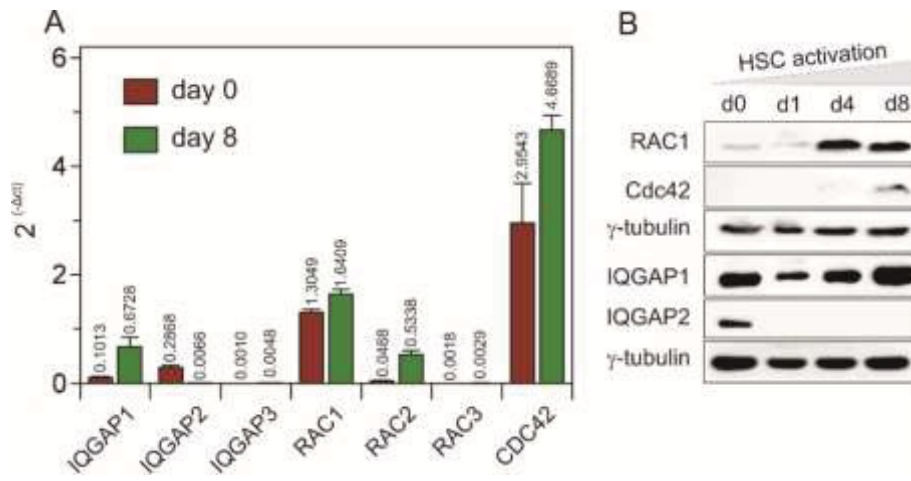
Nouri *et al.*, Figure 1

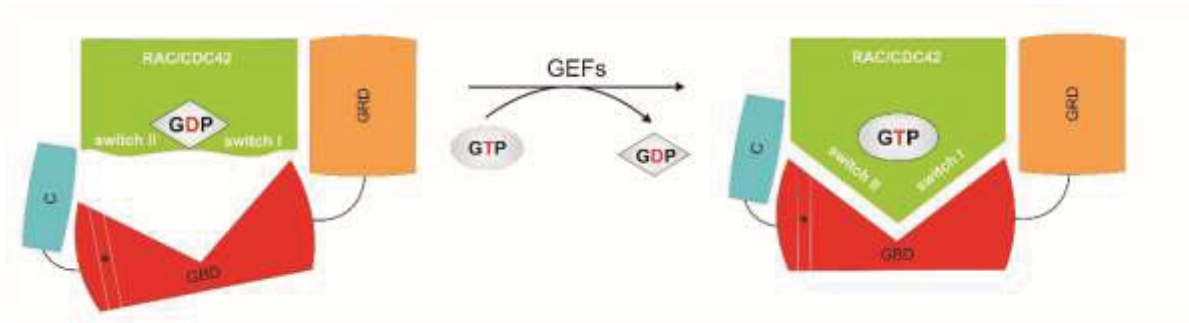
Nouri *et al.*, Figure 2

Nouri *et al.*, Figure 3

Nouri *et al.*, Figure 4

Nouri *et al.*, Figure 5

Nouri *et al.*, Figure 6

Nouri *et al.*, Figure 7

SUPPORTING INFORMATION

IQGAP1 interaction with RHO family proteins revisited: kinetic and equilibrium evidence for two distinct binding sites*

Kazem Nouri¹, Eyad K. Fansa^{1§}, Ehsan Amin¹, Saeideh Nakhaei-Rad¹, Radovan Dvorsky¹, Lothar Gremer², David J. Timson³, Lutz Schmitt⁴, Dieter Häussinger⁵, and Mohammad R. Ahmadian^{1@}

¹Institute of Biochemistry and Molecular Biology II, Medical faculty of the Heinrich-Heine University, 40225 Düsseldorf, Germany

²Institute of Physical Biology, Heinrich-Heine University, Düsseldorf, Germany

³School of Pharmacy and Biomolecular Sciences, University of Brighton, Huxley Building, Lewes Road, Brighton BN2 4GJ, United Kingdom

⁴Institute of Biochemistry, Heinrich-Heine University, Düsseldorf, Germany

⁵Clinic of Gastroenterology, Hepatology and Infectious Diseases, Medical Faculty of the Heinrich-Heine University, Düsseldorf, Germany

Table S1: Primer sequences were obtained from Primer Bank (<http://pga.mgh.harvard.edu/primerbank>) with small modifications match with rat sequences.

Target	Primer	Source
IQGAP1	FW: 5'-GAGAAGACCGTTTTGGAGCTAAT -'3 RV: 5'-GGGTGAGGCTATGCTCAGG -'3	NM_001 1 08489.1
IQGAP2	FW: 5'-GCTGTCAAACTTCAGCAGAC-'3 RV: 5'- AGGTTGTCTACACAGGTCTTGA-'3	XM_008760685.1
IQGAP3	FW: 5'-AACTTCTGGCTTTCTGCGGTA -'3 RV: 5'-AATGCAGTAGATCACCCGAGG-'3	NM_001 1 91 709.1
RAC1	FW: 5'- ACGGAGCCGTTGGTAAAACC-'3 RV: 5'- AGACGGTGGGGATGTACTCTC-'3	NM_1 34366.1
RAC2	FW: 5'- GACAGTAAACCTGTGAACCTGG-'3 RV: 5'- CTGACTAGCGAGAAGCAGATG-'3	XM_006242028.1
RAC3	FW: 5'- TATCCCCACAGTTTTCGACAAC-'3 RV: 5'-GAGAGTGGCCGAAGCCTAT -'3	XM_006247966.1
CDC42	FW: 5'-GAAAATGTGAAAGAAAAGTGGGTG-'3 RV: 5'-TCTGGAGTAATAGGCTTCTGTTTG-'3	XM_006239270.1
HPRT1	FW: 5'-AAG TGT TGG ATA CAG GCC AGA-'3 RV: 5'-GGC TTT GTA CTT GGC TTT TCC-'3	self-designed

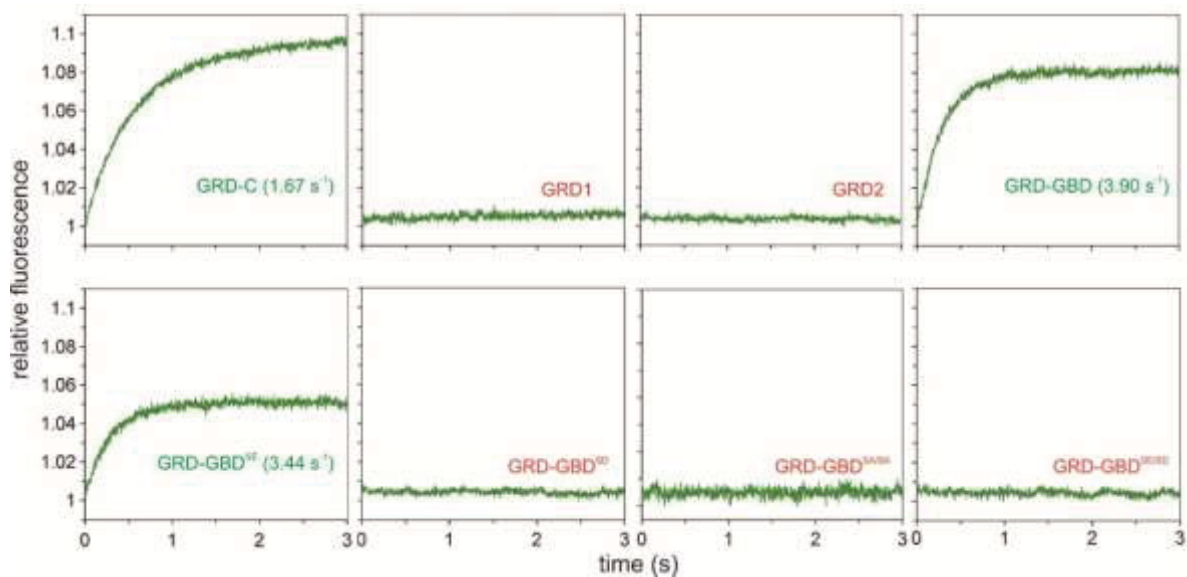
Nouri *et al.* Figure S1

Figure S1. IQGAP1^{GBD} is crucial for the interaction with RAC1. Association of RAC1 mantGppNHp labeled (0.2 μM) and various IQGAP1 variants (2 μM) were measured. In contrast to GRD-C, GRD-GBD, and GRD-GBD^{SE} variants of IQGAP1, GRD1, GRD2, and GRD-GBD variants (SD, SE/SD, and SA/SA) failed to associate with RAC1. Calculated k_{obs} values for associating IQGAP1 fragments with RAC1 are shown in parenthesis.

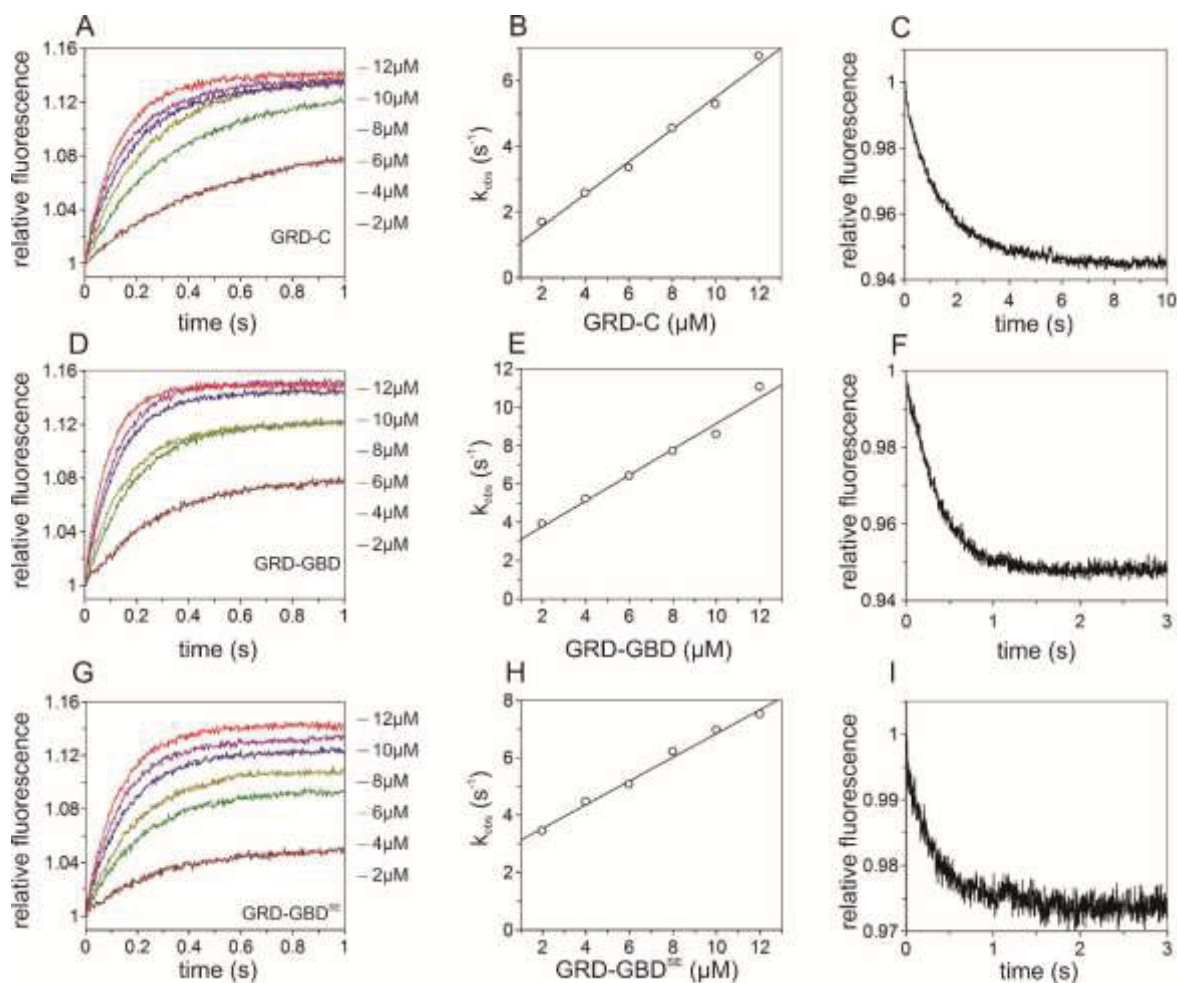
Nouri *et al.* Figure S2

Figure S2. Kinetic measurements of GRD-C, GRD-GBD, and GRD-GBD^{SE} association with RAC1. Association of mantGppNHp-RAC1 (0.2 μM) with increasing concentrations (2-12 μM) of IQGAP1, association rates (k_{on}), and dissociation of IQGAP1 (2 μM) from RAC1-mantGppNHp (0.2 μM) in the presence of unlabeled RAC1-GppNHp (10 μM) are shown for (A-C) GRD-C, (D-F) GRD-GBD, and (G-I) GRD-GBD^{SE}, respectively. Quantitative data are presented in figure 4B.

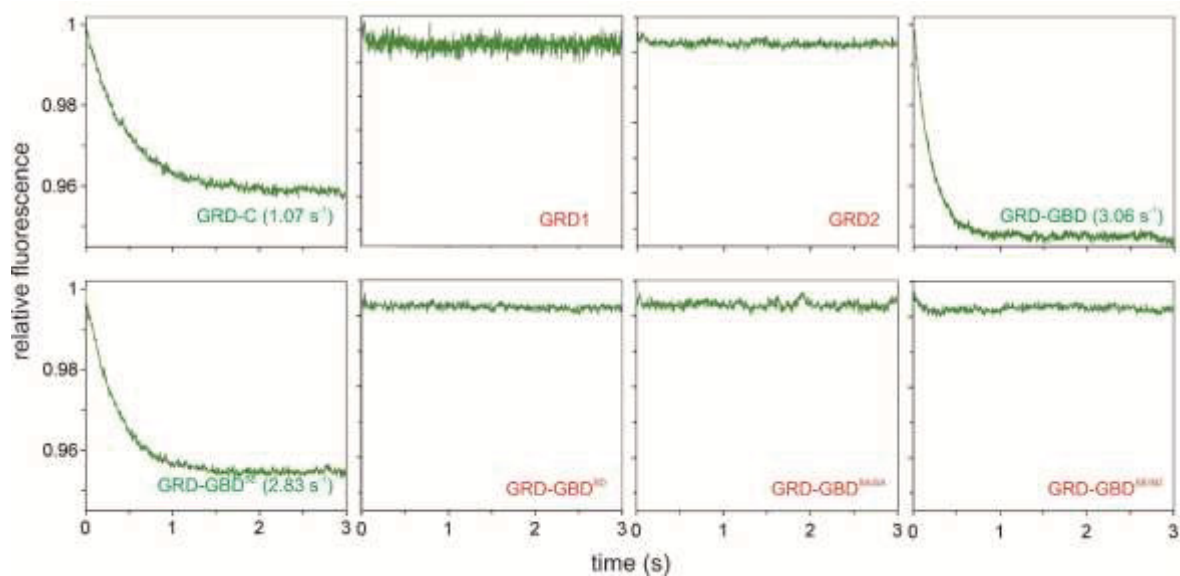
Nouri *et al.* Figure S3

Figure S3. IQGAP1^{GBD} is essential for the CDC42 interaction. Association of different IQGAP1 variants (2 μM) with CDC42-mantGppNHp (0.2 μM) was measured under the same conditions as in S1. CDC42 associates with GRD-C, GDR-GBD, and GRD-GBR^{SE}, but not with GRD1, GRD2, and GDR-GBD variants (SD, SE/SD and SA/SA). k_{obs} values are presented in parenthesis in front of each associating fragment.

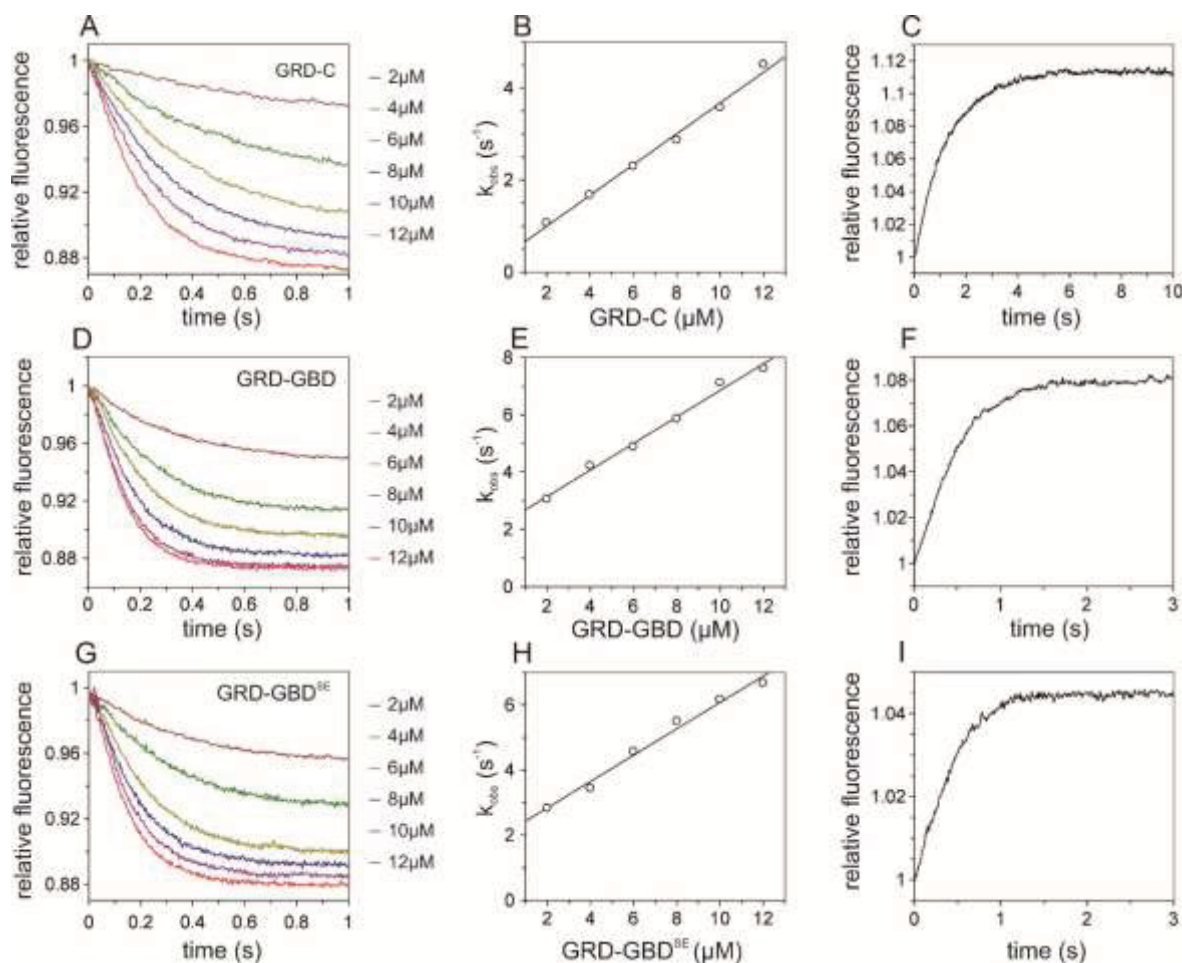
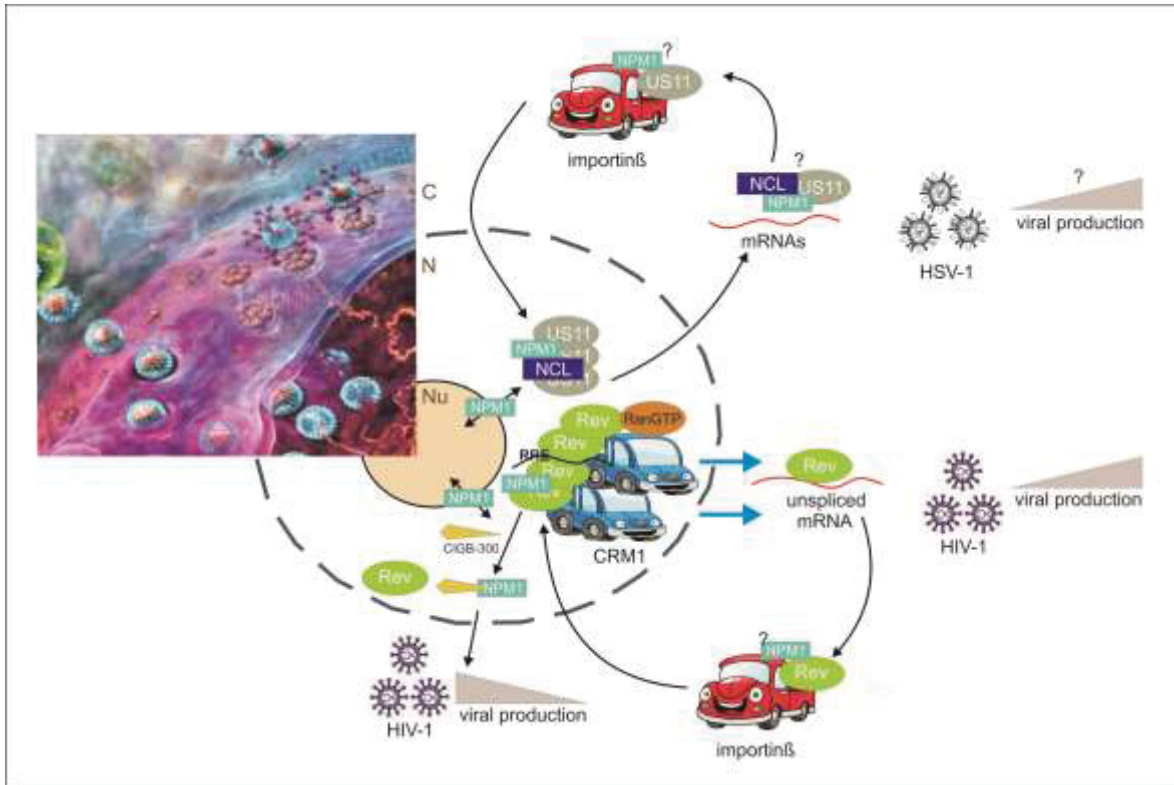
Nouri *et al.* Figure S4

Figure S4. Kinetic measurements of GRD-C, GRD-GBD, and GRD-GBD^{SE} association with CDC42. Kinetic measurements were performed under the same conditions as in S2. Association of mantGppNHp-CDC42 (0.2 μM) with increasing concentrations (2-12 μM) of IQGAP1 proteins, association rates (k_{on}), and dissociation of IQGAP1 (2 μM) from CDC42-mantGppNHp (0.2 μM) in the presence of unlabeled CDC42-GppNHp (10 μM) are shown for GRD-C (A-C), GRD-GBD (D-F), and GRD-GBD^{SE} (G-I), respectively. Corresponding quantitative data are presented in figure 4C.

Chapter V

Biophysical Characterization of Nucleophosmin Interactions with Human Immunodeficiency Virus Rev and Herpes Simplex Virus US11

Graphical abstract



Status: PLOS One, in press, November 2015

Impact factor: 3.25

Own Proportion to this work: 90 %

Design, cloning, expression, and purification of Rev, NPM1, and US11 variants
Designing and performing almost all the experiments
Designing and writing the manuscript

Biophysical Characterization of Nucleophosmin Interactions with Human Immunodeficiency Virus Rev and Herpes Simplex Virus US11

Kazem Nouri¹, Jens M. Moll¹, Lech-Gustav Milroy², Anika Hain³, Radovan Dvorsky¹, Ehsan Amin¹, Michael Lenders⁴, Luitgard Nagel-Steger^{5,6}, Sebastian Howe⁷, Sander H. J. Smits⁴, Hartmut Hengel^{7,8}, Lutz Schmitt⁴, Carsten Münk³, Luc Brunsveld², and Mohammad R. Ahmadian^{1*}

¹Institute of Biochemistry and Molecular Biology II, Medical Faculty, Heinrich-Heine University, Düsseldorf, Germany

²Laboratory of Chemical Biology & Institute of Complex Molecular Systems, Department of Biomedical Engineering, Technische Universiteit Eindhoven, Eindhoven, Netherlands

³Clinic for Gastroenterology, Hepatology and Infectiology, Medical Faculty, Heinrich-Heine University, Düsseldorf, Germany

⁴Institute of Biochemistry, Heinrich-Heine University, Düsseldorf, Germany

⁵Institute of Complex Systems (ICS-6), Research Centre Jülich, Jülich, Germany

⁶Institute of Physical Biology, Heinrich-Heine University, Düsseldorf, Germany

⁷Institute of Virology, Medical Faculty, Heinrich-Heine University, Düsseldorf, Germany

⁸Institute of Virology, University Medical Center Freiburg

* Corresponding author

reza.ahmadian@uni-duesseldorf.de (MRA)

Running title: NPM1 interaction with viral proteins

Abbreviations: aa, amino acid; A1-A3, acidic regions 1-3; aSEC, analytical SEC; CBB, Coomassie Brilliant Blue; Cterm, C-terminal; f, fluoresceinated; FL, full-length; HSV-1, herpes simplex virus type 1; HIV-1, human immunodeficiency virus type 1; HRBD, histone and RNA-binding domains; IP, immunoprecipitation; ITC, isothermal titration calorimetry; MALS, multi angle light scattering; NES, nuclear export signal; NLS, nuclear localization signal; NoLS, nucleolar localization signal; NPM1, nucleophosmin; Nterm, N-terminal; OD, oligomerization domain; PD, pull-down; RBD, RNA-binding domain; SEC, size exclusion chromatography.

Abstract

Nucleophosmin (NPM1, also known as B23, numatrin or NO38) is a pentameric RNA-binding protein with RNA and protein chaperon functions. NPM1 has increasingly emerged as a potential cellular factor that directly associates with viral proteins; however, the significance of these interactions in each case is still not clear. In this study, we have investigated the physical interaction of NPM1 with both human immunodeficiency virus type 1 (HIV-1) Rev and Herpes Simplex virus type 1 (HSV-1) US11, two functionally homologous proteins. Both viral proteins show, in mechanistically different modes, high affinity for a binding site on the N-terminal oligomerization domain of NPM1. Rev, additionally, exhibits low-affinity for the central histone-binding domain of NPM1. We also showed that the proapoptotic cyclic peptide CIGB-300 specifically binds to NPM1 oligomerization domain and blocks its association with Rev and US11. Moreover, HIV-1 virus production was significantly reduced in the cells treated with CIGB-300. Results of this study suggest that targeting NPM1 may represent a useful approach for antiviral intervention.

Key words: B23, CIGB-300, cyclic peptide, herpes simplex virus, histone-binding domain, HIV-1, HSV-1, human immunodeficiency virus, NO38, NPM1, numatrin, oligomerization domain, Rev, US11

Introduction

Nucleophosmin (NPM1, also known as B23, numatrin, NO38) is a multifunctional phosphoprotein, predominantly localized in the nucleoli, which participates extensively in RNA regulatory mechanisms including transcription, ribosome assembly and biogenesis, mRNA stability, translation and microRNA processing [1,2]. NPM1 (294 amino acids; 37 kDa) consists of an N-terminal oligomerization domain (OD), a central histone binding domain (HBD) and a C-terminal RNA-binding domain (RBD) (Fig. 1A) [3]. It also contains nuclear localization signals (NLSs) at the N-terminus, central nuclear exports signals (NESs) and a nucleolar localization signal (NoLS) at the very C-terminus (Fig. 1A). NPM1 shuttles between the nucleus and cytoplasm and accordingly, a proportion of nucleolar NPM1 constantly translocates to the nucleoplasm and inner nuclear membrane as well as to the cytoplasm and inner and outer plasma membrane [2,4,5]. Due to this ability, NPM1 has been implicated in many stages of viral infection through interaction with a multitude of proteins from heterologous viruses (Table 1), including Human immunodeficiency virus type 1 (HIV-1) Rev [4], Human T-cell leukemia virus type 1 (HTLV-1) Rex [6] and Herpes simplex virus type 1 (HSV-1) UL24 [7].

Rev is 116 amino acid long and its RNA-binding domain is composed of an arginine-rich motif (ARM), which binds to various HIV-1 RNA stem loop structures [8]. The RNA-binding domain of Rev also acts as a nuclear/nucleolar targeting signal, which can deliver cytoplasmic proteins to the nucleus or nucleolus [8,9]. Many host proteins including DDX1, DDX3, eIF5A, exportin-1, hRIP/Rab, Matrin-3, NPM1, PIMT, and RNA helicase A have been suggested to bind to Rev prior to induction of its nuclear translocation [10-13]. NPM1 interaction with Rev appears to be necessary for nucleolar localization of Rev [4]. In fact, the HIV-1 Rev response element, a segment of viral RNA, represents a nuclear export signal, which triggers, *via* Rev binding, the nucleocytoplasmic shuttling of viral transcripts in infected cells [14]. A similar mechanism is controlled by Rex responsive element [15]. Most interestingly, US11, a protein of HSV-1, has the potential of directly binding to the Rev and Rex response elements and functionally substituting for Rev and Rex functions [4,14].

HSV-1 virions have four morphologically separate structures, a DNA core, capsid, tegument, and envelope. Tegument proteins fill the space between the capsid and the envelope [16]. US11 is a tegument protein and approximately 600 to 1,000 molecules per virion are released in the target cell upon virus entry [17]. It is a multifunctional protein involved in posttranscriptional regulation of gene expression and in biological processes related to the survival of cells following environmental stress [18,19]. US11 is localized in the nucleus and the cytoplasm, but especially accumulates in the nucleolus [20,21]. It has been reported that US11 has RNA-binding activity and can associate strongly with ribosomes and has also been found in rRNA and polysome containing fractions [17,22]. US11 also interacts with several host proteins, including nucleolin [23], ubiquitous kinesin heavy chain (uKHC) [24], homeodomain-interacting protein kinases 2 (HIPK2) [19], and protein kinase R (PKR) [25], which in turn counteracts the antiviral host defense system. Furthermore, although US11 protein is not essential for viral growth in cell cultures, it plays a vital role in the cells subjected to thermal stress [26], recovery of protein synthesis and survival in heat shock-treated cells [27].

In this study we investigated Rev-NPM1 interaction and found that Rev shows high-affinity binding to two domains of NPM1, OD and HBD, in an RNA-independent manner. Due to the

functional homology of US11 with both HIV-1 Rev and HTLV-1 Rex, it was tempting to examine US11 binding to NPM1. The achievements in this study demonstrates, for the first time, a physical interaction between the C-terminal domain of US11 and NPM1^{OD} in an RNA-independent manner. The Rev and US11 association with NPM1 was prevented by a cyclic peptide, CIGB-300, which also bound to NPM1^{OD} but not to the other NPM1 domains. Cell-based experiments revealed a significant reduction of HIV-1 virus production in the presence of CIGB-300. Thus, the association of nucleolar protein NPM1 with the viral proteins Rev and US11 may advance our understanding of HIV and HSV pathology and further implies that NPM1 can be exploited as a therapeutic target for infectious diseases.

Materials and Methods

Constructs

The coding sequence of NPM1 full-length (NPM1^{FL}, aa 1-294), kindly provided by F. Carrier [28]. Oligomerization domain (NPM1^{OD}, aa 1-122), histone and RNA-binding domains (NPM1^{HRBD}, aa120-294), histone binding domain (NPM1^{HRBD}, aa 120-241), RNA-binding domain (NPM1^{RBD}, aa 241-294), HSV-1 US11 full-length (US11^{FL}, aa 1-152), Nterm (US11^{Nterm}, aa 1-84) and Cterm (US11^{Cterm}, aa 79-152) as well as HIV-1 Rev full-length (Rev^{FL}, aa 1-116) were amplified by PCR and cloned into pGEX-4T1-Ntev or pET-23b to obtain GST-fusion or His-tagged proteins. The Myc-tagged HSV-1 US11^{FL} was cloned into pcDNA3.1-Myc for expression in eukaryotic cells. pNL4-3 was used to produce replication competent HIV-1 [29].

Cell culture

COS-7 and HeLa cells were obtained from German Collection of Microorganisms and Cell Cultures (Braunschweig, Germany). TZM-bl Cells were from NIH AIDS reagent program and HOS.CD4.CXCR4 cells were from CFAR (Centers for AIDS Research). All cells were grown in DMEM supplemented with 10% fetal bovine serum (FBS) (Life Technologies) and penicillin/streptomycin (Life Technologies) as antibiotics. Cells were grown in a humidified CO₂ (5%) atmosphere at 37°C. Trypsin/EDTA was from Genaxxon Bioscience GmbH (Ulm, Germany).

Antibodies and fluorescent probes

Mouse monoclonal anti-NPM1 (ab10530) recognizing the C-terminal 68-amino acids and rabbit monoclonal anti-NPM1 (ab52644) recognizing the N-terminal 122-amino acids were from Abcam (Cambridge, United Kingdom), Rabbit monoclonal anti-myc from Cell Signaling Technology, Inc. (Boston, USA), Alexa fluor 488 mouse anti-rabbit IgG and Alexa fluor 633, and goat anti-mouse IgG from Molecular Probes (Oregon, USA), and normal monoclonal Rabbit IgG (sc-2027) was from Santa Cruz Biotechnology, Texas, USA.

Proteins

For protein expression the *Escherichia coli* strains BL21(DE3), pLysS BL21(DE3), CodonPlusRIL, or BL21(Rosetta), were transformed and used to purify the respective protein as previously described [30,31]. All purified proteins were analyzed by SDS-PAGE (Fig. 1B) and stored as either tag-fused or cleaved protein at -80°C.

Transient transfection

COS-7 and HeLa cells were transfected using the TurboFect transfection reagent according to the manufacturer's instructions (Thermo Scientific) in 24-well plates or 10 cm dishes by using 0.5 µg or 5 µg plasmid DNA per transfection, respectively.

Confocal laser scanning microscopy

Confocal imaging was performed using a LSM510-Meta confocal microscope (Zeiss, Jena, Germany) as previously reported [5].

Immunoblotting

Proteins were heated in Laemmli sample buffer and subjected to SDS-PAGE. The proteins were transferred to nitrocellulose membranes (Hybond C, GE Healthcare) using Mini Trans-Blot cell (100 volt for 1 h) (BIO-RAD, USA), and immunoblotted using monoclonal primary antibody to mouse NPM1 antibody (Abcam), rabbit NPM1 antibody (Abcam), and rabbit myc antibody (Cell Signaling) for 1 h. After three washing steps, membranes were incubated with polyclonal horseradish peroxidase-coupled secondary antibodies for 1 h and signals were visualized by the ECL detection system (GE Healthcare) and images were collected using the ChemoCam Imager ECL (INTAS science imaging, Germany).

Immunoprecipitation

COS-7 cells were transiently transfected with cDNA encoding Myc-tagged US11. After 48 h, an equal number of the cells were lysed in a buffer, containing 30 mM Tris/HCl, pH 7.5, 150 mM NaCl, 1 mM EDTA, 1% Triton X-100, 2.5 mM Na-pyrophosphate, 1 mM β -glycerophosphate, 1 mM sodium vanadate, and one EDTA-free protease inhibitor cocktail tablet (Roche, Mannheim, Germany). Lysates were centrifuged at 12,000 \times g for 2 min. The supernatant was precleared with protein G agarose (Roche, Mannheim, Germany) and divided to three parts for IgG control, beads control and IP, and then incubated with an anti-myc antibody (Cell Signaling) overnight at 4°C. Afterwards, protein G-Agarose beads were added to the lysate for 1 h before recovering the beads by centrifugation at 500 \times g for 5 min at 4°C. The beads were washed 4-times in the lysis buffer, and resuspended in Laemmli sample buffer. Precipitates and total cell lysate were subjected to SDS-PAGE, and Western blotting as described above.

Analytical size exclusion chromatography (aSEC)

The complex formation of NPM1^{OD} and US11^{FL} was analyzed using a superdex 200 10/30 column (GE Healthcare, Uppsala, Sweden) and a buffer, containing 30 mM Tris-HCl (pH 7.5), 150 mM NaCl, 5 mM MgCl₂, and 3 mM dithiothreitol. The flow rate was sustained at 0.5 ml/min. Fractions were collected at a volume of 0.5 ml and then peak fractions were visualized by 12.5% SDS-PAGE gel and staining using coomassie brilliant blue (CBB).

Pull-down assay

GST, GST-fused NPM1 and HSV-1 US11 variants as well as HIV-1 Rev were expressed in *E. coli* and purified using standard protocols [30,31]. In order to obtain prey proteins the GST-tag was cleaved off with purified tobacco etch virus (tev) protease and removed by reverse GSH affinity purification. Pull-down experiments were performed by adding 50 μ g purified proteins, e.g. HIV-1 Rev and HSV US11 variants, or COS-7 cell lysate transfected with pcDNA-mycUS11^{FL} to 25 μ g of GST-fused NPM1 proteins, immobilized on 100 μ l glutathione-conjugated Sepharose 4B beads (Macherey-Nagel, Duren, Germany). The mixture was incubated at 4°C for 1 h in a buffer containing 30 mM Tris/HCl, pH 7.5, 150 mM NaCl, 5 mM MgCl₂, and 3 mM Dithiothreitol. In cases of RNase treatments, 70 U RNase A (Qiagen, Hilden, Germany) were added to the same buffer in order to determine an RNA dependent interaction between the NPM1 variants and HIV-1 Rev. After four washing steps with the same buffer, proteins retained on the beads were heat-denatured (7 min at 90°C) and analyzed by SDS-PAGE followed by coomassie brilliant blue (CBB)

staining or by Western blotting. Mixed samples prior to pull-down (PD) analysis were used as input controls.

Isothermal titration calorimetry (ITC)

All proteins were prepared in ITC buffer, containing 30 mM Tris-HCl, pH 7.5, 150 mM NaCl, 5 mM MgCl₂, and 1 mM Tris (2-carboxyethyl) phosphine (TCEP) on a size exclusion chromatography (SEC) column (Superdex 200, 16/60, GE Healthcare, Uppsala, Sweden). ITC measurements were performed at 25°C using a VP-ITC system (Microcal, Northampton, MA, USA) as previously reported [32]. The final data analysis was carried out using Origin software (Microcal). The experimental data were evaluated using Origin 7.0 software (Microcal) to determine the binding parameters including association constant (K_a), number of binding sites (n), and enthalpy (ΔH). Control measurements were carried out by titrating buffer to the protein.

Analytical Ultracentrifugation (AUC)

Sedimentation velocity centrifugation experiments at 50,000 rpm and 20°C were carried out in a Beckman Optima XL-A (Beckman-Coulter, Brea, CA, USA), equipped with absorption optics, and a four-hole rotor. Samples (volume 400 μ L) were filled into standard aluminum double sector cells with quartz glass windows. Measurements were performed in absorbance mode at detection wavelengths 230 nm. Radial scans were recorded with 30 μ m radial resolution at \sim 1.5 min intervals. The software package SEDFIT v 14.1 (www.analyticalultracentrifugation.com) was used for data evaluation. After editing time-invariant, noise was calculated and subtracted. In SEDFIT continuous sedimentation coefficient distributions $c(s)$ were determined with 0.05 S resolution and F-ratio = 0.95. Suitable s -value ranges between 0 and 20 S and f/f_0 between 1 and 4 were chosen. Buffer density and viscosity had been calculated with SEDNTERP v 20111201 beta (bitcwiki.sr.unh.edu) [33]. The partial specific volume of NPM1^{OD} fragment, NPM1^{FL} and US11^{FL} were calculated according to the method of Cohn and Edsall [34] as implemented in SEDNTERP. NPM1^{OD} was analyzed at 0.25 concentrations in 30 mM Tris-HCl, pH 7.5, 150 mM NaCl, and TCEP (1 mM). After equilibrium was reached, concentration profiles were recorded with 10 μ m radial resolution and averaging of seven single registrations per radial value. Equilibria had been established at 14,000, 16,000, 25,000, 42,000 and 50,000 rpm. Data evaluation was performed using SEDPHAT.

Multi angle light scattering (MALS)

MALS experiments were performed as described [35]. Briefly, light scattering measurement of purified NPM1^{OD} alone or combined with US11^{FL} was performed on a MALS instrument (miniDAWN™ TREOS). For exact protein mass calculation, UV absorptions at 280 nm (Agilent Infinity 1260) and refractive index (RI) signals (OptilabRex, Wyatt Technology) were collected. Raw data was analyzed and processed using ASTRA software (Wyatt Technology) to calculate molecular mass averages and polydispersity indexes of analyzed protein samples.

CIGB-300 synthesis

The CIGB-300 peptide was synthesized at room temperature by manual solid-phase peptide synthesis using a Rink Amide resin (0.59 mmol/g loading). Briefly, the resin (200 μ mole scale) was pre-swollen by suspending in 3 mL of NMP for 10 min and the N-terminal Fmoc-protecting group cleaved by treating the resin with 3 mL of a stock solution of 20% piperidine (v/v) in *N*-methyl-2-pyrrolidone (NMP) (2 x 5 min). Each amino acid coupling was performed by pre-mixing 2 mL of a 0.4 M stock solution of *O*-Benzotriazole-*N,N,N',N'*-tetramethyluronium-hexafluoro-phosphate (HBTU) in NMP with 4 mL of a 0.2 M stock solution of the amino acid building block in NMP,

followed by 2 mL of a 1.6 M stock solution of *N,N*-diisopropylethylamine (DIPEA) stock solution, also in NMP. The reaction mixture was added immediately to the resin and the reaction vessel agitated at ambient temperature for 30 min. Each amino acid coupling was performed twice. For the coupling of the fluorescein isothiocyanate (FITC) dye, an amino acid linker (Fmoc-O1Pen-OH, Iris Biotech GmbH) was first coupled to the N-terminus, the Fmoc group deprotected under standard conditions, and then the resin was incubated with 7 eq. of FITC and 14 eq. of DIPEA in DMSO at RT for 18 h. The linear peptides (with and without FITC dye) were simultaneously deprotected and cleaved from the Rink Amide resin using a 92.5/2.5/2.5/2.5 (v/v) mixture of trifluoroacetic acid (TFA)/H₂O/triisopropylsilane (TIS)/ ethanedithiol (EDT), and then precipitated in ice-cold diethyl ether. Finally, disulfide formation was performed by stirring the crude peptide in phosphate buffer (pH 7.5) with 1% v/v DMSO at RT for 48 h to afford either CIGB-300 or fluoresceinated CIGB-300 after purification by reverse-phase HPLC using an Alltima HP C18 column (5 μm, length 125 mm, ID: 20 mm) and 0.1% trifluoroacetic acid (TFA) in H₂O/MeCN as mobile phase. The pure peptides were analyzed by LC-MS using a Shimadzu LC Controller V2.0, LCQ Deca XP Mass Spectrometer V2.0, Alltima C18-column 125 x 2.0 mm, Surveyor AS and PDA with solvent eluent conditions: CH₃CN/H₂O/1% TFA. The Rink Amide resin and all amino acid building blocks were purchased from Novabiochem®. HBTU, DIPEA, NMP, HPLC-grade CH₃CN and HPLC-grade TFA were all purchased from Biosolve B.V. Diethyl ether was purchased from Actu-All Chemicals. FITC, ethanedithiol, and triisopropylsilane were all purchased from Sigma-Aldrich. H₂O refers to Millipore-grade distilled water. Summary of LC-MS data (ESI): CIGB-300; [M+5TFA+3H]³⁺: 1210.25 (theoretical), 1210.13 (found); [M+6TFA+3H]³⁺: 1248.26 (theoretical), 1248.20 (found); fluoresceinated CIGB-300; [M+5TFA+3H]³⁺: 1335.61 (theoretical), 1335.73 (found); [M+6TFA+3H]³⁺: 1373.95 (theoretical), 1373.60 (found).

Fluorescence polarization

Fluoresceinated CIGB-300 (also referred to as FITC-labelled CIGB-300) was synthesized as described above. Increasing amounts of different variants of NPM1, GST-Rev, GST-US11 and GST as a negative control were titrated into FITC-labeled CIGB-300 (0.1 μM) in a buffer containing 30 mM Tris/HCl (pH 7.5), 150 mM NaCl, 5 mM MgCl₂, 1 mM tris-(2-carboxyethyl) phosphine and a total volume of 200 μl at 25°C using a Fluoromax 4 fluorimeter. Displacement assay was performed by titrating increasing amount of Rev and US11 to the complex of NPM1 and FITC-labelled CIGB-300. The concentration dependent binding curve was fitted using a quadratic ligand binding equation.

Virus production assay

HOS.CD4.CXCR4 were seeded in a 24 well plate with 2.5x10⁴ cells per well. One part was treated with 100 μM CIGB-300 peptide for 30 min at 37°C and one part was left untreated. Cells were infected with HIV-1 NL4-3 (MOI 1) and after 6 h cells were washed to remove input virus. Cell culture supernatant was collected 48 h and 72 h after infection. Virus titer in the supernatant was determined by infection of TZM-bl cells and luciferase measurement three days later using the *Steady-Glo Luciferase Assay System* (Promega).

Structural bioinformatics

Model of the complex between NPM1 and CIGB-300 was created in two steps. Tat part of the peptide was first docked to the structure of NPM1 (PDB ID: 4N8M) [36] with the help of Haddock web portal (<http://haddock.org/>). Acidic residues on three subunits were defined as active residues for docking while the setup of the Easy interface was used. Docked pose with best score

that enables building of cyclic part of the peptide was then used in the second step. Model of the cyclic peptide was first generated and then placed with program CHARMM [37] in different orientations and positions on the surface of NPM1 in a way that enabled its interaction with the Tat portion of the peptide construct. After linking, the geometry of whole complex was optimized by energy minimization applying 500 steps of steepest descent method. Complex with lowest minimized energy was used as a final mode.

Results

HIV-1 Rev directly binds to two distinct regions of NPM1

Previous reports have shown that NPM1 is co-localized and co-immunoprecipitated with HIV-1 Rev in cells [4,38]. To investigate a direct interaction between NPM1 and Rev, pull-down experiments under cell-free conditions were performed using Rev^{FL} and NPM1 variants as GST-fusion proteins. As indicated in Fig. 2A (upper panel), Rev^{FL} interacts with NPM1^{FL}, NPM1^{OD}, NPM1^{HBD} and NPM1^{HRBD}, but not with the NPM1^{RBD}, suggesting that two different regions of NPM1, namely OD and HBD, have tight physical interaction with the HIV-1 Rev. To show whether this interaction is RNA-dependent, the pull-down experiments were performed under the same conditions in the presence of RNase A. As shown in Figure 2A (lower panel), RNase treatment had no effect on HIV-1 Rev association with NPM1. These results clearly indicate that HIV-1 Rev specifically binds to NPM1, and the binding is not RNA-dependent.

Next, we purified all proteins in high quantities (Fig. 1B), and after cleaving the tag, isothermal titration calorimetry (ITC) experiments were conducted in order to examine the stoichiometry of binding and to determine the binding affinity of Rev^{FL} for the NPM1 variants. Consistent with the data obtained by pull-down assay, Rev^{FL} revealed variable affinity for the NPM1 variants with calculated dissociation constants (K_d) between 18 and 0.013 μ M for 1:1 stoichiometry (Figs. 2B, S1A-C Fig.; Table 2). No interaction was detected between Rev^{FL} and NPM1^{RBD} (Fig. 2C) suggesting that a low micromolar affinity for the interaction between Rev and NPM1^{HRBD} actually stems from the central histone binding domain of NPM1 (NPM1^{HBD}). The obtained dissociation constant (K_d) for the Rev^{FL} and NPM1^{HBD} interaction was 5.8 μ M indicating a stronger affinity for Rev^{FL} as compared to that of NPM1^{HRBD}, which could be due to a binding site that partially masked by the C-terminal RBD.

HSV-1 US11 associates with NPM1 in cells

The fact that Rev physically binds to NPM1 and US11 alone can fulfill Rex and Rev's function in transactivating envelope glycoprotein gene expression [14], led us to examine a potential US11-NPM1 interaction. We first analyzed the intracellular distribution of endogenous NPM1 and overexpressed myc-US11 in HeLa cells using confocal imaging. Figure 3A shows a nucleolar co-localization of NPM1 and US11 where the overall pattern of these proteins is different. In contrast to a predominant nucleolar localization of NPM1, US11 was found in the cytoplasm and also accumulated, to certain extent, in the nucleoli. To confirm the association of US11 with NPM1, COS-7 cells overexpressing myc-US11 were lysed and endogenous NPM1 was immunoprecipitated. Fig. 3B shows that NPM1 co-precipitated with myc-US11 indicating that US11 forms a complex with NPM1. We, next, used purified GST-NPM1^{FL} and pulled down myc-US11, transiently overexpressed in COS-7 cells. As shown in Fig. 3C, the myc-US11^{FL} clearly bound

to NPM1^{FL}, but not to the GST control, indicating that there may be a direct interaction between US11 and NPM1.

US11 associates with NPM1^{OD} in its oligomeric state

To clarify whether the interaction observed above is a direct interaction, we used purified, RNase A treated NPM1 and US11 variants from *E. coli*. Fig. 4A shows that NPM1^{FL} and NPM1^{OD} but not NPM1^{HRBD} and NPM1^{RBD}, directly interact with US11^{FL}. We repeated the experiments to map the NPM1 binding region of US11 by using purified, GST-fused, N-terminal and C-terminal fragments of US11. As shown in Fig. 4A, both US11^{Cterm} and US11^{Nterm} bound, with the same pattern as US11^{FL} bound to NPM1^{FL} and NPM1^{OD}. However, binding affinities of isolated N- or C-terminal domains of US11 towards NPM1 seemed markedly reduced compared to the full-length protein. In the light of above mentioned, we conclude that NPM1 and US11 physically interact with each other *via* NPM1^{OD} and largely US11^{Cterm}.

Next, ITC measurement was also performed to determine the binding affinity between NPM1 and US11 by titrating NPM1^{FL} (1.2 mM) to US11^{FL} solution (60 μ M); both proteins were treated with RNase A. As shown in Fig. 4B, the association of NPM1^{FL} with US11^{FL} is endothermic (positive peaks). As a control experiment, buffer was titrated to 60 μ M US11^{FL} under the same experimental condition with no calorimetric changes (Fig. 4C). Based on ITC analysis we estimated an apparent K_d value of 4 μ M. The NPM1^{OD} interaction with US11^{FL} was also analyzed by aSEC combined with MALS, after treating the proteins with RNase A. Fig. 4D (lower panel) shows a co-elution of the RNase-treated NPM1^{OD} and US11^{FL} proteins from the Superdex 200 (10/300) column indicating that these proteins form a complex. MALS analysis revealed that NPM1^{OD} oligomerized to a pentameric state and formed a 1:1 complex with the monomeric US11^{FL} (Fig. 4D upper panel). To further investigate the oligomerization states of US11 and NPM1, AUC experiments were performed. Results obtained were consistent with the MALS data, and revealed that NPM1^{FL} and NPM1^{OD} are pentameric and globular while US11^{FL} was monomeric and adopts an elongated structure (Table 3 and S2 Fig.). Together, the data clearly demonstrates that US11 selectively binds to the N-terminal oligomerization domain of NPM1 in an RNA-independent manner.

Displacement of the NPM1-CIGB-300 complex by Rev and US11

Synthetic peptide CIGB-300 (also called p15-Tat; Fig. 5A) has been described as a proapoptotic and anti-cancer peptide, which directly targets and antagonizes NPM1 function in cancer cells [39,40]. Fluorescence polarization analysis revealed that a FITC-labelled CIGB-300 tightly associates with NPM1^{FL} and NPM1^{OD} but not with NPM1^{HRBD} and NPM1^{RBD} (Fig. 5B). Calculated K_d values for the FITC-labelled CIGB-300 interaction with NPM1^{FL} and NPM1^{OD} were 1.4 and 6.6 μ M, respectively.

We used the NPM1^{FL}- FITC-labelled CIGB-300 complex to further investigate NPM1 interactions with Rev and US11. The idea here was that titrating Rev or US11 to the complex may result in displacement of NPM1^{FL} from the FITC-labelled CIGB-300. Fig. 5C shows that increasing concentrations of US11, but not Rev, significantly displaced NPM1^{FL} from the FITC-labelled CIGB-300 complex. This result was surprising for two reasons: First, Rev binds NPM1 in a higher nanomolar range (Table 2) and should be able to compete with CIGB-300 provided that both bind to the same surface of the NPM1 protein. Interestingly, Rev revealed a 30-fold lower affinity for NPM1^{FL} as compared to NPM1^{OD} (Table 2), which may explain why Rev did not displace NPM1^{FL}

from FITC-labelled CIGB-300. Second, US11, which evidently exhibits an approximately 10-fold lower binding affinity for NPM1^{FL} as compared to Rev, is able to displace NPM1^{FL} from its complex with the synthetic FITC-labelled CIGB-300 (Fig. 5C). To address this issue we repeated the displacement experiments under the same conditions as before but used the FITC-labelled CIGB-300 complex with NPM1^{OD} instead of NPM1^{FL}. Data obtained revealed that both Rev and US11 efficiently displace FITC-labelled CIGB-300 by binding to NPM1^{OD} (Fig. 5D), indicating that Rev, US11 and FITC-labelled CIGB-300 have overlapping binding sites on NPM1^{OD}.

To obtain a first structural assessment of NPM1^{OD} site targeted by CIGB-300 we conducted a multistage protein-ligand docking approach. Assuming that basic part of CIGB-300 determines the binding, its Tat tail was docked in the first step. In the second step, the cyclic part was placed on the surface of NPM1^{OD} and linked to the peptide fulfilling geometry and energy criteria. Whole peptide contacted three out of five monomeric units of the pentameric NPM1^{OD}, but in a way that enables five copies of CIGB-300 to be generated without sterical clashes (Fig. 5E). It is important to note that a stoichiometry of 1:1 emerged spontaneously, as the criteria that five peptides should bind to NPM1^{OD} pentamer was not applied while generating of the model. The feature that CIGB-300 wraps around at least several monomeric units (Fig. 5E, middle panel) points to a stabilization effect of bound peptides and is consistent with the model of NPM1 in complex with R-rich proteins, such as p19^{ARF}, ARF6, Rev and the ribosomal protein L5 [36].

HIV-1 production is influenced in CIGB-300 treated cells

In order to investigate the possible role of NPM1-Rev interaction for HIV-1 replication, HOS-CD4.CXCR4 cells were incubated with CIGB-300 for 30 min or left untreated. After removing the peptide, cells were infected with HIV-1 (clone NL4.3, MOI 1). Culture supernatants were collected 48 and 72 h post infection and were quantified by titration on the HIV-1 reporter cells TZM-bl. In cells treated with CIGB-300, the virus production was reduced by 63% and 70% after 48 h and 72 h post infection, respectively (Fig. 6). Thus, CIGB-300 may interfere with an NPM1-Rev interaction in cells and affect Rev-dependent gene expression and subsequently HIV infection.

Discussion

Since its discovery 34 years ago, intensive research has been performed on NPM1. NPM1 is ubiquitously expressed and significantly upregulated in response to cellular stress signals [18,19,41,42] leading to the alteration of nucleolar structures and its re-localization to other cellular compartments. As a global effector, it has been implicated in maintenance of genomic stability, transcriptional gene regulation, ribosome biogenesis, centrosome duplication, DNA repair, control of cellular senescence, protection against radiation-induced apoptosis, tumor suppression, and has been increasingly emerging as a potential cellular factor for viral infection (see Table 1). Most of these functions have hitherto remained obscure and unexplained.

To shed light on the association of NPM1 with viral proteins, we have investigated its physical interaction with HIV-1 protein Rev and HSV-1 protein US11. Based on our results Rev exhibits affinity towards two NPM1 binding sites: on the pentameric, N-terminal oligomerization domain (NPM1^{OD}) and on the central histone-binding domain (NPM1^{HBD}), while HSV-US11 has only one binding site on NPM1^{OD}. We suggest that the different NPM1 domains interact in a mechanistically different mode with the Rev and US11 proteins. Rev association with NPM1 is the result of presumably an RNA-independent bimodal binding mechanism, according to our data, of (i) a low-affinity binding to the histone-binding domain of NPM1 (K_d 5.8 μ M) and (ii) a very high-

affinity binding to oligomerization domain of NPM1 (K_d 0.013 μ M), leading to an overall 0.4 μ M K_d value for the full-length NPM1 (Table 2). In the case of the NPM1-US11 interaction, we observed a strong binding of US11 to NPM1^{OD}, which is most probably achieved *via* its C-terminal RBD (US11^{Cterm}; See Figs. 1A and 4A). While the data regarding US11 reports its unprecedented direct interaction with NPM1, our measurements with Rev confirm previously obtained observations. It has been shown that two different transcripts of NPM1, B23.1 and B23.2, prevent the aggregation of Rev *via* their proposed chaperone activity [43]. B23.1, which was also used in this study, is identical to B23.2 but has a 35-amino acid longer C-terminus. As the prevention of Rev aggregation by both constructs was nearly identical, this C-terminus was excluded from the interaction with Rev [43], which is in agreement with our results from PD and ITC experiments (Fig. 2, S1A-C Fig. and Table 2). Our finding of a 1:1 ratio ($n \approx 0.84$) between NPM1 and Rev obtained by ITC (Table 2) is also consistent with earlier studies that have suggested a stoichiometric interaction between NPM1 and Rev, and a maximal stimulation of the import of Rev into the nucleus by NPM1 at a 1:1 molar ratio [4,43]. This stoichiometric ratio suggests that NPM1^{FL} exhibits one binding site for one HIV-1 Rev molecule. Since Rev has the tendency to aggregate also under normal physiological conditions [44], it is very likely that NPM1, by acting as a molecular chaperone, increases Rev's solubility and mobility during the import into and throughout the nucleus.

US11 is an abundant HSV-1 protein, which is expressed late during infection [45]. It has been reported that US11 functionally substitutes Rev and Rex proteins by stimulating expression of glycoproteins required for retroviral envelope synthesis [14]. US11 interaction with cellular proteins may, therefore, be required during HSV-1 infection. However, so far, only a few proteins including 2'-5'-oligoadenylate synthetase [46], cellular kinesin light-chain-related protein PAT1 [45], human ubiquitous kinesin heavy chain [24], protein kinase R (PKR) [47], protein activator of the interferon-induced protein kinase (PACT) [48], and nucleolin [23] have been reported. NPM1 and nucleolin are among the most abundant nucleolar proteins [5] with high functional but not structural similarities. They are usually found in the granular components and dense fibrillar components of nucleoli, have the same distribution as US11 [49], and are re-localized during HSV-1 infection [7,50]. With NPM1, we have identified in this study a new nucleolar protein partner for US11 and characterized the subdomains responsible for their interactions. US11 has two domains (Fig. 1A): An N-terminal domain called effector domain (ED) and a C-terminal RNA-binding domain (RBD). C-terminal domain consisting of 20–24 XPR (X, any amino acid; P, proline; R, arginine) repeats has a polyproline type II helix organization and is usually engaged in interactions with other proteins [15]. US11^{ED} is necessary for transactivation of gene expression, transport, and mRNA translation [15]. Therefore, we designed two deletion variants of US11 (N- and C- terminus) to determine the part involved in the interaction with NPM1. In contrast to nucleolin, which has been reported to interact with the C-terminus of US11 [23], our data clearly shows that both domains are apparently required for the interaction with NPM1. The C-terminal domain of US11, which is involved in the nucleolar localization of US11, binds to NPM1 stronger than the N-terminal domain (Fig. 4A). Since C-terminus of US11 is rich in arginine, these results support the idea that arginine-rich motif (R-rich) mediates the interactions with NPM1 [36]. Synthetic peptide CIGB-300 used in our investigation also falls into this category as it is the conjugate of R-rich peptide Tat, and the cyclic peptide (hence is called p15-Tat; Fig. 5A). This peptide, which has been described as a proapoptotic peptide with antiproliferative activity *in vitro* and antitumoral activity

in vivo [51], has been reported to directly bind to NPM1 [39,40]. We observed in this study that only NPM1^{OD}, but not the other domains of NPM1, associates with fCIGB-300. Interestingly, the K_d value for the fCIGB-300 interaction with NPM1^{FL}, derived from our polarization measurements (Fig. 5B), was indicative of almost 5-fold higher affinity than that of fCIGB-300-NPM1^{OD} interaction. This higher affinity can be explained by an avidity effect that originates from core N-terminal domain and the dynamic flexible tails, similarly to the model proposed for nucleoplasmin interaction with histones [52]. NPM1^{OD} is followed by the two highly acidic regions with disordered structure and a C-terminal RBD that folds as a three-helix bundle [53]. The biological significance of the acidic regions (A1-A3; Fig. 1A) has not been established. The A1 region in NPM1^{OD} has been recently shown to play a crucial role in the interaction with R-rich motifs of NPM1 binding proteins, such as p19ARF, ARF6, the ribosomal protein L5, and HIV1 Rev [36]. A model of the complex between NPM1^{OD} and CIGB-300 provided insights into different sites for the association of the CIGB-300 peptide, especially the R-rich motif of the CPP^{Tat} contacting negative charges of the A1 region of NPM1^{OD} (Figs. 1A and 5E). Additionally, our displacement experiment with Rev indicates that CIGB-300 shares the same binding site on NPM1 and may act as an inhibitor of NPM1-Rev interaction. Most likely for the same reason, we observed a reduced expression of viral production in HIV-1 infected cells treated with the CIGB-300 peptide (Fig. 6).

Furthermore, our displacement data shows that the NPM1-US11 interaction was also modulated by CIGB-300 (Figs. 5C and 5D). Thus, it is tempting to speculate that US11 and Rev, two functionally homologous viral proteins, share a similar binding site on NPM1 as suggested in this study for CIGB-300. An amino acid sequence analysis revealed clear differences in the R-rich motifs between Rev (³⁸RRNRRRRWRARAR⁴⁸) and US11, which consists of 21 'XPR' repeat motifs in US11^{Cterm}. R-rich motifs act as NLS by binding to the nuclear import receptors in nuclear translocation of viral proteins [10,12,54,55]. On the other hand, nucleolar shuttling and accumulation of Rev requires interaction with NPM1 [4,12]. US11 is similarly shuttling between the nucleus and the cytoplasm in transiently transfected cells and HSV-1-infected cells [20,56]. Mutagenesis and modeling studies of the C-terminus of US11, containing XPR repeats, have shown that this region is critical for both nucleolar accumulation of US11 and its nucleocytoplasmic export [15,57]. As mentioned above, CIGB-300 has the cell penetrating peptide Tat with R-rich motif, which corresponds to the presumed nuclear localization signal (NLS). Tat moves across the nuclear envelope and consequently drives CIGB-300 to the nucleus. Thus, we hypothesize that, (i) R-rich motifs of viral proteins serve as NPM1 binding sites that facilitate their nuclear transport analogous to NLS-importin system, and (ii) NPM1 most likely acts as an auxiliary factor for R-rich motif-containing viral proteins, such as HIV-1 Rev and HSV-1 US11, and achieves their transport into different nuclear compartments and subnuclear domains, leading to nuclear egress of infectious viral particles. Thus, NPM1 seems to represent a key protein in viral infections that is hijacked by invading pathogens to facilitate infection. As a consequence, NPM1 may represent a novel promising target for antiviral therapeutic intervention.

Conflict of interest

The authors declare no conflict of interest.

Acknowledgments

We thank Saeideh Nakhaei-Rad, Lothar Gremer and Roland P. Piekorz for discussions, Heiner Schaal for plasmid SVtat–rev-envRL, Ilse Meyer for technical assistance, and Mohammad M. Akbarzadeh and Mehdi Y. Matak for critical reading of the manuscript. This work was funded in part by the International Graduate School of Protein Science and Technology (iGRASP), the Research Commission of the Medical Faculty and the Strategic Research Fund (SFF) of Heinrich-Heine University Düsseldorf, the International Research Training Group 1902 (IRTG 1902) “Intra- and interorgan communication of the cardiovascular system”, the German Research Foundation (Deutsche Forschungsgemeinschaft or DFG) through the Collaborative Research Center 974 (SFB 974) “Communication and Systems Relevance during Liver Injury and Regeneration”, and GRK 1045 “Modulation of host cell function”. C.M. is supported by the Heinz Ansmann foundation. A.H. is supported by the Jürgen Manchot Foundation, Molecules of Infection Graduate School.

References

1. Colombo E, Alcalay M, Pelicci PG (2011) Nucleophosmin and its complex network: a possible therapeutic target in hematological diseases. *Oncogene* 30: 2595-2609.
2. Okuwaki M, Matsumoto K, Tsujimoto M, Nagata K (2001) Function of nucleophosmin/B23, a nucleolar acidic protein, as a histone chaperone. *FEBS Lett* 506: 272-276.
3. Okuwaki M (2007) The Structure and Functions of NPM1/Nucleophosmin/B23, a Multifunctional Nucleolar Acidic Protein. *Journal of Biochemistry* 143: 441-448.
4. Fankhauser C, Izaurralde E, Adachi Y, Wingfield P, Laemmli UK (1991) Specific complex of human immunodeficiency virus type 1 rev and nucleolar B23 proteins: dissociation by the Rev response element. *Mol Cell Biol* 11: 2567-2575.
5. Taha MS, Nouri K, Milroy LG, Moll JM, Herrmann C, et al. (2014) Subcellular fractionation and localization studies reveal a direct interaction of the fragile X mental retardation protein (FMRP) with nucleolin. *PLoS ONE* 9: e91465.
6. Adachi Y, Copeland TD, Hatanaka M, Oroszlan S (1993) Nucleolar targeting signal of Rex protein of human T-cell leukemia virus type I specifically binds to nucleolar shuttle protein B-23. *J Biol Chem* 268: 13930-13934.
7. Lymberopoulos MH, Bourget A, Abdeljelil NB, Pearson A (2011) Involvement of the UL24 protein in herpes simplex virus 1-induced dispersal of B23 and in nuclear egress. *Virology* 412: 341-348.
8. Hope TJ (1999) The ins and outs of HIV Rev. *Arch Biochem Biophys* 365: 186-191.
9. Cochrane AW, Perkins A, Rosen CA (1990) Identification of sequences important in the nucleolar localization of human immunodeficiency virus Rev: relevance of nucleolar localization to function. *J Virol* 64: 881-885.
10. Suhasini M, Reddy TR (2009) Cellular proteins and HIV-1 Rev function. *Curr HIV Res* 7: 91-100.
11. Kula A, Guerra J, Knezevich A, Kleva D, Myers MP, et al. (2011) Characterization of the HIV-1 RNA associated proteome identifies MatrIn 3 as a nuclear cofactor of Rev function. *Retrovirology* 8: 1742-4690.
12. Lin MH, Sivakumaran H, Apolloni A, Wei T, Jans DA, et al. (2012) Nullbasic, a potent anti-HIV tat mutant, induces CRM1-dependent disruption of HIV rev trafficking. *PLoS ONE* 7: e51466.
13. He JJ, Henao-Mejia J, Liu Y (2009) Sam68 functions in nuclear export and translation of HIV-1 RNA. *RNA Biol* 6: 384-386.
14. Diaz JJ, Dodon MD, Schaerer-Uthurralt N, Simonin D, Kindbeiter K, et al. (1996) Post-transcriptional transactivation of human retroviral envelope glycoprotein expression by herpes simplex virus Us11 protein. *Nature* 379: 273-277.
15. Schaerer-Uthurralt N, Erard M, Kindbeiter K, Madjar JJ, Diaz JJ (1998) Distinct domains in herpes simplex virus type 1 US11 protein mediate post-transcriptional transactivation of human T-lymphotropic virus type I envelope glycoprotein gene expression and specific binding to the Rex responsive element. *J Gen Virol* 79: 1593-1602.
16. Kelly BJ, Fraefel C, Cunningham AL, Diefenbach RJ (2009) Functional roles of the tegument proteins of herpes simplex virus type 1. *Virus Res* 145: 173-186.
17. Roller RJ, Monk LL, Stuart D, Roizman B (1996) Structure and function in the herpes simplex virus 1 RNA-binding protein U(s)11: mapping of the domain required for ribosomal and nucleolar association and RNA binding in vitro. *J Virol* 70: 2842-2851.
18. Mulvey M, Arias C, Mohr I (2006) Resistance of mRNA translation to acute endoplasmic reticulum stress-inducing agents in herpes simplex virus type 1-infected cells requires multiple virus-encoded functions. *J Virol* 80: 7354-7363.
19. Giraud S, Diaz-Latoud C, Hacot S, Textoris J, Bourette RP, et al. (2004) US11 of herpes simplex virus type 1 interacts with HIPK2 and antagonizes HIPK2-induced cell growth arrest. *J Virol* 78: 2984-2993.
20. Xing J, Wu F, Pan W, Zheng C (2010) Molecular anatomy of subcellular localization of HSV-1 tegument protein US11 in living cells. *Virus Research* 153: 71-81.
21. Salsman J, Zimmerman N, Chen T, Domagala M, Frappier L (2008) Genome-wide screen of three herpesviruses for protein subcellular localization and alteration of PML nuclear bodies. *PLoS Pathog* 4: e1000100.
22. Roller RJ, Roizman B (1991) Herpes simplex virus 1 RNA-binding protein US11 negatively regulates the accumulation of a truncated viral mRNA. *J Virol* 65: 5873-5879.
23. Greco A, Arata L, Soler E, Gaume X, Coute Y, et al. (2011) Nucleolin Interacts with US11 Protein of Herpes Simplex Virus 1 and Is Involved in Its Trafficking. *Journal of Virology* 86: 1449-1457.
24. Diefenbach RJ, Miranda-Saksena M, Diefenbach E, Holland DJ, Boadle RA, et al. (2002) Herpes simplex virus tegument protein US11 interacts with conventional kinesin heavy chain. *J Virol* 76: 3282-3291.

25. Cassady KA, Gross M (2002) The herpes simplex virus type 1 U(S)11 protein interacts with protein kinase R in infected cells and requires a 30-amino-acid sequence adjacent to a kinase substrate domain. *J Virol* 76: 2029-2035.
26. Brown SM, Harland J (1987) Three mutants of herpes simplex virus type 2: one lacking the genes US10, US11 and US12 and two in which Rs has been extended by 6 kb to 0.91 map units with loss of Us sequences between 0.94 and the Us/TRs junction. *J Gen Virol* 68: 1-18.
27. Diaz-Latoud C, Diaz JJ, Fabre-Jonca N, Kindbeiter K, Madjar JJ, et al. (1997) Herpes simplex virus Us11 protein enhances recovery of protein synthesis and survival in heat shock treated HeLa cells. *Cell Stress Chaperones* 2: 119-131.
28. Yang C, Maiguel DA, Carrier F (2002) Identification of nucleolin and nucleophosmin as genotoxic stress-responsive RNA-binding proteins. *Nucleic Acids Res* 30: 2251-2260.
29. Widera M, Erkelenz S, Hillebrand F, Krikoni A, Widera D, et al. (2013) An intronic G run within HIV-1 intron 2 is critical for splicing regulation of vif mRNA. *J Virol* 87: 2707-2720.
30. Jaiswal M, Dubey BN, Koessmeier KT, Gremer L, Ahmadian MR (2012) Biochemical assays to characterize Rho GTPases. *Methods in molecular biology* 827: 37-58.
31. Eberth A, Ahmadian MR (2009) In vitro GEF and GAP assays. *Curr Protoc Cell Biol* Chapter 14: Unit 14 19.
32. Risse SL, Vaz B, Burton MF, Aspenstrom P, Piekorz RP, et al. (2013) SH3-mediated targeting of Wrch1/RhoU by multiple adaptor proteins. *Biol Chem* 394: 421-432.
33. Wennerberg K, Der CJ (2004) Rho-family GTPases: it's not only Rac and Rho (and I like it). *J Cell Sci* 117: 1301-1312.
34. Lam BD, Hordijk PL (2013) The Rac1 hypervariable region in targeting and signaling: a tail of many stories. *Small GTPases* 4: 78-89.
35. Thakur HC, Singh M, Nagel-Steger L, Kremer J, Prumbaum D, et al. (2014) The centrosomal adaptor TACC3 and the microtubule polymerase chTOG interact via defined C-terminal subdomains in an Aurora-A kinase-independent manner. *J Biol Chem* 289: 74-88.
36. Mitrea DM, Grace CR, Buljan M, Yun MK, Pytel NJ, et al. (2014) Structural polymorphism in the N-terminal oligomerization domain of NPM1. *Proc Natl Acad Sci U S A* 111: 4466-4471.
37. Brooks BR, Brooks CL, 3rd, Mackerell AD, Jr., Nilsson L, Petrella RJ, et al. (2009) CHARMM: the biomolecular simulation program. *J Comput Chem* 30: 1545-1614.
38. Miyazaki Y, Nosaka T, Hatanaka M (1996) The post-transcriptional regulator Rev of HIV: implications for its interaction with the nucleolar protein B23. *Biochimie* 78: 1081-1086.
39. Perera Y, Farina HG, Gil J, Rodriguez A, Benavent F, et al. (2009) Anticancer peptide CIGB-300 binds to nucleophosmin/B23, impairs its CK2-mediated phosphorylation, and leads to apoptosis through its nucleolar disassembly activity. *Molecular Cancer Therapeutics* 8: 1189-1196.
40. Perera Y, Costales HC, Diaz Y, Reyes O, Farina HG, et al. (2012) Sensitivity of tumor cells towards CIGB-300 anticancer peptide relies on its nucleolar localization. *J Pept Sci* 18: 215-223.
41. Kurki S, Peltonen K, Laiho M (2004) Nucleophosmin, HDM2 and p53: players in UV damage incited nucleolar stress response. *Cell Cycle* 3: 976-979.
42. Lindstrom MS, Zhang Y (2006) B23 and ARF: friends or foes? *Cell Biochem Biophys* 46: 79-90.
43. Szebeni A, Olson MO (1999) Nucleolar protein B23 has molecular chaperone activities. *Protein Sci* 8: 905-912.
44. DiMattia MA, Watts NR, Stahl SJ, Rader C, Wingfield PT, et al. (2010) Implications of the HIV-1 Rev dimer structure at 3.2 Å resolution for multimeric binding to the Rev response element. *Proc Natl Acad Sci U S A* 107: 5810-5814.
45. Benboudjema L, Mulvey M, Gao Y, Pimplikar SW, Mohr I (2003) Association of the herpes simplex virus type 1 Us11 gene product with the cellular kinesin light-chain-related protein PAT1 results in the redistribution of both polypeptides. *J Virol* 77: 9192-9203.
46. Sanchez R, Mohr I (2007) Inhibition of cellular 2'-5' oligoadenylate synthetase by the herpes simplex virus type 1 Us11 protein. *J Virol* 81: 3455-3464.
47. Khoo D, Perez C, Mohr I (2002) Characterization of RNA determinants recognized by the arginine- and proline-rich region of Us11, a herpes simplex virus type 1-encoded double-stranded RNA binding protein that prevents PKR activation. *J Virol* 76: 11971-11981.
48. Peters GA, Khoo D, Mohr I, Sen GC (2002) Inhibition of PACT-mediated activation of PKR by the herpes simplex virus type 1 Us11 protein. *J Virol* 76: 11054-11064.
49. Besse S, Diaz JJ, Pichard E, Kindbeiter K, Madjar JJ, et al. (1996) In situ hybridization and immuno-electron microscope analyses of the Us11 gene of herpes simplex virus type 1 during transient expression. *Chromosoma* 104: 434-444.

50. Lymberopoulos MH, Pearson A (2007) Involvement of UL24 in herpes-simplex-virus-1-induced dispersal of nucleolin. *Virology* 363: 397-409.
51. Perea SE, Reyes O, Baladron I, Perera Y, Farina H, et al. (2008) CIGB-300, a novel proapoptotic peptide that impairs the CK2 phosphorylation and exhibits anticancer properties both in vitro and in vivo. *Molecular and Cellular Biochemistry* 316: 163-167.
52. Taneva SG, Bañuelos S, Falces J, Arregi I, Muga A, et al. (2009) A Mechanism for Histone Chaperoning Activity of Nucleoplasmin: Thermodynamic and Structural Models. *Journal of Molecular Biology* 393: 448-463.
53. Gallo A, Lo Sterzo C, Mori M, Di Matteo A, Bertini I, et al. (2012) Structure of Nucleophosmin DNA-binding Domain and Analysis of Its Complex with a G-quadruplex Sequence from the c-MYC Promoter. *Journal of Biological Chemistry* 287: 26539-26548.
54. Jeang KT, Xiao H, Rich EA (1999) Multifaceted activities of the HIV-1 transactivator of transcription, Tat. *J Biol Chem* 274: 28837-28840.
55. Cardarelli F, Serresi M, Bizzarri R, Giacca M, Beltram F (2007) In vivo study of HIV-1 Tat arginine-rich motif unveils its transport properties. *Mol Ther* 15: 1313-1322.
56. Attrill HL, Cumming SA, Clements JB, Graham SV (2002) The herpes simplex virus type 1 US11 protein binds the coterminal UL12, UL13, and UL14 RNAs and regulates UL13 expression in vivo. *J Virol* 76: 8090-8100.
57. Catez F, Erard M, Schaerer-Uthurralt N, Kindbeiter K, Madjar JJ, et al. (2002) Unique Motif for Nucleolar Retention and Nuclear Export Regulated by Phosphorylation. *Molecular and Cellular Biology* 22: 1126-1139.
58. Bevington JM, Needham PG, Verrill KC, Collaco RF, Basrur V, et al. (2007) Adeno-associated virus interactions with B23/Nucleophosmin: identification of sub-nucleolar virion regions. *Virology* 357: 102-113.
59. Matthews DA (2001) Adenovirus protein V induces redistribution of nucleolin and B23 from nucleolus to cytoplasm. *J Virol* 75: 1031-1038.
60. Ugai H, Dobbins GC, Wang M, Le LP, Matthews DA, et al. (2012) Adenoviral protein V promotes a process of viral assembly through nucleophosmin 1. *Virology* 432: 283-295.
61. Okuwaki M, Iwamatsu A, Tsujimoto M, Nagata K (2001) Identification of nucleophosmin/B23, an acidic nucleolar protein, as a stimulatory factor for in vitro replication of adenovirus DNA complexed with viral basic core proteins. *J Mol Biol* 311: 41-55.
62. Samad MA, Okuwaki M, Haruki H, Nagata K (2007) Physical and functional interaction between a nucleolar protein nucleophosmin/B23 and adenovirus basic core proteins. *FEBS Lett* 581: 3283-3288.
63. Samad MA, Komatsu T, Okuwaki M, Nagata K (2012) B23/nucleophosmin is involved in regulation of adenovirus chromatin structure at late infection stages, but not in virus replication and transcription. *J Gen Virol* 93: 1328-1338.
64. Abraham R, Mudaliar P, Jaleel A, Srikanth J, Sreekumar E (2015) High throughput proteomic analysis and a comparative review identify the nuclear chaperone, Nucleophosmin among the common set of proteins modulated in Chikungunya virus infection. *J Proteomics* 120: 126-141.
65. Malik-Soni N, Frappier L (2012) Proteomic profiling of EBNA1-host protein interactions in latent and lytic Epstein-Barr virus infections. *J Virol* 86: 6999-7002.
66. Malik-Soni N, Frappier L (2014) Nucleophosmin contributes to the transcriptional activation function of the Epstein-Barr virus EBNA1 protein. *J Virol* 88: 2323-2326.
67. Liu CD, Chen YL, Min YL, Zhao B, Cheng CP, et al. (2012) The nuclear chaperone nucleophosmin escorts an Epstein-Barr Virus nuclear antigen to establish transcriptional cascades for latent infection in human B cells. *PLoS Pathog* 8: e1003084.
68. Bazot Q, Deschamps T, Tafforeau L, Siouda M, Leblanc P, et al. (2014) Epstein-Barr virus nuclear antigen 3A protein regulates CDKN2B transcription via interaction with MIZ-1. *Nucleic Acids Res* 42: 9700-9716.
69. Aminev AG, Amineva SP, Palmenberg AC (2003) Encephalomyocarditis viral protein 2A localizes to nucleoli and inhibits cap-dependent mRNA translation. *Virus Res* 95: 45-57.
70. Ning B, Shih C (2004) Nucleolar localization of human hepatitis B virus capsid protein. *J Virol* 78: 13653-13668.
71. Lee SJ, Shim HY, Hsieh A, Min JY, Jung G (2009) Hepatitis B virus core interacts with the host cell nucleolar protein, nucleophosmin 1. *J Microbiol* 47: 746-752.
72. Jeong H, Cho MH, Park SG, Jung G (2014) Interaction between nucleophosmin and HBV core protein increases HBV capsid assembly. *FEBS Lett* 588: 851-858.
73. Li WH, Miao XH, Qi ZT, Ni W, Zhu SY, et al. (2009) Proteomic analysis of differently expressed proteins in human hepatocellular carcinoma cell lines HepG2 with transfecting hepatitis B virus X gene. *Chin Med J (Engl)* 122: 15-23.

74. Ahuja R, Kapoor NR, Kumar V (2015) The HBx oncoprotein of hepatitis B virus engages nucleophosmin to promote rDNA transcription and cellular proliferation. *Biochim Biophys Acta* 1850: 1783-1795.
75. Mai RT, Yeh TS, Kao CF, Sun SK, Huang HH, et al. (2006) Hepatitis C virus core protein recruits nucleolar phosphoprotein B23 and coactivator p300 to relieve the repression effect of transcriptional factor YY1 on B23 gene expression. *Oncogene* 25: 448-462.
76. Huang WH, Yung BY, Syu WJ, Lee YH (2001) The nucleolar phosphoprotein B23 interacts with hepatitis delta antigens and modulates the hepatitis delta virus RNA replication. *J Biol Chem* 276: 25166-25175.
77. Marasco WA, Szilvay AM, Kalland KH, Helland DG, Reyes HM, et al. (1994) Spatial association of HIV-1 tat protein and the nucleolar transport protein B23 in stably transfected Jurkat T-cells. *Arch Virol* 139: 133-154.
78. Li YP (1997) Protein B23 is an important human factor for the nucleolar localization of the human immunodeficiency virus protein Tat. *J Virol* 71: 4098-4102.
79. Gadad SS, Rajan RE, Senapati P, Chatterjee S, Shandilya J, et al. (2011) HIV-1 infection induces acetylation of NPM1 that facilitates Tat localization and enhances viral transactivation. *J Mol Biol* 410: 997-1007.
80. Oliveira AP, Simabuco FM, Tamura RE, Guerrero MC, Ribeiro PG, et al. (2013) Human respiratory syncytial virus N, P and M protein interactions in HEK-293T cells. *Virus Res* 177: 108-112.
81. Tsuda Y, Mori Y, Abe T, Yamashita T, Okamoto T, et al. (2006) Nucleolar protein B23 interacts with Japanese encephalitis virus core protein and participates in viral replication. *Microbiol Immunol* 50: 225-234.
82. Sarek G, Jarviluoma A, Moore HM, Tojkander S, Vartia S, et al. (2010) Nucleophosmin phosphorylation by v-cyclin-CDK6 controls KSHV latency. *PLoS Pathog* 6: 1000818.
83. Duan Z, Chen J, Xu H, Zhu J, Li Q, et al. (2014) The nucleolar phosphoprotein B23 targets Newcastle disease virus matrix protein to the nucleoli and facilitates viral replication. *Virology* 452-453: 212-222.
84. Lv M, Chen J, Shi H, Chen X, Fan X, et al. (2011) [Co-localization analysis between porcine epidemic diarrhea virus nucleocapsid protein and nucleolar phosphoprotein B23.1]. *Wei Sheng Wu Xue Bao* 51: 643-647.

Table 1 - Nucleophosmin involvement in multiple viral infections.

Virus ^a	Partner	Domain	Effect/observation	References
AAV	Rep	n.d.	Viral assembly	[58]
Adenovirus	Core protein V	n.d.	NPM1 re-localization, Replication, Viral assembly	[59,60]
	Basic core protein	n.d.	Transcription, Replication	[61]
	Core protein V, pre-VII	n.d.	Replication, chromatin assembly	[62,63]
CHIKV	n.d.	n.d.	n.d.	[64]
EBV	EBNA1	HBD	Transcription	[65,66]
	EBNA2	OD	Transcription, latency	[67]
	EBNA3	n.d.	Transcription	[68]
EMCV	3BCD	n.d.	Nuclear transport	[69]
HBV	core protein 149	n.d.	Capsid assembly	[70-72]
	X protein	n.d.	n.d.	[73,74]
HCV	Core protein	n.d.	Transcription	[75]
HDV	Antigen	n.d.	n.d.	[76]
HIV-1	Rev	OD, HBD	n.d.	[4]; this study
	Tat	n.d.	NPM1 acetylation, transcription	[77-79],
HRSV	Matrix protein	n.d.	Replication	[80]
HSV-1	UL24	n.d.	NPM1 re-localization	[7]
	US11	OD	n.d.	this study
HTLV-1	Rex	HBD	n.d.	[6]
JEV	Core protein	OD	Replication	[81]
KSHV	LANA	n.d.	NPM1 phosphorylation (T199), latency	[82]
NDV	Matrix protein M	RBD	NPM1 re-localization, Replication	[83]
PEDV	N protein	n.d.	Nucleolar co-localization	[84]

^a Virus abbreviation: AAV, Adeno-associated virus; EBV, Epstein Barr virus; CHIKV, Chikungunya virus; EMCV, Encephalomyocarditis virus; HBV, Hepatitis B virus; HCV, Hepatitis C virus; HDV, Hepatitis delta virus; HIV-1, Human immunodeficiency virus type 1; HRSV, Human respiratory syncytial virus; HSV-1, Herpes simplex virus type 1; HTLV1, Human T-cell leukemia virus type 1; JEV, Japanese encephalitis virus; KSHV, **Kaposi's sarcoma-associated herpes virus**; NDV, Newcastle disease virus; PEDV, porcine epidemic diarrhea virus. n.d., not determined.

Table 2 - ITC data for HIV-1 Rev^{FL} interaction with NPM1 variants.

Protein	K_d (μM) ^a	ΔH (kcal/mol)	$T\Delta S$ (kcal/mol)	n (sites)
NPM1 ^{FL}	0.41	-16.50±0.47	-0.66	0.84
NPM1 ^{OD}	0.013	-3.79±0.11	-0.58	0.94
NPM1 ^{HRBD}	18	-3.23±0.31	-0.27	0.76
NPM1 ^{HBD}	5.8	-1.71±0.20	-0.71	0.85
NPM1 ^{RBD}	no binding	-	-	-

K_a , association constant; K_d , dissociation constant; ΔH , enthalpy; n, binding stoichiometry (number of binding sites). HIV-1 Rev^{FL} did not show any binding to the RNA-binding domain (RBD) of NPM1. All measurements were performed at 25 °C. ^a K_d values were calculated from $K_d = 1/K_a$.

Table 3 - AUC-SV data for NPM1^{FL}, NPM1^{OD}, and US11^{FL}, respectively.

Proteins	$S_{20,w}$ (S)	Std. dev.	f/f_0	MW (kDa)
NPM1 ^{FL}	6.7	0.52	1.5	146
NPM1 ^{OD}	4.5	0.14	1.27 – 1.40	63.3
US11 ^{FL}	1.4	0.20	1.4 - 1.7	15.3

MW, molecular weight; $S_{20,w}$ (S), sedimentation rate at 20 °C; f/f_0 , frictional coefficient. In all three cases the values refer to a single, dominant species, which represented more than 90 % of the sample.

Figure legends

Fig. 1. Schematic representation of domain organization, various constructs and proteins of NPM1, HSV-1 US11, and HIV-1 Rev.

(A) Domains and various constructs of NPM1, US11 and Rev. The numbers indicate the N- and C-terminal amino acids of the respective constructs used in this study. A1-A3, acidic regions 1-3; Cterm, C-terminal; ED, effector domain; FL, full-length; HRBD, histone and RNA-binding domains; HBD, histone binding domain; NES, nuclear export signal; NLS, nuclear localization signal; NoLS, nucleolar localization signal; Nterm, N-terminal; OD, oligomerization domain; RBD, RNA-binding domain. (B) Coomassie brilliant blue (CBB) stained SDS-PAGE of purified proteins used in this study.

Fig. 2. Direct NPM1 interaction with HIV-1 Rev.

(A) Qualitative interaction analysis by GST pull-down assay and subsequent CBB staining. NPM1 FL, OD and HRBD, but not RBD, displayed a selective interaction with HIV-1 Rev (upper panel), which was also observed after an RNase A treatment (lower panel). (B) Quantitative interaction analysis by ITC. The binding parameters for the interaction between NPM1^{FL} and Rev were obtained using ITC. Titration of NPM1^{FL} (750 μ M) to Rev^{FL} (35 μ M) showed an exothermic response (negative peaks) indicating that Rev selectively interacts with NPM1^{FL}. The upper graph shows calorimetric changes plotted versus the time and the lower graph represents the changes in temperature according to the molar ratio of the interacting proteins. (C) No interaction was observed in a control experiments by titrating NPM1^{RBD} (300 μ M) to Rev^{FL} (30 μ M).

Fig. 3. NPM1 association with HSV-1 US11 in the cell.

(A) Nucleolar colocalization of endogenous NPM1 with myc-US11. Confocal images of HeLa cells transfected with myc-US11 were obtained by staining endogenous NPM1 (Mouse anti-NPM1 (ab10530)), myc-US11 (anti-myc antibody), and filamentous actin (rhodamine-phalloidin). For clarity, a boxed area in the merged panel shows colocalization of NPM1 and US11 in the nucleolus as pointed by arrows. Scale bar: 20 μ m. (B) Myc-US11 associates with endogenous NPM1 in COS-7 cells. NPM1 was co-immunoprecipitated with myc-US11 overexpressed in COS-7 cells using anti-myc antibody. A normal Rabbit IgG and sample without antibody were used as IP controls. Input, 5% of total cell lysate; IP, immunoprecipitation; IB, immunoblotting. (C) Myc-US11^{FL} displayed an interaction with NPM1^{FL}. Myc-US11^{FL} was pulled down with the GST-fusion NPM1^{FL}, but not with GST, which was used as a negative control. Samples prior pull-down (PD) analysis were used as input control.

Fig. 4. Physical interaction of HSV-1 US11 with NPM1.

(A) C-terminal region of US11 largely contributes to NPM1 interaction. Pull-down experiments were conducted with purified proteins in the presence of RNase A by using GST-fused US11^{FL}, US11^{Nterm}, US11^{Cterm}, and GST as a negative control. For the detection of NPM1 variants two different antibodies were used, ab52644 recognized an N-terminal epitope containing in NPM1^{FL} and NPM1^{OD}, and ab10530 recognized a C-terminal epitope containing in NPM1^{HRBD} and NPM1^{RBD}. The same pattern of interaction was obtained for the N-terminal and the C-terminal parts of US11, although the interaction between NPM1^{FL} and NPM1^{OD} with US11^{Nterm} was much weaker than with US11^{Cterm}. The exposure time was 1 min for all the blots. (B-C) US11 binds NPM1 with a binding constant in the low micromolar range. To measure the binding parameter for the NPM1-US11 interaction, 1.2 mM NPM1^{FL} (B) and buffer (C) were titrated to 60 μ M US11^{FL}. Both NPM1 and US11 were treated with RNase A. Conditions were the same as described in Fig. 2. US11

binding to NPM1 is an endothermic reaction. **(D)** US11 binds to a pentameric NPM1. aSEC-MALS/RI analysis of NPM1^{OD}, US11^{FL}, and a mixture of both proteins revealed an oligomeric nature of NPM1^{OD} with a molecular weight (MW) of 66.1 kDa corresponding to the pentameric form. Obtained MW for US11 was 16.6 kDa, which matches the theoretical MW of 16.7 kDa for a monomeric US11 (upper panel). SDS-PAGE and CBB staining of the aSEC (Superdex 200, 10/300) elution fractions of NPM1^{OD}, US11^{FL}, and a mixture of both clearly revealed a NPM1-US11 complex formation (lower panel). Both NPM1 and US11 were treated with RNase A. The MW of this complex corresponds to 76.6 kDa for a pentameric NPM1^{OD}, and a monomeric US11^{FL}. A MW of 21.8 kDa was measured that is estimated to an unbound US11^{FL}.

Fig. 5. The synthetic peptide CIGB-300 competes with Rev and US11 by binding NPM1^{OD} with high-affinity.

(A) CIGB-300 consists of the cyclic P15 (blue) and the Tat (purple) peptides, and labeled with fluorescein (green; FITC). **(B)** Fluorescence polarization experiments conducted by titrating increasing amounts of NPM1 variants, Rev, US11, and GST to 0.1 μ M FITC-labelled CIGB-300 (f CIGB-300). A high affinity interaction with the peptide was only observed for NPM1^{FL} and NPM1^{OD}, resulting from an increase of polarization, but not for Rev, US11, GST, and the other NPM1 variants. **(C-D)** Contrary to US11, Rev only displaced NPM1^{OD} from its fCIGB-300 complex. Displacement experiments were performed by adding increasing amounts of Rev or US11 to the NPM1^{FL}-fCIGB-300 complex **(C)** or to the NPM1^{OD}-fCIGB-300 complex **(D)**. **(E)** A proposed NPM1^{OD}-CIGB-300 docking model of pentameric NPM1^{OD} structure in the complex with CIGB-300. Cyclic part (blue) and basic part (purple) of the peptide shown as sticks and ribbons wraps around several monomeric units of NPM1 represented by surfaces in different colors shown in top view (left), rotated orientation (middle), and the bottom view (right).

Fig. 6. CIGB300 treatment interferes with HIV-1 production.

CIGB-300 treated or untreated HOS.CD4.CXCR4 cells were infected with NL4.3 virus at an MOI of 1. Culture supernatant was collected 48 and 72 h post infection and virus titer was determined. The figure shows one representative experiment out of four, in which virus quantification was performed by TZM-bl cell titration. Values are the means \pm S.D. of three measurements. Statistical significance (P) was calculated by the Student's t-test: ***P<0.002; **P<0.02.

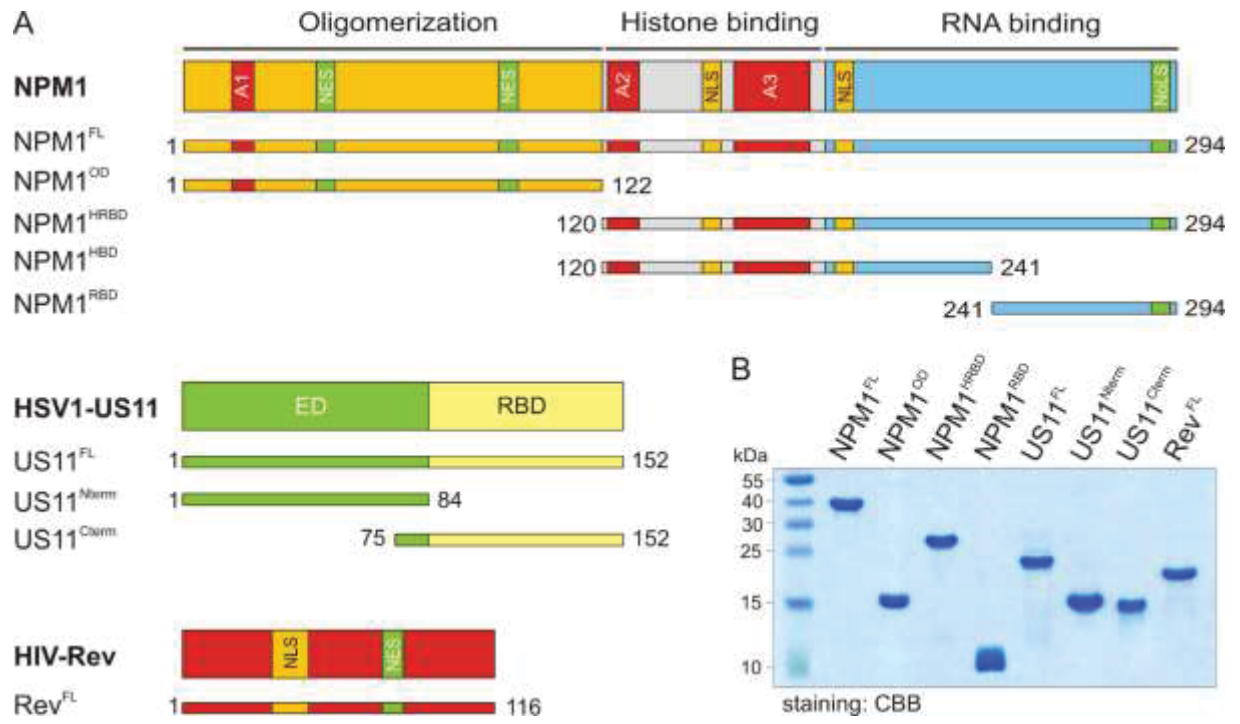
Supporting Information

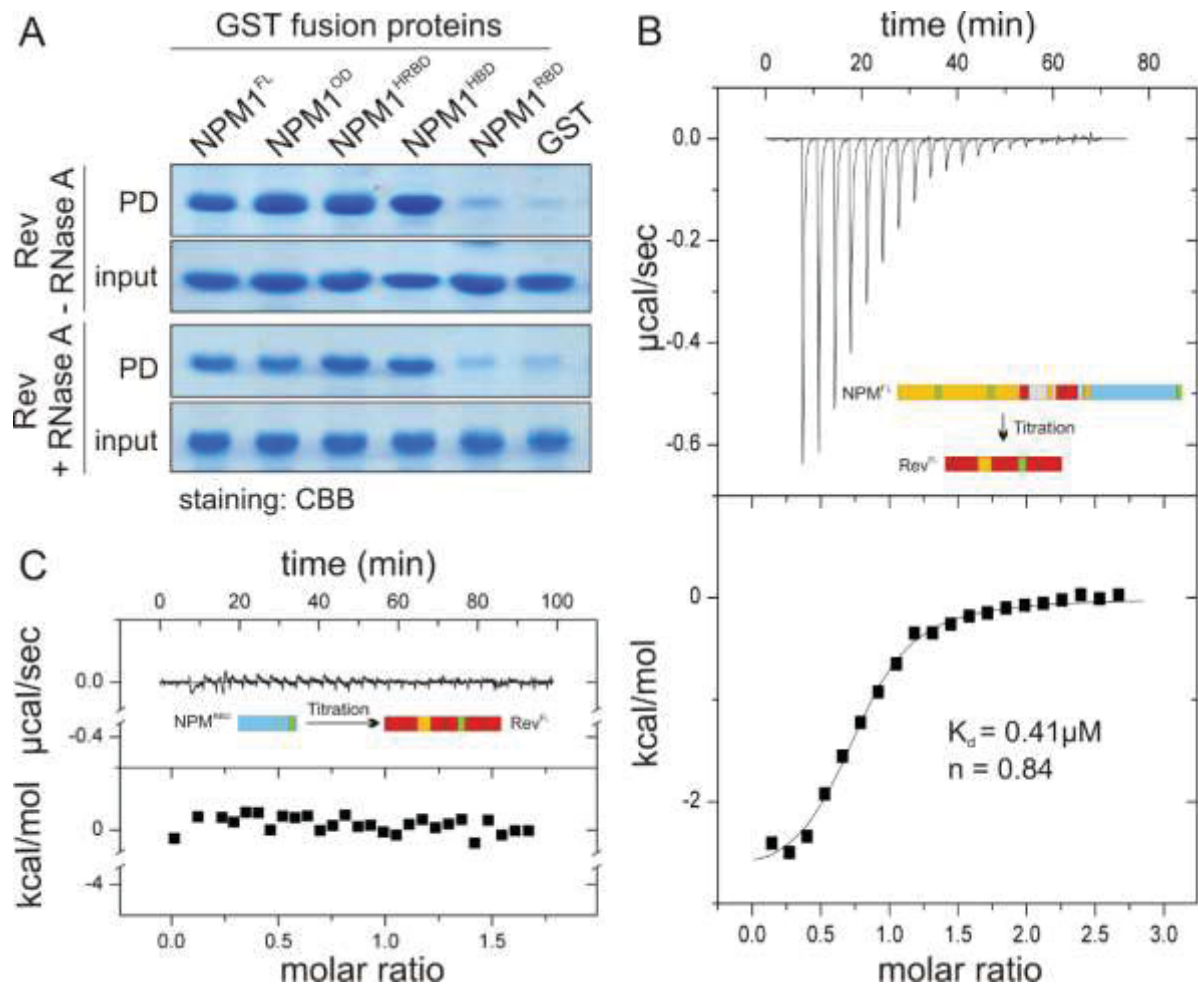
S1 Fig. Physical interaction of HIV-1 Rev with NPM1.

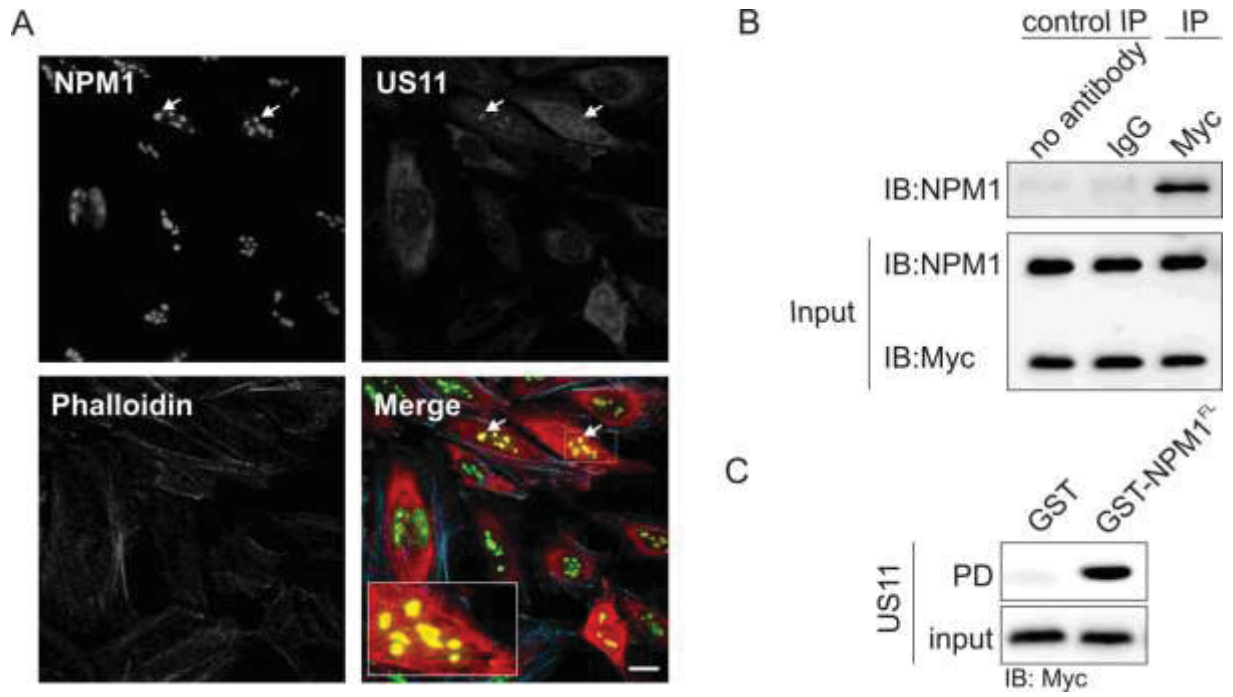
Quantitative interaction analysis were performed by ITC at 25°C by titrating (A) NPM1OD (450 μ M) to 30 μ M HIV-1 Rev, (B) NPM1HBD (350 μ M) to 25 μ M HIV-1 Rev and (C) NPM1HRBD (800 μ M) to 50 μ M HIV-1 Rev, respectively. The upper graph shows calorimetric changes plotted versus the time, and the lower graph represents the changes in temperature according to the molar ratio of the interacting proteins.

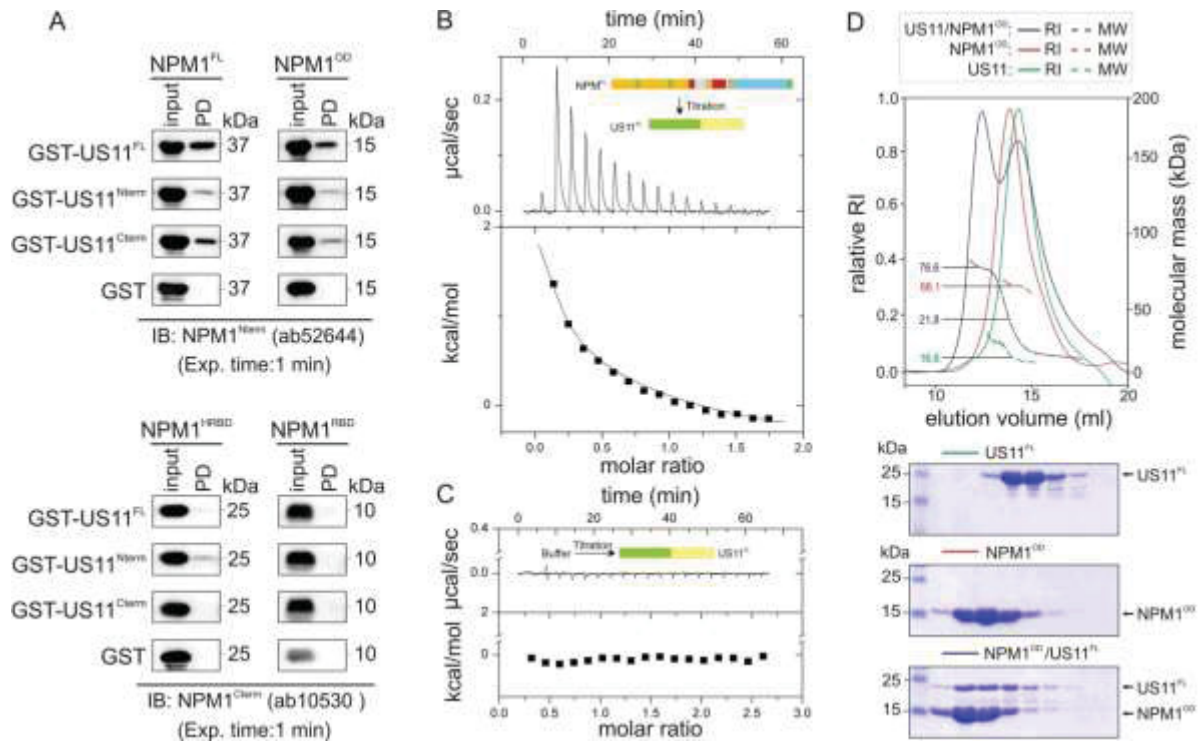
S2 Fig. Analytical ultracentrifugation for the determination of the oligomeric state and molecular mass of US11 and NPM1.

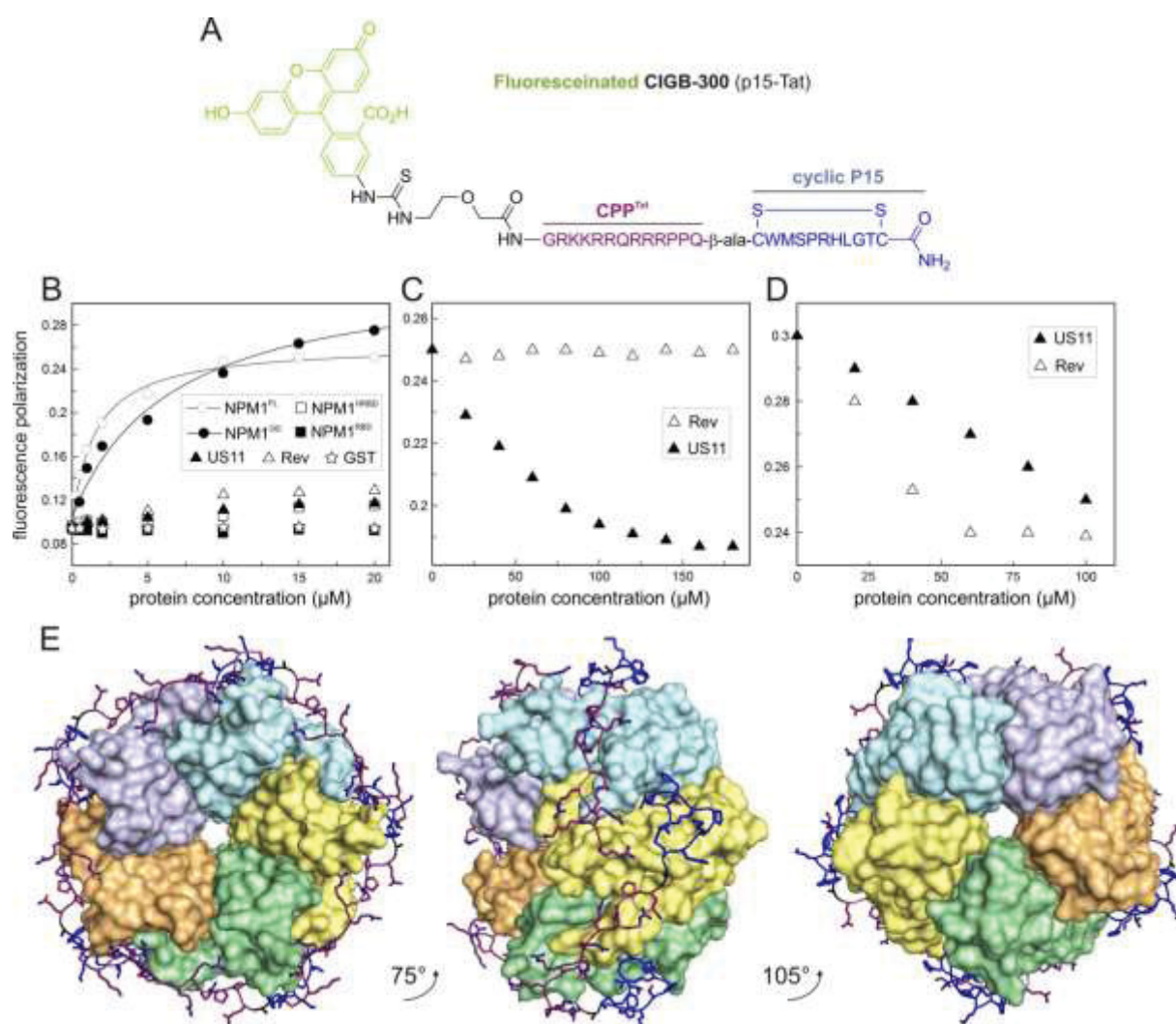
(A) Sedimentation velocity analysis of US11^{FL} and NPM1^{FL} at 35,000 rpm and 20 °C. Graphs show the evaluated $c(s)$ distributions obtained by SEDFIT. For presentation, curves had been normalized to maximum peak height. Results revealed that NPM1^{FL} and US11^{FL} are pentameric and monomeric, respectively. **(B)** The left panel contains data obtained from the sedimentation velocity analysis of NPM1^{OD}, which shows the population of pentamer, and the right panel are data obtained from sedimentation equilibrium analysis of 0.25 μ M NPM1^{OD} at 14000 (purple), 16000 (blue), 25000 (cyan), 42000 (green) and 50000 rpm (yellow) at 20°C. Experimentally determined concentration profiles were fitted globally with a single species model resulting in a molecular mass of 65180 \pm 640 Da corresponding to a pentamer of NPM1^{OD}. The experimental data together with the fitted concentration profiles are shown on the top, and at the bottom, residuals from the fit are documented.

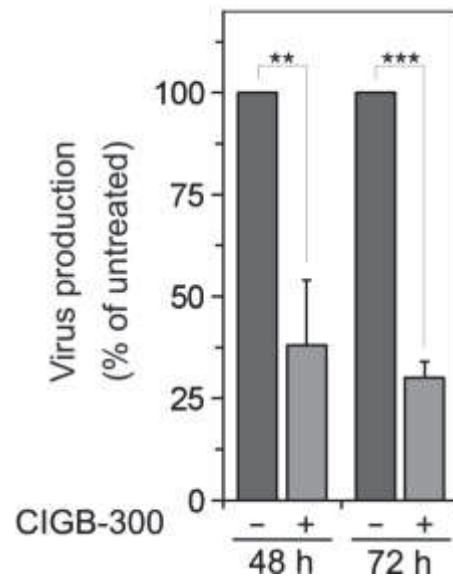
Nouri *et al.*, Fig. 1

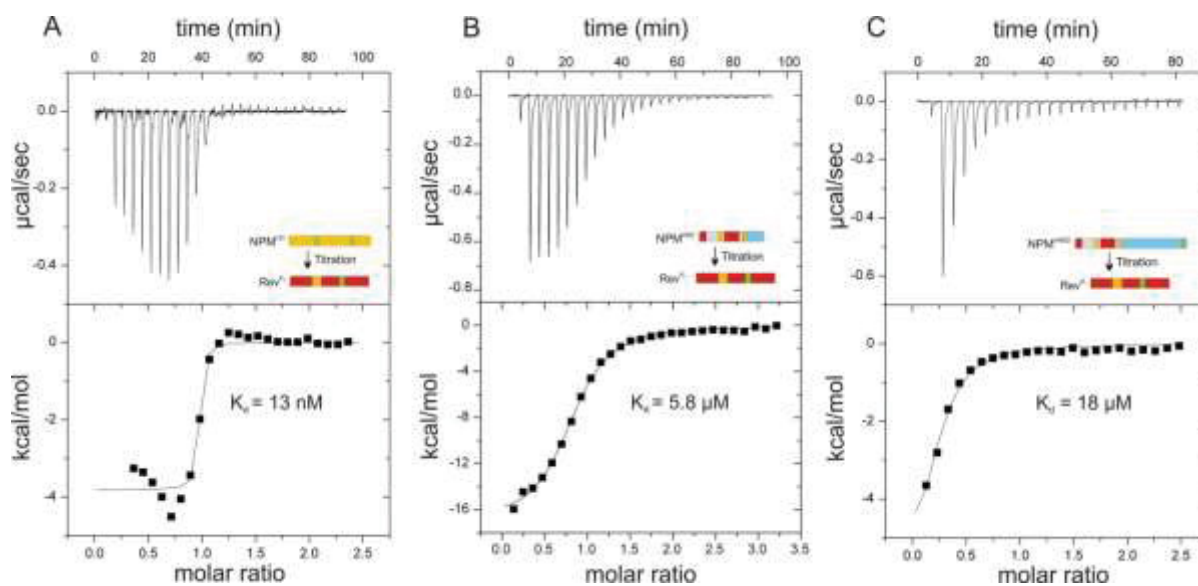
Nouri *et al.*, Fig. 2

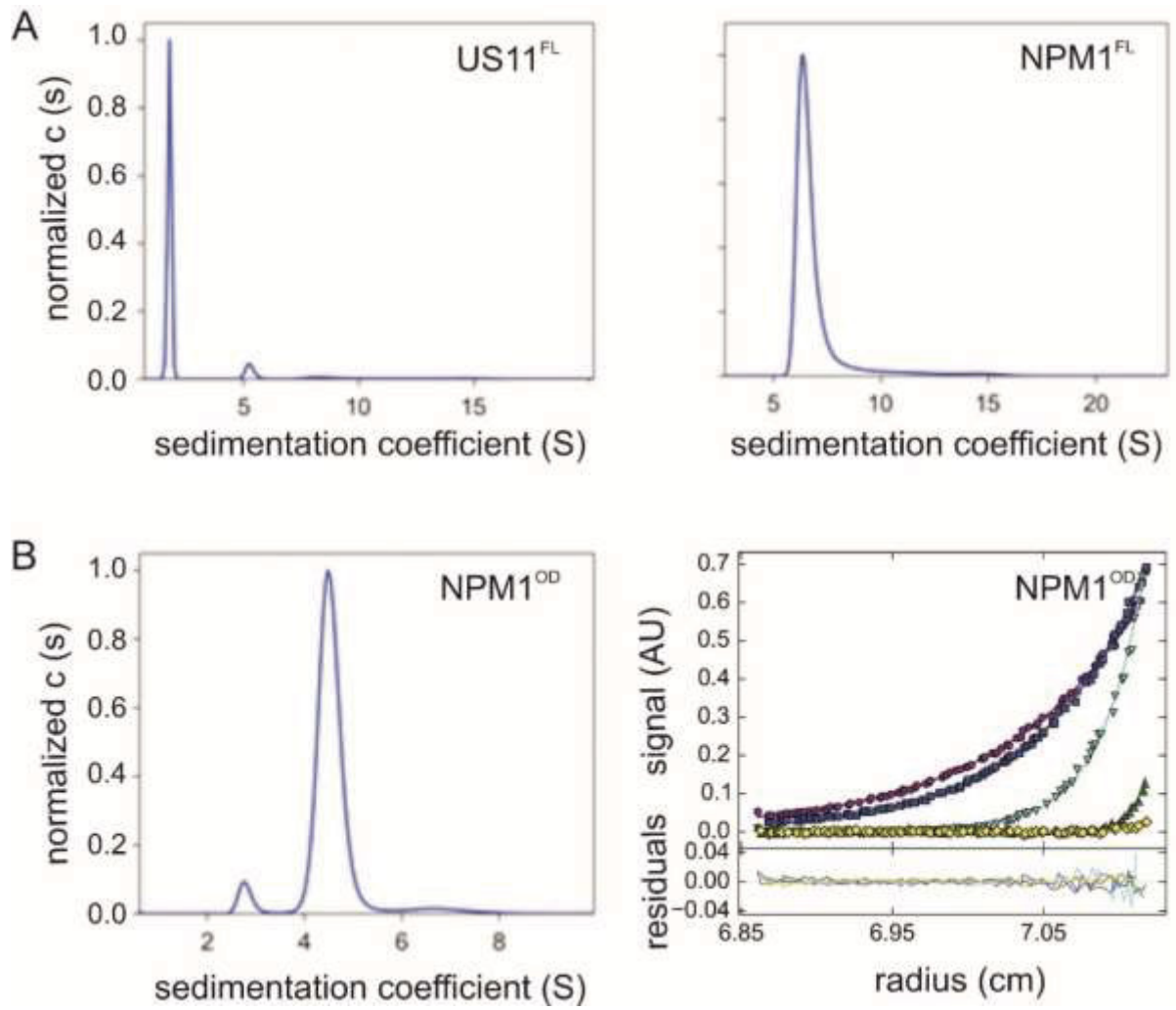
Nouri *et al.*, Fig. 3

Nouri *et al.*, Fig. 4

Nouri *et al.*, Fig. 5

Nouri *et al.*, Fig. 6

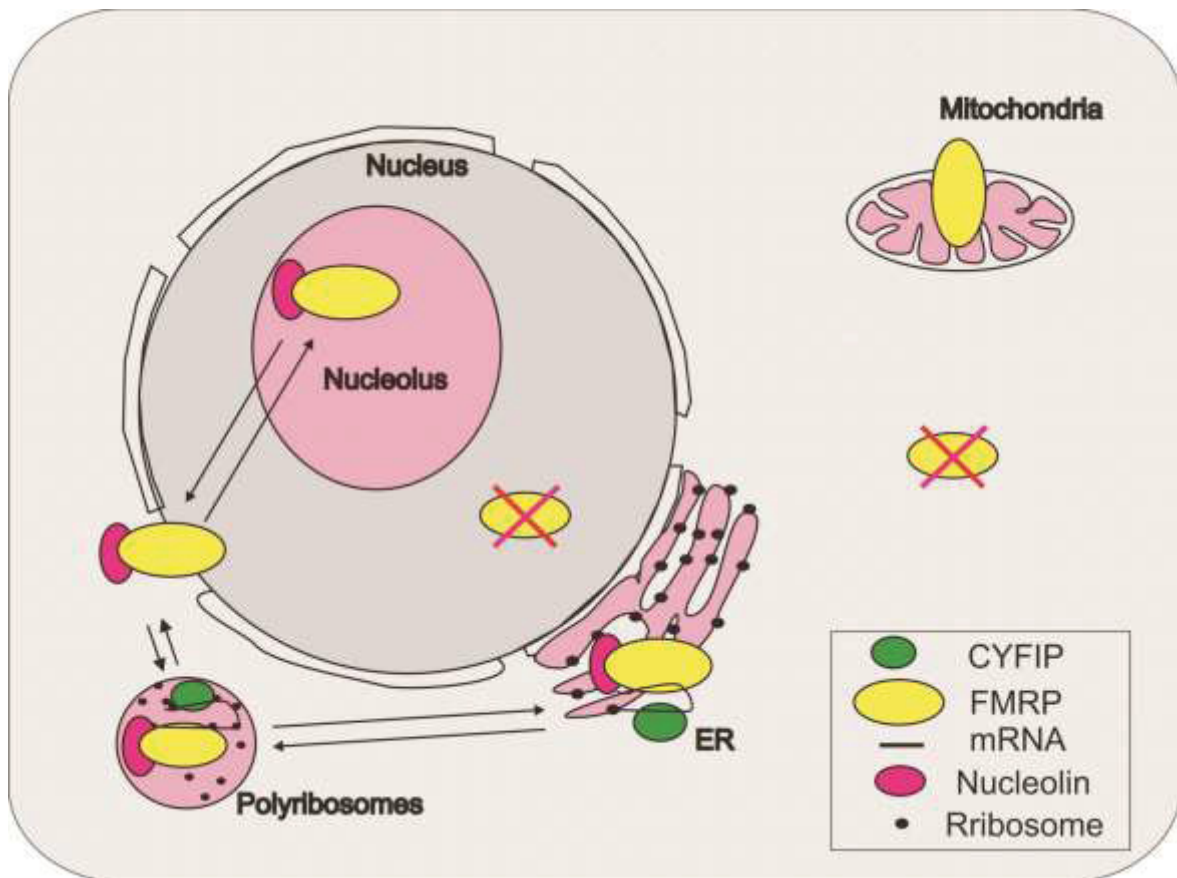
Nouri *et al.*, Fig. S1

Nouri *et al.*, Fig. S2

Chapter VI

Subcellular Fractionation and Localization Studies Reveal a Direct Interaction of the Fragile X Mental Retardation Protein (FMRP) with Nucleolin

Graphical abstract



Status: Published in PLOS One, March 21, 2014
Impact factor: 3.25
Own Proportion to this work: 20 %

Design, expression, and purification of nucleolin RGG (GAR)

Preparing IAEDANS-labeled fluorescent RGG

Interaction study of FMRP and RGG

Partially writing and revising the manuscript

Subcellular Fractionation and Localization Studies Reveal a Direct Interaction of the Fragile X Mental Retardation Protein (FMRP) with Nucleolin

Mohamed S. Taha¹, Kazem Nouri¹, Lech G. Milroy², Jens M. Moll¹, Christian Herrmann³, Luc Brunsveld², Roland P. Piekorz¹, Mohammad R. Ahmadian^{1*}

¹ Institute of Biochemistry and Molecular Biology II, Medical Faculty of the Heinrich-Heine-University, Düsseldorf, Germany, ² Laboratory of Chemical Biology and Institute of Complex Molecular Systems, Department of Biomedical Engineering, Technische Universiteit Eindhoven, Eindhoven, the Netherlands, ³ Department of Physical Chemistry I, Ruhr University Bochum, Bochum, Germany

Abstract

Fragile X mental Retardation Protein (FMRP) is a well-known regulator of local translation of its mRNA targets in neurons. However, despite its ubiquitous expression, the role of FMRP remains ill-defined in other cell types. In this study we investigated the subcellular distribution of FMRP and its protein complexes in HeLa cells using confocal imaging as well as detergent-free fractionation and size exclusion protocols. We found FMRP localized exclusively to solid compartments, including cytosolic heavy and light membranes, mitochondria, nuclear membrane and nucleoli. Interestingly, FMRP was associated with nucleolin in both a high molecular weight ribosomal and translation-associated complex (~6 MDa) in the cytosol, and a low molecular weight complex (~200 kDa) in the nucleoli. Consistently, we identified two functional nucleolar localization signals (NoLSs) in FMRP that are responsible for a strong nucleolar colocalization of the C-terminus of FMRP with nucleolin, and a direct interaction of the N-terminus of FMRP with the arginine-glycine-glycine (RGG) domain of nucleolin. Taken together, we propose a novel mechanism by which a transient nucleolar localization of FMRP underlies a strong nucleocytoplasmic translocation, most likely in a complex with nucleolin and possibly ribosomes, in order to regulate translation of its target mRNAs.

Citation: Taha MS, Nouri K, Milroy LG, Moll JM, Herrmann C, et al. (2014) Subcellular Fractionation and Localization Studies Reveal a Direct Interaction of the Fragile X Mental Retardation Protein (FMRP) with Nucleolin. PLoS ONE 9(3): e91465. doi:10.1371/journal.pone.0091465

Editor: Barbara Bardoni, CNRS UMR7275, France

Received: November 10, 2013; **Accepted:** February 11, 2014; **Published:** March 21, 2014

Copyright: © 2014 Taha et al. This is an open-access article distributed under the terms of the Creative Commons Attribution License, which permits unrestricted use, distribution, and reproduction in any medium, provided the original author and source are credited.

Funding: This work was supported in part by the German Academic Exchange Service (DAAD), the International Graduate School of Protein Science and Technology (IGRASP) and by the Strategic Research Fund (SRF) of the Heinrich-Heine University Düsseldorf (Grant F-2012/79-6). The funders had no role in study design, data collection and analysis, decision to publish, or preparation of the manuscript.

Competing Interests: The authors have declared that no competing interests exist.

* E-mail: reza.ahmadian@uni-duesseldorf.de

Introduction

Fragile X syndrome (FXS) is one of the most common forms of inherited mental retardation, which is associated with various behavioral and physiological abnormalities, including social withdrawal, anxiety, intellectual disability, epilepsy and autism [1,2,3]. FXS is caused by the absence of the fragile X mental retardation protein (FMRP) [4,5,6], which belongs to the RNA-binding, fragile X related protein (FXRP) family that includes also the fragile X related proteins 1 and 2 (FXR1P and FXR2P) [7,8].

FMRP is ubiquitously expressed with higher abundance in the brain and testis [7,9]. Studies by a number of laboratories have shown that FMRP is a regulator of protein translation and associates with the translation machinery [4,10]. FMRP is associated with messenger ribonucleoprotein (mRNP) particles and large polyribosomal complexes in the cytoplasm of various cell types [11,12,13,14]. FMRP consists of an N-terminal dimerization domain, a central region containing two K homology (KH1 and KH2) domains and a C-terminus encompassing the arginine-glycine-glycine (RGG) region [15,16]. The N-terminal and central regions of FMRP are highly conserved among the FXRPs, while the C-terminal shows significant variability [7]. FMRP is known to play roles in nucleocytoplasmic shuttling of mRNA by a non-

canonical nuclear localization signal (NLS) and a nuclear export signal (NES) [17,18,19,20]. Different mechanisms for the nuclear export of FMRP have been suggested involving CRM1/exportin1 [20] and/or the nuclear export factor family proteins [17]. In addition, FXR1P and FXR2P have been reported to contain a nucleolar localization signal (NoLS) at their C-termini, which is not reported yet in FMRP [7] although its nucleolar localization has been described previously [21].

Several FMRP interacting proteins have been identified so far. FXR1P and FXR2P are structurally and functionally related to FMRP. They additionally harbor a functional nucleolar targeting signal [7]. The cytoplasmic interacting FMR1 protein (CYFIP; also known as p140 and PIR121, respectively), a binding partner of FMRP [22], acts as a downstream effector of Rac1 thereby linking Rac1 to actin dynamics and lamellipodia formation. Activated Rac1 binds CYFIP and sequesters it from its complex with FMRP, which in turn is then released to regulate protein translation [23]. Moreover, nuclear FMRP interacting protein 1 (NUFIP1) has been identified as a nuclear RNA binding protein [24]. Other molecules described in FMRP protein complexes include the RNA-induced silencing complex (RISC), argonaute 2

(AGO2), Dicer, the 82-kDa FMRP interacting protein (82-FIP), as well as eukaryotic initiation factor 5 (eIF5) and nucleolin [25,26,27].

When six different cell lines were analyzed, i.e. Cos-7, HEK 293, HeLa, MDCK II, MEF, and NIH3T3, we found the strongest FMRP expression in HeLa cells. Thus, we investigated in this study the subcellular localization and interaction of FMRP with its binding partners in HeLa cells using an anti-FMRP antibody (ab17722) that has been successfully analyzed in FMR1 knockout mice [3]. Our novel findings reveal that FMRP localizes predominantly in different cellular compartments, including mitochondria and nucleoli. Interestingly, FMRP was found to be associated with nucleolin in two distinct protein complexes, a cytosolic high molecular weight translation-associated complex and a nucleolar, low molecular weight complex. Using purified proteins we show that the N-terminus of FMRP undergoes a direct protein-protein interaction with the C-terminal RGG domain of nucleolin. We further demonstrate that the nucleolar localization of FMRP is specifically regulated by two functional NLSs in its C-terminus.

Results and Discussion

FMRP localization at different subcellular compartments in HeLa cells

In a first step we employed confocal laser scanning microscopy (cLSM) to analyze the intracellular distribution of endogenous FMRP in HeLa cells. Cells were co-stained with antibodies specific for several endogenous markers, i.e. cellular organelles and compartments. As indicated in Figure 1, FMRP can be detected at almost every compartment of the cell. No colocalization could be found with the plasma membrane and filamentous actin (F-actin) when costained with antibodies against the transmembrane protein Na⁺/K⁺-ATPase and fluorescent phalloidin, respectively (Fig. 1A). FMRP considerably colocalized in perinuclear regions and at endomembranes with its binding partner CYFIP, the 60S acidic ribosomal protein p0 (RPLP0), the eukaryotic initiation factor 5 (eIF5) [26], and calreticulin (a marker of the endoplasmic reticulum). Of note, the mitochondrially encoded cytochrome c oxidase subunit II (MTCO2; also known as COX-2) showed a clear colocalization with FMRP suggesting that FMRP may be associated with the mitochondrial (see below).

Only a very weak colocalization could be detected under these conditions when employing markers for the nuclear membrane (NUP62) as well as antibodies specific for lamin B1 and surprisingly, also nucleolin (Fig. 1B). Interestingly, nucleolin has been previously reported to be part of FMRP protein complexes linked to translational inhibition [26]. Although FMRP was not clearly detectable in the nucleus under these conditions, it is important to note that FMRP contains both NLS and NES sequences [15], with the latter playing a putative role in nucleocytoplasmic shuttling of ribosomes probably in association with nucleolin [26].

Subfractionation and biochemical characterization of intracellular FMRP localization

Next, the cellular compartmentalization of FMRP and its interacting partners in HeLa cells was investigated in greater detail by establishing a detergent-free differential centrifugation protocol through sucrose cushions as described in Material and Methods. Thereby, we obtained six distinct fractions, including heavy membrane fraction (plasma membrane, mitochondria and rough endoplasmic reticulum or rER), light membrane fraction (smooth endoplasmic reticulum or sER, and free polysomes), cytoplasm fraction including lysosomes, nuclear membranes together with

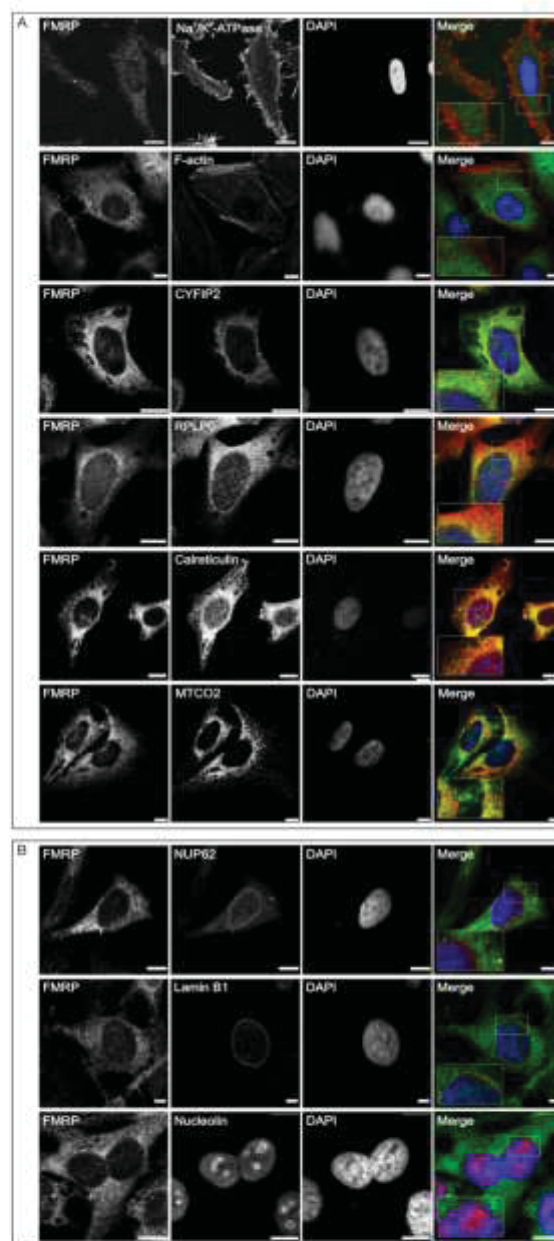


Figure 1. FMRP is localized at various intracellular sites in HeLa cells. Confocal laser scanning microscopy (cLSM) images of HeLa cells depicting endogenous FMRP (green channel) costained with various cytosolic (A) and nuclear (B) markers (red channel), including antibodies against CYFIP2, RPLP0 (ribosomal proteins), nucleolin (nucleolar marker), MTCO2 (mitochondrial protein), NUP62 (nucleoporins), lamin B1 (nuclear intermediate filament proteins), and calreticulin (endoplasmic reticulum marker). Detection of Na⁺/K⁺-ATPase and phalloidin staining were used to detect the cellular membrane and F-actin, respectively. DNA was stained by using DAPI (blue channel). Boxed areas in the merged panels depict enlarged areas of interest. Scale bar: 10µm.
doi:10.1371/journal.pone.0091465.g001

rER attached to the outer nuclear membrane, and lastly fractions containing the nucleoplasm and nucleoli (Fig. 2A). To evaluate the separation quality of the isolated sub-cellular fractions we used antibodies directed against specific marker proteins (Fig. 2B). The transmembrane protein Na⁺/K⁺-ATPase that is also expressed in HeLa cells, was consistently found in the heavy membrane and the light membrane fractions. Trace amounts of Na⁺/K⁺-ATPase were detected in the nuclear fractions, where it has been suggested to play a physiological role in Ca²⁺ homeostasis [28]. Another membrane marker found in the heavy membrane fraction, which undergoes palmitoylation and localizes to the plasma membrane [29], is α subunit of the G_{q/11} protein ($\alpha_{q/11}$). Glyceraldehyde-3-phosphate dehydrogenase (GAPDH) is largely present in the cytoplasmic fraction with comparable amounts also in heavy and light membranes. GAPDH has been reported to bind specifically to certain integral membrane proteins that are located in the plasma membrane, such as Na⁺/K⁺-ATPase [30]. GAPDH is also associated with the GTPase Rab2 at the ER and Golgi apparatus [31]. The early endosome antigen 1 (EEA1) was used as endosomal marker to show that endosomes primarily exist in the cytoplasm and light membrane fractions [32]. NUP62 as a marker for the nuclear membrane, as well as lamin B1 and histone H3 as nuclear markers were employed and were also detected in the nucleolar fraction and the nuclear membrane as well as in the nucleoplasm in the case of lamin B1 [33]. Lastly, nucleolin and nucleophosmin (also called B23, NO38 or numatrin) were used as nucleolar markers. Both proteins were found not only in nuclear fractions but also in the light and heavy membranes. Interestingly, similar to nucleolin, also nucleophosmin has been implicated in the modulation of multiple cellular processes outside the nucleus [34].

Immunoblot analysis of all fractions using the above mentioned marker proteins revealed that FMRP and phospho-FMRP (Serine 499) exists predominantly in solid compartments, such as the cytosolic heavy and light membranes, the nuclear membrane, and also the nucleoli (Fig. 2B). FMRP appeared on the immunoblots in two major bands with molecular masses of 72 and 80 kDa, consistent with several previous studies [8,9,12,26,35,36]. The fact that FMRP is part of a large mRNP complex (~600 kDa) [12] strongly indicates that the amounts of soluble FMRP must be very low. Consistent with this, no significant amounts of FMRP were detected in both the cytoplasm and in the nucleoplasm (Fig. 2B). The FMRP content in the respective fractions was calculated using the following approach: (i) The relative intensity of each protein band was determined by densitometric evaluation of FMRP immunoblot signal intensities; (ii) obtained intensities of each fraction were divided by the intensity obtained for FMRP in the total cell lysate and multiplied by the protein amounts used in every fraction; (iii) the obtained FMRP concentration in each fraction was divided by the total FMRP concentration and multiplied by 100. Accordingly, the FMRP content was 42.5% in the heavy membrane fraction, 22.5% in light membranes, 13.3% in the nuclear membrane fraction, and 21.7% in the nucleoli-containing fraction. The nucleolin content in these fractions, calculated in the same way, were 15.9%, 20.8%, 13.3% and 50.0%, respectively.

In addition to FMRP, we also analyzed the presence of proteins by immunoblot detection, which are either part of the translational machinery or known to modulate FMRP function in a RNA-dependent manner. Interestingly, the small GTPase Rac1 and its effector CYFIP revealed fractionation patterns, which were very similar to FMRP. CYFIP isoforms 1 and 2 were previously found in a complex with FMRP in HeLa cells [37], suggesting that FMRP may not discriminate between both highly conserved

CYFIP isoforms. However, in contrast to CYFIP, Rac1 was found not only in the heavy and light membrane fractions, but also in the cytoplasm. Cytoplasmic Rac1 exists in complex with its regulator guanine nucleotide dissociation inhibitor GDI α [38]. Nuclear shuttling of Rac1 depends on its C-terminal polybasic region [39]. The nuclear import receptor karyopherin $\alpha 2$ has been shown to directly bind to and to translocate Rac1 into the nucleus [40]. It has been reported that GFP-CYFIP2 accumulates in the nucleus and that CYFIP2 is capable of undergoing CRM-1/exportin-dependent nucleocytoplasmic shuttling [41]. The roles of both CYFIP and Rac1 in the nucleus are still unclear. Nuclear Rac1 was found in complex with numerous proteins and may thus play different roles [40], including the regulation of cell division [42].

The light membrane fractions contained the largest population of proteins which are linked to the translational machinery, such as ribosomal RPLP0 and the initiation factor eIF5. The high amount of cytoplasmic eIF5 in the absence of FMRP, CYFIP, and ribosomes (including RPLP0) indicates that the association of eIF5 with the translation machinery is independent of FMRP [27]. The presence of FMRP, CYFIP, RPLP0, and also eIF5 in the nuclear membrane fraction is most likely based on their association with the rER.

An interesting observation was that nucleolin, another multi-functional RNA-binding phosphoprotein, was found in all FMRP-containing fractions (Fig. 2B). Nucleolin, which has been previously reported to exist in the FMRP-containing protein complexes in murine fibroblasts [26] and human embryonic kidney 293T cells [27], resembles FMRP as it contains an NLS and is able to shuttle between the nucleolus and cytoplasm [43]. It is involved in various processes, including chromatin remodeling, rRNA processing, ribosome biogenesis in the nucleolus, nucleocytoplasmic shuttling of ribosomes, mRNA stabilization, and translation [44]. FMRP contains both a NLS and NES [15] and also undergoes nucleocytoplasmic shuttling [17,19,20] and is, like nucleolin [45], associated with mRNP particles and large polyribosomal complexes [11,12,13,14,46]. Thus, the presence of FMRP in the nucleolar fraction [11] led us to speculate about a possible concerted role of FMRP and nucleolin in nucleocytoplasmic shuttling of ribosomes and escorting mRNAs to the translational machinery. Similar to FMRP, nucleolin is associated with neurodegenerative disorders, such as Huntington's disease, Alzheimer disease, Down syndrome, and progressive supranuclear palsy [47].

Another interesting observation in this study was the association of FMRP with mitochondria (Fig. 1A). To further prove this finding we investigated a possible localization of FMRP in or on mitochondria by isolating highly enriched mitochondria fraction from the heavy membrane fraction of the HeLa cells (Fig. 2A; see Materials and Methods). As illustrated in Figure 2C, a considerable amount of FMRP appeared to exist in the mitochondria like the mitochondrial markers MTCO2 and ACAT1 (Acetyl-CoA acetyltransferase), where also slight amounts of nuclear proteins, such as histone H3 and nucleolin, were also detected. This suggests that the mitochondrial fraction contained nuclear impurity. Nonetheless, our result clearly indicate that FMRP is either physically associated with the outer mitochondrial membrane, eventually as part of p-bodies and stress granules [48,49] or it is sorted into the mitochondrial matrix. The latter was reported in both EBV-transformed human lymphoblastoid cells using cell fractionation and rat brain neurons using electron microscopy [18]. These observations are in line with the studies suggesting possible mitochondria-associated functions of FMRP, e.g. in preventing apoptosis as a downstream effector of metabotropic glutamate receptors [50] and/or controlling mitochondrial protein

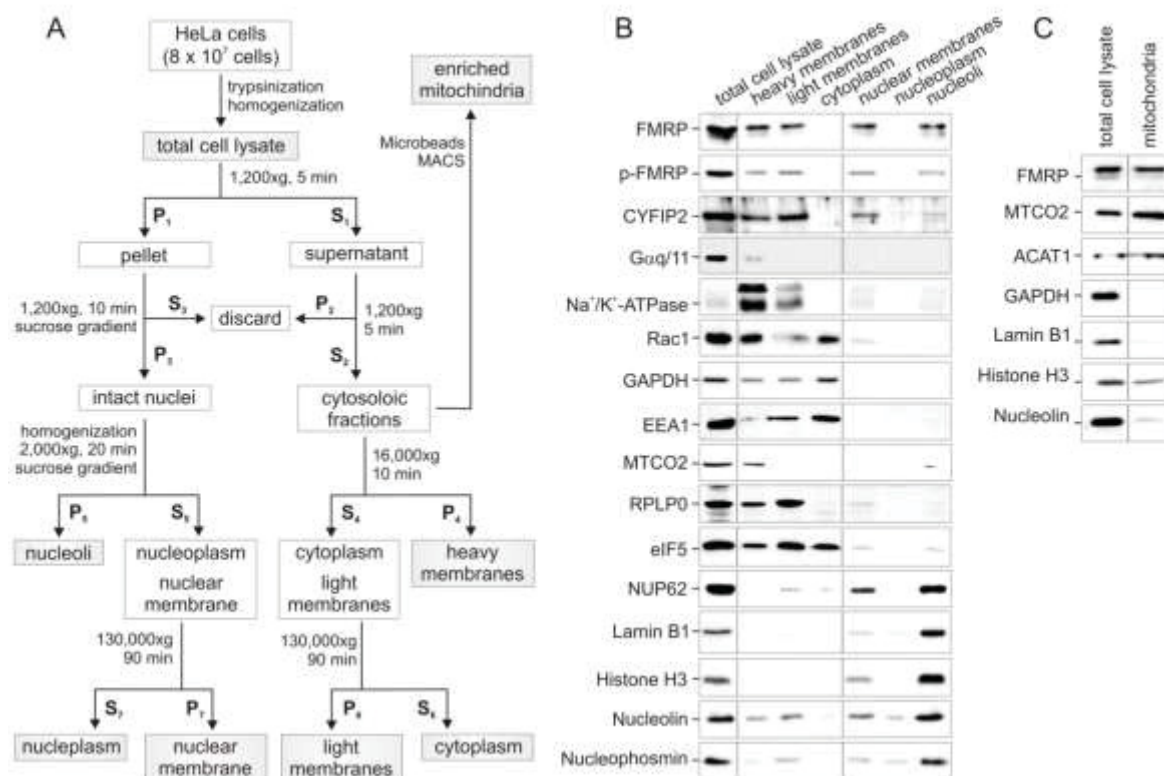


Figure 2. FMRP shows a diverse subcellular distribution pattern in HeLa cells as revealed by subcellular fractionation analysis. (A) Experimental cell fractionation procedure employing several differential centrifugation steps. Cells were fractionated into six distinct fractions, including heavy membrane (plasma membrane and rough endoplasmic reticulum), light membrane (polysomes, golgi apparatus, smooth endoplasmic reticulum), cytoplasm (cytoplasm and lysosomes), enriched nuclear membrane (containing rough endoplasmic reticulum), nucleoplasm, and nucleoli. S_i supernatant; P_i pellet. (B) FMRP is largely absent in the cytoplasm and nucleoplasm and predominantly localizes to solid compartments. The protein concentrations were normalized in all fractions with exception of the nucleoplasm due its low protein content as compared to the other fractions. In each lane, 5 μg proteins were loaded except for the nucleoplasm, where one μg was used. In addition to FMRP and its binding partner CYFIP, the fractions were analyzed by using different subcellular marker, including Gαq/11, Na⁺/K⁺-ATPase and Rac1 (plasma membrane), EEA2 (endosomes), GAPDH (cytoplasm), eIF5 and RPLP0 (ribosomes and rough ER). Nuclear markers included histone H3 and lamin B1. Nucleolin was used as nucleolar marker. (C) Detection of FMRP in mitochondria. The presence of FMRP in isolated mitochondrial fraction was analyzed by SDS-PAGE and immunoblotting, using antibodies against FMRP, two mitochondrial proteins MTCO2 and ACAT1, the cytosolic GAPDH as well as the nuclear proteins lamin B1, histone H3 and nucleolin. Equal protein amounts of the mitochondrial fraction and the total cell lysate were used.

doi:10.1371/journal.pone.0091465.g002

translation [50,51]. Interestingly, partial reduction in the FMRP amount in pre-mutation FMR1 knock-in mice has been shown to correlate with the mitochondrial number and function [52], and to lead to mitochondrial dystrophy [50] and elevated mitochondrial oxidative stress in FXS patients [53]. However, the role of FMRP on/in mitochondria is unclear [51] and requires further investigation.

FMRP coexists with nucleolin in two distinct, nucleolar and cytosolic complexes

To further characterize the colocalization and a possible (functional) interaction of FMRP and nucleolin, the light membrane and nucleolar fractions were further analyzed using analytical size exclusion chromatography on a superose 6 HR column calibrated with molecular weight standards (see Material and Methods). As indicated in Figures 3A and 3B, intact FMRP-containing protein complexes of both samples showed a different separation and elution profile. Proteins in the light membrane

fraction eluted in the void volume suggesting that the FMRP complexes exhibit a native molecular weight of at least ~6 MDa (void volume of the superose 6 HR column). Such a cytosolic high molecular weight complex may consist of polyribosomes (~4.2 MDa/80S ribosome), mRNPs particles and/or additional components or regulators of the translational machinery [11,13,35]. In lymphoblasts, FMRP has been shown previously to be part of a protein complex of ~600 kDa (void volume of the superdex 200 column), which contain the 60 S ribosomal protein RPLP0 as well as the FMRP-related FXR1P and FXR2P [35]. Such a FMRP protein complex has been shown in HeLa cells to be associated with actively translating polyribosomes [13].

In contrast, the FMRP complexes of the nucleolar fraction exhibited a rather low molecular weight of approximately 200 kDa. Immunoblot analysis of both peak fractions further suggested that nucleolin exists in two different FMRP complexes, i.e. in the cytosolic and nucleolar compartments. Based on the detection of nucleolin, CYFIP, and RPLP0 (Fig. 3A) in the light

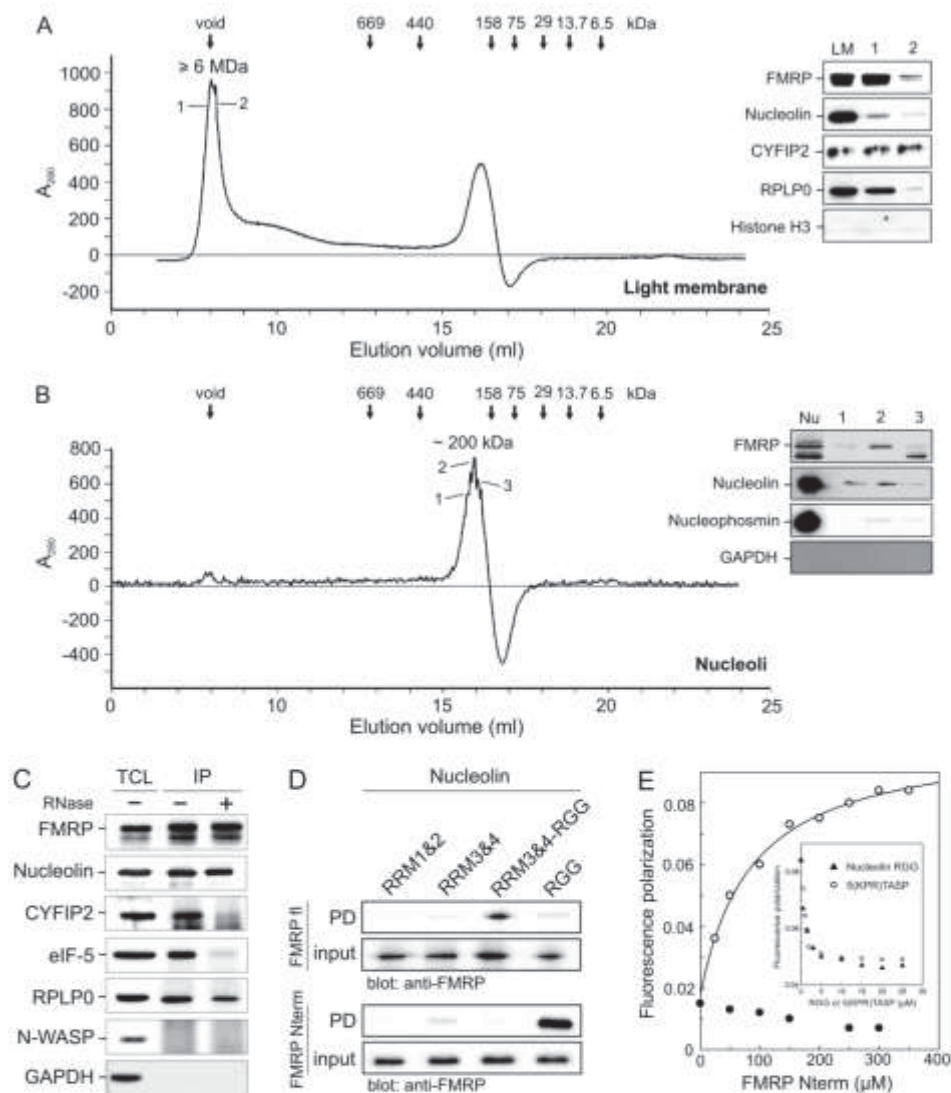


Figure 3. FMRP and nucleolin interact in both cytosolic high molecular weight and nuclear low molecular weight complexes. (A, B) Native FMRP protein complexes were fractionated by loading the light membrane (A) and nucleolar (B) fractions on a superose 6 size exclusion chromatography column. The absorbance of the column eluent at 280 nm (A_{280}) was plotted against the elution volume (ml). Different FMRP binding partners and markers are shown, including histone H3 and GAPDH as negative controls in the endomembrane and nucleolar fractions, respectively. The elution positions of standard proteins employed include thyroglobulin (669 kDa), ferritin (440 kDa), aldolase (158 kDa), ovalbumin (75 kDa), carbonic anhydrase (29 kDa), ribonuclease (13.7 kDa), and aprotinin (6.5 kDa). The peak fractions, as indicated by a solid line, were subjected to SDS-PAGE and immunoblotting using antibodies against FMRP (71 kDa), nucleolin (76 kDa), CYFIP2 (146 kDa), RPLP0 (34 kDa) and eIF5 (58 kDa). LM, light membrane; Nu, nucleoli. The molecular mass of the peak fractions is indicated above the peaks. (C) Interaction of FMRP with CYFIP, nucleolin, eIF5, and RPLP0 as analyzed by co-immunoprecipitation. Endogenous FMRP was immunoprecipitated from HeLa cell lysates using an anti-FMRP antibody before and after RNase treatment. FMRP co-precipitated with nucleolin, RPLP0, eIF5, and CYFIP2. Interaction with the latter two proteins was sensitive to RNase treatment. Proteins were visualized by using antibodies against FMRP, nucleolin, eIF5, CYFIP2 and RPLP0. N-WASP and GAPDH were used as a negative IP controls. IP, immunoprecipitation; TCL, total cell lysate. (D) Direct interaction between FMRP and nucleolin. GST pull-down experiments were conducted by mixing bacterial lysate expressing His-tagged FMRP fl (upper panel) or FMRP Nterm (lower panel) with different GST-fused nucleolin proteins (RRM1&2, aa 284–466; RRM3&4, aa 467–644; RRM3&4-RGG, aa 499–710; RGG, aa 645–710) immobilized on GSH sepharose beads. Proteins retained on the beads were resolved by SDS-PAGE and processed for Western blot using a monoclonal antibody against FMRP. Mixed samples before performing pulldown (PD) analysis were used as input control. (E) Low-affinity interaction between the FMRP Nterm and the nucleolin RGG. Fluorescence polarization assay was used as a tool for monitoring the interaction of the FMRP Nterm (increasing concentrations as indicated) with the IAEDANS-labeled fluorescent RGG (0.5 μ M) (open circles). As negative controls, FMRP Nterm was titrated into IAEDANS alone (0.5 μ M) (closed circles). The inset depicts the displacement of FMRP Nterm from IAEDANS-labeled fluorescent RGG by increasing concentrations of unlabeled RGG and the synthetic peptide construct 5(KPR)TASP. doi:10.1371/journal.pone.0091465.g003

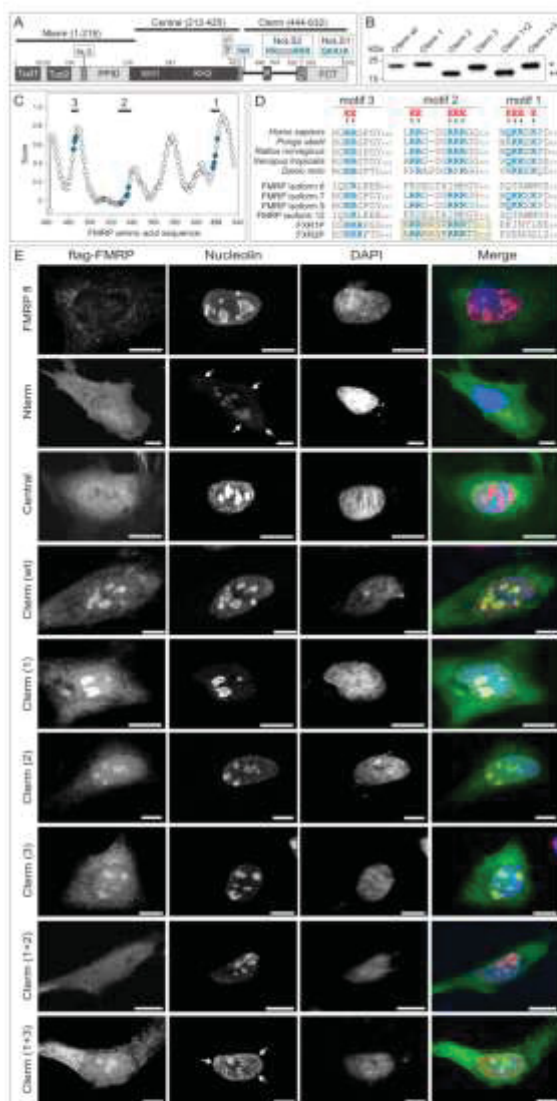


Figure 4. The C-terminal region of FMRP contains evolutionary conserved nucleolar localization signals. (A) Domain organization and motifs of FMRP. Schematic diagram of FMRP architectures highlights major domains and motifs. FCT, FMRP C-terminus; KH1 and KH2, tandem K (described first in the hnRNP K protein) homology domain; NES, nuclear export signal; NLS, nuclear localization signal; NoLS, nucleolar localization signal; PPIID, protein-protein interaction domain; RGG, arginine-glycine-glycine region; P, phosphorylation sites; Tud1 and Tud2, tandem Tudor (also called Agenet) domains. The C-terminal region (Cterm; aa 444–632) of FMRP contains two NoLSs, identified in this study. Two further FMRP fragment used were Nterm (1–218) and a Central region (212–425). (B) Overexpression of the Cterm wild-type (wt) and its variants on HeLa cells. Cterm 1: QKKEK changed to EEEeE; Cterm 2: RRGDGRRR changed to EEgdgEE; Cterm 3: RR changed to EE; Cterm 1 2: a combination of Cterm 1 and 2 mutations; Cterm 1 3: a combination of Cterm 1 and 3 mutations. Cterm 2 and Cterm 1 2 revealed a change in protein mobility (**) as compared to the wild-type and the other variants (*). (C) NoLS prediction of FMRP Cterm using the NoLS predictor program [58]. Graph shows the probability of NoLS distribution (represented by score) plotted against the amino acid sequence of FMRP Cterm (444–632). Three motifs and critical positively

charged residues are marked blue. (D) Multiple sequence alignment of the three predicted NoLS motifs 1, 2, and 3 of FMRP Cterm from different species (upper panel) as well as FMRP transcripts and homologous proteins (lower panel). Basic residues (blue), which are changed to glutamic acids (red) are highlighted. Upper panel: FMRP sequences from different species are human (accession number 544328), orangutan (197102198), rat (30794228), frog (53749722) and zebrafish (23308667). Lower panel: FMRP transcripts and homologous proteins are transcript 6 (297374777), 7 (297374779), 9 (297374791) and 12 (297374789) as well as FXR1P (61835148) and FXR2P (259013556). (E) Nucleolar localization of FMRP. cLSM images of HeLa cells transfected with FMRP fl, Nterm, Central, Cterm (wt) and Cterm variants (anti-flag; green channel) costained with endogenous nucleolin (anti-nucleolin; red channel) and DNA (DAPI; blue channel) revealed that Cterm (wt), (1), (2), (3) and (1 3) colocalize with nucleolin in the nucleolus. In contrast this colocalization was absent in the case of Cterm (1 2). Cytoplasmic distribution of FMRP Nterm and the subnuclear distribution of endogenous nucleolin are highlighted by arrows. Scale bar: 10 μ m. doi:10.1371/journal.pone.0091465.g004

membrane-associated FMRP complex, we assume that this cytosolic high molecular weight complex is even much larger than 5–6 MDa and also contains programmed ribosomes and polysomes [54]. In contrast, the low molecular weight FMRP complex may contain one nucleolin molecule (76 kDa) and two FMRP molecules (71 kDa), as FMRP is able to dimerize *in vitro* N-terminal domain [15]. This complex may also exist in a 1:1 stoichiometry since endogenous nucleolin runs approximately at 110 kDa (data not shown).

In order to further characterize the interaction between FMRP and nucleolin as critical translational regulators, we performed immunoprecipitation studies using HeLa cell lysates with and without RNase treatment using FMRP-specific antibodies. As indicated in Figure 3C, nucleolin, CYFIP, RPLP0, and also eIF5 were efficiently co-immunoprecipitated and found in a complex with FMRP. Here, CYFIP and eIF5 dissociated almost completely from the complexes when the samples were treated with RNase A. These data strongly suggest that eIF5 and CYFIP association with FMRP within the translation machinery is RNA-dependent. In contrast to the FMRP-eIF5 relationship in translational initiation, which remains unclear, the FMRP-CYFIP complex has been shown to display a translational repression activity [10], which additionally requires eIF4E [36]. Of particular relevance may be the finding that association of FMRP with nucleolin and RPLP0 was not affected by RNase A treatment (Fig 3C). Consistent with this result, FMRP was previously detected in the same protein complex with RPLP0 [35], as well as with nucleolin, FXR1P, FXR2P, and different mRNAs, including FMRP mRNA [26]. In contrast to the high molecular weight, cytosolic FMRP complex, which most likely controls translation, the role of the low molecular weight nucleolar FMRP-nucleolin complex remains unclear.

In summary our results show that FMRP is predominantly present in two complexes residing in the light membrane and the nucleoli. These macromolecular complexes significantly differ in size and composition. Direct FMRP interaction partners identified by co-immunoprecipitation include nucleolin and RPLP0. In addition, there seems to be an indirect, RNA-mediated interaction of FMRP with CYFIP and eIF5.

FMRP binds directly to nucleolin

Our data about the existence of different FMRP-nucleolin protein complexes prompted us to map the FMRP-nucleolin interaction at the protein level. We performed GST pulldown experiments under cell-free conditions by using His₆-tagged full

length (fl) as well as the N-terminal region (Nterm) of FMRP (aa 1–218; Fig. 4A) and various nucleolin subdomains as Glutathion-S-transferase (GST) fusion proteins. As indicated in Figure 3D, both FMRP variants were able to directly bind to nucleolin subdomains, although with different patterns. FMRP fl strongly bound a construct encompassing the RRM3&4-RGG (aa 499–710) domains of nucleolin and to a weaker extent also to RRM3&4 (aa 467–644) domains and the C-terminal RGG domain (aa 645–710) of nucleolin. This picture was, however, greatly different for interaction studies using the N-terminus of FMRP. The strongest interaction was found between the N-terminus of FMRP and the RGG domain of nucleolin. Binding of the FMRP N-terminus to the RRM3&4 fragment was as weak as that of FMRP fl, and binding of RRM3&4-RGG domains was also not much pronounced. Both FMRP constructs did not reveal any interaction with RRM1&2 (aa 284–466) domains of nucleolin (Fig. 3D).

In order to determine the binding affinity between FMRP Nterm and nucleolin RGG, we used the advantage of fluorescence polarization. Therefore, we labeled RGG with the fluorescence reporter group IAEDANS. As shown in Figure 3E, we notably observed an incremental increase in fluorescence polarization in the presence of increasing amounts of FMRP Nterm but not with IAEDANS alone. From this data a dissociation constant (K_d) value of 87 μ M was calculated illustrating a low-affinity FMRP-nucleolin interaction. Competition experiments were next performed to prove this complex formation using the purified, unlabeled RGG domain of nucleolin and a synthetic peptide construct 5(KPR)/TASP, which has been reported previously to bind nucleolin [55]. As indicated in Figure 3E, the unlabeled RGG domain and the peptide construct efficiently displaced FMRP Nterm from its complex with the fluorescent RGG domain by binding to FMRP Nterm and the fluorescent RGG domain, respectively.

The nucleolin-binding N-terminus of FMRP harbors due to its various subdomains different interaction characteristics (Fig. 4A) [10]. It contains two conserved Tudor domains (Tud1 and Tud2; also called N-terminal domain of FMRP 1 and 2 or NDF1 and NDF2 [16]) that are part of the proposed royal family of protein domains, also including Agenet, MBT, PWWP, and chromo domains [56]. The Tudor domains of FMRP, FXR1P, and FXR2P have been shown to selectively bind trimethylated lysines peptides derived from histones H3K9 and H4K20 [16,57]. The Tud2 domain of FMRP has also been shown to physically bind 82-FIP (82-kDa FMRP Interacting Protein) [16], which has been identified as a component of FMRP-containing mRNP complexes [25]. The Tud2 domain of FMRP has been proposed to be a stronger target for interactions as compared to Tud1, possibly because of its plasticity and availability of exposed hydrophobic cavities [16].

Taken together, our findings suggest that the N-terminus of FMRP is responsible for its physical interaction with nucleolin. The FMRP binding epitope on nucleolin could be identified as the RGG region, which has been implicated in facilitating a variety of protein and RNA interactions [44].

FMRP contains a functional nucleolar localization signal (NoLS)

The fact that FMRP was clearly detectable in the nucleolar fraction similar to nucleolin (Fig. 2B), and that both proteins directly interact with each other (Fig. 3D), was remarkable, especially because FMRP was found to be associated with the granular component of the nucleolus using immunogold labeling and electron microscopy [21]. In order to clarify the significance of these observations, we subjected FMRP to a mutational analysis

by studying the colocalization of different FMRP subdomains with endogenous nucleolin in HeLa cells. Most remarkably, we found that in contrast to FMRP full-length (fl), the N-terminus (called Nterm; aa 1–218), and the central KH domains (called central; aa 212–425), a C-terminal region of FMRP (called Cterm; aa 444–632) clearly colocalized with nucleolin in the nucleolus (Fig. 4E), when overexpressed in HeLa cells. These data strongly suggest that FMRP Cterm must encompass one or more functional NoLS motifs.

Therefore, we next screened for the presence of NoLS motifs in FMRP Cterm by employing a NoLS prediction software (<http://www.compbio.dundee.ac.uk/www-nod/>) [58]. This analysis showed that there are at least three putative NoLS motifs at the C-terminus of FMRP (Fig. 4C), which are partially conserved in other organisms and within different FMRP isoforms and related proteins. One of these NoLS motifs (motif 2; Fig. 4D) has been previously described for the FMRP-related proteins FRX1P and FRX2P [59]. Interestingly, FMRP isoforms 6 and 12, which lack both NoLS1 and NoLS2 (Fig. 4D), have been very recently reported to localize to Cajal bodies in the nucleus [60], due to a different C-terminal region. Cajal bodies participate in the biogenesis of small nuclear ribonucleoproteins (snRNPs) with which FMRP isoforms are associated [61].

To analyze the potential roles of these motifs, we substituted the positively charged residues in all three motifs with negatively charged glutamic acids (E) in the context of the Cterm construct (Fig. 4D). Transient transfection experiments of HeLa cells have shown that Cterm mutants of motifs 1 and 2 (Cterm 1 and 2), but not motif 3 (Cterm 3), resulted in a significant reduction of their nucleolar localization as compared to the wild-type situation (Cterm wt) (Fig. 4E). This effect was stronger when we combined the substitution of both motifs 1 and 2. Consequently, overexpressed Cterm 1 2, when compared to Cterm 1 3, was localized at other subcellular regions, but not in the nucleolus (Fig. 4E). In addition, a subnuclear distribution of nucleolin was observed when Cterm 1 3 was overexpressed (Fig. 4E). Thus, our data clearly demonstrate the existence of at least two evolutionary conserved and functional motifs (NoLS1 and NoLS2) that are crucial for nucleolar localization of FMRP.

The fact that FMRP, which contains functional NLS and NoLSs, was predominantly found in the cytoplasm (Figures 1A, 1B and 4E) can be explained by the presence of different nuclear export mechanisms [17,19,20]. However, it is rather intriguing that nucleolin, which lacks NES and NoLS (data not shown), almost completely localized to the nucleolus (Figs. 1A, 1B and 4E). The presence of two NoLS motifs in FMRP and the fact that it selectively binds nucleolin led us to speculate that FMRP may facilitate nuclear and nucleolar import of nucleolin in a kind of piggyback mechanism. Next to the Tudor domains is a non-canonical NLS within the FMRP Nterm [17,19,62], which most likely facilitates FMRP shuttling into the nucleus [10,37]. This piggyback hypothesis is nicely supported by the observation that overexpression of FMRP Nterm resulted in the subcellular redistribution of nucleolin (Fig. 4E). FMRP Nterm competes for nucleolin binding with endogenous FMRP and prevents the FMRP-mediated nucleolin targeting to the nucleolus. This function of FMRP obviously is rather significant especially because a missense mutation in the NLS of the FMR1 gene, altering a conserved arginine residue at position 138 to glutamine (R138Q), may represent an important cause associated with developmental delay [63]. An rRNA-mediated nucleolar localization of nucleolin has been proposed in an early study that has shown that the C-terminal regions of nucleolin, containing the RRMs and the RGG domain, are essential for nucleolar accumulation of nucleolin [64].

Thus, it is very likely that a concerted interaction of FMRP with nucleolin regulates the transport of rRNAs and ribosomal proteins towards the nucleolus and the export of ribosomes from the nucleolus as well as mRNAs and mRNP particles from the nucleus [10,26,44,65]. It is important to note that nucleolin may be addressed in the nucleolus by a FMRP-independent mechanism since it has its own NLS [64]. Accordingly, nucleolin and FMRP could assemble in the nucleoplasm or in the nucleolus in order to accomplish ribosomal biogenesis and ribosome or mRNP particle export.

An important question to be addressed is why FMRP is predominantly cytoplasmic, although it contains functional NES and NoLS motifs. Several explanations for this paradox are proposed: (1) The NLS and eventually the NoLS motifs of FMRP may be masked in the context of FMRP fl through an intramolecular or intermolecular mechanism that need to be released for example by posttranslational modifications [19]. FMRP phosphorylation of conserved residues (Ser497, Ser500, Thr502 and Ser504) is located within the phosphorylation (P) region close to the identified NoLS motifs (Fig. 4A) [46,66] and may also have modulatory impacts on the FMRP redistribution [67]. (2) Interestingly, NoLS2 is an integral part of the RGG region of FMRP, and arginine methylations in and around this region have been reported to regulate the association of FMRP with polyribosomes and mRNA [48,54]. This may suggest that nucleolar localization of FMRP, possibly in complex with nucleolin, may well be a prerequisite for FMRP association with and nuclear export of target mRNAs and ribosomes [17,68]. (3) The fact that FMRP fl predominantly localizes in the cytosolic compartments supports the notion that FMRP, due to its two NES motifs, underlies an efficient mechanism for nuclear export. Consistent with this, deletion of the NES motifs has been shown to result in FMRP accumulation in the nucleus [17].

Conclusions

The discovery of the FMR1 gene defects over twenty-two years ago [69] has led to significant advances in understanding the critical role of FMRP in synaptic plasticity and the molecular events of the fragile X mental retardation syndrome [2,6,14,67]. Despite the bulk of data concerning the molecular properties of FMRP and despite the growing body of evidence on its functional significance especially in neurons, the molecular mechanisms by which FMRP plays a role in RNA transport and metabolism, translation regulation, cytoskeleton remodeling, and cell motility still remain to be elucidated.

This study describes the thorough investigation of physical and functional niches of FMRP by analyzing the subcellular distribution of endogenous FMRP and its complexes under native conditions in HeLa cells. Confocal microscopy imaging subcellular fractionation and precipitation experiments provide valuable insights into (i) FMRP association with various nuclear and cytosolic fractions of variable molecular weights, (ii) uncovered a direct interaction between FMRP N-terminus and the RGG domain of nucleolin, and (iii) identified the existence of two functional NoLSs at the C-terminus of FMRP. Our data open new perspectives of a possible mechanistic link between nucleolar ribosome biogenesis, RNA shuttling and the cytoplasmic translational machinery that may be dependent on distinct functional subsets of FMRP-nucleolin complexes.

This study also demonstrates the presence of FMRP-containing complexes in the nucleus and the cytoplasm. These complexes contain nucleolin and other crucial factors for RNA processing and translational control. A direct interaction of FMRP with

nucleolin was identified by RNase digestion experiments and interaction studies using purified proteins. We were further able to identify the responsible binding epitopes as the N-terminus of FMRP and the RGG domain of nucleolin. A potential functional role of the FMRP-nucleolin complex formation may be nucleocytoplasmic shuttling of nucleolin provided by the presence of functional NLS, NoLSs and NESs existing in FMRP.

Future biophysical investigations of FMRP beyond differential cell fractionation and size exclusion chromatography will eventually require the use of blue native polyacrylamide gel electrophoresis, which is in combination with mass spectroscopy a powerful strategy for further separation and identification of native multi-protein FMRP complexes. These will provide an essential framework for uncovering the molecular niches and the physical environment of FMRP endowed of specific, molecular properties, and may ultimately open new perspectives in elucidating the molecular mechanisms of FMRP regulation and function.

Materials and Methods

Constructs

Nterm (aa 1–218) and Cterm (aa 444–632) of human FMRP, RRM3&4-RGG (aa 499–710) and RGG (aa 645–710) of human nucleolin were amplified by standard PCR and cloned into pGEX-4T1 and pGEX-4T1-Ntev. Full length FMRP (FMRP-fl; aa 1–632) was cloned into pET23b as a His-tag fused protein. Moreover, FMRP-fl, Nterm (aa 1–218), Central (aa 212–425) and Cterm (aa 444–632) were cloned into pcDNA 3.1-FLAG. RRM1&2 (aa 284–466), RRM3&4 (aa 467–644), RRM3&4-RGG (aa 499–710) and RGG (aa 645–707) of human nucleolin were kindly provided by F. Carrier [70].

Cell culture

Various cell lines, including Cos-7, HEK 293, HeLa and NIH3T3, were obtained from the German Collection of Microorganisms and Cell Cultures (DSMZ, Braunschweig, Germany), MDCK II from the American Type Culture Collection (ATCC, Manassas, USA), and wild-type murine embryonic fibroblasts (MEFs) from our laboratory. All cell lines were grown in DMEM supplemented with 10% fetal bovine serum (FBS) (Life Technologies, Darmstadt, Germany) and penicillin/streptomycin as antibiotics. Trypsin/EDTA was from Genaxxon Bioscience GmbH, Ulm, Germany.

Antibodies and fluorescent probes

Anti-FMRP (F6072) was purchased from US Biological (Swampscott, United States); anti-FMRP (ab17722), anti-FMRP (phospho S499) (ab48127), anti-calreticulin (ab4), anti-Lamin B1 (ab16048), anti-RPLP0 (ab88872), anti-CYFIP2 (AB95969), anti-nucleolin (ab22758), anti-MTC02 (AB3298), anti-nucleophosmin (ab10530), anti-ACAT1 (ab71407) and anti-EEA1 (ab2900) were purchased from Abcam (Cambridge, United Kingdom); anti-eIF5 (SC-28309), anti-N-WASP (sc-100964), and anti-G $\alpha_{q/11}$ (sc-392) were from Santa Cruz biotechnology (Texas, USA); anti-nucleoporin p62 (610498) and anti-Rac1 (610651) were from BD Transduction (New Jersey, USA); anti-Histone H3 (9715) and anti-GAPDH (2118) were from Cell Signaling (Boston, USA) and anti-Actin (MAB1501) from Millipore (Temecula, U.S.A.); Anti-Na⁺/K⁺ ATPase (A276), anti-FLAG (F3165) and DAPI were obtained from Sigma-Aldrich. Alexa fluor 546 phalloidin and the secondary antibodies Alexa fluor 488 goat anti-rabbit IgG and Alexa fluor 633 goat anti-mouse IgG were obtained from Molecular Probes (Oregon, USA).

Proteins

Escherichia coli BL21(DE3) pLysS, BL21(DE3) CodonPlus-RIL, or BL21(Rosetta) strains transformed with the respective construct were grown until an OD600 value of 0.7 and thereafter induced with 0.1 mM isopropyl- β -D-thiogalactopyranoside (IPTG) overnight at 25°C. All proteins were purified as described [71,72].

Transient transfection

HeLa cells were transfected using the TurboFect (Thermo Scientific) transfection reagent according to the manufacturer's instructions in 6-well plates employing 4 μ g DNA per transfection.

Immunofluorescence microscopy

HeLa cells grown on glass coverslips were fixed with 4% paraformaldehyde for 20 min, permeabilized with 0.25% triton-X100 in PBS for 10 min, and thereafter blocked for 1 h in a solution containing 3% BSA in 0.25% triton-X100/PBS. Cells were incubated with primary and secondary antibodies for 1 h and finally counterstained with DAPI (4,6-diamidino-2-phenylindole dihydrochloride) for 5 min and mounted using the prolong gold anti-fade reagent (Molecular Probes, Eugene, USA). Images were obtained as single optical slides using a LSM510-Meta confocal microscope (Zeiss, Jena, Germany) equipped with a 40x/1.3 immersion objective and excitation wavelengths of 364 nm, 488 nm, and 546 nm.

Subcellular fractionation by differential centrifugation

A differential centrifugation method was combined with the use of sucrose cushions in this study to fractionate HeLa cells. In addition, we avoided detergents and sonication in order to keep subcellular protein complexes intact. HeLa cells were homogenized by using a pre-chilled 7 ml Dounce homogenizer in a detergent-free lysis buffer containing 10 mM Tris/HCl (pH 7.4), 10 mM NaCl, 0.5 mM MgCl₂, and EDTA-free protease inhibitor cocktail (Roche, Berlin, Germany). The homogenates were centrifuged at 2,000xg for 5 min at 4°C. The pellets were resuspended in 250 mM sucrose solution containing 10 mM MgCl₂ and centrifuged through an 880 mM sucrose cushion containing 0.5 mM MgCl₂ at 1,200xg for 10 min in order to obtain the crude nuclear and cytoplasmic fractions. The supernatants were further subjected to a 16,000xg centrifugation step for 10 min to isolate the heavy membrane pellet and the post-nuclear supernatant. The post-nuclear supernatants were then centrifuged for 1.5 h at 130,000xg. The resulting pellets contained the light membrane fraction and polysomes. Nuclei were resuspended in lysis buffer and gently homogenized using a Balch homogenizer (clearance of 8 μ m) and 8-10 up-and-down strokes. Homogenized nuclei were centrifuged through a cushion of 880 mM sucrose containing 0.5 mM MgCl₂ at 2000xg for 20 min to isolate the nucleolar pellet and post-nucleolar supernatant. The post-nucleolar supernatant was finally centrifuged for 1.5 h at 130,000xg. The resulting pellets contained the nuclear membranes and the supernatants the nucleoplasmic fractions. All fractionation steps were carried out at 4°C. Protein concentration of all fractions was determined by the Bradford assay (Bio-Rad, Hercules, CA). All fractions were divided into two samples. One sample was mixed with 5x SDS-PAGE loading buffer and 6 μ g of total protein was subjected to SDS-PAGE. The other sample was analyzed using size exclusion chromatography.

Isolation of mitochondria

HeLa cell mitochondria were isolated from the heavy membrane fraction (see above) using a modified protocol described previously [73]. This fraction was subjected to PEB buffer (PBS buffer, pH 7.2, 2 mM EDTA and 0.5% bovine serum albumin) and incubated with 30 μ l anti-TOM22 MicroBeads (Miltenyi Biotec, Bergisch Gladbach, Germany) for 1 h at 4°C. The mixture was loaded onto a pre-equilibrated MACS column (Miltenyi Biotec), which was placed in the magnetic field of a MACS separator (Miltenyi Biotec). The column was washed three times with 3 ml PEB buffer and retained mitochondria were finally eluted in a volume of 1.5 ml. Mitochondrial solution was centrifuged at 13,000xg for 1 min. The mitochondria-containing pellet was washed two times using 0.32 M sucrose, 1 mM EDTA, and 10 mM Tris/HCl. After centrifugation (13,000xg, 1 min) the mitochondrial pellet was resuspended in 20 mM Tris/HCl (pH 7.5) and equal protein amount of mitochondrial fraction and total cell lysate were subjected to SDS-PAGE and immunoblotting analysis.

Analytical size exclusion chromatography (aSEC)

Analytical size exclusion chromatography was employed for further separation of FMRP complexes in the endomembrane and nucleolar fractions using a superose-6 HR 10/30 column (GE Healthcare, Uppsala, Sweden) and a buffer containing 30 mM HEPES (pH 7.6), 5 mM MgCl₂, 150 mM NaCl, and 3 mM DTT. The optimal separation range of the column is 5 kDa to 5 MDa, with an exclusion limit of 40 MDa (GE Healthcare, Uppsala, Sweden). The flow rate was maintained at 0.5 ml/min. Fractions were collected at a volume of 0.5 ml. Peak fractions were visualized by 15% SDS-PAGE gel and staining using Coomassie brilliant blue (CBB).

Immunoprecipitation

For immunoprecipitation of FMRP protein complexes from cellular extracts, HeLa cells were lysed in a buffer containing 20 mM Tris/HCl (pH 7.5), 150 mM NaCl, 1 mM EDTA, 1% triton X-100, 2.5 mM Na-pyrophosphate, 1 mM β -glycerophosphate, 1 mM sodium vanadate, one EDTA-free protease inhibitor cocktail tablet (Roche, Mannheim, Germany), and 70 U RNase A (Qiagen, Hilden, Germany) in order to determine RNA dependent interacting partners of FMRP. Lysates were centrifuged at 10,000xg for 10 min. The supernatant was precleared with protein A/G plus-agarose (sc-2003, Santa Cruz Biotechnology, Texas, USA) and then incubated with an anti-FMRP antibody (5 μ g/ml; ab17722; Abcam, Cambridge, UK) overnight at 4°C. Thereafter, protein A/G plus-agarose beads were added to the lysate for 1 h before recovering the beads by centrifugation at 664xg for 5 min at 4°C. The beads were washed 4-times in the lysis buffer, resuspended in SDS-PAGE loading buffer and analyzed by SDS-PAGE and Western blotting using a BioRad Mini-PROTEAN system (BioRad, Hercules, CA).

Pull-down assay

GST pull-down experiments were conducted by adding 500 μ g of bacterial lysate expressing His-tagged FMRP fl or 50 μ g FMRP Nterm purified protein with 25 μ g of different GST-fused nucleolin proteins (RRM1&2, aa 284–466; RRM3&4, aa 467–644; RRM3&4-RGG, aa 499–710; RGG, aa 645–710) immobilized on 30 μ l glutathione-conjugated Sepharose 4B beads (Macherey-Nagel, Duren, Germany). The mixture was incubated at 4°C for 45 min in buffer, containing 50 mM Tris/HCl, pH 8.0, 150 mM NaCl, 1 mM DTT, 5% glycerol. After washing for five

times with the same buffer proteins retained on the beads were resolved by SDS-PAGE and processed for immunoblotting using a monoclonal antibody against FMRP. Mixed samples prior to pull-down (PD) analysis were used as input controls.

Peptide synthesis

The template assembled synthetic peptide 5(KPR)/TASP [74,75] was synthesized by manual solid-phase peptide synthesis on Rink Amide resin (Novabiochem, 100–200 mesh, 0.59 mmol/g loading) using standard Fmoc/HBTU peptide coupling conditions. Briefly, the resin (200 μ mol) was pre-swollen by suspending in 3 ml of *N*-methyl-2-pyrrolidone (NMP) for 10 min followed by deprotection of the fluorenylmethyloxycarbonyl (Fmoc)-protecting group using 3 ml of 20% piperidine (v/v) in NMP (2 \times 5 min). Each amino acid coupling was performed by mixing 2 ml of a 0.4 M stock solution of *O*-Benzotriazole-*N,N,N,N*-tetramethyluronium-hexafluoro-phosphate (HBTU) with 4 ml of a 0.2 M NMP stock solution of the amino acid, followed by 2 ml of a 1.6 M NMP stock solution of *N,N*-diisopropylethylamine (DIPEA). The reaction mixture was added immediately to the resin and the reaction vessel agitated at ambient temperature for 30 min. For the synthesis of the peptide backbone, the *N*- α -Fmoc-protected amino acid building blocks were introduced sequentially and in the following order (single coupling): Fmoc-Cys(Trt)-OH, Fmoc-Gly-OH, Fmoc-Lys(Alloc)-OH, Fmoc-Glu(Bu)-OH, Fmoc-Pro-OH, Fmoc-Gly-OH, Fmoc-Lys(Alloc)-OH, Fmoc-Lys(Boc)-OH, Fmoc-Lys(Alloc)-OH. Prior to the introduction of the peptide side-chains, orthogonal cleavage of the allyloxycarbonyl (alloc)-protecting groups was performed by suspending the pre-swollen resin (10 min, dichloromethane, CH₂Cl₂) in a CH₂Cl₂ solution of *tetrakis*-(triphenylphosphine)palladium(0) (0.1 eq. per alloc group) and *N,N*-dimethylbarbituric acid (5 eq. per alloc group), according to a recently described protocol [76]. For the synthesis of the peptide side-chains, triple couplings were necessary to introduce the Fmoc-R(Pbf)-OH, Fmoc-Pro-OH and Fmoc-Lys(Bu)-OH building blocks. The 5(KPR)/TASP peptide was cleaved from the resin using a 92.5/2.5/2.5/2.5 (v/v) mixture of trifluoroacetic acid (TFA)/H₂O/trisopropylsilane (TIS)/ethanedithiol (EDT), and then precipitated in ice-cold diethyl ether. The peptide construct was then purified by

reverse-phase HPLC using an Alltima HP C18 column (5 μ m, length 125 mm, ID: 20 mm) and 0.1% TFA in H₂O/MeCN as mobile phase. The pure peptides were analyzed by LC-MS using a Shimadzu LC Controller V2.0, LCQ Deca XP Mass Spectrometer V2.0, Alltima C18-column 125 \times 2.0 mm, Surveyor AS and PDA with solvent eluent conditions: CH₃CN/H₂O/1% TFA (C₁₃₂H₂₄₀N₃₁O₂₇S₇, [M + 3H]³⁺ Calculated: 1003.31; Measured: 1003.80). The identity of the peptides was verified by MALDI (C₁₃₂H₂₄₄N₃₁O₂₇S₇, [M H]⁺ Calculated: 3008.98; Measured: 3007.98). The Rink Amide resin and all amino acid building blocks were purchased from Novabiochem®. HBTU, *N,N*-diisopropylamine, *N*-methyl-2-pyrrolidone, CH₂Cl₂, HPLC-grade CH₃CN and HPLC-grade TFA were all purchased from Biosolve B.V. Diethyl ether was purchased from Actua-All Chemicals. [(PPh₃)₄Pd], *N,N*-dimethylbarbituric acid, ethanedithiol, and trisopropylsilane were all purchased from Sigma-Aldrich. H₂O refers to Millipore grade distilled water.

Fluorescence polarization

Fluorescence labeling of the nucleolin RGG with the fluorescence reporter group *N*-(iodoacetaminoethyl)-1-naphthylamine-5-sulfonic acid (IAEDANS; Sigma, Deisenhofen, Germany) was performed as previously described [72]. Increasing amounts of FMRP Nterm (50, 100, 150, 200, 250, 300 and 350 μ M) were titrated into IAEDANS-labeled fluorescent RGG (0.5 μ M) in a buffer, containing 30 mM Tris/HCl (pH 7.5), 150 mM NaCl, 5 mM MgCl₂, 1 mM tris-(2-carboxyethyl) phosphine and a total volume of 200 μ l at 25 °C using a Fluoromax 4 fluorimeter. The concentration dependent binding curve was fitted using a quadratic ligand binding equation.

Acknowledgments

We thank France Carrier for providing us nucleolin constructs and Ehsan Amin, Radovan Dvorsky, and Saideh Nakhaei-Rad for discussions.

Author Contributions

Conceived and designed the experiments: MST LB CH RPP MRA. Performed the experiments: MST LGM JMM KN. Analyzed the data: MST LGM CH RPP MRA. Contributed reagents/materials/analysis tools: LGM LB CH RPP MRA. Wrote the paper: LGM MST KN MRA.

References

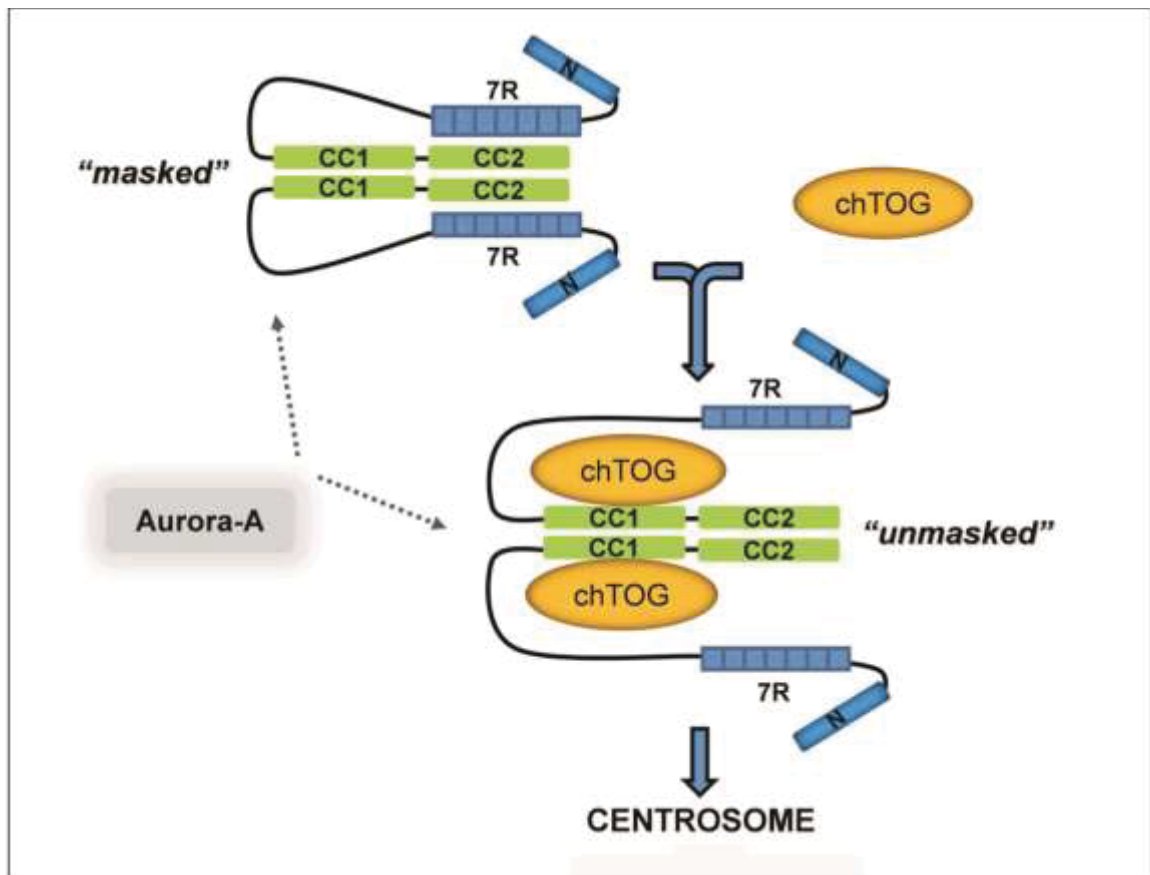
- Krueger DD, Bear MF (2011) Toward fulfilling the promise of molecular medicine in fragile X syndrome. *Annu Rev Med* 62: 411–429.
- Wang T, Bray SM, Warren ST (2012) New perspectives on the biology of fragile X syndrome. *Curr Opin Genet Dev* 22: 256–263.
- Darnell JC, Van Driesche SJ, Zhang C, Hung KY, Mele A, et al. (2011) FMRP stalls ribosomal translocation on mRNAs linked to synaptic function and autism. *Cell* 146: 247–261.
- Incamagli A, Tiedge H (2013) Translational control at the synapse: role of RNA regulators. *Trends Biochem Sci* 38: 47–55.
- Bardoni B, Davidovic L, Bensaid M, Khandjian EW (2006) The fragile X syndrome: exploring its molecular basis and seeking a treatment. *Expert Rev Mol Med* 8: 1–16.
- Kim M, Cerman S (2012) Fragile X mental retardation protein: past, present and future. *Curr Protein Pept Sci* 13: 350–371.
- Hoogeveen AT, Willemsen R, Oostra BA (2002) Fragile X syndrome, the fragile X related proteins, and animal models. *Microsc Res Tech* 57: 148–155.
- Davidovic L, Durand N, Khalilallah O, Tabet R, Barbry P, et al. (2013) A novel role for the RNA-binding protein FXRIP in myoblasts cell-cycle progression by modulating p21/Cdkn1a/Cip1/Waf1 mRNA stability. *PLoS Genet* 9: e1003367.
- El Fatimy R, Tremblay S, Dury AY, Solomon S, De Koninck P, et al. (2012) Fragile X mental retardation protein interacts with the RNA-binding protein Caprin1 in neuronal RiboNucleoProtein complexes [corrected]. *PLoS One* 7: e39330.
- Saito MR, Bray SM, Warren ST (2012) Molecular mechanisms of fragile X syndrome: a twenty-year perspective. *Annu Rev Pathol* 7: 219–245.
- Feng Y, Aboher D, Eberhart DE, Brown V, Malter HE, et al. (1997) FMRP associates with polyribosomes as an mRNP, and the 1304N mutation of severe fragile X syndrome abolishes this association. *Mol Cell* 1: 109–118.
- Tamanini F, Meijer N, Verheij C, Willems PJ, Galjaard H, et al. (1996) FMRP is associated to the ribosomes via RNA. *Hum Mol Genet* 5: 809–813.
- Coelin F, Bouillon M, Fortin A, Morin S, Rousseau F, et al. (1997) The fragile X mental retardation protein is associated with poly(A) mRNA in actively translating polyribosomes. *Hum Mol Genet* 6: 1465–1472.
- Sidorov MS, Aertlich BD, Bear MF (2013) Fragile X mental retardation protein and synaptic plasticity. *Mol Brain* 6: 15.
- Adinolfi S, Ramos A, Martin SR, Dal Poz F, Pucci P, et al. (2003) The N-terminus of the fragile X mental retardation protein contains a novel domain involved in dimerization and RNA binding. *Biochemistry* 42: 10437–10444.
- Ramos A, Hollingsworth D, Adinolfi S, Castets M, Kelly G, et al. (2006) The structure of the N-terminal domain of the fragile X mental retardation protein: a platform for protein-protein interaction. *Structure* 14: 21–31.
- Kim M, Bellini M, Cerman S (2009) Fragile X mental retardation protein FMRP binds mRNAs in the nucleus. *Mol Cell Biol* 29: 214–228.
- Feng Y, Gurekani CA, Eberhart DE, Yi H, Warren ST, et al. (1997) Fragile X mental retardation protein: nucleocytoplasmic shuttling and association with somatodendritic ribosomes. *J Neurosci* 17: 1539–1547.
- Bardoni B, Sittler A, Shen Y, Mandel JL (1997) Analysis of domains affecting intracellular localizations of the FMRP protein. *Neurobiol Dis* 4: 329–336.
- Tamanini F, Bontekoe C, Bakker CE, van Uuren L, Anar B, et al. (1999) Different targets for the fragile X-related proteins revealed by their distinct nuclear localizations. *Hum Mol Genet* 8: 863–869.

21. Willemssen R, Bontekoe C, Tamamini F, Galjaard H, Hoogeveen A, et al. (1996) Association of FMRP with ribosomal precursor particles in the nucleolus. *Biochem Biophys Res Commun* 225: 27–33.
22. Schenck A, Bardoni B, Moro A, Bagni C, Mandel JL (2001) A highly conserved protein family interacting with the fragile X mental retardation protein (FMRP) and displaying selective interactions with FMRP-related proteins FXR1P and FXR2P. *Proc Natl Acad Sci U S A* 98: 8844–8849.
23. Schenck A, Bardoni B, Laugmann C, Harden N, Mandel JL, et al. (2003) CYFIP/Sra-1 controls neuronal connectivity in *Drosophila* and links the Rac1 GTPase pathway to the fragile X protein. *Neuron* 38: 487–498.
24. Bardoni B, Willemssen R, Wellet JJ, Schenck A, Severijnen LA, et al. (2003) NUFIP1 (nuclear FMRP interacting protein 1) is a nucleocytoplasmic shuttling protein associated with active synaptosomes. *Exp Cell Res* 289: 95–107.
25. Bardoni B, Castets M, Huot ME, Schenck A, Adinolfi S, et al. (2003) 82-FIP, a novel FMRP (fragile X mental retardation protein) interacting protein, shows a cell cycle-dependent intracellular localization. *Hum Mol Genet* 12: 1609–1620.
26. Ceman S, Brons V, Warren ST (1999) Isolation of an FMRP-associated messenger ribonucleoprotein particle and identification of nucleolin and the fragile X-related proteins as components of the complex. *Mol Cell Biol* 19: 7925–7932.
27. Villare P, Marion RM, Orin J (2004) The composition of Staufen-containing RNA granules from human cells indicates their role in the regulated transport and translation of messenger RNAs. *Nucleic Acids Res* 32: 2411–2420.
28. Gaha C, Artigas P, Gatto C (2012) Nuclear Na⁺/K⁺-ATPase plays an active role in nucleoplasmic Ca²⁺ homeostasis. *J Cell Sci* 125: 6137–6147.
29. Adjobo-Hermans MJ, Goedhart J, van Weeren L, Nijmeijer S, Manders EM, et al. (2011) Real-time visualization of heterotrimeric G protein Gq activation in living cells. *BMC Biol* 9: 32.
30. Seidler NW (2013) Compartmentation of GAPDH. *Adv Exp Med Biol* 983: 61–101.
31. Tisdale EJ, Kelly C, Arteale CR (2004) Glyceraldehyde-3-phosphate dehydrogenase interacts with Rab2 and plays an essential role in endoplasmic reticulum to Golgi transport exclusive of its glycolytic activity. *J Biol Chem* 279: 54046–54052.
32. Mu FT, Callaghan JM, Steele-Mortimer O, Stenmark H, Parton RG, et al. (1995) EEA1, an early endosome-associated protein. EEA1 is a conserved alpha-helical peripheral membrane protein flanked by cysteine “fingers” and contains a calmodulin-binding IQ motif. *J Biol Chem* 270: 13503–13511.
33. Shimi T, Butts-Israeli V, Adams SA, Hamanaka RB, Goldman AE, et al. (2011) The role of nuclear lamin B1 in cell proliferation and senescence. *Genes Dev* 25: 2579–2593.
34. Colombo E, Alcalay M, Pefeci FG (2011) Nucleophosmin and its complex network: a possible therapeutic target in hematological diseases. *Oncogene* 30: 2593–2609.
35. Tamamini F, Van Umen L, Bakker C, Sacchi N, Galjaard H, et al. (1999) Oligomerization properties of fragile-X mental-retardation protein (FMRP) and the fragile-X-related proteins FXR1P and FXR2P. *Biochem J* 343 Pt 3: 517–523.
36. Napoli L, Mercaldo V, Boyd PP, Eleuteri B, Zalfa F, et al. (2008) The fragile X syndrome protein represses activity-dependent translation through CYFIP1, a new 4E-BP. *Cell* 134: 1042–1054.
37. Bardoni B, Schenck A, Mandel JL (2001) The Fragile X mental retardation protein. *Brain Res Bull* 56: 375–382.
38. Garcia-Mata R, Boulter E, Berridge K (2011) The ‘invisible hand’: regulation of RHO GTPases by RHOGEFs. *Nat Rev Mol Cell Biol* 12: 493–504.
39. Lanning CC, Dackiwala JL, Ruiz-Velasco R, Shafer SH, Williams CL (2004) The Rac1 C-terminal polybasic region regulates the nuclear localization and protein degradation of Rac1. *J Biol Chem* 279: 44197–44210.
40. Sambrook K, Bielek H, Schradl K, Schmidt G, Klugbauer N (2010) The nuclear import of the small GTPase Rac1 is mediated by the direct interaction with karyopherin alpha2. *Traffic* 11: 198–209.
41. Jackson RS, 2nd, Cho YJ, Stein S, Liang P (2007) CYFIP2, a direct p53 target, is leptomycin-B sensitive. *Cell Cycle* 6: 95–103.
42. Michalson D, Alidi W, Guardavaccaro D, Zhou M, Ahearn I, et al. (2008) Rac1 accumulates in the nucleus during the G2 phase of the cell cycle and promotes cell division. *J Cell Biol* 181: 485–496.
43. Tajrishvili MM, Tuteja R, Tuteja N (2011) Nucleolin: The most abundant multifunctional phosphoprotein of nucleolus. *Commun Integr Biol* 4: 267–275.
44. Abdelmohsen K, Gorospe M (2012) RNA-binding protein nucleolin in disease. *RNA Biol* 9: 799–808.
45. Brendel C, Rehbein M, Krievanamp HJ, Buck F, Richter D, et al. (2004) Characterization of Staufen 1 ribonucleoprotein complexes. *Biochem J* 384: 239–246.
46. Ceman S, O'Donnell WT, Reed M, Patton S, Pohl J, et al. (2003) Phosphorylation influences the translation state of FMRP-associated polyribosomes. *Hum Mol Genet* 12: 3295–3305.
47. Caxle WM, Kitson E, Li J, Bracler J, Zhang J (2009) A role for a novel protein, nucleolin, in Parkinson's disease. *Neurosci Lett* 459: 11–15.
48. Dolzhanskaya N, Merz G, Aletta JM, Demman RB (2006) Methylation regulates the intracellular protein-protein and protein-RNA interactions of FMRP. *J Cell Sci* 119: 1933–1946.
49. Huang L, Moller S, Souquere S, Le Roy F, Ernault-Lange M, et al. (2011) Mitochondria associate with P-bodies and modulate microRNA-mediated RNA interference. *J Biol Chem* 286: 24219–24230.
50. Ross-Inta C, Omanska-Khasek A, Wong S, Barrow C, Garcia-Arocena D, et al. (2010) Evidence of mitochondrial dysfunction in fragile X-associated tremor/ataxia syndrome. *Biochem J* 429: 545–552.
51. Yao A, Jin S, Li X, Liu Z, Ma X, et al. (2011) *Drosophila* FMRP regulates microtubule network formation and axonal transport of mitochondria. *Hum Mol Genet* 20: 51–63.
52. Kaplan ES, Cao Z, Hulsizer S, Tassone F, Berman RE, et al. (2012) Early mitochondrial abnormalities in hippocampal neurons cultured from Fmr1 pre-mutation mouse model. *J Neurochem* 123: 613–621.
53. McLennan Y, Polussa J, Tassone F, Hagerman R (2011) Fragile x syndrome. *Curr Genomics* 12: 216–224.
54. Blackwell E, Zhang X, Ceman S (2010) Arginines of the RGG box regulate FMRP association with polyribosomes and mRNA. *Hum Mol Genet* 19: 1314–1325.
55. Callebaut C, Blanco J, Benkirane N, Krust B, Jacotot E, et al. (1998) Identification of V3 loop-binding proteins as potential receptors implicated in the binding of HIV particles to CD4(+) cells. *J Biol Chem* 273: 21988–21997.
56. Maurer-Stroh S, Dickens NJ, Hughes-Davies L, Kozzarides T, Eisenhaber F, et al. (2003) The Tudor domain ‘Royal Family’: Tudor, plant Ageret, Chromo, PWWP and MBT domains. *Trends Biochem Sci* 28: 69–74.
57. Adams-Crisaba MA, Gao Y, Bian C, Amaya MF, Lam R, et al. (2010) Structural studies of the tandem Tudor domains of fragile X mental retardation related proteins FXR1 and FXR2. *PLoS One* 5: e13559.
58. Scott MS, Troshin PV, Barton GJ (2011) NoD: a Nucleolar localization sequence detector for eukaryotic and viral proteins. *BMC Bioinformatics* 12: 317.
59. Tamamini F, Kirkpatrick LL, Schonkrogen J, van Umen L, Bontekoe C, et al. (2000) The fragile X-related proteins FXR1P and FXR2P contain a functional nucleolar-targeting signal equivalent to the HIV-1 regulatory proteins. *Hum Mol Genet* 9: 1487–1493.
60. Dury AY, El Fatimy R, Tremblay S, Rose TM, Côté J, et al. (2013) Nuclear Fragile X Mental Retardation Protein Is localized to Cajal Bodies. *PLoS Genetics* 9: e1003890.
61. Brackett DM, Qing F, Amieux PS, Sellers DL, Horner PJ, et al. (2013) FMR1 transcript isoforms: association with polyribosomes; regional and developmental expression in mouse brain. *PLoS One* 8: e58296.
62. Sittler A, Devys D, Weber C, Mandel JL (1996) Alternative splicing of exon 14 determines nuclear or cytoplasmic localisation of fmr1 protein isoforms. *Hum Mol Genet* 5: 95–102.
63. Collins SC, Bray SM, Solih JA, Cutler DJ, Coffee B, et al. (2010) Identification of novel FMR1 variants by massively parallel sequencing in developmentally delayed males. *Am J Med Genet A* 152A: 2512–2520.
64. Schmidt-Zachmann MS, Nigg EA (1993) Protein localization to the nucleolus: a search for targeting domains in nucleolin. *J Cell Sci* 105 (Pt 3): 799–806.
65. Ceman S, Nelson R, Warren ST (2000) Identification of mouse YB1/p50 as a component of the FMRP-associated mRNP particle. *Biochem Biophys Res Commun* 279: 904–908.
66. Narayanan U, Nalavadi V, Nakamoto M, Thomas G, Ceman S, et al. (2008) S6K1 phosphorylates and regulates fragile X mental retardation protein (FMRP) with the neuronal protein synthesis-dependent mammalian target of rapamycin (mTOR) signaling cascade. *J Biol Chem* 283: 18478–18482.
67. Bassell GJ, Warren ST (2008) Fragile X syndrome: loss of local mRNA regulation alters synaptic development and function. *Neuron* 60: 201–214.
68. Darnell JC, Klamm E (2013) The translation of translational control by FMRP: therapeutic targets for FXS. *Nat Neurosci*.
69. Verkerk AJ, Pieretti M, Sutcliffe JS, Fu YH, Kuhl DP, et al. (1991) Identification of a gene (FMR-1) containing a CCG repeat coincident with a breakpoint cluster region exhibiting length variation in fragile X syndrome. *Cell* 65: 905–914.
70. Yang C, Maigaal DA, Carrier F (2002) Identification of nucleolin and nucleophosmin as genotoxic stress-responsive RNA-binding proteins. *Nucleic Acids Res* 30: 2251–2260.
71. Eberth A, Ahmadian MR (2009) In vitro GEF and GAP assays. *Current protocols in cell biology/editorial board, Juan S Bonifacio [et al] Chapter 14: Unit 14 19.*
72. Jainwal M, Gremer L, Dvorsky R, Haessler LG, Cirstea IC, et al. (2011) Mechanistic insights into specificity, activity, and regulatory elements of the regulator of G-protein signaling (RGS)-containing Rho-specific guanine nucleotide exchange factors (GEFs) p115, PDZ-RhoGEF (PRG), and leukemia-associated RhoGEF (LARG). *J Biol Chem* 286: 18202–18212.
73. Robinson MS, Sablensler DA, Foster SD (2010) Rapid inactivation of proteins by rapamycin-induced rerouting to mitochondria. *Dev Cell* 18: 324–331.
74. Callebaut C, Jacotot E, Guichard G, Krust B, Rey-Caillie M, et al. (1996) Inhibition of HIV infection by pseudopeptides blocking viral envelope glycoprotein-mediated membrane fusion and cell death. *Virology* 218: 181–192.
75. Callebaut C, Jacotot E, Krust B, Guichard G, Blanco J, et al. (1997) Pseudopeptide TASP inhibitors of HIV entry bind specifically to a 95-kDa cell surface protein. *J Biol Chem* 272: 7159–7166.
76. Wojcik F, Mosca S, Hartmann L (2012) Solid-phase synthesis of asymmetrically branched sequence-defined poly(oligo)amidoamines. *J Org Chem* 77: 4226–4234.

Chapter VII

The Centrosomal Adaptor TACC3 and the Microtubule Polymerase chTOG Interact *via* Defined C-terminal Subdomains in an Aurora-A Kinase-independent Manner

Graphical abstract



Status: Published in the Journal of Biological Chemistry, January 3, 2014

Impact factor: 4.57

Own Proportion to this work: 10 %

Purification of chTOG-A and -B

Analytical size exclusion chromatography

ITC measurement

Pull-down experiment

Partially writing and revising the manuscript

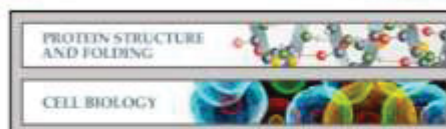


Protein Structure and Folding:
**The Centrosomal Adaptor TACC3 and the
 Microtubule Polymerase chTOG Interact
 via Defined C-terminal Subdomains in an
 Aurora-A Kinase-independent Manner**

Harish C. Thakur, Madhurendra Singh,
 Luitgard Nagel-Steger, Jana Kremer, Daniel
 Prumbaum, Eyad Kalawy Fansa, Hakima
 Ezzahoui, Kazem Nouri, Lothar Gremer,
 André Abts, Lutz Schmitt, Stefan Raunser,
 Mohammad R. Ahmadian and Roland P.
 Piekorz

J. Biol. Chem. 2014, 289:74-88.

doi: 10.1074/jbc.M113.532333 originally published online November 22, 2013



Access the most updated version of this article at doi: [10.1074/jbc.M113.532333](https://doi.org/10.1074/jbc.M113.532333)

Find articles, minireviews, Reflections and Classics on similar topics on the [JBC Affinity Sites](#).

Alerts:

- [When this article is cited](#)
- [When a correction for this article is posted](#)

[Click here](#) to choose from all of JBC's e-mail alerts

Supplemental material:

<http://www.jbc.org/content/suppl/2013/11/22/M113.532333.DC1.html>

This article cites 81 references, 39 of which can be accessed free at
<http://www.jbc.org/content/289/1/74.full.html#ref-list-1>

The Centrosomal Adaptor TACC3 and the Microtubule Polymerase chTOG Interact via Defined C-terminal Subdomains in an Aurora-A Kinase-independent Manner^{*[5]}

Received for publication, November 4, 2013. Published, JBC Papers in Press, November 22, 2013, DOI 10.1074/jbc.M113.532333

Harish C. Thakur^{1†}, Madhurendra Singh², Luitgard Nagel-Steger^{3*}, Jana Kremer¹, Daniel Prumbaum¹, Eyad Kalawy Fansa^{4,2}, Hakima Ezzahoui¹, Kazem Nouri¹, Lothar Gremer^{5*}, André Abts^{**}, Lutz Schmitt^{**}, Stefan Raunser¹, Mohammad R. Ahmadian^{4,2}, and Roland P. Piekorz^{2,3}

From the ¹Institut für Biochemie und Molekularbiologie II, Medizinische Fakultät der Heinrich-Heine-Universität, D-40225 Düsseldorf, Germany, ²Institut für Physikalische Biologie, Heinrich-Heine-Universität, 40225 Düsseldorf, Germany, ³ICS-6, Strukturbiologie, Forschungszentrum, 52425 Jülich, Germany, ⁴Institut für Biochemie, Heinrich-Heine-Universität, 40225 Düsseldorf, Germany, and ⁵Max-Planck-Institut für Molekulare Physiologie, 44227 Dortmund, Germany

Background: The TACC3-chTOG protein complex is essential for mitotic spindle assembly.

Results: TACC3-chTOG binding is directed and mediated by specific intradomain and interdomain interactions that are not affected by Aurora-A kinase.

Conclusion: Formation of the TACC3-chTOG complex is Aurora-A-independent, in contrast to its recruitment to the spindle apparatus.

Significance: Novel insight into regulation and domain specificity of TACC3-chTOG interaction is provided.

The cancer-associated, centrosomal adaptor protein TACC3 (transforming acidic coiled-coil 3) and its direct effector, the microtubule polymerase chTOG (colonic and hepatic tumor overexpressed gene), play a crucial function in centrosome-driven mitotic spindle assembly. It is unclear how TACC3 interacts with chTOG. Here, we show that the C-terminal TACC domain of TACC3 and a C-terminal fragment adjacent to the TOG domains of chTOG mediate the interaction between these two proteins. Interestingly, the TACC domain consists of two functionally distinct subdomains, CC1 (amino acids (aa) 414–530) and CC2 (aa 530–630). Whereas CC1 is responsible for the interaction with chTOG, CC2 performs an intradomain interaction with the central repeat region of TACC3, thereby masking the TACC domain before effector binding. Contrary to previous findings, our data clearly demonstrate that Aurora-A kinase does not regulate TACC3-chTOG complex formation, indicating that Aurora-A solely functions as a recruitment factor for the TACC3-chTOG complex to centrosomes and proximal mitotic spindles. We identified with CC1 and CC2, two functionally diverse modules within the TACC domain of TACC3

that modulate and mediate, respectively, TACC3 interaction with chTOG required for spindle assembly and microtubule dynamics during mitotic cell division.

The centrosome represents the main microtubule (MT)⁴ organizing center in all metazoans and is thereby responsible for equal partitioning of chromosomes to daughter cells during the mitotic phase of the cell cycle (1–5). Numerical and structural abnormalities of centrosomes are associated with aneuploidy, chromosomal instability and transformation, developmental defects, apoptotic cell death, and cell cycle arrest through induction of premature senescence (6–12). Cancer cells *e.g.* counteract extra centrosomes and, therefore, the danger of multipolar divisions and excess aneuploidy/cell death through centrosome clustering (13–15). This process became an attractive pharmacological tumor target (16, 17).

During the cell cycle centrosomes undergo a division and maturation process called the centrosome cycle (4, 18, 19). Mitotic centrosomes are structurally made up of one pair of centrioles surrounded by the pericentriolar matrix (20). More than two hundred proteins are involved in centrosome assembly, organization, and function (19, 21–23). These proteins have structural, functional/enzymatic, and regulatory/signaling roles in MT nucleation and spindle dynamics, mitotic progression, and cytokinesis (24). Recent work by the Mitocheck consortium (25, 26) provided a global confirmation of known and identification of novel cell division genes and their protein

^{*}This work was supported by a fellowship of the NRW (North Rhine-Westphalia) graduate school "BioStruct: Biological Structures in Molecular Medicine and Biotechnology" (to H. C. T.), the Deutsche Forschungsgemeinschaft (SFB 728/TP A5 to R. P. P.), the research commission of the medical faculty of the Heinrich-Heine-University (grants to R. P. P. and M. R. A.), the strategic research fund of the Heinrich-Heine-University (grants to R. P. P. and M. R. A.), and the International Graduate School of Protein Science and Technology (iGRASP; to K. N. and M. R. A.).

^[5]This article contains supplemental Table S1 and Figs. S1–S11.

[†]Present address: Wellcome Trust Centre for Cell Biology, The University of Edinburgh, Edinburgh EH9 3JR, Scotland, United Kingdom.

²Supported by Bundesministerium für Bildung und Forschung (NGFNplus program Grant 01GS08100).

³To whom correspondence should be addressed: Institut für Biochemie und Molekularbiologie II, Universitätsklinikum der Heinrich-Heine-Universität, D-40225 Düsseldorf, Germany. Tel.: 49-211-81-12739; Fax: 49-211-81-12726; E-mail: Roland.Piekorz@uni-duesseldorf.de.

⁴The abbreviations used are: MT, microtubule; aa, amino acid; SEC, size exclusion chromatography; aSEC, analytical SEC; CBB, Coomassie Brilliant Blue; CC, coiled-coil; chTOG, colonic and hepatic tumor overexpressed gene; ITC, isothermal titration calorimetry; 7R, serine-proline-glutamate-rich repeat region; TACC, transforming acidic coiled-coil; XMAP215, *Xenopus* microtubule associated protein 215 kDa; ARNT, aryl hydrocarbon receptor nuclear translocator.

Molecular Basis of TACC3-chTOG Complex Formation

complexes that require biochemical and functional elucidation in greater detail.

Members of the centrosomal TACC (transforming acidic coiled-coil) family of proteins are important structural components of the mitotic spindle apparatus (27–29). TACCs are conserved in all metazoans and play a vital role as adaptor proteins in the regulation of centrosomal integrity and spindle MT stability and dynamics (27, 28, 30–34). Vertebrates express three TACC isoforms, TACC1, TACC2, and TACC3, of which the latter is typically found at high levels in proliferative and regenerative cell types and tissues (35–37). During the cell cycle TACC3 expression increases strongly in the G₂/M phase (38) followed by Cdh1-dependent degradation of TACC3 during mitotic exit (39). TACC3 deficiency leads to growth retardation and embryonic lethality (38, 40), in line with the anti-proliferative impact of shRNA mediated gene silencing of TACC3 (41, 42).

A crucial regulator of TACC3 is the mitotic kinase Aurora-A that phosphorylates TACC3 (pTACC3) and thereby determines its differential centrosomal/proximal spindle (pTACC3) versus distal spindle MT (TACC3) localization during (pro-)metaphase (43–46). Interestingly, recent findings expand the function of TACC3 and the Aurora-A-TACC3 axis to the regulation of kinetochore-microtubule connections (47) and central spindle assembly at later stages of mitosis (48), respectively. Other known TACC3 binding partners with regulatory/effector functions include the endocytic and vesicle trafficking protein clathrin (*i.e.* clathrin heavy chain) (49, 50) that binds to the clathrin interaction domain of pTACC3 to ensure intermicrotubule bridging and mitotic spindle organization (51, 52). Moreover, the evolutionary conserved interaction between TACCs and MT polymerases of the XMAP215 family is crucial for spindle pole stabilization and growth of centrosomal MTs (43, 46, 53). Family members, which comprise XMAP215 in *Xenopus laevis*, Msps in *Drosophila melanogaster*, and chTOG/CKAP5 (cytoskeleton associated protein 5) in *Homo sapiens*, are identified by the presence of several "TOG" domains involved in MT binding.

TACC proteins are structurally characterized by a rather variable N-terminal region of which the approximately first 100 residues are uniquely conserved among vertebrate TACC3 isoforms. Further features include a central serine-proline-glutamate-rich repeat region (28, 33) that in the case of murine TACC3 is characterized by seven perfect repeats of 24 amino acids each (thereafter referred to as "7R") (33, 38) as well as a highly conserved, coiled-coil-containing C terminus (thereafter referred to as "CC" or "TACC domain"). This signature domain is composed of ~200 amino acids (aa) (27, 33, 55), required for centrosomal localization, and known to be involved in protein-protein interaction (28). Here, TACC proteins interact from yeast to human through their TACC domain with the C terminus of XMAP215 family members (28, 46, 56, 57), thereby targeting them to spindle poles. In contrast, the functional role of the N-terminal part of TACC3 outside of the TACC domain is rather undefined besides being a substrate for Aurora-A-mediated phosphorylation that is required for centrosomal and proximal spindle localization of TACC3 (28).

From the analysis of *X. laevis* TACC3, it has been proposed that the N-terminal part masks the TACC domain and thereby inhibits its function (58, 59). Aurora-A mediated phosphorylation of TACC3 was implicated to "unmask" and thereby expose the TACC domain to intermolecular interaction with XMAP215 (46, 59). However, the molecular basis/details of the masking/unmasking mechanism of the TACC domain and its interaction with the C terminus of XMAP215 remained enigmatic. Here, we subjected recombinant murine TACC3 and the C-terminal part of the murine XMAP215 homologue chTOG to a deletion and biochemical interaction analysis. We identify within the TACC domain two functionally distinct subdomains, CC1 (aa 414–530) and CC2 (aa 530–630), which are involved in interdomain and intradomain protein interaction, respectively. We demonstrate that TACC3 forms a stable intramolecular complex through the interaction of 7R with CC2 (TACC domain "masked"). Interestingly, the C terminus of chTOG (aa 1806–2032) right hand to the putative MT-interacting TOG6 domain (52) binds selectively to the CC1 module and thereby disrupts the intramolecular CC2–7R complex, thereby giving rise to the effector-bound state of the TACC domain (TACC domain "unmasked"). Neither intradomain interaction of TACC3 nor its binding to chTOG was affected by Aurora-A kinase. Thus, consecutive intra- and intermolecular protein interactions direct and determine TACC3-chTOG complex formation before its Aurora-A-regulated centrosomal and proximal spindle recruitment required for MT growth and mitotic spindle assembly.

EXPERIMENTAL PROCEDURES

In Silico Analysis of TACC3—Protein sequences of TACC family members were retrieved from the NCBI database and used for further analysis. For sequence alignment and evolutionary analysis of conserved domains, the ClustalW multiple sequence alignment algorithm was used (60), and alignment was analyzed with JALVIEW. Further analysis of the coiled-coil boundary in the TACC domain of murine TACC3 was performed using the COILS server in 14, 21, and 28 residue scan mode (61). Algorithms and tools from the EXPASY proteomic server were employed for sequence-based protein characterization.

Cloning of Expression Constructs—Coding sequences for murine TACC3 and its variants were amplified using sequence-specific primer and cloned into the pGEX-4T1-NTEV expression vector. The following constructs were created: full-length TACC3 (aa 1–630); TACC3-ΔN (Δ1–118); TACC3-ΔR (Δ141–308), lacking the serine-proline-glutamate-rich repeat region; TACC3-ΔNΔR (Δ1–118 and Δ141–308); 7R (aa 119–324) comprising the serine-proline-glutamate-rich repeat region; CC (TACC domain; aa 414–630); CC1 (aa 414–530); CC2 (aa 530–630) (62). Moreover, pGEX-4T1-NTEV-based expression constructs for C-terminal fragments of human chTOG were created: chTOG-Cterm (aa 1574–2032), chTOG-A (aa 1544–1805), and chTOG-B (aa 1806–2032). To generate TACC3 deletion mutants fused at the C terminus to GFP, the following constructs were cloned in a pEGFP-N1 (Clontech)-based vector: full-length TACC3; TACC-ΔCC1 and TACC-ΔCC2 lacking the CC1 or CC2 subdomains, respec-

Molecular Basis of TACC3-chTOG Complex Formation

tively; TACC- Δ CC lacking the entire TACC domain. All constructs were validated by DNA sequencing.

Overexpression and Purification—GST fusion proteins were overexpressed in *Escherichia coli* BL21 Rosetta strain (Novagen). Protein extraction was carried out by incubating cells at 4 °C with DNase I (10 μ g/ml) followed by cell lysis in a microfluidizer (model M110S, Microfluidics Corp.) at a pressure of 10,000 p.s.i. Bacterial lysates were centrifuged to collect soluble fractions, and GST-tagged proteins were isolated from the supernatant via GST affinity purification. Upon cleavage of the GST tag with tobacco etch virus protease (4 units/mg, 4 °C, overnight) or thrombin (2 units/mg, 4 °C, overnight) proteins were subjected to gel filtration using a standard buffer containing 30 mM Tris-HCl, pH 7.5, 200 mM NaCl, 3 mM DTT, and 2 mM EDTA. The GST tag from the TACC3- Δ N and TACC3- Δ N Δ R deletion mutants could not be cleaved by tobacco etch virus protease for unknown reasons (data not shown), thus employing thrombin for both GST tag removal and cleavage at the internal site (supplemental Fig. S4). The final purity was analyzed on SDS-PAGE, proteins were concentrated using centrifugal ultrafiltration devices (Amicon Ultra; Millipore), and protein concentration was determined by the Bradford assay. For mass spectrometric analysis of thrombin-cleaved TACC3, the protein was desalted by passing through NAP-25 columns (GE Healthcare) and analyzed by MALDI-TOF at the central BMFZ facility of the Heinrich-Heine-University Düsseldorf.

Immunoblotting—Proteins were separated using SDS-PAGE gels and transferred to nitrocellulose membranes (Hybond C, GE Healthcare). Blots were probed overnight with primary antibodies: α TACC3 (N18) and α TACC3 (C18), both generated in rabbits (38), are specific for the N and C terminus of murine TACC3, respectively; α GST (Abcam); α chTOG (Abcam, QED Bioscience/Acris, and Novus Biologicals); α GFP (Roche Applied Science). After three washing steps membranes were incubated with horseradish peroxidase-coupled secondary antibodies for 1 h. Signals were visualized by the ECL detection system (GE Healthcare), and images were collected using the INTAS chemostar imager.

Analytical Gel Filtration/Size Exclusion Chromatography (SEC)—Gel filtration was performed using a Superose 6 10/300 GL column connected to an ÄKTATM purifier (GE Healthcare) and UV900 detector. For molecular weight determination, the column was calibrated with standard proteins of known molecular mass: thyroglobulin (669 kDa), ferritin (440 kDa), aldolase (158 kDa), ovalbumin (43 kDa), carbonic anhydrase (29 kDa), ribonuclease A (13.7 kDa), and aprotinin (6.5 kDa). Protein samples (50–200 μ g) were injected onto the preequilibrated column, and elution fractions of 0.5 ml were collected. Elution profiles were recorded using UNICORN4.11 software, and peak fractions were analyzed by SDS-PAGE followed by Coomassie Brilliant Blue (CBB) staining and immunoblotting.

GST Pulldown Assay—GST, GST-fused TACC3 variants, and fragments of the C terminus of chTOG (chTOG-Cterm) were expressed in *E. coli* and purified using standard protocols. To obtain prey proteins, the GST tag was cleaved off with tobacco etch virus protease and cleared by reverse GSH affinity purification. GSH-Sepharose beads (GE Healthcare) in a 100- μ l volume were washed 3 times with standard buffer. GST and

GST-fused proteins (10–20 μ M) were added and incubated in a final volume of 200 μ l at 4 °C for 1 h. Blocking with 5% BSA (2 h at 4 °C) was performed followed by three washing steps with standard buffer (30 mM Tris-HCl, pH 7.5, 200 mM NaCl, 3 mM DTT, 2 mM EDTA). Finally, samples were incubated at an equimolar ratio with prey proteins at 4 °C for 2 h. After five washing steps, 100 μ l of 2 \times Laemmli buffer was added, and samples were heat-denatured (5 min at 95 °C) and analyzed by SDS-PAGE followed by CBB staining and immunoblotting.

Isothermal Titration Calorimetry (ITC)—Purified TACC3 variants and chTOG-Cterm were first subjected to gel filtration (Superose 6 XK16/60) using ITC buffer (30 mM Tris-HCl, pH 7.5, 200 mM NaCl, 1 mM Tris(2-carboxyethyl)phosphine, 2 mM EDTA). For the 7R fragment, buffer was exchanged by overnight dialysis against ITC buffer using Slide-A-Lyzer dialysis cassettes (Thermo Scientific). All ITC measurements were carried out at 20 °C using a VP-ITC microcalorimeter (Microcal) (63, 64). Proteins were loaded into the sample cell and titrated with their putative interaction partners (10–15-fold higher protein concentration in the syringe compared with the concentration in the cell; titration volume 8, 10, or 15 μ l; spacing of 150–180 s; reference power of 13 μ cal s⁻¹, stirring at 310 rpm). The final data analysis was carried out using Origin software (Microcal Software). The experimental data were evaluated using Origin 7.0 software (Microcal Software) to determine the binding parameters, including association constant (K_a), number of binding sites (N), and enthalpy (ΔH). Control measurements were performed by titrating buffer to the protein and vice versa.

Immunoprecipitation—Purified TACC3 proteins before and after thrombin cleavage (~10–15 μ g) were mixed with 2 μ l of rabbit antisera (α TACC3 N18 or α TACC3 C18) (38) and incubated overnight at 4 °C. Thereafter, 25 μ l of protein A/G-agarose (Santa Cruz Biotechnology) preabsorbed with BSA was added, and the volume was adjusted to 100 μ l with IP buffer (30 mM Tris-HCl, 200 mM NaCl, 2 mM EDTA). After an incubation period of 1 h the beads were washed with IP buffer, and protein complexes were eluted with 2 \times Laemmli loading buffer and analyzed by SDS-PAGE and immunoblotting using primary antibodies (N18, C18) and horseradish peroxidase-conjugated secondary antibodies. Moreover, total cell lysates from HEK293 cells, which were transfected with expression vectors for TACC3 or TACC3 deletion mutants fused C-terminally to GFP, were prepared essentially as described (32) and thereafter subjected to immunoprecipitation using α GFP antibodies (Roche Applied Science). chTOG was detected in the co-immunoprecipitates using an α chTOG antibody from QED Bioscience/Acris.

Protein Kinase Assay—Purified human Aurora-A kinase (Signal Chem) was employed according to the manufacturer's instructions. In brief, kinase assays were performed in a volume of 25 μ l by mixing 5 μ l (0.1 μ g/ μ l) of Aurora-A kinase (diluted in kinase assay buffer: 5 mM MOPS, pH 7.2, 2.5 mM β -glycerol phosphate, 5 mM MgCl₂, 1 mM EGTA, 0.4 mM EDTA, 50 ng/ μ l BSA) with 1 μ g of purified TACC3 protein (before and after thrombin cleavage) or 1 μ g of the TACC3-chTOG complex as a substrate. The final volume was adjusted to 20 μ l with double distilled H₂O, and reactions were started by adding 5 μ l of 10

Molecular Basis of TACC3-chTOG Complex Formation

mM ATP (dissolved in 25 mM MOPS, pH 7.2, 12.5 mM β -glycerol phosphate, 25 mM $MgCl_2$, 5 mM EGTA, 0.4 mM EDTA). Reactions were incubated at 30 °C for 15 min and stopped by the addition of 10 μ l of 2 \times Laemmli loading buffer. Samples were separated by SDS-PAGE, and phosphorylated proteins were subsequently detected by Pro-Q Diamond (Molecular Probes, Invitrogen) and CBB staining.

Eukaryotic Cell Culture—HEK293 and HeLa cells were cultured in Dulbecco's modified Eagle's medium supplemented with 10% fetal calf serum (Invitrogen), 2 mM L-glutamine, 100 units/ml penicillin, and 100 μ g/ml streptomycin. GFP-fused TACC3 expression vectors were transfected into HEK293 cells using the TurboFect transfection reagent (ThermoScientific). The Aurora-A kinase inhibitor MLN8237 (Selleckchem) was applied in cell culture at a concentration of 0.5 μ M for 2 h (65).

Confocal Laser Scanning Microscopy—Cells were seeded at densities of 8×10^3 cells/cm² on coverslips and fixed with ice-cold methanol/acetone (1:1) for 20 min at -20 °C upon MLN8237 treatment. Subsequently, cells were incubated in IF buffer (4% bovine serum albumin, 0.05% saponin in PBS) for 1 h and stained in IF buffer with the following primary antibodies at the indicated dilutions: anti- α -tubulin (DM1a, 1:500, Sigma, or YOL1/34, Acris Antibodies, Hiddenhausen, Germany); α TACC3 (H300 or D2, Santa Cruz Biotechnology); anti- γ -tubulin (GTU-88, 1:100, Sigma); α chTOG (1:500, Acris); α pT288 Aurora-A (1:500; Cell Signaling). DNA was detected using 4,6-diamidino-2-phenylindole (DAPI, 1 mg/ml; Sigma). Analyses were performed with a LSM510-Meta confocal microscope (Zeiss) equipped with 40/1.3 or 63/1.4 immersion objectives and excitation wavelengths of 364, 488, 543, and 633 nm.

RESULTS

The TACC Domain of TACC3 Consists of Two Distinct Coiled-coil Subdomains—To examine the primary structure of murine TACC3 and thereby define functional modules in TACC3, sequence alignments of vertebrate TACC family members were performed. Consistent with previous findings (28, 33, 55), the N termini of TACC3 isoforms are characterized by a variable length and different amino acid composition as compared with other vertebrate TACC family members. Interestingly, the first 100 amino acids of TACC3 isoforms display a sequence identity of up to 75% (data not shown) followed by the central repeat region that in the case of murine TACC3 comprises seven conserved serine-proline-glutamate-rich repeats (7R) each consisting of 24 amino acids. Interestingly, coiled-coil prediction analysis indicated the presence of one breaking region that divides the C-terminal TACC domain of mammalian TACC3 proteins into two coiled-coil-containing subdomains, CC1 and CC2 (supplemental Fig. S1). Here, CC2 clearly revealed a higher amino acid sequence identity than the CC1 subdomain (supplemental Fig. S2). Overall, the domain organization of vertebrate TACC3 proteins emphasizes their isoform-specific functional roles as compared with TACC1 and TACC2. That is exemplified by the embryonic lethality caused by TACC3 deficiency, which is not observed for TACC2 deficiency (37, 38, 40), as well as by the selective interaction of the aryl hydrocarbon receptor nuclear translocator (ARNT) with TACC3 but not with TACC1 and TACC2 (66).

Moreover, we identified a unique and functional thrombin cleavage site (⁴¹⁰LEPR/GL⁴¹⁵) close to the TACC domain of murine TACC3 (Fig. 1A) that is absent in all other TACC3 proteins and TACC isoforms. This cleavage site resembles a *bona fide* recognition site for thrombin (⁴¹⁰LVPR/GS⁴¹⁵). Although the thrombin site present in murine TACC3 might not have any physiological relevance, it was used as a tool in this study to analyze the intra- and intermolecular interaction of murine TACC3.

Purification of Deletion Mutants and Fragments of TACC3 and chTOG—Based on the *in silico* analysis we cloned murine TACC3 and its variants (supplemental Fig. S3) as well as C-terminal fragments of chTOG (supplemental Fig. S5A) into the prokaryotic expression vector pGEX-4T1-NTEV. Proteins fused N-terminally to glutathione S-transferase (GST) were purified, cleaved using tobacco etch virus protease to remove the GST tag, and finally separated by gel filtration and/or reverse glutathione affinity chromatography (supplemental Figs. S4 and S5, B and C). Thrombin cleavage of TACC3 resulted in two fragments, a larger N-terminal part (TACC3-N7R, aa 1–413) and a smaller C-terminal fragment (CC, aa 414–630) containing the TACC domain (Fig. 1A and supplemental Fig. S4A). The identity and size of the CC fragment (25.2 kDa) was corroborated by mass spectrometry using MALDI-TOF. The adaptability of the thrombin site was also confirmed for the deletion mutants TACC3- Δ R, TACC3- Δ N, and TACC3- Δ N Δ R (supplemental Fig. S3 and S4).

Intradomain Association Leads to an Intramolecular Masked State of TACC3—We next subjected TACC3 to analytical size exclusion chromatography (aSEC) using a Superose 6 10/300 column. Interestingly, TACC3 eluted before and after thrombin cleavage in peak fractions with apparent molecular masses of ~1200 and ~630 kDa, respectively (Fig. 1B), the latter being unexpectedly the only peak detected after thrombin cleavage. Subsequent peak fraction analysis by SDS-PAGE and CBB staining as well as immunoblotting demonstrated the co-elution of both fragments, TACC3-N7R and CC (Fig. 1C). These findings strongly suggested the formation of a tight complex between the N- and C-terminal parts of TACC3. We confirmed this intramolecular interaction by co-immunoprecipitation of TACC3 before and after thrombin cleavage using antibodies specific for the N or C termini of murine TACC3 (38). As indicated in Fig. 1D, TACC3-N7R and CC was co-immunoprecipitated in both directions. Of note, thrombin cleavage of TACC3 did not result in changes in its secondary structure as indicated from circular dichroism measurements (supplemental Fig. S11A).

The Intramolecular Interaction of TACC3 Is Mediated between the 7R and CC2 Domains—To identify the domains involved in intradomain TACC3 interaction, we deleted the conserved N-terminal region (Δ 1–118; TACC- Δ N) and the central 7R region (Δ 141–308; TACC3- Δ R) (supplemental Fig. S3). The respective purified TACC3 variants were analyzed before and after thrombin cleavage by aSEC. The absence of the first 118 amino acids did not have any detectable effect on the elution pattern of TACC3- Δ N that was comparable to full-length TACC3 (Fig. 2B). Also, upon thrombin cleavage, both protein fragments (named TACC3-7R and TACC3-CC in Fig.

Molecular Basis of TACC3-chTOG Complex Formation

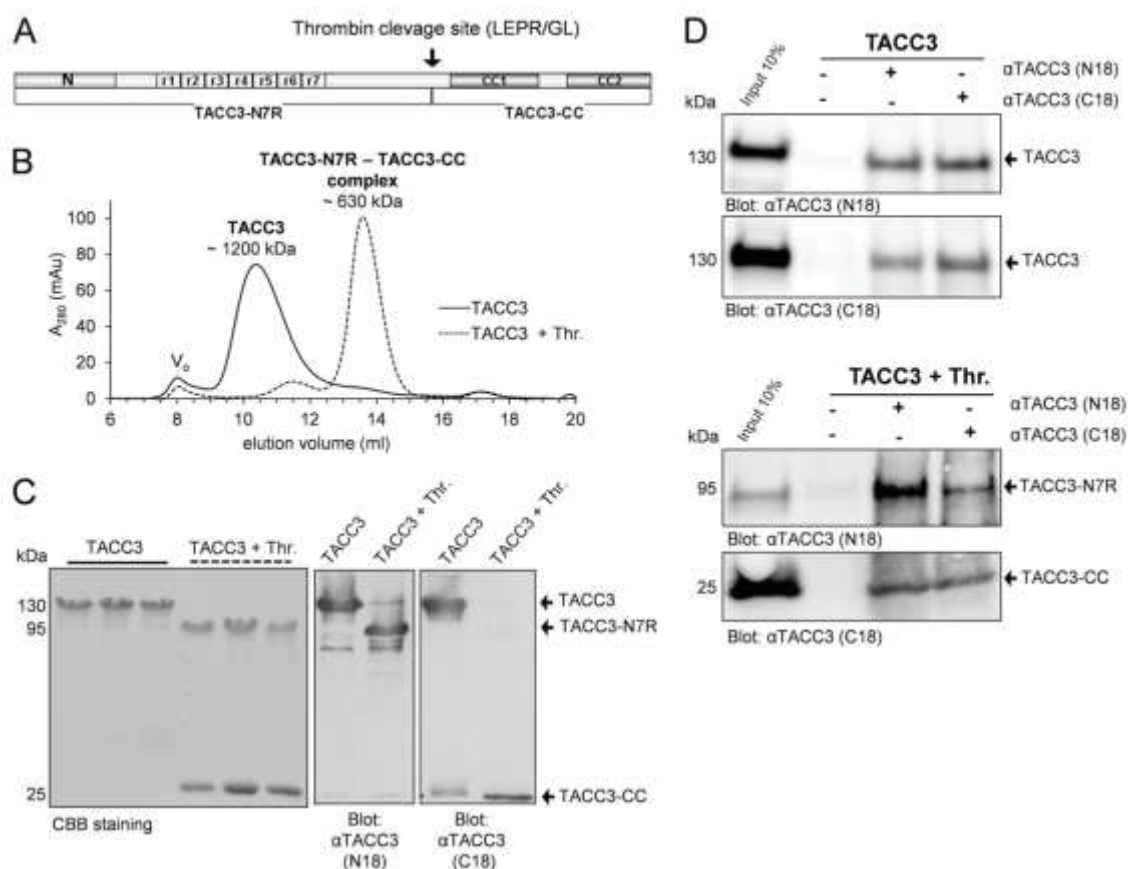


FIGURE 1. Thrombin cleavage of murine TACC3 generates two N- and C-terminal fragments staying in one intramolecular complex. *A*, a novel and unique thrombin site divides TACC3 into two separate parts, TACC3-N7R and TACC3-CC. *N* specifies the conserved ~100 amino acid residues at the N terminus. CC1 and CC2 indicate two distinct coiled-coil subdomains in the C terminus. *r1* to *r7* denotes the central region in TACC3 consisting of seven serine-proline-glutamate-rich repeats (7R). *B*, determination of the apparent molecular mass of TACC3 by aSEC (Superpose 6, 10/300). Elution profiles of TACC3 before (solid line) and after thrombin cleavage (dashed line) are indicated. V_0 , void volume. *mAu*, milliabsorbance units. *C*, peak elution fractions were analyzed by SDS-PAGE followed by CBB staining (left panel) and immunoblotting (central and right panels employing N18 and C18 antibodies directed against the N- or C-terminal end of TACC3, respectively) (38). *D*, co-immunoprecipitation analysis of TACC3 before (upper panel) and after thrombin cleavage (lower panel) was performed either without antibody input (beads control, lane 2) or by using N18 and C18 antibodies (lanes 3 and 4). *Thr.*, thrombin.

2) still co-eluted in one peak, suggesting that the conserved N-terminal region is not essentially involved in the intramolecular interaction of TACC3. In contrast, deletion of the 7R region abolished intradomain binding and resulted after thrombin cleavage in the separation of the fragments (named TACC3-N and TACC3-CC in Fig. 3) in two distinct peaks with apparent molecular masses of 160 and 630 kDa, respectively). Their identity was reconfirmed by immunoblot analysis (Fig. 3C). Thus, the central serine-proline-glutamate-rich repeat region (7R) is required for the intramolecular interaction with the C-terminal CC domain.

We further validated this finding by subjecting the isolated domains, *i.e.* GST-7R (bait) and CC (prey) (supplemental Fig. S3) to pulldown-based interaction analysis. GST alone was used as the control. Although CC showed an unspecific binding to the beads, we could still detect a clearly stronger binding of CC when GST-7R was used as bait and analyzed by immunoblotting (Fig. 3D). Last, to determine the region within the TACC

domain that binds to the central repeat region, we purified 7R and the CC subdomains CC1 and CC2 (supplemental Fig. S3 and S4E) and analyzed their interaction by employing ITC. As indicated in Fig. 3E, significant calorimetric changes as well as changes in the temperature as a function of the molar ratio of the interacting proteins were observed when 7R was titrated onto CC2. In contrast, binding of 7R to CC1 could not be detected (Fig. 3E, lower panel). We conclude that the central repeat region, *i.e.* 7R, binds selectively to CC2 and thereby mediates intramolecular TACC3 binding potentially masking the C terminus of TACC3 before intermolecular protein interaction.

TACC3 Interacts with chTOG via Its CC1 Domain—We next characterized the interdomain binding between TACC3 and its major effector, the MT polymerase chTOG. We employed the C terminus of chTOG as bait (GST-chTOG-Cterm; supplemental Fig. S5) in pulldown assays demonstrating a strong interaction between chTOG-Cterm and the CC domain of

Molecular Basis of TACC3-chTOG Complex Formation

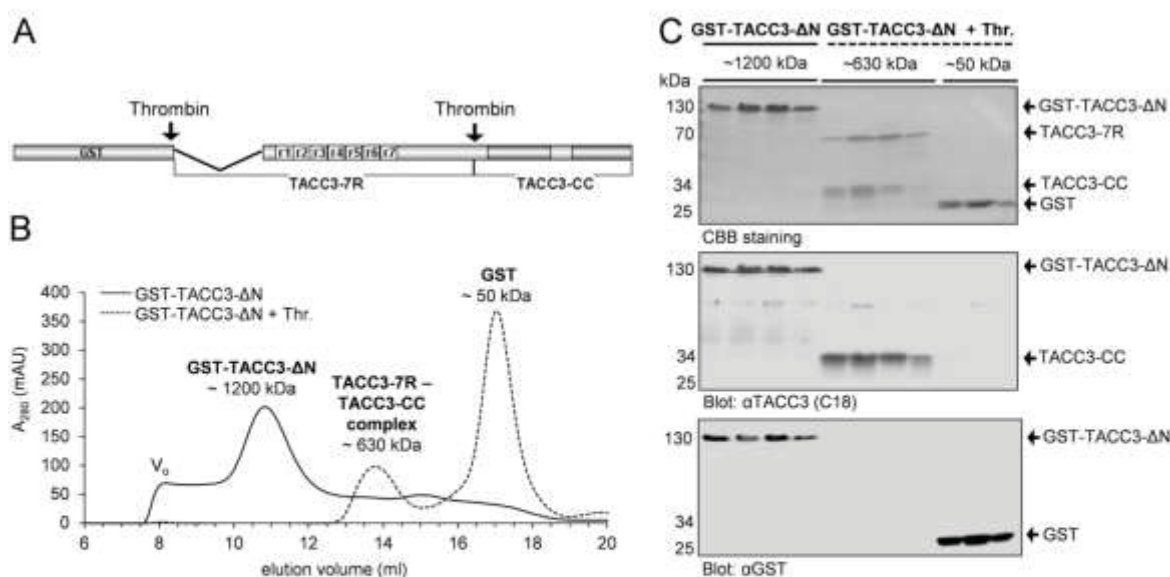


FIGURE 2. The N-terminal 118 amino acids are not involved in intramolecular complex formation of murine TACC3. *A*, primary structure of TACC3-ΔN lacking the N-terminal part of 118 aa. *B*, aSEC (Superpose 6, 10/300) elution profiles of GST-TACC3-ΔN before (solid line) and after (dashed line) thrombin cleavage. V_0 , void volume. mAU, milliabsorbance units. *C*, peak elution fractions were analyzed by SDS-PAGE followed by CBB staining (upper panel) and immunoblotting using anti-TACC3 C18 (middle panel) or anti-GST antibodies (lower panel). GST was used as a control.

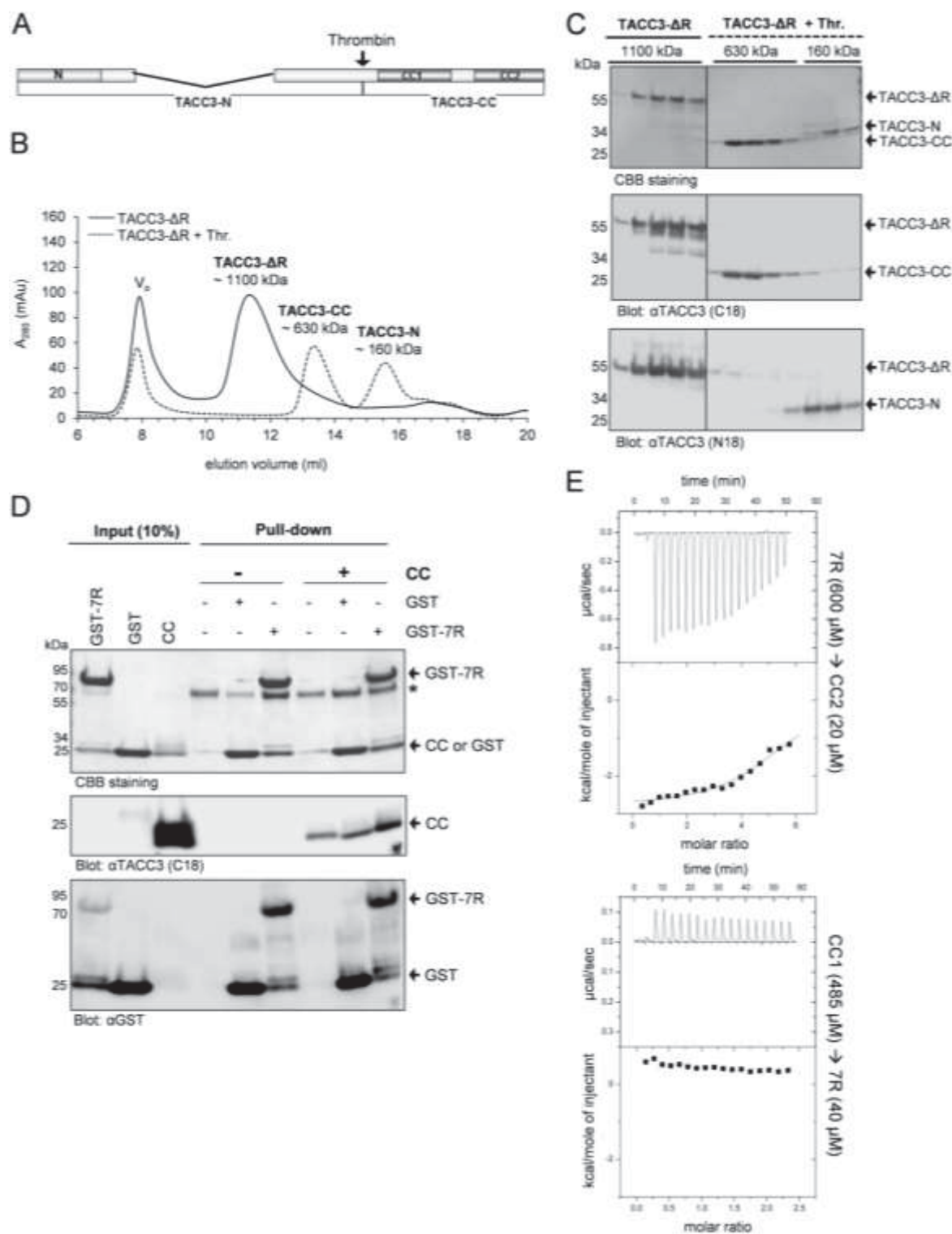
TACC3 (Fig. 4A). Interestingly, when analyzing the relative contribution of the two coiled-coil-containing subdomains of the TACC domain (*i.e.* CC1 and CC2; supplemental Fig. S3) to chTOG-Cterm binding in aSEC experiments, we observed a prominent peak shift of CC1 mixed with chTOG-Cterm that did not occur in the case of CC2 (Fig. 4, *B* and *C*). This selective CC1-chTOG-Cterm interaction was still observable in the presence of equimolar amounts of CC2, *i.e.* when mixing and analyzing all three fragments together (Fig. 4D). Of note, CC1 and CC2 did not interact with each other (supplemental Fig. S7). Subsequent ITC-based binding measurements revealed a strong association between CC1 and chTOG-Cterm with a K_d of 0.7 μM and a binding stoichiometry ($n = 0.83$) of nearly 1:1 (Fig. 4E). Consistent with the aSEC data, we did not detect any interaction between CC2 and chTOG-Cterm in ITC experiments (Fig. 4E). Importantly, we confirmed these findings also *in vivo* by expressing deletion mutants of TACC3 lacking either the TACC domain (CC) or one of its subdomains (*i.e.* CC1 or CC2) in HEK293 cells as C-terminally tagged GFP fusion proteins. Transfected cells were subjected to co-immunoprecipitation analysis using GFP-specific antibodies. As indicated in Fig. 5, deletion of CC1, but not of the CC2 subdomain, abrogated interaction with endogenous chTOG, strongly indicating that also under *in vivo* conditions the CC1 domain specifically determines binding of TACC3 to chTOG.

chTOG Binds to TACC3 via a C-terminal Region after the MT-interacting TOG Domains—Having localized CC1 as part in the TACC domain that binds to the C terminus of chTOG, we now narrowed down the TACC3 interacting part within the C terminus of chTOG. For this, we purified and analyzed two subdomains, chTOG-A (aa 1544–1805), which contains the putative, MT-interacting TOG6 domain (52), and chTOG-B

(aa 1806–2032) within the C terminus of chTOG (supplemental Fig. S5). As indicated in the pulldown-based interaction analysis in Fig. 6, chTOG-B, but not chTOG-A, efficiently bound to TACC3 or its isolated CC1 domain. Consistent with this, employing aSEC and subsequent peak fraction analysis on SDS-PAGE, we observed a clear complex formation for chTOG-B-CC1 but no interaction and peak shift when chTOG-A and CC1 were mixed together (supplemental Fig. 10, *A* and *B*). Thus, chTOG binds specifically via a C-terminal fragment adjacent to the putative MT-binding TOG6 domain to the CC1 domain of TACC3.

Interaction of chTOG with TACC3 Abrogates Intradomain Masking of TACC3—Based on the findings above, we next addressed the relation between the intradomain TACC3 interaction (mediated through 7R and CC2) and intermolecular CC1-chTOG-Cterm binding thereby analyzing the “directionality” of formation of these protein complexes. As indicated in Fig. 7A, GST-fused chTOG-Cterm was able to pull down full-length TACC3 or its C terminus (CC) produced upon thrombin cleavage of TACC3. However, in the latter case, the N-terminal part of TACC3 (TACC3-N7R) could not be detected in GST-chTOG-Cterm pulldown complexes by immunoblotting (Fig. 7A, *last lane*) strongly indicating that chTOG-Cterm binding uncouples the intramolecular TACC3 interaction. These findings were further validated by subjecting the TACC3-chTOG-Cterm protein complex before and after thrombin cleavage to aSEC. Fig. 7B shows that both TACC3 alone and TACC3 bound to chTOG-Cterm eluted on aSEC comparably at a peak fraction equivalent to an apparent molecular mass of ~1200 kDa. In contrast, when TACC3 was prebound to chTOG-Cterm and then subjected to thrombin cleavage, a shift of the TACC3 complex (TACC3-N7R-CC; apparent mass of ~630 kDa) toward an

Molecular Basis of TACC3-chTOG Complex Formation



Molecular Basis of TACC3-chTOG Complex Formation

earlier elution volume corresponding to an apparent mass of ~800 kDa was detected (Fig. 7C). SDS-PAGE analysis confirmed that this peak shift was due to the interaction of chTOG-Cterm with the TACC domain, once more indicating that the intramolecular interaction between 7R and CC2 is relieved upon chTOG-Cterm binding to CC1. We conclude that 7R-CC2 and CC1-chTOG-Cterm are consecutive and mutually exclusive interactions representing the two distinct masked and unmasked states of the C-terminal TACC domain of TACC3.

Aurora-A Kinase Does Not Interfere with TACC3-chTOG Complex Formation—Aurora-A kinase phosphorylates and targets TACC3 to centrosomes and proximal mitotic spindles as a prerequisite for TACC3-chTOG protein complex-dependent centrosomal MT assembly and dynamics (43–46). Sequence alignment and phosphorylation prediction revealed that murine TACC3 displays three putative Aurora-A phosphorylation sites (Ser-34, -341, and -347) that are localized in the N-terminal part outside of the CC domain (Fig. 1A) and are conserved in human TACC3 (Ser-34, -552, and -558) as well as *X. laevis* TACC3 (Ser-33, -620, and -626) (28). Our *in vitro* data presented above already indicated that Aurora-A-mediated phosphorylation of TACC3 is not required to expose the TACC domain for intermolecular protein interaction. However, the time point when Aurora-A phosphorylates TACC3, *i.e.* before or after chTOG binding, remained unclear. We, therefore, subjected (i) TACC3 before and after thrombin cleavage, (ii) TACC3- Δ R lacking the central repeat region required for intramolecular masking, and (iii) TACC3 prebound to chTOG-Cterm to *in vitro* kinase assays. As shown in Fig. 8, under all these conditions the N terminus of TACC3 outside of the TACC domain was efficiently phosphorylated by Aurora-A kinase. Thus, Aurora-A phosphorylates TACC3 independent from the masked or unmasked status of the TACC domain and does thereby not discriminate between the unbound or chTOG-bound state.

These *in vitro* findings were also tested *in vivo* by employing the Aurora-A kinase inhibitor MLN8237 in cell culture under conditions where Aurora-A kinase activity (as monitored by autophosphorylation at Thr-288) was abrogated (supplemental Fig. S8A). As indicated in supplemental Fig. 8, B–D, MLN8237-mediated inhibition of Aurora-A kinase impaired spindle formation and colocalization of TACC3 and chTOG to microtubules and spindle poles. However, centrosomal colocalization of TACC3 and chTOG was still detectable despite the occurrence of fragmented centrosomes. Consistent with this, employing co-immunoprecipitation analysis, interaction of TACC3 with chTOG was still detectable in MLN8237-treated cells (supplemental Fig. S9). Taken together, these findings emphasize that Aurora-A functions solely as a recruitment factor of the TACC3-chTOG complex to centrosomes and proximal

spindle microtubules (43–46) without affecting its formation and protein interaction.

DISCUSSION

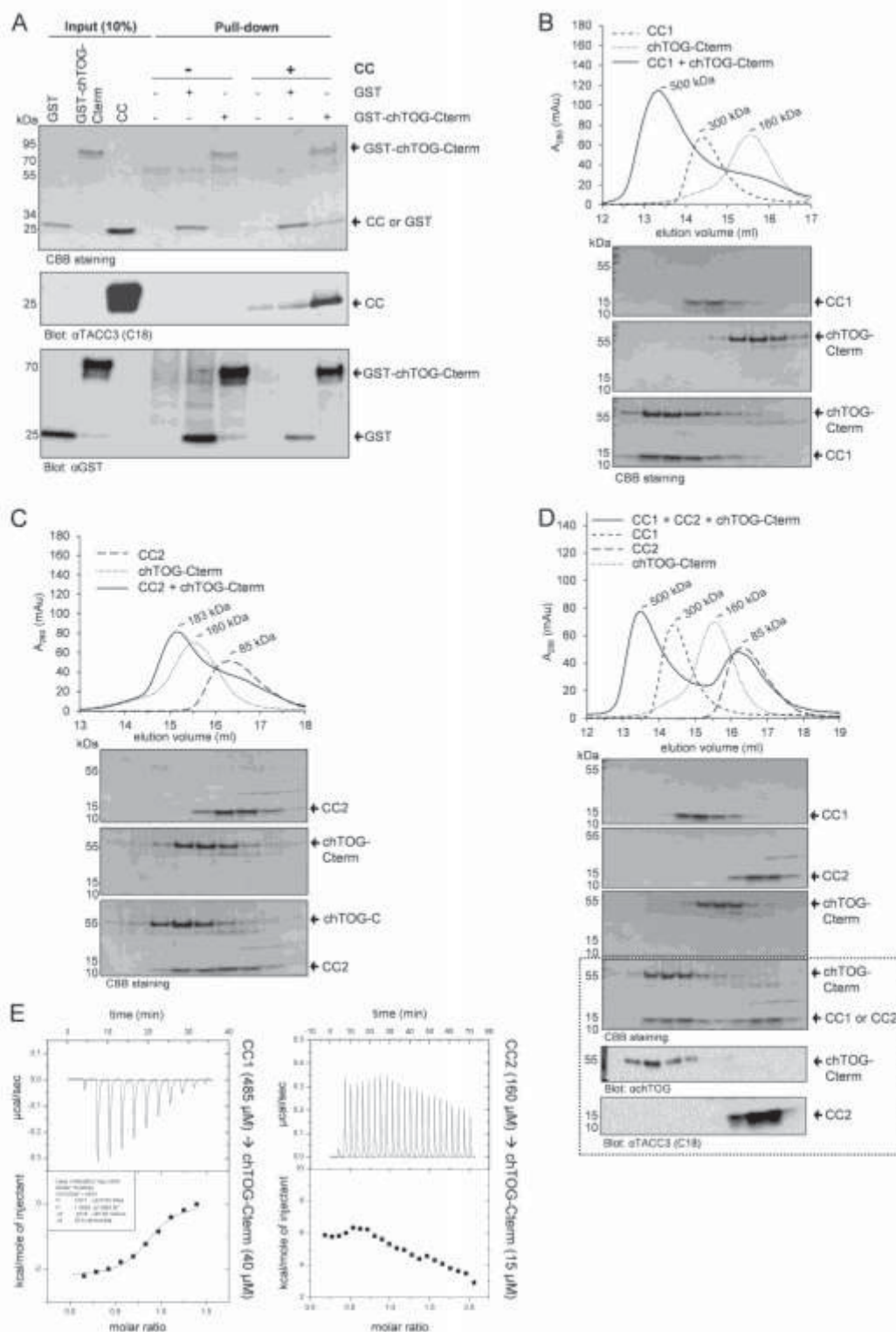
This study provides novel molecular insight into the basis of spindle MT stability and dynamics during mitosis by determining the interaction between the centrosomal adaptor protein TACC3 and the MT polymerase chTOG. The main findings of our work are as follows. 1) The C-terminal TACC domain of TACC3 consists of two functionally distinct modules, CC1 and CC2. 2) CC2 performs an intradomain interaction with the central repeat region (7R), a complex that masks intermolecular interaction of TACC3. 3) chTOG directly binds CC1 via a C-terminal fragment adjacent to N-terminal MT binding TOG domains. 4) Aurora-A kinase, a major regulator of TACC3, does not interfere with TACC3-chTOG complex formation either *in vitro* or *in vivo*. 5) Thus, Aurora-A solely acts as a centrosomal/proximal spindle recruitment factor for the TACC3-chTOG complex consistent with previous findings (43–46).

Our data argue against the possibility that the evolutionary conserved interaction between TACC3 and chTOG family members, as observed by several groups (31, 53, 58, 59, 67), requires the complete TACC domain. By analyzing the TACC3-chTOG protein complex, we define CC1 as an chTOG interacting domain. Moreover, we show that the deletion mutant TACC3- Δ CC1, in contrast to TACC3- Δ CC2, fails to co-immunoprecipitate/interact with chTOG *in vivo* (Fig. 5). Our findings are consistent with recent work of Hood *et al.* (52) that has analyzed the interaction of human TACC3 and chTOG isoforms using a deletion mapping approach. The authors narrowed down the corresponding human CC1 domain to a short region of 12 amino acids (aa 673–684) that appears to be sufficient for chTOG binding and chTOG localization on spindle MTs *in vivo* (52). Interestingly, centrosomal localization of chTOG was apparently reduced but still detectable, further indicating that chTOG may be recruited to centrosomes via both TACC3-dependent and -independent mechanisms.

As indicated in our model (Fig. 9), the mutually exclusive intradomain 7R-CC2 and interdomain CC1-chTOG interactions, respectively, provide novel functional insight into the subdomain selectivity and directionality of TACC3-chTOG complex formation. Our findings obtained by ITC analysis (Figs. 3E and 4E) are of particular relevance by providing clear insights into differential binding affinities for a strong chTOG-Cterm-CC1 interaction *versus* a weak 7R-CC2 interaction. Accordingly, we propose that chTOG binding to CC1 results in a conformational change of the CC2 subdomain, which is in turn released from its intramolecular complex with 7R and hence unmasks both CC2 and the central repeat region of

FIGURE 3. Deletion of the central repeat (7R) domain prevents intramolecular TACC3 complex formation. A, primary structure of TACC3- Δ R lacking the 7R domain. B, elution profile of TACC3- Δ R on analytical gel filtration (Superose 6, 10/300) before (solid line) and after (dashed line) thrombin cleavage. V_0 , void volume. C, peak elution fractions were analyzed on SDS-PAGE (4–15% gradient gel) followed by CBB staining (upper panel) and immunoblotting using the indicated antibodies (middle and lower panels). Thr., thrombin. D, the interaction between the isolated repeat region (7R) and the TACC domain (CC) was analyzed by pulldown assays and immunoblotting using N18 and C18 antibodies against TACC3. The asterisk indicates bovine albumin used to reduce unspecific binding to GSH-Sepharose beads. E, analysis of the interaction between 7R and subdomains of the TACC domain (CC1, CC2) employing ITC. Heat changes after association of the indicated protein fragments indicate that 7R selectively interacts with CC2 (upper panel) but not CC1 (lower panel). See supplemental Fig. S6 for experimental ITC controls.

Molecular Basis of TACC3-chTOG Complex Formation



Molecular Basis of TACC3-chTOG Complex Formation

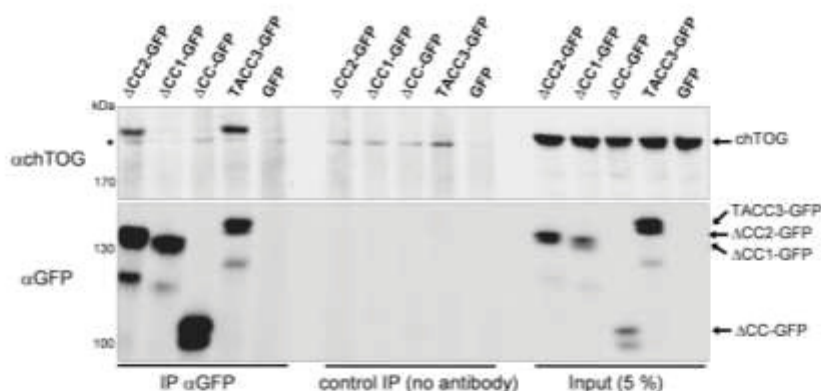


FIGURE 5. The CC1 subdomain is required for binding of TACC3 to chTOG *in vivo*. HEK293 cells were transfected with expression constructs for TACC3 or the indicated C-terminal deletion mutants all C-terminally fused to GFP. After 48 h, total cell lysates were prepared and subjected to co-immunoprecipitation analysis using a GFP-specific antibody followed by SDS-PAGE analysis and detection of chTOG in the immunoprecipitates. mAu, milliabsorbance units; IP, immunoprecipitation. The asterisk indicates an unspecific band.

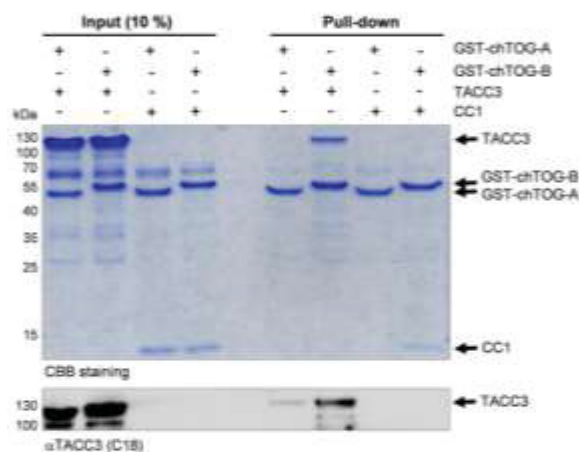


FIGURE 6. The C terminus of chTOG following the six TOG domains binds to the CC1 subdomain of TACC3. The interaction between the C terminus of chTOG (divided into the subfragments chTOG-A and chTOG-B; supplemental Fig. S5) with full-length TACC3 or its CC1 subdomain was analyzed by pull-down assays and subsequently detected by CBB staining and immunoblotting using antibodies against the C-terminal end of TACC3 (C18). chTOG-B, but not the TOG6 domain containing fragment chTOG-A (supplemental Fig. S5), displays a selective interaction with TACC3.

TACC3. As a consequence, not only CC2, but also 7R may become available for further interactions with other downstream binding partners. However, in the latter case, no protein is currently known that binds to the central repeat domain of TACC3 despite the presence of *bona fide* PXXP binding motifs known to interact with SH3 domain-containing proteins in intracellular signaling processes. This is different for the TACC domain that has been identified by yeast two hybrid-based

screening as well as pulldown and immunoprecipitation assays as major binding partner for various, functionally rather diverse proteins. These include factors involved in cortical neurogenesis (Cep192, DOCK7) (68, 69), hematopoietic development (FOG-1) (70), hypoxia response and gene expression (ARNT) (66), transcriptional regulation (MBD2) (71), and regulation of mTOR signaling (TSC2) (55). Interestingly, FOG-1 and ARNT have been proposed to bind to a region containing the last 20 residues of the CC2 subdomain (66, 72). Consistently, CC2 may be involved not only in intradomain but also in intermolecular protein interactions, whereas CC1 may only undergo intermolecular effector binding.

Aurora-A-mediated phosphorylation of TACC3 seems not to interfere with TACC3 intradomain and TACC3-chTOG interdomain interactions under *in vitro* conditions (Fig. 8). Accordingly, *in vivo*, TACC3-chTOG interaction and centrosomal colocalization was still detectable in HeLa cells that have been subjected to treatment with the Aurora-A kinase inhibitor MLN8237 (supplemental Figs. S8 and S9). These findings also contradict the previous model proposing that Aurora-A-mediated phosphorylation of *X. laevis* TACC3 triggers unmasking of the TACC domain and thereby exposes it for intermolecular interaction (*i.e.* XMAP215 binding) and centrosomal targeting (46, 59). In fact, Aurora-A-mediated phosphorylation of TACC3 seems to be solely required for targeting of the TACC3-chTOG complex to centrosomes and spindle MTs (28, 44). In the latter case, pTACC-chTOG interacts with another key effector in mitotic spindle assembly, the clathrin heavy chain, thereby cross-linking and stabilizing MT bundles (31, 51, 52).

Based on this study a sequential function of TACC3-chTOG effector complexes in the course of mitosis can be proposed.

FIGURE 4. The CC1 subdomain of TACC3 mediates chTOG binding. A, interaction between the C terminus of chTOG (chTOG-Cterm; aa 1574–2032; supplemental Fig. S6) and the CC domain of TACC3 was analyzed by pull-down assays and immunoblotting using antibodies against the C-terminal end of TACC3 (C18) and GST. B and C, binding of purified TACC subdomains (CC1 or CC2) to chTOG-Cterm was analyzed by aSEC (superpose 6, 10/300) followed by SDS-PAGE and CBB staining of the respective peak fractions. D, chTOG-Cterm interacts in a competition experiment selectively with CC1 when mixed with both CC1 and CC2 fragments. Samples were analyzed by aSEC followed by SDS-PAGE and CBB staining of the respective peak fractions. The dotted box indicates elution fractions from the analysis of the CC1 + CC2 + chTOG-Cterm mixture employing anti-chTOG and anti-TACC3 (C18 recognizing CC2, but not CC1) antibodies. E, analysis of binding of chTOG-Cterm to CC1 (left panel) and CC2 (right panel) using ITC confirms selective protein complex formation between chTOG-Cterm and CC1. See supplemental Fig. S6 for experimental ITC controls.

Molecular Basis of TACC3-chTOG Complex Formation

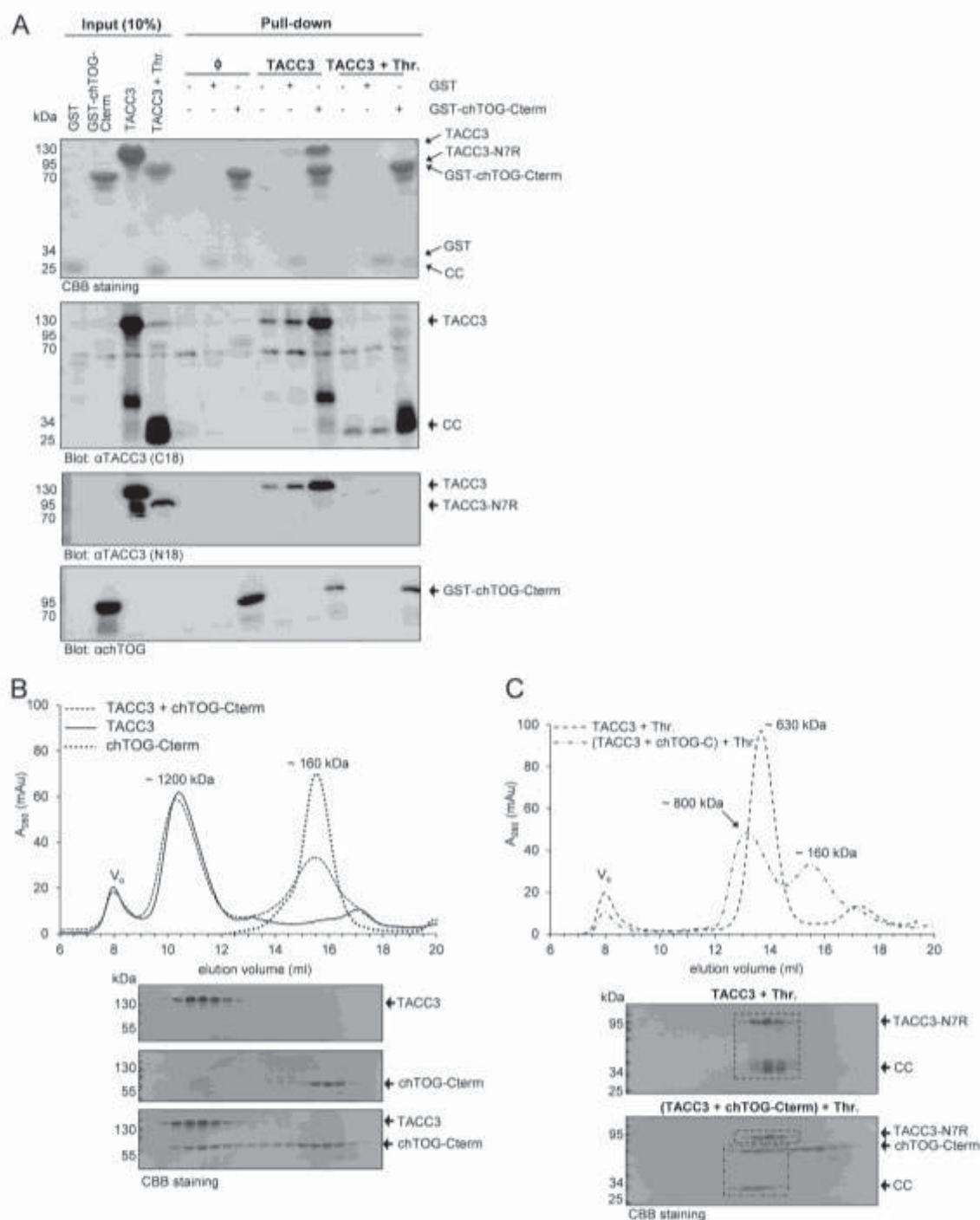


FIGURE 7. Binding of chTOG-Cterm to TACC3 disrupts the intradomain interaction of TACC3. *A*, the interaction between chTOG-Cterm and thrombin-cleaved TACC3 was analyzed by pulldown assays and immunoblotting using the indicated antibodies. Intradomain interaction of TACC3-N7R with CC is thereby abrogated upon chTOG-Cterm binding, as chTOG-Cterm pulls down CC but not TACC3-N7R (*last lane*). *B* and *C*, aSEC-based analysis of the TACC3-chTOG-Cterm complex was performed employing uncleaved TACC3 (*B*) or thrombin-cleaved TACC3 either alone or prebound to chTOG-Cterm (*C*). Peak fractions were analyzed by SDS-PAGE and CBB staining. The *dashed lines* within the CBB-stained SDS-PAGE gels highlight the peak shift of the chTOG-Cterm-CC complex (but not of TACC3-N7R) after thrombin cleavage. *mAu*, millabsorbance units.

Molecular Basis of TACC3-chTOG Complex Formation

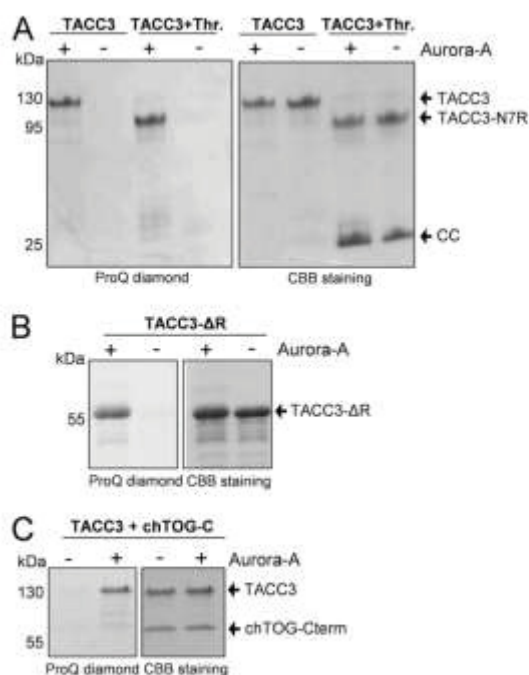


FIGURE 8. Aurora-A kinase phosphorylates murine TACC3 *in vitro* independent from its intra- or intermolecular binding status. Kinase assays were performed in the presence and absence of purified Aurora-A kinase employing uncleaved and thrombin-cleaved TACC3 (A), TACC3-ΔR (B), and the TACC3-chTOG-C-term complex (C). Phosphorylated protein fragments were visualized by ProQ diamond staining. Thr., thrombin.

TACC3 interacts with the C terminus of chTOG thereby targeting it in an Aurora-A-dependent manner to spindle poles. On the other hand, the evolutionary conserved N terminus of chTOG likely comprises MT-stabilizing activity as demonstrated for XMAP215. In particular, XMAP215/chTOG proteins contain a variable number of TOG domains that bind to $\alpha\beta$ -tubulin heterodimers, load them as MT polymerase (73) to the plus ends of MTs, and thereby inhibit "MT catastrophes." In contrast, the C-terminal part of XMAP215 (and likely also chTOG) suppresses MT growth by promoting MT catastrophes (74). Therefore, the engagement of chTOG-C-term by the CC1 subdomain of TACC3 during G₂/M transition and metaphase might be a vital step in shifting the equilibrium toward MT polymerization. Upon mitotic exit, Cdh1 and ubiquitin-dependent degradation of TACC3 (39) then "disengages" the MT catastrophe promoting activity of the C terminus of XMAP215/chTOG. As a consequence, a shift of the equilibrium occurs toward MT "shrinkage" and disassembly of the spindle apparatus. Thus, TACC3 family members may function as "engagement factors" for the C terminus of XMAP215/chTOG to ensure a dynamic balance between MT rescue and catastrophe during the course of mitosis.

Besides a better molecular understanding regarding the mechanism and directionality of TACC3-chTOG interaction, we furthermore obtained novel insight into the unusual biophysical properties of TACC3. Analysis by aSEC (e.g. Fig. 1) clearly demonstrated that TACC3 displays a higher oligomeric

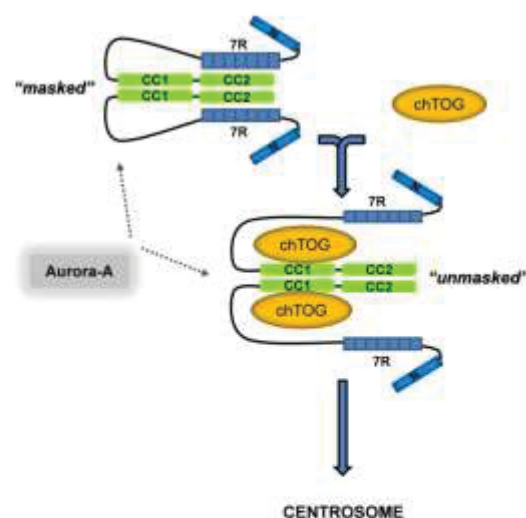


FIGURE 9. Integrative model for the domain specificity and directionality of TACC3-chTOG complex formation. We propose that the intradomain (7R-CC2; TACC3 masked) and intermolecular (CC1-chTOG; TACC3 unmasked) binding states of TACC3 are mutually exclusive, thereby defining a directionality of TACC3 regulated adaptor function toward chTOG binding and function. TACC3 can be phosphorylated by Aurora-A kinase in both binding states, indicating that Aurora-A acts as a centrosomal recruitment factor but is not involved in exposing the TACC domain for intermolecular interaction with chTOG or TACC3-chTOG complex formation. Moreover, based on biophysical characterization of murine TACC3 (supplemental Fig. 11, B and C, and supplemental Table S1; Ref. 34) we conclude that TACC3 displays an oligomeric to oligomeric state. Thr., thrombin.

mass and/or an elongated rod-like structure, obviously due to the presence of the coiled-coil containing TACC domain that elutes inherently at an apparent molecular mass of ~630 kDa (Fig. 3B). Moreover, endogenous TACC3 or FLAG-tagged TACC3 from transfected eukaryotic cells behaves on aSEC comparable to purified TACC3 (data not shown). These findings are in accordance with the observation that TACC isoforms overexpressed in HeLa cells form in a TACC domain-dependent manner punctuate-like structures resembling cytoplasmic polymers (data not shown) (27). Employing further analytical methods including multiangle light scattering and analytical ultracentrifugation allowed us to conclude that TACC3 is characterized by a oligomeric (*i.e.* dimeric to hexameric) structure and a highly extended shape (supplemental Fig. 11, B and C, and supplemental Table S1). These findings are consistent with data from electron microscopic analysis where TACC3 depicts an elongated, fiber-like appearance (34). Another abnormality of murine TACC3 represents its migration in SDS-PAGE gels at 120–130 kDa (Fig. 1C) as compared with its theoretical molecular mass of 70.5 kDa. Interestingly, this unusual "gel shifting" is not based on the presence of the coiled-coil containing TACC domain (data not shown) but is rather caused by the central repeat region (supplemental Fig. S4, B versus A). As proof, deletion of the 7R domain restored normal gel migration of TACC3 (Fig. 3C and supplemental Fig. S4B). Of note, abnormal SDS-PAGE migration of acidic proteins can be caused by an altered binding of surfactants (like SDS) (75), a possibility that remains to be clarified for TACC3 and in particular the 7R domain.

Molecular Basis of TACC3-chTOG Complex Formation

Biological and pathobiological roles of TACC3 are underlined by several observations. TACC3 deficiency leads to severe growth retardation and embryonic lethality (38, 40). This is in line with the anti-proliferative and cell cycle arrest/senescence-inducing impact of shRNA-mediated gene silencing of TACC3 (41, 42). Moreover, it could be shown that TACC3 depletion sensitizes cells to the apoptotic and senescence-inducing effects of mitotic spindle poisons. Accordingly, inducible gene disruption of TACC3 *in vivo* in the p53^{-/-} sarcomatous model is highly effective in causing apoptotic tumor regression (76). Interestingly, besides quantitative deregulation of gene expression of TACC isoforms in several tumor types, TACC1 and TACC3 point mutants have been identified in melanoma and ovarian cancer patients (77, 78). Moreover, oncogenic fusions between TACC and fibroblast growth factor receptor genes have been recently described in glioblastoma multiforme and bladder cancer patients (79, 80). The impact of these structural and tumor-associated alterations on Aurora-A-mediated regulation and function of TACCs is currently unknown and requires a more in-depth molecular understanding of TACC-effector interactions. Irrespective, it is tempting to speculate that these TACC mutants translate through loss-of-function or gain-of-function mechanisms into chromosomal instability and aneuploidy and thereby support cellular transformation (81, 82). Taken all these points into account, TACC3 represents an attractive antitumor target that may be at least indirectly drug-treatable at the level of its interactome. This assumption is supported by the recent identification of small drugs that act as inhibitors of protein-protein interaction and thereby impair the half-life and stability of TACC3 (KSH101), disrupt the TACC3-ARNT complex (KG-548), or inhibit the function of the TACC3-chTOG complex (spindlactone) (54, 66, 83, 84).

Acknowledgments—We thank Britta Tschapek for help in setting up the multiangle light scattering method and Jürgen Scheller and members of the Institute of Biochemistry and Molecular Biology II for input and fruitful comments during the course of this work and on the manuscript.

REFERENCES

- Bornens, M. (2012) The centrosome in cells and organisms. *Science* **335**, 422–426.
- Compton, D. A. (2000) Spindle assembly in animal cells. *Annu. Rev. Biochem.* **69**, 95–114.
- Delgeyr, N., Sillibourne, J., and Bornens, M. (2005) Microtubule nucleation and anchoring at the centrosome are independent processes linked by ninein function. *J. Cell Sci.* **118**, 1565–1575.
- Mattison, C., and Winey, M. (2006) *The Centrosome Cycle/Cell Cycle Regulation* (Kaldis, P., ed.) pp. 925–925. Springer, Berlin.
- Nigg, E. A. (2004) *Centrosomes in Development and Disease*. Wiley-VCH Verlag, Weinheim.
- Anderhub, S. J., Krämer, A., and Maier, B. (2012) Centrosome amplification in tumorigenesis. *Cancer Lett.* **322**, 8–17.
- Basto, R., Brunk, K., Vinadogova, T., Peel, N., Franz, A., Khodjakov, A., and Raff, J. W. (2008) Centrosome amplification can initiate tumorigenesis in flies. *Cell* **133**, 1032–1042.
- Bettencourt-Dias, M., Hildebrandt, F., Pellman, D., Woods, G., and Godinho, S. A. (2011) Centrosomes and cilia in human disease. *Trends Genet.* **27**, 307–315.
- Chan, J. Y. (2011) A clinical overview of centrosome amplification in human cancers. *Int. J. Biol. Sci.* **7**, 1122–1144.
- Mardin, B. R., and Schiebel, E. (2012) Breaking the ties that bind. new advances in centrosome biology. *J. Cell Biol.* **197**, 11–18.
- Schmidt, S., Esumann, F., Cirstea, I. C., Kuck, F., Thakur, H. C., Singh, M., Kletke, A., Janicke, R. U., Wiek, C., Hanenberg, H., Ahmadian, M. R., Schulze-Osthoff, K., Nürnberg, B., and Piekorz, R. P. (2010) The centrosome and mitotic spindle apparatus in cancer and senescence. *Cell Cycle* **9**, 4469–4473.
- Zyss, D., and Gergely, F. (2009) Centrosome function in cancer. Guilty or innocent? *Trends Cell Biol.* **19**, 334–346.
- Fielding, A. B., Lim, S., Montgomery, K., Dobrev, I., and Dedhar, S. (2011) A critical role of integrin-linked kinase, ch-TOG, and TACC3 in centrosome clustering in cancer cells. *Oncogene* **30**, 521–534.
- Kwon, M., Godinho, S. A., Chandhok, N. S., Ganem, N. J., Azoune, A., Thery, M., and Pellman, D. (2008) Mechanisms to suppress multipolar divisions in cancer cells with extra centrosomes. *Genes Dev.* **22**, 2189–2203.
- Marthiens, V., Piel, M., and Basto, R. (2012) Never tear us apart. The importance of centrosome clustering. *J. Cell Sci.* **125**, 3281–3292.
- Krämer, A., Maier, B., and Bartek, J. (2011) Centrosome clustering and chromosomal (in)stability. A matter of life and death. *Mol. Oncol.* **5**, 324–335.
- Raub, M. S., Breitkreutz, I., Anderhub, S., Rønne, M. H., Leber, B., Larsen, T. O., Weiz, L., Konotop, G., Hayden, P. J., Podar, K., Fraehauf, J., Nissen, F., Mier, W., Haberkorn, U., Ho, A. D., Goldschmidt, H., Anderson, K. C., Clausen, M. H., and Krämer, A. (2012) GF-15, a novel inhibitor of centrosome clustering, suppresses tumor cell growth *in vitro* and *in vivo*. *Cancer Res.* **72**, 5374–5385.
- Meraldi, P., and Nigg, E. A. (2002) The centrosome cycle. *FEBS Lett.* **521**, 9–13.
- Nigg, E. A., and Stearns, T. (2011) The centrosome cycle. Centriole biogenesis, duplication, and inherent asymmetries. *Nat. Cell Biol.* **13**, 1154–1160.
- Cunha-Ferreira, I., Bento, I., and Bettencourt-Dias, M. (2009) From zero to many. Control of centriole number in development and disease. *Traffic* **10**, 482–498.
- Andersen, J. S., Wilkinson, C. J., Mayor, T., Mortensen, P., Nigg, E. A., and Mann, M. (2003) Proteomic characterization of the human centrosome by protein correlation profiling. *Nature* **426**, 570–574.
- Jakobsen, L., Vanselow, K., Skogs, M., Toyoda, Y., Linnberg, E., Poser, I., Falkenby, L. G., Benneisen, M., Westendorp, J., Nigg, E. A., Uhlen, M., Hyman, A. A., and Andersen, J. S. (2011) Novel asymmetrically localizing components of human centrosomes identified by complementary proteomics methods. *EMBO J.* **30**, 1520–1535.
- Müller, H., Schmidt, D., Steinbrink, S., Mirgorodskaya, E., Lehmann, V., Habermann, K., Dreher, F., Gustavsson, N., Kessler, T., Lebrach, H., Herwig, R., Gebom, J., Ploubidou, A., Boutros, M., and Lange, B. M. (2010) Proteomic and functional analysis of the mitotic *Drosophila* centrosome. *EMBO J.* **29**, 3344–3357.
- Doxsey, S., McCullum, D., and Theurkauf, W. (2005) Centrosomes in cellular regulation. *Annu. Rev. Cell Dev. Biol.* **21**, 411–434.
- Hutchins, J. R., Toyoda, Y., Hegemann, B., Poser, I., Hériché, J. K., Sykora, M. M., Augsburg, M., Hudcz, O., Buschhorn, B. A., Bulkescher, J., Conrad, C., Comartin, D., Schleifler, A., Sarov, M., Pozniakovskiy, A., Slabicki, M. M., Schloissnig, S., Steinmacher, I., Leschner, M., Szykora, A., Lawo, S., Pelletier, L., Stark, H., Nasmyth, K., Ellenberg, J., Durbin, R., Buchholz, F., Mechtler, K., Hyman, A. A., and Peters, J. M. (2010) Systematic analysis of human protein complexes identifies chromosome segregation proteins. *Science* **328**, 593–599.
- Neumann, B., Walter, T., Hériché, J. K., Bulkescher, J., Erle, H., Conrad, C., Rogers, P., Poser, I., Held, M., Liebel, U., Cetin, C., Sieckmann, F., Pau, G., Kahbe, R., Wünsche, A., Satagopam, V., Schmitz, M. H., Chapuis, C., Gerlich, D. W., Schneider, R., Eils, R., Huber, W., Peters, J. M., Hyman, A. A., Durbin, R., Pepperkok, R., and Ellenberg, J. (2010) Phenotypic profiling of the human genome by time-lapse microscopy reveals cell division genes. *Nature* **464**, 721–727.
- Gergely, F., Karlsson, C., Still, L., Cowell, J., Kilmartin, J., and Raff, J. W. (2000) The TACC domain identifies a family of centrosomal proteins that

Molecular Basis of TACC3-chTOG Complex Formation

- can interact with microtubules. *Proc. Natl. Acad. Sci. U.S.A.* **97**, 14352–14357
28. Peset, L., and Vernos, I. (2008) The TACC proteins. TACC-ling microtubule dynamics and centrosome function. *Trends Cell Biol.* **18**, 379–388
 29. Raff, J. W. (2002) Centrosomes and cancer. Lessons from a TACC. *Trends Cell Biol.* **12**, 222–225
 30. Gergely, F. (2002) Centrosomal TACCtics. *Biosessays* **24**, 915–925
 31. Hood, F. E., and Royle, S. J. (2011) Pulling it together. The mitotic function of TACC3. *Bioarchitecture* **1**, 105–109
 32. Schneider, L., Essmann, F., Kletke, A., Rio, P., Hanenberg, H., Wetzel, W., Schulze-Osthoff, K., Nürnberg, B., and Piekorz, R. P. (2007) The transforming acidic coiled coil 3 protein is essential for spindle-dependent chromosome alignment and mitotic survival. *J. Biol. Chem.* **282**, 29273–29283
 33. Still, I. H., Vettaikorumakankav, A. K., DiMatteo, A., and Liang, P. (2004) Structure-function evolution of the transforming acidic coiled coil genes revealed by analysis of phylogenetically diverse organisms. *BMC Evol. Biol.* **4**, 16
 34. Thakur, H. C., Singh, M., Nagel-Steger, L., Prumbaum, D., Fansa, E. K., Gremer, L., Ezzahoui, H., Abts, A., Schmitt, L., Raunser, S., Ahmadian, M. R., and Piekorz, R. P. (2013) Role of centrosomal adaptor proteins of the TACC family in the regulation of microtubule dynamics during mitotic cell division. *Biol. Chem.* **394**, 1411–1423
 35. Hao, Z., Stoler, M. H., Sen, B., Shore, A., Westbrook, A., Flickinger, C. J., Herr, J. C., and Coonrod, S. A. (2002) TACC3 expression and localization in the murine egg and ovary. *Mol. Reprod. Dev.* **63**, 291–299
 36. Sadek, C. M., Pelto-Huikko, M., Tujague, M., Steffensen, K. R., Wennerholm, M., and Gustafsson, J. A. (2003) TACC3 expression is tightly regulated during early differentiation. *Gene Expr. Patterns* **3**, 203–211
 37. Schuendeln, M. M., Piekorz, R. P., Wichmann, C., Lee, Y., McKinnon, P. J., Boyd, K., Takahashi, Y., and Ihle, J. N. (2004) The centrosomal, putative tumor suppressor protein TACC2 is dispensable for normal development, and deficiency does not lead to cancer. *Mol. Cell. Biol.* **24**, 6403–6409
 38. Piekorz, R. P., Hoffmeyer, A., Duntsch, C. D., McKay, C., Nakajima, H., Sexl, V., Snyder, L., Reh, J., and Ihle, J. N. (2002) The centrosomal protein TACC3 is essential for hematopoietic stem cell function and genetically interfaces with p53-regulated apoptosis. *EMBO J.* **21**, 653–664
 39. Jeng, J. C., Lin, Y. M., Lin, C. H., and Shih, H. M. (2009) Cdh1 controls the stability of TACC3. *Cell Cycle* **8**, 3529–3536
 40. Yao, R., Natsume, Y., and Noda, T. (2007) TACC3 is required for the proper mitosis of sclerotome mesenchymal cells during formation of the axial skeleton. *Cancer Sci.* **98**, 555–562
 41. Schmidt, S., Schneider, L., Essmann, F., Cirstea, I. C., Kuck, F., Kletke, A., Jänicke, R. U., Wiek, C., Hanenberg, H., Ahmadian, M. R., Schulze-Osthoff, K., Nürnberg, B., and Piekorz, R. P. (2010) The centrosomal protein TACC3 controls paclitaxel sensitivity by modulating a premature senescence program. *Oncogene* **29**, 6184–6192
 42. Schneider, L., Essmann, F., Kletke, A., Rio, P., Hanenberg, H., Schulze-Osthoff, K., Nürnberg, B., and Piekorz, R. P. (2008) TACC3 depletion sensitizes to paclitaxel-induced cell death and overrides p21WAF-mediated cell cycle arrest. *Oncogene* **27**, 116–125
 43. Barros, T. P., Kinoshita, K., Hyman, A. A., and Raff, J. W. (2005) Aurora A activates D-TACC-Msps complexes exclusively at centrosomes to stabilize centrosomal microtubules. *J. Cell Biol.* **170**, 1039–1046
 44. Kinoshita, K., Noetzel, T. L., Pelletier, L., Mechtler, K., Drechsel, D. N., Schwager, A., Lee, M., Raff, J. W., and Hyman, A. A. (2005) Aurora A phosphorylation of TACC3/maskin is required for centrosome-dependent microtubule assembly in mitosis. *J. Cell Biol.* **170**, 1047–1055
 45. LeRoy, P. J., Hunter, J. J., Hoar, K. M., Burke, K. E., Shinde, V., Ruan, J., Bowman, D., Galvin, K., and Ecsedy, J. A. (2007) Localization of human TACC3 to mitotic spindles is mediated by phosphorylation on Ser-558 by Aurora A. A novel pharmacodynamic method for measuring Aurora A activity. *Cancer Res.* **67**, 5362–5370
 46. Peset, I., Seiler, J., Sardon, T., Bejarano, I. A., Rybina, S., and Vernos, I. (2005) Function and regulation of Maskin, a TACC family protein, in microtubule growth during mitosis. *J. Cell Biol.* **170**, 1057–1066
 47. Fu, W., Chen, H., Wang, G., Luo, J., Deng, Z., Xin, G., Xu, N., Guo, X., Lei, J., Jiang, Q., and Zhang, C. (2013) Self-assembly and sorting of acentrosomal microtubules by TACC3 facilitate kinetochore capture during the mitotic spindle assembly. *Proc. Natl. Acad. Sci. U.S.A.* **110**, 15295–15300
 48. Lioutas, A., and Vernos, I. (2013) Aurora A kinase and its substrate TACC3 are required for central spindle assembly. *EMBO Rep.* **14**, 829–836
 49. Fu, W., Jiang, Q., and Zhang, C. (2011) Novel functions of endocytic player clathrin in mitosis. *Cell Res.* **21**, 1655–1661
 50. Royle, S. J. (2012) The role of clathrin in mitotic spindle organisation. *J. Cell Sci.* **125**, 19–28
 51. Booth, D. G., Hood, F. E., Prior, I. A., and Royle, S. J. (2011) A TACC3/chTOG/clathrin complex stabilises kinetochore fibres by inter-microtubule bridging. *EMBO J.* **30**, 906–919
 52. Hood, F. E., Williams, S. J., Burgess, S. G., Richards, M. W., Roth, D., Straube, A., Pfuhl, M., Bayliss, R., and Royle, S. J. (2013) Coordination of adjacent domains mediates TACC3-chTOG-clathrin assembly and mitotic spindle binding. *J. Cell Biol.* **202**, 463–478
 53. Gergely, F., Draviam, V. M., and Raff, J. W. (2003) The chTOG/XMAP215 protein is essential for spindle pole organization in human somatic cells. *Genes Dev.* **17**, 336–341
 54. Yao, R., Kondoh, Y., Natsume, Y., Yamanaka, H., Inoue, M., Toki, H., Takagi, R., Shimizu, T., Yamori, T., Osada, H., and Noda, T. (2013) A small compound targeting TACC3 revealed its different spatiotemporal contributions for spindle assembly in cancer cells. *Oncogene* DOI:10.1038/onc.2013.382
 55. Gómez-Baldó, L., Schmidt, S., Maxwell, C. A., Bonifaci, N., Gabaldón, T., Vidalain, P. O., Senapedis, W., Kletke, A., Rosing, M., Barnekow, A., Rotapel, R., Capellá, G., Vidal, M., Astrinidis, A., Piekorz, R. P., and Pujana, M. A. (2010) TACC3-TSC2 maintains nuclear envelope structure and controls cell division. *Cell Cycle* **9**, 1143–1155
 56. Lauffart, B., Howell, S. J., Tasch, J. E., Cowell, J. K., and Still, I. H. (2002) Interaction of the transforming acidic coiled-coil 1 (TACC1) protein with chTOG and GAS41/NuB1 suggests multiple TACC1-containing protein complexes in human cells. *Biochem. J.* **363**, 195–200
 57. Sato, M., Vardy, L., Angel Garcia, M., Koonrugsa, N., and Toda, T. (2004) Interdependency of fission yeast Alp14/TOG and coiled coil protein Alp7 in microtubule localization and bipolar spindle formation. *Mol. Biol. Cell* **15**, 1609–1622
 58. Albee, A. J., Tao, W., and Wiese, C. (2006) Phosphorylation of maskin by Aurora-A is regulated by RanGTP and importin β . *J. Biol. Chem.* **281**, 38293–38301
 59. Albee, A. J., and Wiese, C. (2008) Xenopus TACC3/maskin is not required for microtubule stability but is required for anchoring microtubules at the centrosome. *Mol. Biol. Cell* **19**, 3347–3356
 60. Thompson, J. D., Higgins, D. G., and Gibson, T. J. (1994) ClustalW. Improving the sensitivity of progressive multiple sequence alignment through sequence weighting, position-specific gap penalties and weight matrix choice. *Nucleic Acids Res.* **22**, 4673–4680
 61. Lupas, A., Van Dyke, M., and Stock, J. (1991) Predicting coiled coils from protein sequences. *Science* **252**, 1162–1164
 62. Thakur, H. C. (2012) *Biochemical and biophysical characterization of the centrosomal protein TACC3*. Doctoral dissertation, Faculty of Mathematics and Natural Sciences of the Heinrich Heine University, Düsseldorf, Germany
 63. Eberth, A., Lundmark, R., Gremer, L., Dvorsky, R., Koessmeier, K. T., McMahon, H. T., and Ahmadian, M. R. (2009) A BAR domain-mediated autoinhibitory mechanism for RhoGAPs of the GRAF family. *Biochem. J.* **417**, 371–377
 64. Risse, S. L., Vaz, B., Burton, M. F., Aspenström, P., Piekorz, R. P., Brunsfeld, L., and Ahmadian, M. R. (2013) SH3-mediated targeting of Wrch1/RhoU by multiple adaptor proteins. *Biol. Chem.* **394**, 421–432
 65. Sardon, T., Pache, R. A., Stein, A., Molina, H., Vernos, I., and Aloy, P. (2010) Uncovering new substrates for Aurora A kinase. *EMBO Rep.* **11**, 977–984
 66. Partch, C. L., and Gardner, K. H. (2011) Coactivators necessary for transcriptional output of the hypoxia inducible factor, HIF, are directly recruited by ARNT PAS-B. *Proc. Natl. Acad. Sci. U.S.A.* **108**, 7739–7744
 67. Cassimeris, L., and Morabito, J. (2004) TOGP, the human homolog of XMAP215/Dis1, is required for centrosome integrity, spindle pole orga-

Molecular Basis of TACC3-chTOG Complex Formation

- nization, and bipolar spindle assembly. *Mol. Biol. Cell* **15**, 1580–1590
68. Xie, Z., Moy, L. Y., Sanada, K., Zhou, Y., Buchman, J. J., and Tsai, L.-H. (2007) Cep120 and TACCs control interkinetic nuclear migration and the neural progenitor pool. *Neuron* **56**, 79–93
 69. Yang, Y. T., Wang, C. L., and Van Aelst, L. (2012) DOCK7 interacts with TACC3 to regulate interkinetic nuclear migration and cortical neurogenesis. *Nat. Neurosci.* **15**, 1201–1210
 70. Garriga-Canut, M., and Orkin, S. H. (2004) Transforming acidic coiled-coil protein 3 (TACC3) controls friend of GATA-1 (FOG-1) subcellular localization and regulates the association between GATA-1 and FOG-1 during hematopoiesis. *J. Biol. Chem.* **279**, 23597–23605
 71. Angrisano, T., Lembo, F., Pero, R., Natale, F., Fusco, A., Avvedimento, V. E., Bruni, C. B., and Chiariotti, L. (2006) TACC3 mediates the association of MBD2 with histone acetyltransferases and relieves transcriptional repression of methylated promoters. *Nucleic Acids Res.* **34**, 364–372
 72. Simpson, R. J., Yi Lee, S. H., Bartle, N., Sum, E. Y., Visvader, J. E., Matthews, J. M., Mackay, J. P., and Crossley, M. (2004) A classic zinc finger from friend of GATA mediates an interaction with the coiled-coil of transforming acidic coiled-coil 3. *J. Biol. Chem.* **279**, 39789–39797
 73. Brouhard, G. J., Stear, J. H., Noetzel, T. L., Al-Bassam, J., Kinoshita, K., Harrison, S. C., Howard, J., and Hyman, A. A. (2008) XMAP215 is a processive microtubule polymerase. *Cell* **132**, 79–88
 74. Popov, A. V., Pozniakovskiy, A., Arnal, I., Antony, C., Ashford, A. J., Kinoshita, K., Tournebise, R., Hyman, A. A., and Karsenti, E. (2001) XMAP215 regulates microtubule dynamics through two distinct domains. *EMBO J.* **20**, 397–410
 75. Shi, Y., Mowery, R. A., Ashley, J., Hentz, M., Ramirez, A. J., Bilgicer, B., Slunt-Brown, H., Borchelt, D. R., and Shaw, B. F. (2012) Abnormal SDS-PAGE migration of cytosolic proteins can identify domains and mechanisms that control surfactant binding. *Protein Sci.* **21**, 1197–1209
 76. Yao, R., Natsume, Y., Saiki, Y., Shioya, H., Takeuchi, K., Yamori, T., Toki, H., Aoki, I., Saga, T., and Noda, T. (2012) Disruption of Tacc3 function leads to *in vivo* tumor regression. *Oncogene* **31**, 135–148
 77. Hodis, E., Watson, I. R., Kryukov, G. V., Arold, S. T., Imielinski, M., Theurillat, J. P., Nickerson, E., Auclair, D., Li, L., Place, C., Dicara, D., Ramos, A. H., Lawrence, M. S., Cibulskis, K., Sivachenko, A., Voet, D., Saksena, G., Stransky, N., Onofrio, R. C., Winckler, W., Ardlie, K., Wagle, N., Wargo, J., Chong, K., Morton, D. L., Stenke-Hale, K., Chen, G., Noble, M., Meyerson, M., Ladbury, J. E., Davies, M. A., Gershenwald, J. E., Wagner, S. N., Hoon, D. S., Schadendorf, D., Lander, E. S., Gabriel, S. B., Getz, G., Garraway, L. A., and Chin, L. (2012) A landscape of driver mutations in melanoma. *Cell* **150**, 251–263
 78. Lauffart, B., Vaughan, M. M., Eddy, R., Chervinsky, D., DiCiuccio, R. A., Black, J. D., and Still, I. H. (2005) Aberrations of TACC1 and TACC3 are associated with ovarian cancer. *BMC Women's Health* **5**, 8
 79. Singh, D., Chan, J. M., Zoppoli, P., Niola, F., Sullivan, R., Castano, A., Liu, E. M., Reichel, I., Porrati, P., Pellegatta, S., Qiu, K., Gao, Z., Ceccarelli, M., Riccardi, R., Brat, D. J., Guha, A., Aldape, K., Golfinos, J. G., Zagzag, D., Mikkelsen, T., Finocchiaro, G., Lasorella, A., Rabadan, R., and Iavarone, A. (2012) Transforming fusions of FGFR and TACC genes in human glioblastoma. *Science* **337**, 1231–1235
 80. Williams, S. V., Hurst, C. D., and Knowles, M. A. (2013) Oncogenic FGFR3 gene fusions in bladder cancer. *Hum. Mol. Genet.* **22**, 795–803
 81. Vitre, B. D., and Cleveland, D. W. (2012) Centrosomes, chromosome instability (CIN) and aneuploidy. *Curr. Opin. Cell Biol.* **24**, 809–815
 82. Holland, A. J., and Cleveland, D. W. (2012) Losing balance. The origin and impact of aneuploidy in cancer. *EMBO Rep.* **13**, 501–514
 83. Guo, Y., Partch, C. L., Key, J., Card, P. B., Pashkov, V., Patel, A., Bruick, R. K., Wurdak, H., and Gardner, K. H. (2013) Regulating the ARNT/TACC3 axis. Multiple approaches to manipulating protein/protein interactions with small molecules. *ACS Chem. Biol.* **8**, 626–635
 84. Wurdak, H., Zhu, S., Min, K. H., Aimone, L., Lairson, L. L., Watson, J., Chópluk, G., Demas, J., Charette, B., Halder, R., Weerapana, E., Cravatt, B. F., Cline, H. T., Peters, E. C., Zhang, J., Walker, J. R., Wu, C., Chang, J., Tuntland, T., Cho, C. Y., and Schultz, P. G. (2010) A small molecule accelerates neuronal differentiation in the adult rat. *Proc. Natl. Acad. Sci. U.S.A.* **107**, 16542–16547

SUPPLEMENTARY EXPERIMENTAL PROCEDURES

Multiangle Light Scattering (MALS) – Light scattering measurement of purified TACC3 (before and after thrombin cleavage) was performed on a MALS instrument (miniDAWN™ TREOS) under asymmetric Flow-Field-Flow-Fractionation conditions (Eclipse™ AF4, Wyatt Technology). Protein separation by size was achieved within a very thin flow against a perpendicular force field. For exact protein mass calculation, UV absorptions at 280 nm (Agilent Infinity 1260) and refractive index signals (OptilabRex, Wyatt Technology) were collected. In particular, AF4 membranes were equilibrated with standard buffer followed by injection of 50 µl of protein sample (3.86 mg/ml). Movement of the protein sample on the AF4 membrane was monitored and degree of scattered light and UV absorption ($A_{280\text{nm}}$) were measured. Raw data were analyzed and processed using ASTRA software (Wyatt Technology) to calculate molecular mass averages and polydispersity indexes of analyzed protein samples.

CD (circular dichroism) spectroscopy – CD spectroscopic measurements were performed on a J715 spectropolarimeter (JASCO) in 50 mM sodium phosphate buffer (1.09% Na_2HPO_4 and 0.13% NaH_2PO_4 , pH 7.5; 150 mM NaCl; 1 mM EDTA). Protein samples were subjected to buffer exchange through gel filtration. The CD spectrum was measured in the wavelength range of 190 nm to 260 nm with a data pitch of 0.2 nm with ten accumulations per reading. The spectrum was recorded and converted into molar ellipticity using the following formula: Molar ellipticity $[\theta]$ in $\text{deg}\cdot\text{cm}^2/\text{dmol} = [\Delta\epsilon \text{ (in mdeg)} \times \text{mean residue weight}] / [\text{pathlength (in mm)} \times \text{concentration (mg/ml)}]$. Final data processing was carried out with help of the K2D3 CD spectra analysis program by selecting 41 data points from 200 nm to 240 nm at a data pitch interval of 1 nm.

Analytical ultracentrifugation sedimentation velocity centrifugation (AUC-SV) – AUC-SV was performed using an Optima XL-A analytical ultracentrifuge (Beckman Coulter) with a 4-hole titanium rotor (AnTi-60; Beckman). For SV experiments, cells with a standard aluminum two-channel centerpiece and quartz windows were used. Samples were prepared by gel filtration using standard buffer and concentrated up to 20 µM. The rotor temperature was equilibrated at 10°C in the vacuum chamber. After loading the sample (400 µl) as well as reference buffer (420 µl), radial scans at 280 nm with 20 µm radial resolution were recorded at 3 to 5 min intervals during sedimentation at 37,000 rpm. Partial specific volume of the protein, solvent density, and solvent viscosity were calculated from standard tables using the UltraScan II program (Version 14.3). The collected radial scans were analyzed using the continuous distribution $c(s)$ analysis module in the SEDFIT program (Version 12.1) as well as two-dimensional spectral analysis combined with genetic algorithm (GA) and final Monte Carlo statistics as implemented in UltraScan II. SEDFIT data evaluation was performed as follows: Sedimentation coefficient increments of 0.1 S were used in the appropriate range for each sample. The frictional coefficient was allowed to float during the fitting. The weight average sedimentation coefficient was obtained by integrating the range of sedimentation coefficients in which peaks were present. The $c(s)$ distribution was converted to a $c(s_{20,w})$ distribution using the SEDFIT program. Additional data were evaluated with the UltraScan II software, which in contrast to $c(s)$ in SEDFIT provides each detected species with an individual shape factor, i.e. frictional ratio. After a primary data

evaluation by 2DSA the time invariant noise was subtracted. These noise corrected data were fitted according to a model of non-interacting species with a parsimoniously regulated genetic algorithm to find the sum of solutions of the Lamm equation with the lowest number of individual species that describes the measured data best.

SUPPLEMENTARY TABLES AND FIGURE LEGENDS

TABLE S1. Statistics from analytical ultracentrifugation sedimentation velocity experiments to determine biophysical parameters including the molecular weight of purified murine TACC3 before and after thrombin cleavage. The data revealed the presence of one major species for TACC3 (species 1) and two major species (species 1 and 2) for thrombin cleaved TACC3. The full length protein showed a nearly dimeric molecular mass (1.56 times of the monomeric mass of 70 kDa), sediment faster [$S_{10,w}(S)=3.12$], and displayed a highly extended shape ($f/f_0=2.55$). Upon thrombin cleavage of TACC3, two major species appeared: species 1 (62.3%) displayed a molecular mass of 52.55 kDa and a relatively high sedimentation rate [$S_{10,w}(S)=2.20$] as well as a highly extended shape; species 2 (29.3 %) had a molecular mass of 61.92 kDa, a relatively slow sedimentation rate [$S_{10,w}(S)=1.28$], and a very extended and open conformation ($f/f_0=4.26$). Values in small brackets indicate the results from two independent experiments.

FIGURE S1. *In silico* prediction of coiled-coil subdomains reveals “break regions” within the CC domain of higher vertebrate TACC3 isoforms. The very C-terminal region of TACC family members consisting of 250 residues was subjected to coiled-coil structure prediction using the COILS2 software in scanning modes of 14, 21, and 28 residues (green, blue, and red lines, respectively). *A*, comparison of the TACC domain of TACC3 isoforms from *Takifugu rubripes* (*Tr*-TACC3), *Xenopus laevis* (*Xl*-TACC3/Maskin), *Bos taurus* (*Bt*-TACC3), and *Oryctolagus cuniculus* (*Oc*-TACC3). *B*, comparison of the TACC domain of murine (*Mm*) and human (*Hs*) TACC proteins. Red arrows indicate “break regions” which are typical for TACC3 isoforms and separate the TACC domain into two coiled-coil-containing parts, CC1 and CC2.

FIGURE S2. Multiple sequence alignment of the C-terminal CC domain of vertebrate TACC family members. The arrow indicates the conserved glycine residue used to separate and clone the TACC subdomains CC1 (aa 414-530) and CC2 (aa 530-630) of murine TACC3. The red box indicates the “coiled coil structure breaking region” separating the CC1 and CC2 regions of the TACC domain from each other. Evolutionary, CC1 displays a lower degree of sequence homology when compared to CC2.

FIGURE S3. Domain organization of murine TACC3 deletion variants and fragments analyzed in this study. N specifies the conserved ~100 amino acid residues from the N-terminus of all vertebrate TACC3 isoforms. r1 to r7 denotes the central region in TACC3 consisting of seven serin-proline-rich repeats. CC1 and CC2 indicate two coiled-coil regions in the C-terminus separated by a break region. The internal thrombin cleavage site close to the CC-domain is indicated.

FIGURE S4. Murine TACC3 deletion variants and fragments overexpressed and purified in this study. *A* to *E*, purified proteins as listed in Fig. S3 were analyzed on Coomassie Brilliant Blue stained SDS-PAGE gels. Molecular weights: TACC3, 70.5 kDa; TACC3- Δ R, 52.3 kDa; TACC3- Δ N, 57.2 kDa; TACC3- Δ N Δ R, 39.1 kDa; 7R, 22.0 kDa; CC, 25.2 kDa; CC1, 14.4 kDa; CC2, 11.7 kDa. Note that the abnormal migration of TACC3 in SDS-PAGE gels (~125 kDa; theoretical molecular weight: 70 kDa) is associated with the presence of the seven repeat (7R) region, as its deletion normalizes gel migration to the expected molecular weight.

FIGURE S5. C-terminal chTOG fragments overexpressed and purified in this study. (*A*) Domain organization of murine chTOG and outline of C-terminal fragments analyzed for TACC3 binding. The TOG domains 1 to 5 are implicated in microtubule interaction (1). Fragment A covers also an additional and putative TOG domain (TOG6) that was recently identified (2). (*B,C*) C-terminal fragments of murine chTOG were purified after bacterial expression and analyzed on Coomassie Blue stained SDS-PAGE gels. Calculated molecular weights: chTOG-Cterm, 51.9 kDa; chTOG-A, 29.9 kDa; and chTOG-B, 23.2 kDa. The identity of the chTOG fragments A and B was verified by immunoblotting using α chTOG

antibodies which either recognize only fragment B (α chTOG, #34032 from QED Bioscience/Acris, raised against a peptide of 14 a.a. at the very C-terminus of human chTOG) or both fragments A and B (α chTOG #NB500-182, Novus Biologicals, raised against the C-terminal 301 a.a. of human chTOG) (data not shown). CBB, Commassie Brilliant Blue.

FIGURE S6. Experimental controls for the ITC experiments performed in this study. Control experiments done in the context of Fig. 3E and 4E included titration of CC1 (485 μ M) over buffer (A), buffer on CC2 (40 μ M) (B), 7R (450 μ M) over buffer (C), and CC2 (160 μ M) over buffer (D). The heat release detected in the latter case may indicate changes in the oligomeric behavior of CC2 upon dilution.

FIGURE S7. Lack of interaction between CC1 and CC2 under aSEC conditions points to a parallel coiled-coil structure of the TACC domain. Potential binding of the purified TACC domain fragments CC1 and CC2 to each other was analyzed by analytical size exclusion chromatography (aSEC) followed by SDS-PAGE and CBB staining of the respective peak fractions. The observation that CC1 and CC2 do not interact indicates that the TACC domain of murine TACC3 displays a parallel coiled-coil structure.

FIGURE S8. MLN8237 – mediated inhibition of Aurora-A kinase impairs colocalization of TACC3 and chTOG to spindle microtubules and poles, but does not completely abolish centrosomal TACC3-chTOG colocalization despite centrosomal fragmentation. HeLa cells were treated with DMSO or 0.5 μ M MLN8237 for 2 h. Thereafter, colocalization of the centrosomal marker γ -Tubulin and Aurora-A kinase (autophosphorylated at T288) was analyzed in the absence or presence of the Aurora-A kinase inhibitor MLN8237 (A). (B) and (C) depict confocal section analyses of TACC3 (green)-chTOG (red) colocalization (yellow to orange) at centrosomes and spindles in the absence or presence of MLN8237, respectively. Antibodies against α -Tubulin were used to stain the mitotic spindle apparatus. (D) Magnifications (3.2-fold) of representative confocal pictures depicted in (B) and (C).

FIGURE S9. Binding of TACC3 to chTOG occurs *in vivo* in an Aurora-A – independent manner. HEK293 cells were transfected with expression constructs for TACC3 or the indicated C-terminal deletion mutants all fused C-terminally to GFP. Following 48 h, cells were treated with the Aurora-A inhibitor MLN8237 (0.5 μ M) for 2h. Thereafter, total cell lysates were prepared and subjected to co-immunoprecipitation analysis using a GFP-specific antibody followed by SDS-PAGE and detection of chTOG in the immunoprecipitates.

FIGURE S10. The chTOG-B fragment, but not chTOG-A, interacts with the CC1 subdomain of TACC3. Binding of chTOG-A (A) or chTOG-B (B) (Fig. S5) to the CC1 subdomain of TACC3 was analyzed using analytical size exclusion chromatography (aSEC) followed by SDS-PAGE and CBB staining of the respective peak fractions. A significant peak shift due to complex formation was observed for chTOG-B – CC1, but not for chTOG-A – CC1.

FIGURE S11. Biophysical characterization of purified murine TACC3. A, Thrombin cleavage of TACC3 did not impair its α -helical content and secondary structure as revealed by circular dichroism (CD) measurements. B, Multi Angle Light Scattering (MALS) analysis reveals a polydisperse/oligomeric nature of TACC3 with a molecular mass of ~420 kDa at the maximum UV₂₈₀ absorbance. In contrast, upon thrombin cleavage, TACC3 appears monodisperse with a molecular mass of ~72 kDa that is very close to the monomeric mass of murine TACC3 (70 kDa). C, analytical ultracentrifugation sedimentation velocity experiments analyzing the molecular weight of TACC3 in solution before and after thrombin cleavage (results summarized in Table S1).

SUPPLEMENTARY REFERENCES

1. Al-Bassam, J., and Chang, F. (2011) *Trends Cell Biol* **21**, 604-614
2. Hood, F. E., Williams, S. J., Burgess, S. G., Richards, M. W., Roth, D., Straube, A., Pfuhl, M., Bayliss, R., and Royle, S. J. (2013) *J Cell Biol* **202**, 463-478

Table S1. Biophysical parameters obtained from two independent AUC-SV experiments analyzing murine TACC3 vs. thrombin-cleaved TACC3.

Constructs		Amount (%)	MW (kDa)	$S_{10,w}$ (S)	f/f_0
TACC3	Species 1	87.71	108.91 (108.03, 109.87)	3.12 (3.12, 3.12)	2.55 (2.53, 2.57)
	Species 2	12.29	57.40 (57.10, 58.20)	4.72 (4.68, 4.77)	1.10 (1.09, 1.12)
TACC3 + Thrombin	Species 1	62.30	52.55 (52.17, 52.92)	2.20 (2.19, 2.21)	2.22 (2.21, 2.24)
	Species 2	29.32	61.92 (60.98, 62.86)	1.28 (1.22, 1.27)	4.26 (4.24, 4.29)
	Species 3	8.63	66.09 (63.68, 68.50)	3.78 (3.77, 3.80)	1.51 (1.47, 1.55)

Abbreviations: AUC-SV, analytical ultracentrifugation – sedimentation velocity; MW-molecular weight; $S_{10,w}$ (S), sedimentation rate at 10 °C; f/f_0 , frictional coefficient.

TABLE S1

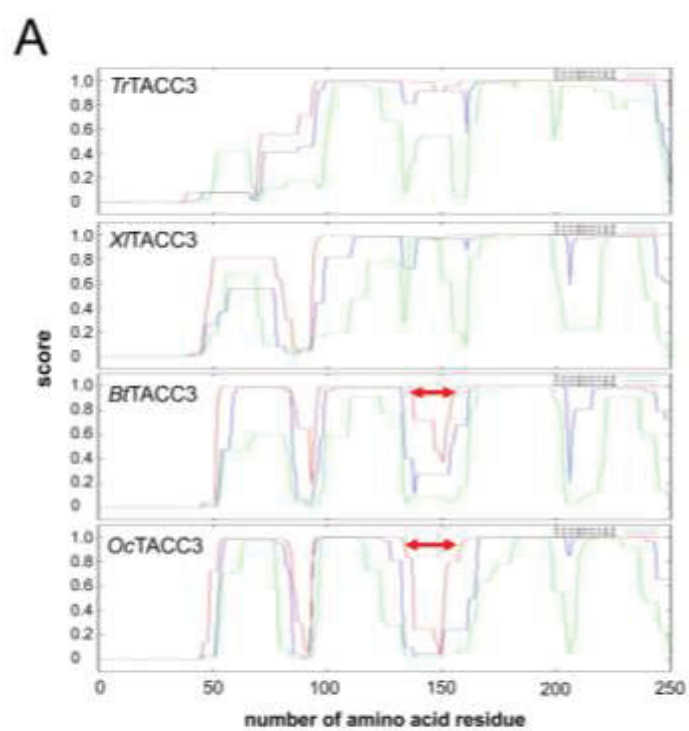


Figure S1

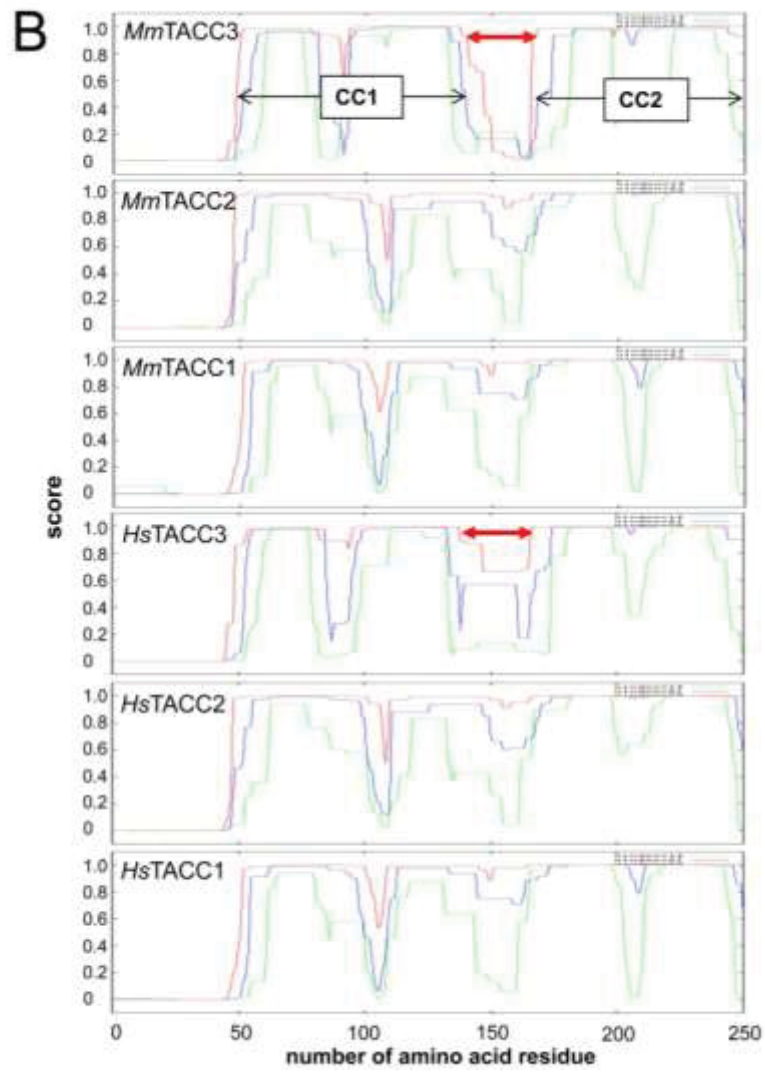


Figure S1

```

MmTACC3 -----RGLLPAEPIVDVLYKYSQKLDVAVVNMQGEEN-----LELKSRYEQLNTRKYLEWQKSVDE 467
HsTACC3 -----GGPPLSTGPIVDLLOYYSQKLDVAVVKATQGEEN-----RELRSRCEELHGRKNEELGKIMDR 678
OcTACC3 -----ILEPSCPPLPVGPIVDVLYRSQRDLDAVQAAGQEN-----LELRSRCEELHTKNEELGKIMDG 576
BtTACC3 -----GAPLLPVGPIVDVLOYYSQKLDLSAVEATQKEN-----EVLRGKCAALQERLLENGKIMDS 650
XtTACC3 -----NPFLSTSDAIVEMLYKYSQKMDAAIEAVRLEVQEKOLEVLEWKTTHKRLYLEVVEGRIIAE 771
TtTACC3 -----QTAHVEESIIEVLYKYSQKMDAAIAKVQAEVEKD-----NCWSAKYKKLLEDGQENRIIAE 718
MmTACC2 SRSRQDTKREAAHPDVSISKTALYSRIGSTEVEKPPGLFGQPDLDSALQVARALEVIKEREVSEWQKYEESRRREVVMRKIVAE 986
HsTACC2 SRSRQDAKREAAHPTDVSISKTALYSRIGTAEVEKPGALFGQPDLDSALQIARALEIITKEREVSEWQKYEESRRREVVMRKIVAE 866
MmTACC1 -----ESPLDGFCLSEAKTAVLTLLIREEIIITKEIENEWKKKYEETREEVLEMRKIVAE 615
HsTACC1 -----ESPLDGFCLSEAKTAVLTLLIREEIIITKEIENEWKKKYEETREEVLEMRKIVAE 644

MmTACC3 FCKIAYKSLAEAKQRELKEIAEDKIQKVLKRDQLNADLNSMERSFSDLKRFKREKREIEGYORNEESLRKYVGECEVKKIEKGG 554
HsTACC3 FEEVYYDAMSEVQKQ---KELSKAEIQKVLKENDQLTTDLNSMERSFSDLKRFKREKREIEGYRNEESLRKQVEDDLARITQLGG 762
OcTACC3 FEGIVYDAMSEVQRQ---KEAARAEVQKVLKDRDLAADLSATEKSFSDLKRFKREKREIEGYRNEESLRKQVEDDAAIVKKAQ 660
BtTACC3 FEGTVYQVMEESOKQ---KELTKAEMDKVLKRNADLTADLHMERFSDLKRFKREKREIEGYRNEESLRKQVEDDIEFVKKAA 734
XtTACC3 FEGTITDILDSRQ---KETAKLELNKVLQEQVQVQDLNSMETSFSELPKRLKQNEALEGYRNEESLRKQVEDDVLVHKKEE 865
TtTACC3 FEEMIAQMMADQEQ---TEESQKOLNEALSENEQVADLNAMERSFSDLKRFKREKREIEGYRNEESLRKQVEDDIAQDQLARIKKEE 802
MmTACC2 YEKTIADMIEDEQRE---KSVSHOTVQDLVLEKEDALADLNSVERSLADLFRYYEMNEVEGFRRNEEVLRRQADELRSVKKKEE 1070
HsTACC2 YEKTIADMIEDEQRE---KSVSHOTVQDLVLEKEDALADLNSVERSLADLFRYYEMNEVEGFRRNEEVLRRQADELRSVKKKEE 950
MmTACC1 YEKTIADMIEDEQRT---SMTSOKSFQDLTMEKEDALADLNSVERSLADLFRYYENLGGLEGFRRNEEVLRRQADELRSVKKKEE 689
HsTACC1 YEKTIADMIEDEQRT---SMTSOKSFQDLTMEKEDALADLNSVERSLADLFRYYENLGGLEGFRRNEEVLRRQADELRSVKKKEE 728

MmTACC3 RYDALKIHAEELRLNEEIAQVRSKAQAEVLKQSRERADMONHSEMTLEQTRIEDELTRICDDLISMEKI 630
HsTACC3 RYDALKAHAEELQLNEEIAQVRSKAQAEALALQSRERKEDMRIQSLEKTVEQTKENEELTRICDDLISMEKI 838
OcTACC3 RYDALKAHAEELKLAEEIAQVRSKAQAEALAFDASMPHADMQIOSLEKTVEQTKENEELTRICDDLISMEKI 736
BtTACC3 KYDALKAQAEELRQASSEEIAQVRSKAQTDALALQAVLRHEGMRVHSLERKVVQKTKENDELTRICDDLISMKRI 810
XtTACC3 RYDALKAHAEELNRRNEEIAHRSKAKSEATLQATLRHEGMKIQSLEKSLERKVEKTKENDELTHLQDFLMEKI 931
TtTACC3 RYDALKAHAEELADANGEIAEVRSKNKAELSAHQLRREQLKAQSLERKSLDQKGRAEELTKLQDEITVQK 878
MmTACC2 RYDALKVHAEELDRANAEIAQVRSKAQEQDAHQASLRHEGLRVDALERTLEQNKIEELTKLQDEIATMGKS 1146
HsTACC2 RYDALKVHAEELDRANAEIAQVRSKAQEQDAHQASLRHEGLRVDALERTLEQNKIEELTKLQDEIATMGKS 1026
MmTACC1 RYDALKVHAEELDRANAEIAQVRSKAQAEALHAGLRHEGMKVESLBRALQKNOIEELTKLQDEIATMGTD 776
HsTACC1 RYDALKIHAEELDKANEEIAQVRSKAKAESALLHGRERHEGMKVESLBRALQKNOIEELTKLQDEIATMGTD 805

```

Figure S2

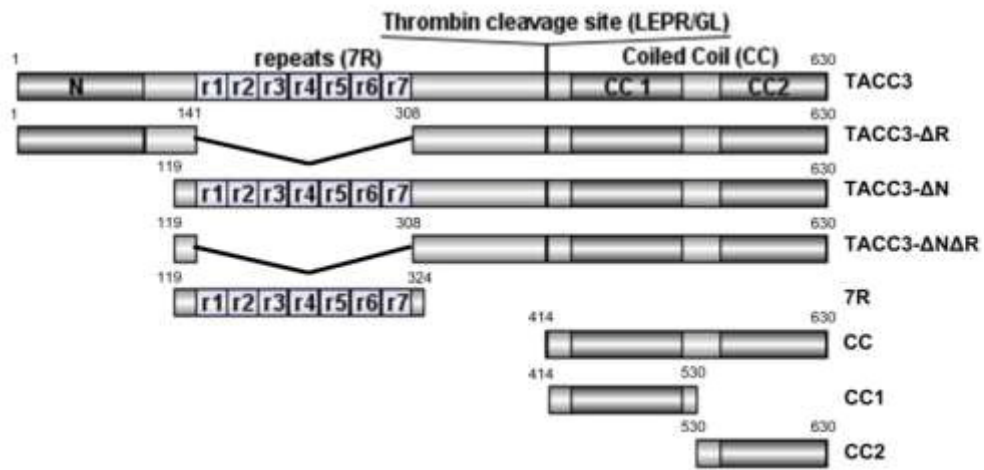


Figure S3

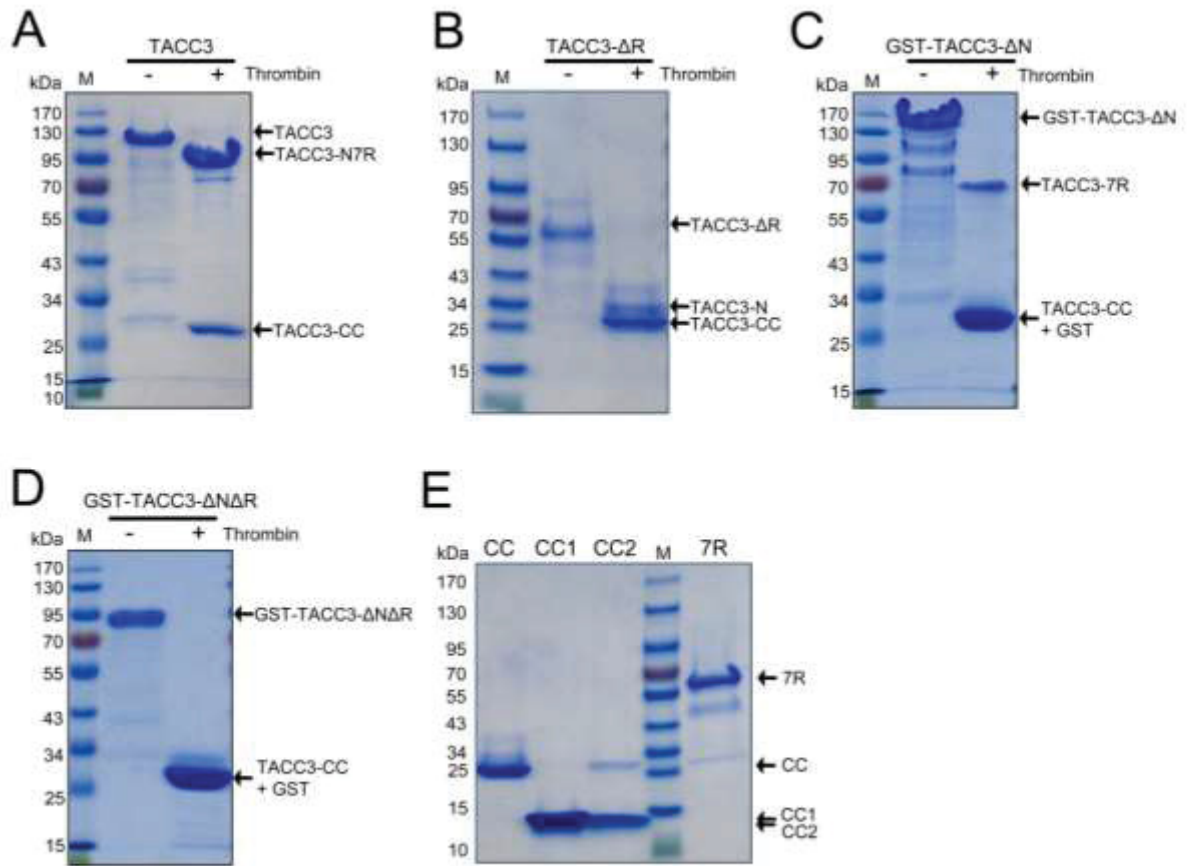
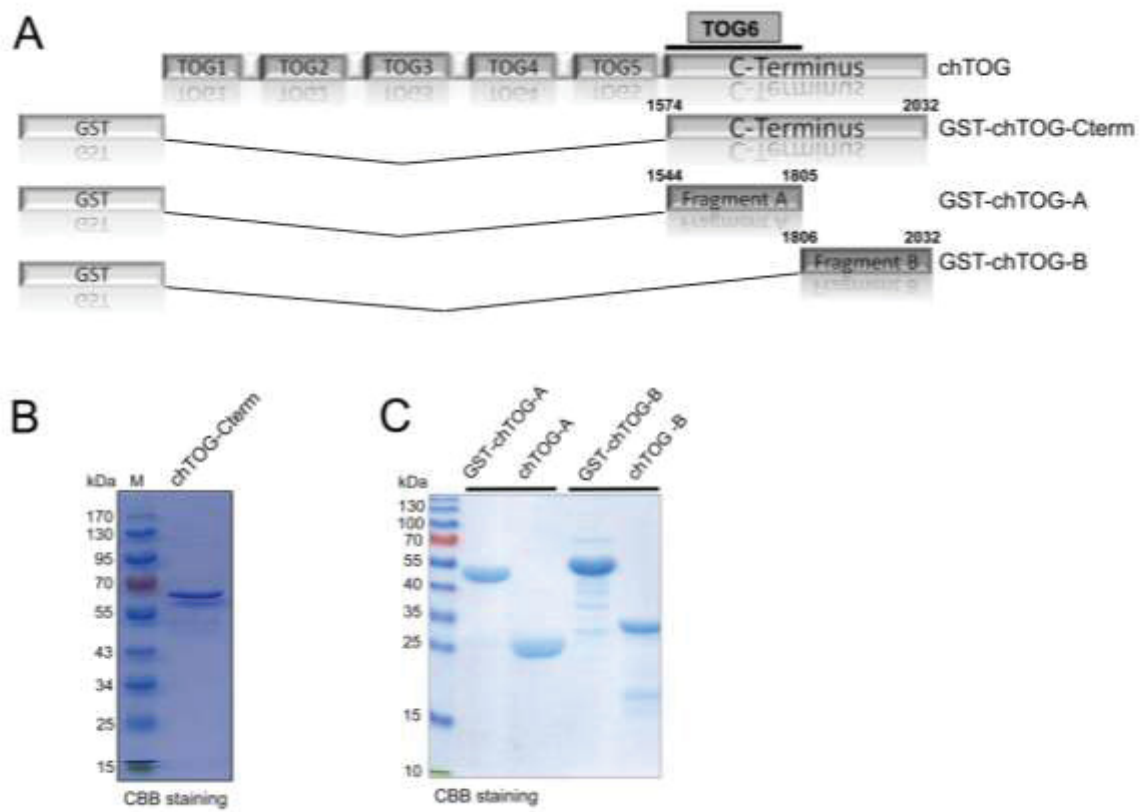


Figure S4



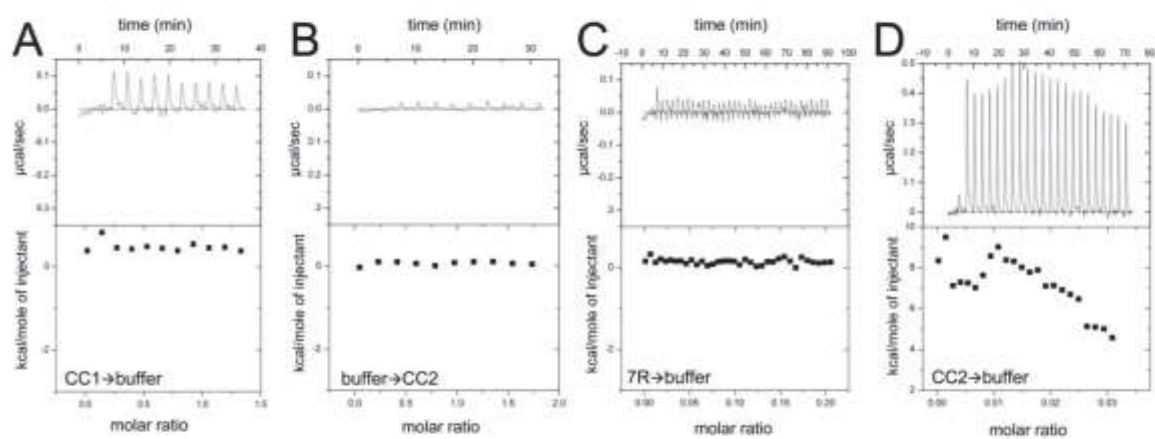


Figure S6

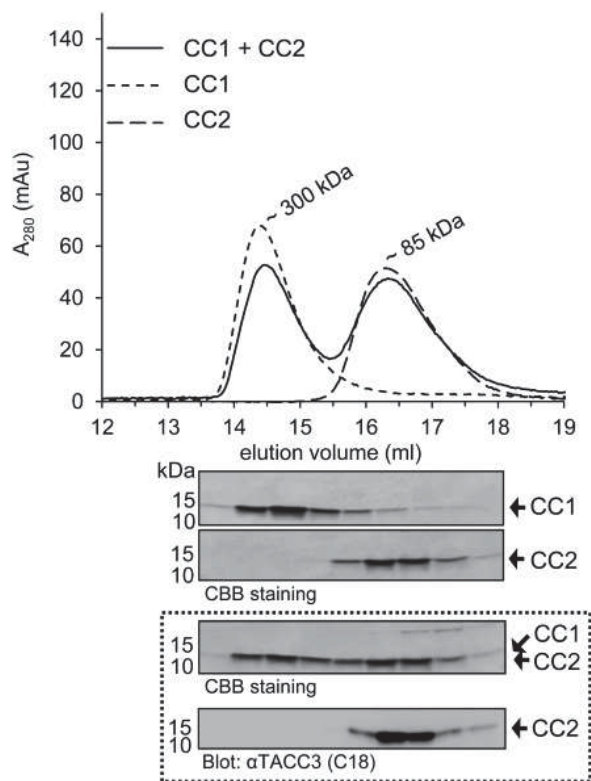


Figure S7

A

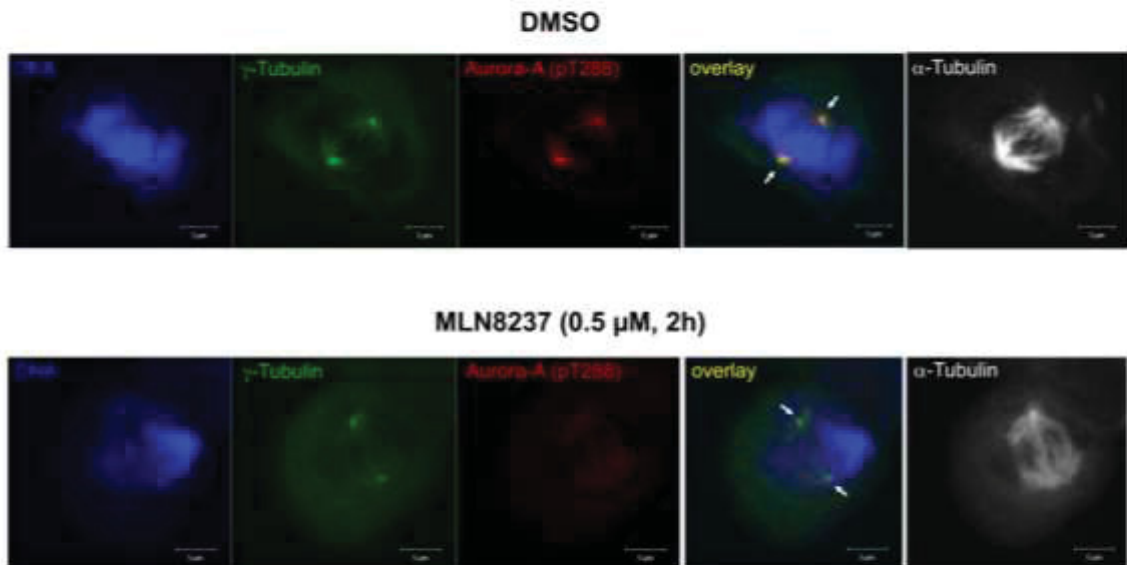


Figure S8

B

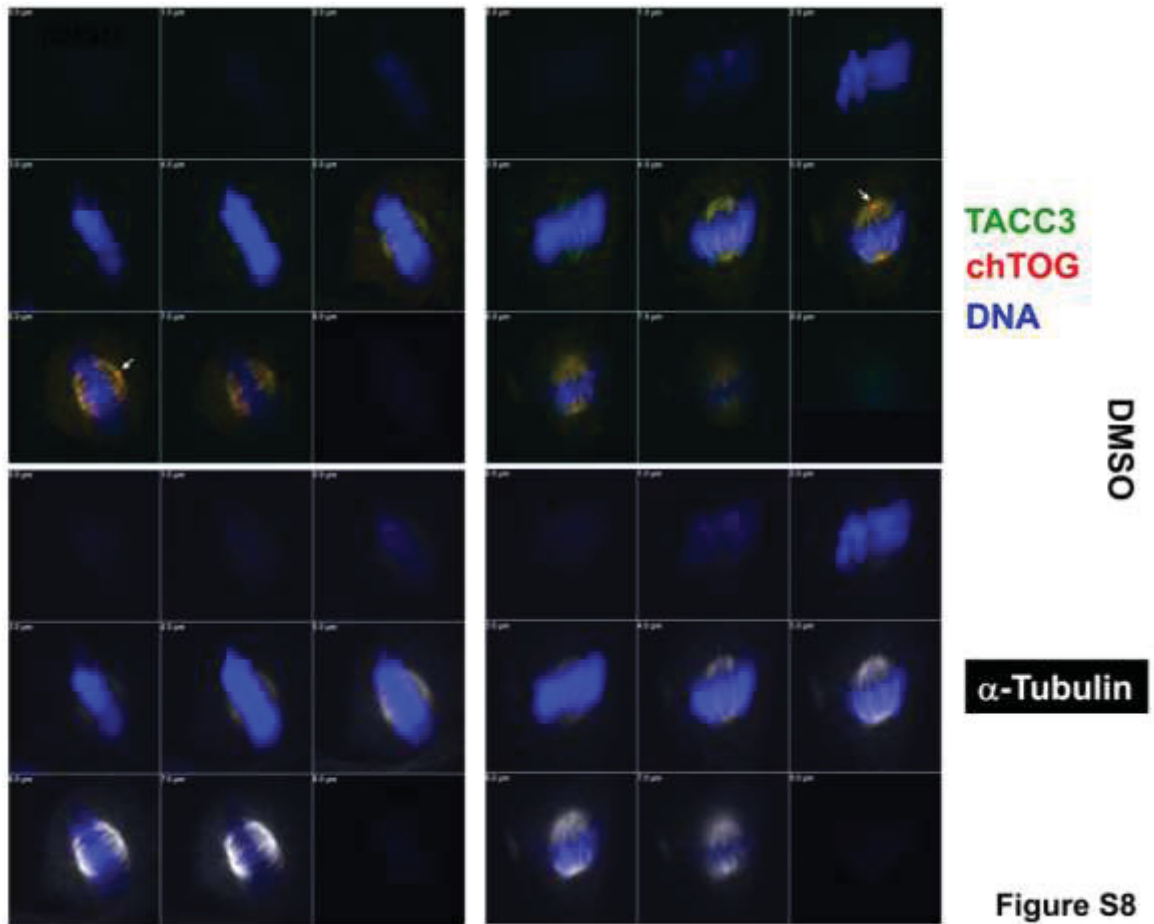
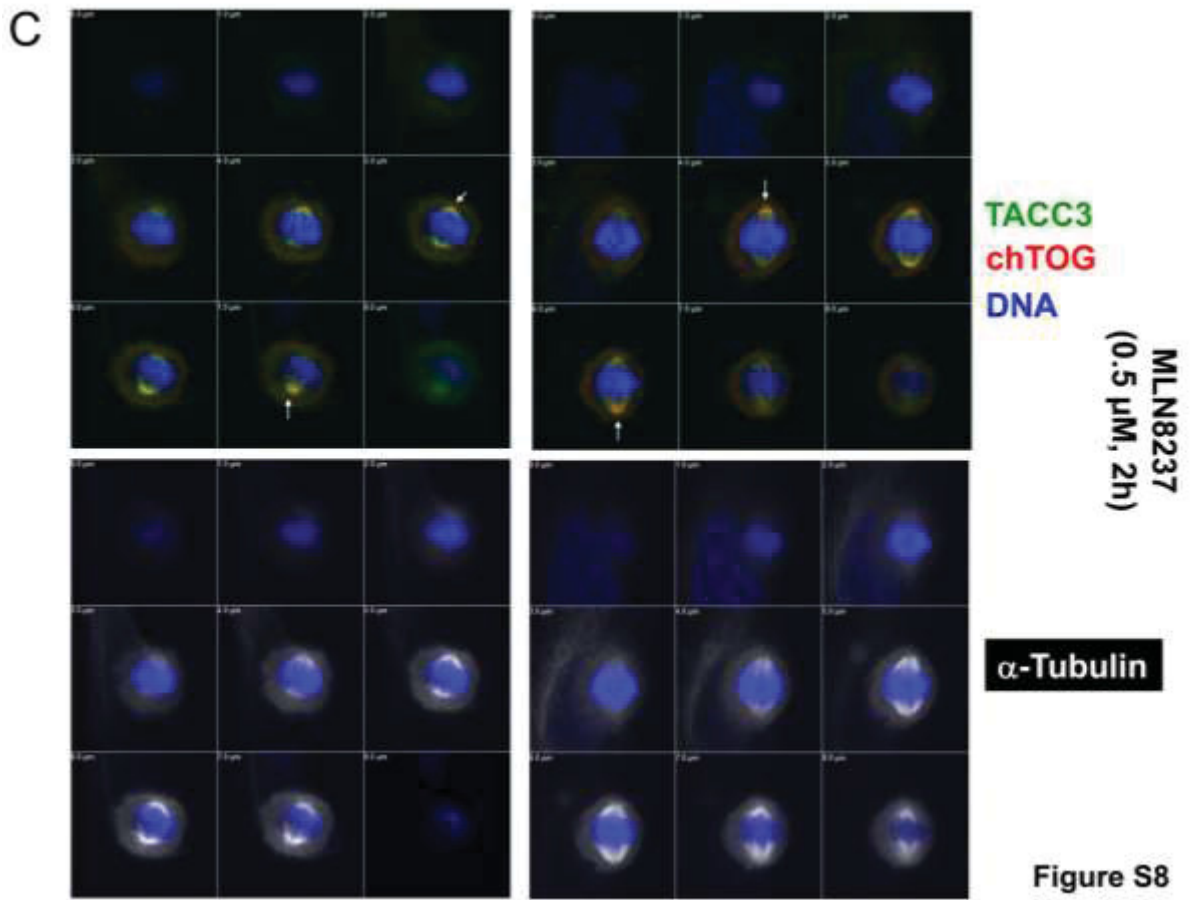


Figure S8



D

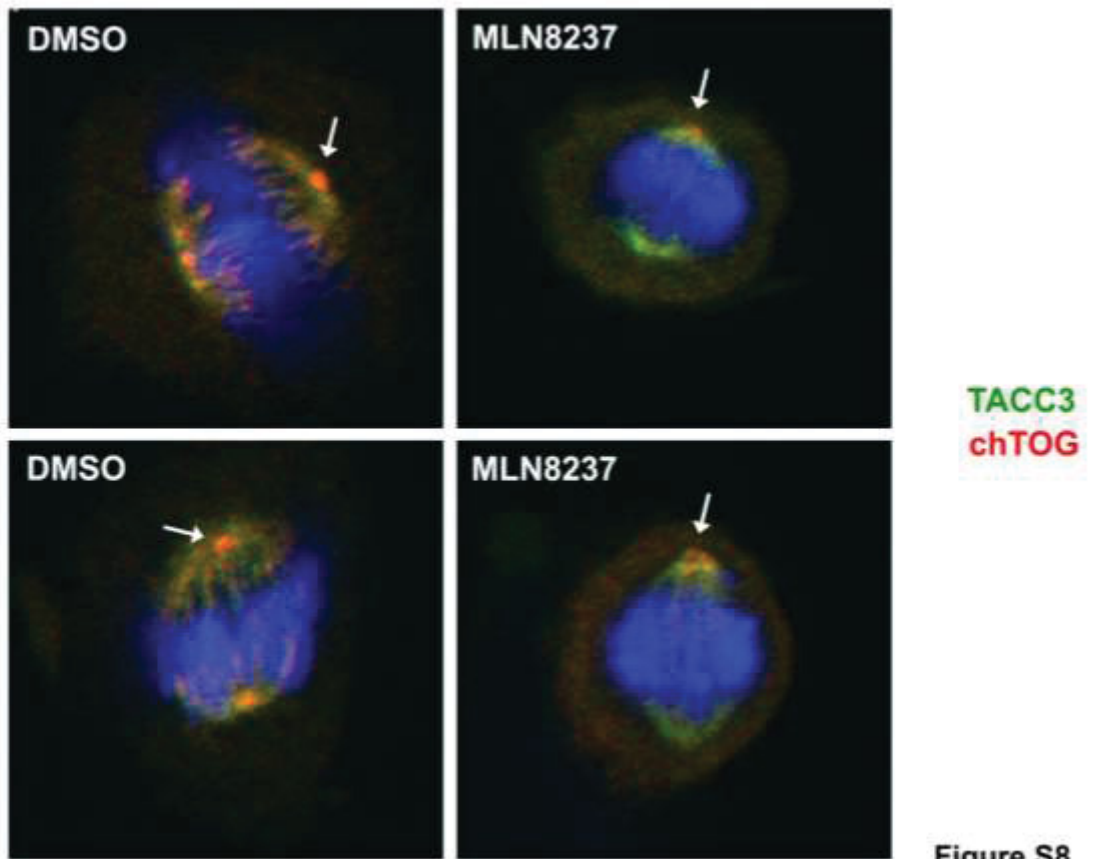


Figure S8

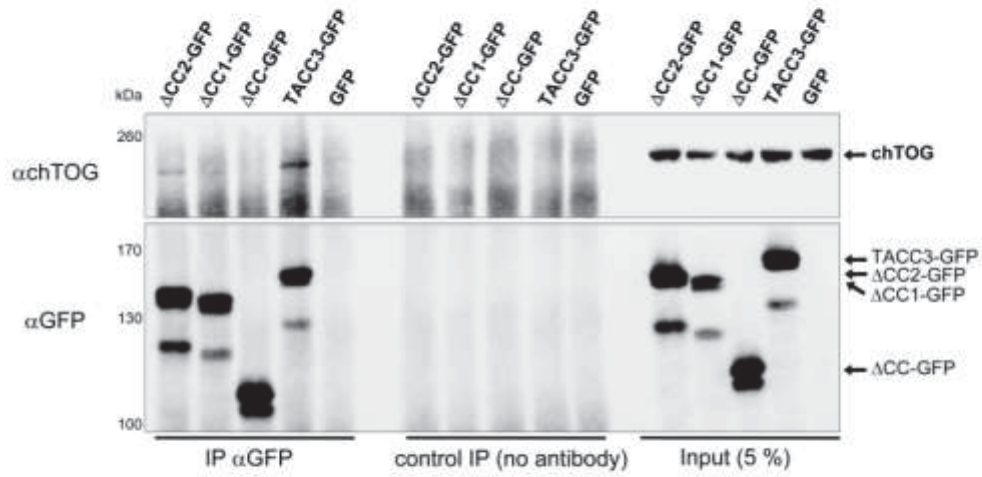


Figure S9

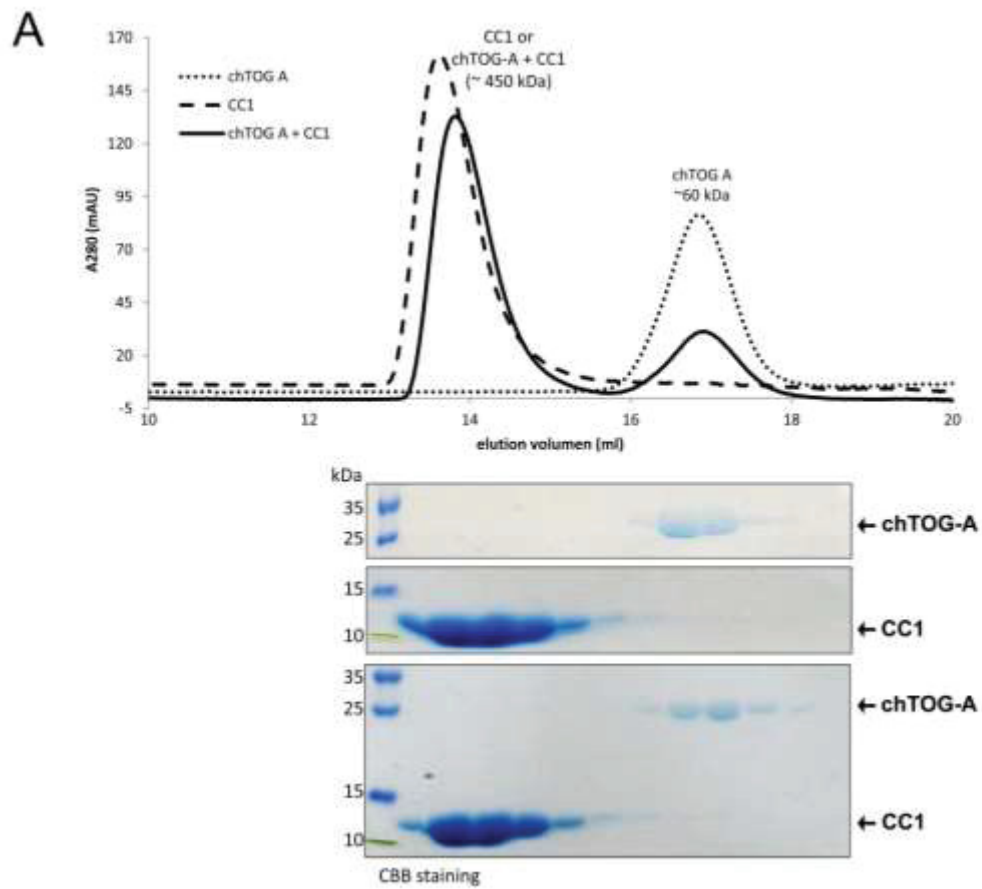


Figure S10

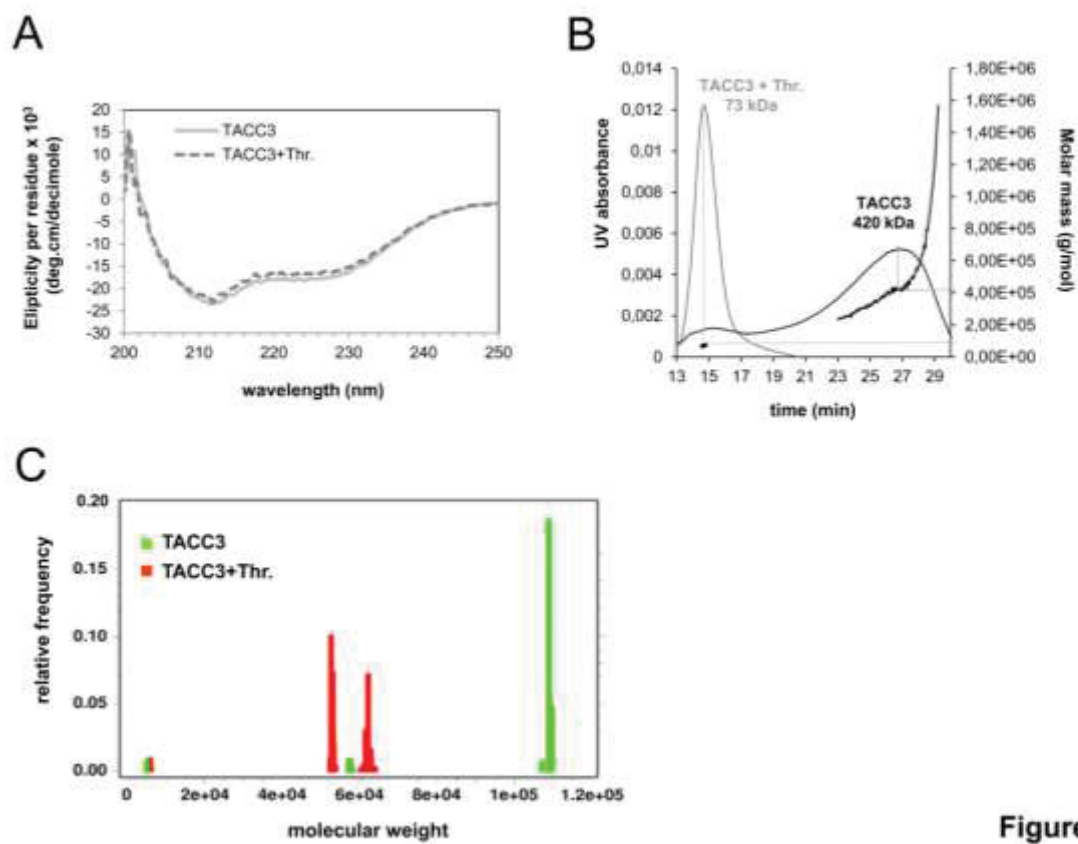


Figure S11

Chapter VIII

General discussion

Kazem Nouri

5 Discussion

During past two decades a principle has appeared asserting that cells achieve specificity in their molecular signaling networks by organizing distinct subsets of proteins in space and time. Spatial organization is required to achieve high-fidelity intracellular information transfer. Proteins can be assembled into specific complexes *via* different ways, including membrane localization, compartmentalization (organelle targeting), and by the assembly of specific protein complexes by scaffold proteins [105,307-309]. These proteins control fidelity and specificity of the information flow within a cell by assembling and linking different types of proteins, e.g., activators, effectors, enzymes, and substrates into signaling circuits. Scaffolds are extremely diverse proteins and could carry out different functions. For instance, the Ste5 and KSR (kinase suppressor of RAS) physically assemble individual kinases that control MAPK pathway localization like membrane anchoring. They are essential for efficient signaling and they can also sequester MAPK signaling proteins from competing inputs [310-312]. Scaffold proteins are not restricted to directing kinase cascades; they can organize other classes of molecules, such as pathogens signaling as well. Pathogens normally use scaffold proteins for rewiring host signaling pathways to turn off or avoid host defenses. For example, the pathogenic bacteria *Yersinia pestis* produces a scaffold-like protein (YopM) that artificially links together two kinases (Rsk1 and Prk2) that do not normally interact [313]. Another example is for the human immunodeficiency virus (HIV) that by producing a scaffold protein, Vif, which bind both APOBEC3G and cullin-E2, destroys the host APOBEC3G protein which is a cytidine deaminase and interferes with viral replication [314]. Another very important and interesting group of scaffold proteins are involved in GTPase (RHO and RAS) signaling. For example, the yeast protein Bem1 promotes the interaction between the GEF, PAK and GTPase substrate, CDC42 [315]. Such coordinated GTPase regulation controls defined morphological behaviors like polarized budding of yeast cells. Another well investigated protein is IQGAP1, which contains several protein-interacting domains that mediate binding to variety of target molecules. This diversity of targets suggests that IQGAP1 coordinates a wide variety of signaling pathways and cellular functions through the assembly of multiprotein complexes [45,118,119]. For example, a ternary complex of CDC42/RAC1 (RHO proteins), IQGAP1 and actin [316], complexes of IQGAP1 containing RAC1/CDC42 and CLIP-170 [140], CDC42 and calmodulin or RAC1 and calmodulin [45], have been described so far. Thus, IQGAP1 play diverse roles in vertebrates, such as nervous system, cardiovascular system, pancreas, lung and kidney.

RAS and RHO proteins such as KRAS, CDC42, and RAC proteins control essential biological processes and are frequently dysregulated in diseases, such as cardiovascular diseases, developmental and neurological disorders, and cancer. A prerequisite for their signaling is

association with and activation of downstream effectors, such as PI3K, B-RAF, WASP, and PAK1. While the role of these effectors is well-investigated, the nature of such a protein-protein recognition process and the mode of interactions for IQGAP1 remain to be established. This study have focused on the interaction of IQGAP1 with the active, GTP-bound form of RHO proteins RAC1 and CDC42 and provides new insights into a two-step binding process that is a prerequisite for IQGAP1 activation and a critical mechanism in temporal regulation and integration of IQGAP1-mediated cellular responses.

From protein scaffolds involved in GTPase signaling, galectin-1 (Gal-1), galectin-3 (Gal-3), nucleophosmin (NPM1), and nucleolin (NCL) are also known to participate in facilitating or enhancing RAS nanoclustering [112-115]. Gal-1 and Gal-3 associate with HRAS and KRAS, and increase nanoclustering of active form of HRAS [115] and KRAS [114], respectively. In addition to be known that NPM1 is a negative regulator of the small GTPase RAC1, and also interacting with ROCK II kinase and playing role in the regulation of centrosome duplication, both NCL and NPM1 bind KRAS and mediates recruitment of KRAS into nanoclusters on the inner leaflet of the plasma membrane [112]. Apart from what is known about the scaffolding role of these two proteins regarding small GTPases, NPM1 and NCL have emerged as an essential host factor for multiple aspects of microbial infection including adhesion at cell surface, entry, intracellular trafficking, regulation of transcription and translation as well as nucleo-cytoplasmic shuttling [172-174,176]. It is increasingly evident that these proteins function as a host-specific target for a large number of viruses and pathogenic bacteria which has raised interest in targeting them therapeutically. While neither direct interaction of NPM1 nor NCL with the RAS isoforms (HRAS, NRAS, and KRAS) was detected, various protein domains of NPM1 and NCL has been used in the present thesis to investigate their interactions with FMRP and viral proteins (HIV1 Rev and HSV1 US11).

5.1 Classical RHO proteins and Juvenile myelomonocytic leukemia (JMML)

In **chapter 2** the biochemical properties of the RHO proteins and their regulatory cycles are described in detail [317]. As it was mentioned before, dysregulation of RHO proteins has been shown to play a vital role in cancer, infectious, cognitive disorders, and cardiovascular diseases. But several aspects of RHO proteins signaling have to be considered yet. Of the RHO family members only RHOA, RAC1, and CDC42 have been widely studied so far and the functions of the other less-characterized members of this protein family await detailed investigation. RHOGDIs associate and extract the RHO proteins from the membrane. Despite the intensive research over the last two decades, the mechanism of this function is not clear yet and the factors displacing the RHO protein from the complex with RHOGDI remain to be elucidated. For the regulation of the 22 RHO proteins more than 70 and 80 GEF and GAP, respectively exist in the human genome. How

these regulators selectively recognize their RHO protein targets is not well understood and majority of GEFs and GAPs in human so far remain uncharacterized. Most of the GEFs and GAPs themselves need to be regulated and require activation through the relief of autoinhibitory elements [318-324]. With a few exceptions [84,325], it is conceptually still unclear how such autoregulatory mechanisms are operated. A better understanding of the specificity and the mode of action of these regulatory proteins is not only fundamentally important for many aspects of biology but also is a master key for the development of drugs against a variety of diseases caused by aberrant functions of RHO proteins.

Another aspect is point mutations in genes related to RHO GTPases, which is very rare. Accordingly, **chapter 3** describes the genetic profiling and whole-exome sequencing (WES) of a large Juvenile myelomonocytic leukemia (JMML) cohort. JMML is a rare and severe myelodysplastic and myeloproliferative neoplasm of early childhood initiated by germline or somatic RAS-activating mutations [78,326-328]. JMML is considered as a unique example of RAS-driven oncogenesis since it is thought to be initiated by mutations, usually described as mutually exclusive, in RAS genes (*NRAS*, *KRAS*) or RAS pathway regulators (PTPN11, NF1 or CBL) [78]. JMML can be sporadic or develop in patients displaying syndromic diseases with constitutional RAS over activation such as Noonan syndrome (NS), type 1-neurofibromatosis (NF1), and CBL syndrome, caused by heterozygous germline mutations in PTPN11, NF1, and CBL respectively [79]. Our study has shown that in addition to RAS and RAS regulators mutation, the RHO GTPase RAC2 is also mutated in some JMML cases [76]. The coexistence of RAC and RAS/MAPK mutations in some tumors and cooperation between oncogenic NRAS and RAC has been previously demonstrated [74]. However, the molecular basis for this interrelationship remained unclear. Our investigations of RAC2 D63V, which predominantly occurs in its active GTP-loaded state as compared to wild-type RAC2 and its constitutive variant RAC2 G12V, have revealed a drastic gain-of-function effect. Interestingly, the analysis of downstream signaling of RAS has shown that RAC2 D63V activates the PI3K/PDK1/AKT and the mTORC2 pathways but has no significant effect on the RAF/MEK/ERK pathway [76]. Furthermore, our data have clearly shown a reversed molecular switch function of RAC2 D63V leading to an accumulation in its active GTP-bound state and undergoing a tight interaction with its effectors, as compared to wild-type RAC2, which may explain its cellular activities towards AKT phosphorylation [76]. This is consistent with several lines of evidence indicating a strong impact of the PI3K/PDK/AKT pathway on JMML [329], and most likely activating the catalytic p110 δ subunit of PI3K, which promote the effects of SHP2 on GM-CSF hypersensitivity [330].

In conclusion, these findings suggest that the RAS-RAC pathway represents a significantly dysregulated subnetwork in JMML and these findings extend and reinforce the notion that JMML is a RASopathy while showing that RAS activation is the major but not the unique player in JMML. Such novel insight into the pathogenesis of JMML should provide functional guidance, prognostic markers and patient selection criteria for new therapeutic options in this very severe childhood leukemia.

5.2 RHO family GTPases and IQGAP1 interaction

It was mentioned before that the interaction of RHO proteins and the downstream effectors such as PAK and WASP is well investigated but the molecular basis of their interaction with another effector, IQGAP1, remains to be elucidated. In **chapter 4** the comprehensive interaction study of different RHO proteins with IQGAP1 C-terminus (here called GRD-C) is presented. Kinetics of these interactions was monitored using stopped-flow fluorescence spectroscopic method. The results clearly indicated that IQGAP1 binds among RHO proteins selectively to RAC- and CDC42-like proteins (RAC1, RAC2, RAC3, RHOG, TC10, and TCL) only in the active GTP form. In contrast to our study which showed that there is no physical interaction between GRD-C and the RHO isoforms RHOA or RHOC, purified from *E. coli*, two studies have reported an association of IQGAP1 with the RHO proteins using immunoprecipitation protocols. *Casteel et al.* have shown that GRD-C interacts with the active, G14V variant of RHOA and RHOC but not with RHOB, in human embryonic kidney 293T cells, and suggested IQGAP1 as a downstream of RHOA [331]. *Bhattacharya et al.* have shown that IQGAP1 binds to both RHOA and p190A-RHOGAP leading to inactivation of RHOA and modulation of contractility of airway smooth muscle cells [162]. We think that observed interaction of IQGAP1 GRD-C with RHOA and RHOC is indirect and may be mediated by another protein in cells, because no direct interaction between IQGAP1 and the RHO isoforms was monitored in our kinetic and equilibrium measurements. However, we do exclude the possibility that other regions at the N-terminal half of IQGAP1 may play a role in the interaction with the RHO isoforms. This can only be investigated with the full-length IQGAP1, whose expression and purification from the baculovirus-insect cell system needs to be established.

Obtained result from individual kinetic measurements displayed the fastest association with RAC2 suggesting that GRD-C-interacting RHO proteins, in spite of tremendous difference in the overall binding affinities, may utilize a homologous set of associating residues in the neighborhood of the fluorescence reporter group. Another point is that these members of the RHO family associate with IQGAP1 more or less in the same time range raising the question whether these interactions may selectively take place in the cells and how temporal regulation

and integration of IQGAP-mediated cellular responses is achieved. RHOG and TC10 interaction with IQGAP2 and IQGAP1, respectively, has been previously reported [57,332]. RHOG has been reported to bind in an activated GTP bound form to the RAC/CDC42-specific effectors MLK3, PLD1, and IQGAP2 which in turn, stimulates some downstream signaling targets of activated RAC1 and CDC42 such as JNK and Akt [332]. Although the consequence of TC10-IQGAP1 interaction is not defined yet, it may control exocytosis and cell polarity for two reasons. Exo70 has been shown to bind to the N-terminal IQGAP1, most likely to the WW motif [333] but probably not to the IQ region because Exo70 was not found as binding partner of this region [119]. In mammals, only RAL (RALA) and TC10 (RHOQ) GTPases have been shown to bind the exocyst complex [334]. TC10-Exo70 interaction is implicated in the tethering of GLUT4 vesicles to the plasma membrane in response to insulin [334-336] and in promoting neurite outgrowth [337-339]. IQGAP1 proteins have been shown to be involved in both processes [119,120,340]. Such a complex interacting network circuit of IQGAP1, which modulates its function in space and time, remains an open and very interesting issue for future studies. Furthermore, TC10 has the fastest and RAC2 the slowest dissociation from GRD-C, respectively, suggesting that an IQGAP1 complex with RAC2 is most stable and may contribute to a longer signal transduction as compared to *e.g.* RAC1, CDC42, RHOG, RAC3, and TC10.

Biochemical analysis along with homology modeling, based on the RAS-RASGAP structure [341], provided up to date a structural model of IQGAP1 GRD contacting the switch regions of the GTP-bound CDC42 [124,141,152,154,166,167,171]. In order to investigate the molecular mechanism of this interaction and reveal the binding domains and interacting residues, different deletion variants of IQGAP1 were designed. Obtained data clearly have shown that GRD1 and GRD2 do not associate with RAC1 and CDC42 under our experimental condition. This was unexpected because GRD has been generally accepted in the IQGAP community as the RAC1- and CDC42-binding domain of the IQGAP1 [124,141,152,154,166,167,171]. In addition, our data have clearly revealed that the region upstream of GRD2 (aa 863-961) is dispensable for the RAC1 and CDC42 interaction. Another interesting issue was the inhibitory effect of the very C-terminal 99 amino acids (C domain) on the GBD determined through a 3-fold faster association of GRD-GBD (lacking the C domain) with RAC1 and CDC42 as compared to GRD-C. This is consistent with what it has been published regarding interaction of GRD and GBD-C domains with each other, favoring the binding to GTP bound CDC42 [342,343]. Moreover, we found that point mutations of the PKC α phosphorylation site (S1443) affect GRD-GBD association with RAC1/CDC42-mantGppNHp and completely abolished GRD-GBD association with RAC1 and CDC42. This is consistent with what has been reported regarding significant reduction in the interaction between IQGAP1 and CDC42-GTP

bound in the presence of phosphatase inhibitor and using MCF10A cell lysate [342]. Works from several groups have shown that shorter IQGAP1 fragments, encompassing the GRD domain, are responsible for RAC1 and CDC42 interaction. However, we did not observe any change in fluorescence when we used a similar protein, GRD2, to measure association kinetic with CDC42 and RAC1 using stopped-flow system. Therefore, to further investigate this point we measured these interactions using fluorescence polarization under equilibrium conditions for both GRD and GRD-C fragments with mantGppNHp-bound RAC1, CDC42, and RHOA. Interestingly, we found that both proteins bind to the GTP-bound state of RAC1 and CDC42 but not to RHOA. Our data have shown that GRD2 exhibits weaker binding to CDC42 and RAC1 10- and 15-folds, respectively as compared with GRD-C. In addition, the K_d value for GRD-GBD S1443D has significantly decreased. Thus, we hypothesised that the binding interface of IQGAP1 interaction with RHO proteins extends beyond the minimal GRD. Mutational data also support our hypothesis that propose GBD but not GRD as the main domain of IQGAP1 associating the switch regions of RAC- and CDC42-like proteins. To prove this proposal, the interaction with GDP-bound state of CDC42 was also conducted under the same condition using fluorescence polarization. Our results have shown that both domains, GRD and GRD-C, indeed interact also with the GDP-bound form of CDC42 with much lower but comparable affinities. This clearly has proved our hypothesis regarding a nucleotide-independent interaction of GRD outside the switch regions of CDC42.

In conclusion, the results indicated that IQGAP1 binds among RHO proteins selectively to RAC- and CDC42-like proteins only in a GTP-dependent manner. Moreover, obtained results suggested that GBD and specifically, serine 1443 phosphorylation is critical for this interaction. Our kinetic and equilibrium measurements clearly challenge the paradigm that the ability of IQGAP1 to interact with RAC/CDC42 proteins is mainly attributed to its GRD. On the contrary, we proposed that the C-terminal half of IQGAP1 utilize at least three functionally distinct units, including GRD, GBD and C, to achieve the interaction with RAC1- and CDC42-like proteins. Remarkably, IQGAP1 seems to employ a different strategy to interact with RAC1 and CDC42 proteins as schematically illustrated in **Figure 9**: (i) GRD undergoes a low-affinity, GDP-/GTP-independent complex with RAC1 and CDC42 proteins outside their switch regions in a way that is independent of the upstream signals, providing it is structurally accessible and available for interactions; (ii) GBD only binds to the RAC1 and CDC42 proteins if they are in an active GTP-bound forms; (iii) the C-terminal region of IQGAP1 may potentiate the IQGAP1 interaction with RAC1 and CDC42 proteins by probably extending the resident time of the respective proteins complexes. Therefore, we unraveled a new level of regulation for the interaction of IQGAP1 with RAC and CDC42 like

proteins. Such a model is very helpful in understanding the mechanism of IQGAP1 activation in the cellular context.

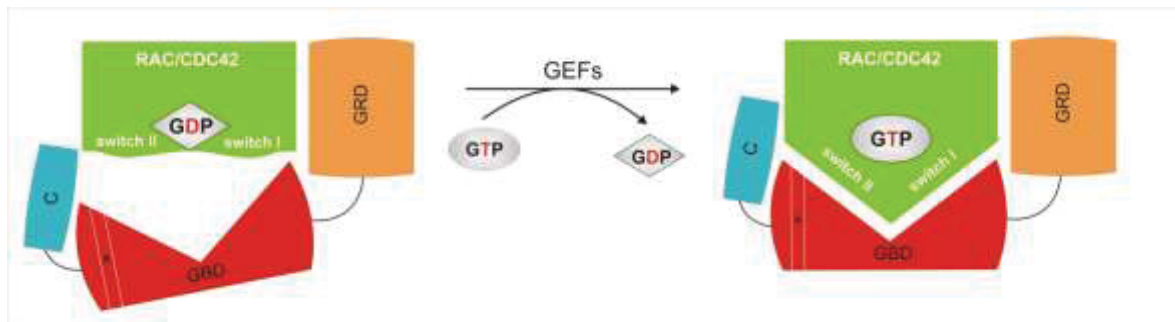


Figure 9. Model for the molecular mechanism of RAC1/CDC42 interaction with IQGAP1 GRD-C. Low-affinity, GDP-/GTP-independent interaction of GRD with RAC1 and CDC42 proteins outside their switch regions. GBD only binds to the RAC1 and CDC42 proteins after GEFs catalyze the exchange of GDP to GTP, and they exist in an active GTP-bound forms. The C-terminal domain of IQGAP1 may potentiate the IQGAP1 interaction with RAC1 and CDC42 proteins by probably extending the resident time of the respective proteins complexes. Figure adopted from chapter 4.

Since a major issue in biology is the isoform specificity, the question to be addressed in the future is that, how the cell controls a specific interaction of IQGAP1 with one of the six identified RHO GTPases interacting IQGAP1. We propose that scaffold proteins, such as calmodulin, may fulfill this function by linking for example RAC1 and IQGAP1 at a distinct area at the plasma membrane. This hypothesis is based on independent published data on individual interaction of calmodulin with both IQGAP1 and RAC1. These studies could be performed in the presence and absence of purified calmodulin and calmodulin/ Ca^{+2} . The physical and biochemical investigations will ultimately advance our knowledge in the field of scaffolds, *e.g.*, calmodulin, as specificity-determining components in signal transduction. Another protein which may play role here is Ajuba [344,345], which has been shown to be required for RAC activation and maintenance of E-cadherin adhesion. However, an interaction between Ajuba and IQGAP1 remains to be shown.

5.3 Nucleophosmin and viral infection

Nucleophosmin (NPM1) is a multifunctional phosphoprotein which has increasingly emerged as a potential cellular factor that directly associates with viral proteins and plays vital role in viral infection. Since its discovery 34 years ago, intensive research has been performed on NPM1. It is ubiquitously expressed and significantly upregulated in response to cellular stress signals leading to the alteration of nucleolar structures and its relocalization to other cellular compartments [346-349]. Due to this ability, NPM1 has been implicated in many stages of viral infection by interacting with a multitude of proteins from heterologous viruses, including Human immunodeficiency virus type 1 (HIV-1) Rev [253], Human T-cell leukemia virus type 1 (HTLV-1) Rex [256], and Herpes simplex virus type 1 (HSV-1) UL24 [252], although the significance of these

interactions in each case until now remained obscure and unexplained. To shed more lights on the association of NPM1 with viral proteins, in **chapter 5** we have investigated NPM1 physical interaction with HIV-1 protein Rev and HSV-1 protein US11 in order to perform binding epitope mapping of NPM1. Rev is 116-amino acids long and its RNA-binding domain is composed of an arginine-rich motif, which binds to different HIV-1 RNA stem loop structures [350]. The RNA-binding domain of Rev acts also as a nuclear/nucleolar targeting signal and can deliver cytoplasmic proteins to the nucleus or nucleolus [271,350]. US11 is an abundant HSV-1 protein, which is expressed late during infection [351]. It has been reported that US11 functionally substitutes Rev and Rex proteins by stimulating expression of glycoproteins required for retroviral envelope synthesis [235]. US11 interaction with cellular proteins is required during HSV-1 infection. In this study, we have identified NPM1 as a new nucleolar protein partner for US11 and characterized the subdomains responsible for their interactions.

Our data indicate that Rev exhibits two NPM1 binding sites on both the pentameric, N-terminal oligomerization domain (NPM1^{OD}) and on the central histone-binding domain (MPM1^{HBD}), while HSV-US11 has only one binding site on NPM1^{OD}. We suggested that the different NPM1 domains interact in a mechanistically different mode with the Rev and US11 proteins. Rev association with NPM1 underlies presumably an RNA-independent bimodal binding mechanism. In the case of the NPM1-US11 interaction, we observed a strong binding of US11 to NPM1^{OD}, which is most probably achieved *via* C-terminal RBD of US11 (US11^{Cterm}), containing arginine rich (R-rich) motif. The C-terminal domain of US11, which is involved in the nucleolar localization of US11, binds NPM1 stronger than the N-terminal domain. Since C-terminus of US11 is rich in arginine, these results nicely support the idea that arginine-rich motif mediates the interactions with NPM1 [352]. While the obtained data regarding US11 report its unprecedented direct interaction with NPM1, our measurements with Rev confirm previously obtained observations. The 1:1 stoichiometric ratio suggests that NPM1^{FL} exhibits one binding site for one HIV-1 Rev molecule. Since Rev has the tendency to aggregate also under normal physiological conditions [353], it is very likely that NPM1, by acting as a molecular chaperone, increases the Rev solubility and mobility during the import into and throughout the nucleus [260].

Furthermore, the interaction of synthetic peptide CIGB-300 and NPM1 was investigated. This peptide has the cell penetrating peptide Tat with R-rich motif. CIGB-300 has been described as a proapoptotic peptide with anti-proliferative activity *in vitro* and anti-tumor activity *in vivo* [262]. We observed in this study that only NPM1^{OD}, and with 5-fold lower affinity compare to NPM1^{FL}, associated with fCIGB-300 but not the other domains of NPM1. This higher affinity can be explained by an avidity effect that originates from core N-terminal domain and the dynamic

flexible tails similarly to the model proposed for nucleoplasmin interaction with histones [354]. Afterward, the molecular docking was used to make a model of CIGB-300-NPM1 interaction. There is an acidic region (A1) in NPM1^{OD} which has been recently shown to play a crucial role in the interaction with R-rich motifs of NPM1 binding proteins, such as p19ARF, ARF6, the ribosomal protein L5, and interestingly HIV-1 Rev [352]. A model of the complex between NPM1^{OD} and CIGB-300 provided insights into different sites for the association of the CIGB-300 peptide, especially the R-rich motif of the Tat contacting negative charges of the A1 region of NPM1^{OD}. Additionally, our displacement experiment with Rev indicates that CIGB-300 shares the same binding site on NPM1 and may act as an inhibitor of NPM1-Rev interaction. Most likely for the same reason we observed a reduced expression of viral production in HIV-1 infected cells treated with the CIGB-300 peptide. In addition, our displacement data have shown that the NPM1-US11 interaction was also modulated by CIGB-300. Thus, it is tempting to speculate that US11 and Rev, two functionally homologous viral proteins, share a similar binding site on NPM1 as suggested in this study for CIGB-300 [260].

Rev, US11, and CIGB-300 contain R-rich motif which acts as NLS by binding to the nuclear import receptors in nuclear translocation of viral proteins [355-358]. In addition to that, Rev, NPM1, and US11 are shuttling between the nucleus and the cytoplasm, and US11 C-terminus is critical for both nucleolar accumulations of US11 and its nucleocytoplasmic export [272,359]. On the other hand, nucleolar shuttling and accumulation of Rev requires interaction with NPM1 [253,358]. Thus, we hypothesize that, (i) R-rich motifs of viral proteins serve as NPM1 binding sites that facilitate their nuclear transport analogous to NLS-importin system, and (ii) NPM1 most likely acts as an auxiliary factor for R-rich motif-containing viral proteins, such as HIV-1 Rev and HSV-1 US11, and achieves their transport into different nuclear compartments and subnuclear domains, leading to nuclear egress of infectious viral particles (**Fig. 10**).

In conclusion, NPM1 seems to represent a key protein in viral infections that is hijacked by invading pathogens to facilitate infection. Unrevealing the association of nucleolar protein NPM1 with the viral proteins Rev and US11 may advance our understanding of HIV and HSV pathology and further imply that NPM1 can be exploited as a therapeutic target for infectious diseases.

In this study only the interaction of these proteins was investigated. The possible regulatory roles and molecular processes in which these proteins are involved during viral infection are still needed to be elucidated.

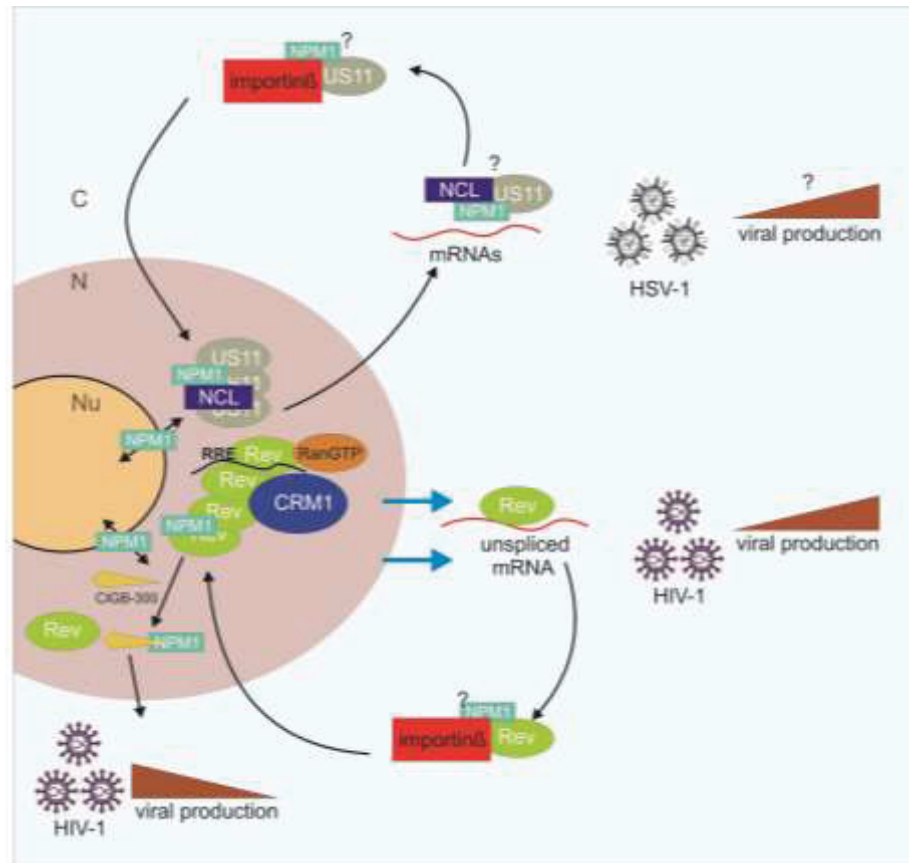


Figure 10. Model for the regulation of nuclear export and import of Rev and US11 viral proteins. After synthesis in the cytoplasm, Rev and US11 are rapidly transported to the nucleus through an interaction of their arginine-rich nuclear localization signal (NLS) with the nuclear import factor importin β . NPM1 may act as an auxiliary protein in this process. The same arginine-rich motif in Rev is responsible for binding to the Rev response element (RRE). The export of unspliced/partially spliced HIV-1 RNA occurs through a CRM1 dependent pathway. NPM1/Rev/CRM1/RanGTP complex cooperates with DDX3 RNA helicase for the export of unspliced/partially spliced HIV-1 RNAs from the nucleus through the nuclear pores. Unlike to HIV-1, the export of HSV-1 RNA is not CRM1 dependent. NCL is required for efficient nuclear egress of HSV-1 nucleocapsids and US11 is a structural protein which is cotransported with capsids, suggesting that NCL and most probably NPM1, through their interactions with US11, could participate in the transport of the viral particles. CIGB-300 shares the same binding site on NPM1 as Rev, and act as an inhibitor of NPM1-Rev interaction. Consequently, reduced expression of viral production in HIV-1 infected cells treated with the CIGB-300 peptide is observed. The question marks show unknown roles of Rev-NPM1 and US11-NPM1 complexes.

5.4 Nucleolin and FMRP interaction

As it was mentioned in introduction, nucleolin (NCL, C23), is multifunctional phosphoprotein predominately localized in nucleoli where it plays key roles in mRNA stability and translation, transcription, ribosome assembly and biogenesis, and microRNA processing. The prerequisite for this multifunctionality is interaction with multitude of other proteins. One of these proteins is the fragile X mental retardation protein (FMRP) which belongs to the RNA-binding, fragile X related protein (FXRP) family [283,360]. Absence of FMRP causes Fragile X syndrome (FXS) which is one of the most common forms of inherited mental retardation, which is associated with various

behavioral and physiological abnormalities, including social withdrawal, anxiety, intellectual disability, epilepsy, and autism [361-363]. **Chapter 6**, describes the physical and functional niches of FMRP by analyzing the subcellular distribution of endogenous FMRP and its complexes under native conditions in HeLa cells. This study demonstrated the presence of FMRP-containing complexes in the nucleus and the cytoplasm. These complexes contain nucleolin and other crucial factors for RNA processing and translational control. A direct interaction of FMRP with nucleolin was identified by RNase digestion experiments and interaction studies using purified proteins. We were further able to identify the responsible binding epitopes as the N-terminus of FMRP and the RGG domain of nucleolin. All to all, obtained results, (i) provided valuable insights into FMRP association with various nuclear and cytosolic fractions of variable molecular weights, (ii) uncovered a direct interaction between FMRP N-terminus and the RGG domain of nucleolin, and (iii) identified the existence of two functional NoLSs at the C-terminus of FMRP [188]. A potential functional role for the FMRP-nucleolin complex formation may be nucleocytoplasmic shuttling of nucleolin provided by the presence of functional NLS, NoLSs, and NESs existing in FMRP. These data open new perspectives of a possible mechanistic link between nucleolar ribosome biogenesis, RNA shuttling, and the cytoplasmic translational machinery that may be dependent on distinct functional subsets of FMRP-nucleolin complexes.

In conclusion, we proposed a novel mechanism by which a transient nucleolar localization of FMRP underlies a strong nucleocytoplasmic translocation, most likely in a complex with nucleolin and possibly ribosomes, in order to regulate translation of its target mRNAs.

6 References

1. Harvey JJ (1964). An Unidentified Virus Which Causes the Rapid Production of Tumours in Mice. *Nature* 204: 1104-1105.
2. Kirsten WH, Mayer LA (1967). Morphologic responses to a murine erythroblastosis virus. *J Natl Cancer Inst* 39: 311-335.
3. Cox AD, Der CJ (2010). Ras history: The saga continues. *Small GTPases* 1: 2-27.
4. Ellis RW, Defeo D, Shih TY, Gonda MA, Young HA, et al. (1981) The p21 src genes of Harvey and Kirsten sarcoma viruses originate from divergent members of a family of normal vertebrate genes. *Nature* 292: 506-511.
5. Goldfarb M, Shimizu K, Perucho M, Wigler M (1982). Isolation and preliminary characterization of a human transforming gene from T24 bladder carcinoma cells. *Nature* 296: 404-409.
6. Pulciani S, Santos E, Lauver AV, Long LK, Aaronson SA, et al. (1982). Oncogenes in solid human tumours. *Nature* 300: 539-542.
7. Shih C, Weinberg RA (1982). Isolation of a transforming sequence from a human bladder carcinoma cell line. *Cell* 29: 161-169.
8. Malumbres M, Barbacid M (2003). RAS oncogenes: the first 30 years. *Nat Rev Cancer* 3: 459-465.
9. Schmidt A, Hall A (2002). Guanine nucleotide exchange factors for Rho GTPases: turning on the switch. *Genes Dev* 16: 1587-1609.
10. Wennerberg K (2005). The Ras superfamily at a glance. *Journal of Cell Science* 118: 843-846.
11. Vetter IR, Wittinghofer A (2001). The guanine nucleotide-binding switch in three dimensions. *Science* 294: 1299-1304.
12. Rojas AM, Fuentes G, Rausell A, Valencia A (2012). The Ras protein superfamily: evolutionary tree and role of conserved amino acids. *J Cell Biol* 196: 189-201.
13. Mitin N, Rossman KL, Der CJ (2005). Signaling interplay in Ras superfamily function. *Curr Biol* 15: R563-574.
14. Zerial M, McBride H (2001). Rab proteins as membrane organizers. *Nature reviews Molecular cell biology* 2: 107-117.
15. Weis K (2003). Regulating access to the genome: nucleocytoplasmic transport throughout the cell cycle. *Cell* 112: 441-451.
16. Munro S (2005). The Arf-like GTPase Arl1 and its role in membrane traffic. *Biochem Soc Trans* 33: 601-605.
17. Nie Z, Hirsch DS, Randazzo PA (2003). Arf and its many interactors. *Curr Opin Cell Biol* 15: 396-404.
18. Wennerberg K, Der CJ (2004). Rho-family GTPases: it's not only Rac and Rho (and I like it). *J Cell Sci* 117: 1301-1312.
19. Narumiya S (1996). The small GTPase Rho: cellular functions and signal transduction. *J Biochem* 120: 215-228.
20. Wittinghofer Ae (2014). Ras Superfamily small G Proteins, Biology and Mechanism, Vol. 1 Springer, Chapter 14, pp 327-340.
21. Hall A (1990). The cellular functions of small GTP-binding proteins. *Science* 249: 635-640.
22. Takai Y, Sasaki T, Matozaki T (2001). Small GTP-binding proteins. *Physiol Rev* 81: 153-208.
23. Via A, Ferre F, Brannetti B, Valencia A, Helmer-Citterich M (2000). Three-dimensional view of the surface motif associated with the P-loop structure: cis and trans cases of convergent evolution. *J Mol Biol* 303: 455-465.
24. Bourne HR, Sanders DA, McCormick F (1990). The GTPase superfamily: a conserved switch for diverse cell functions. *Nature* 348: 125-132.
25. Barbacid M (1987). Ras genes. *Annual review of biochemistry* 56: 779-827.
26. Bos JL (1989). Ras oncogenes in human cancer: a review. *Cancer Res* 49: 4682-4689.
27. Farnsworth CL, Feig LA (1991). Dominant inhibitory mutations in the Mg(2+)-binding site of RasH prevent its activation by GTP. *Mol Cell Biol* 11: 4822-4829.
28. John J, Rensland H, Schlichting I, Vetter I, Borasio GD, et al. (1993). Kinetic and structural analysis of the Mg(2+)-binding site of the guanine nucleotide-binding protein p21H-ras. *J Biol Chem* 268: 923-929.
29. Feig LA (1999). Tools of the trade: use of dominant-inhibitory mutants of Ras-family GTPases. *Nat Cell Biol* 1: E25-27.
30. Spoerner M, Herrmann C, Vetter IR, Kalbitzer HR, Wittinghofer A (2001). Dynamic properties of the Ras switch I region and its importance for binding to effectors. *Proc Natl Acad Sci U S A* 98: 4944-4949.

31. Wittinghofer A, Franken SM, Scheidig AJ, Rensland H, Lautwein A, et al. (1993). Three-dimensional structure and properties of wild-type and mutant H-ras-encoded p21. *Ciba Found Symp* 176: 6-21.
32. Vetter IR (2001). The Guanine Nucleotide-Binding Switch in Three Dimensions. *Science* 294: 1299-1304.
33. Filchtinski D, Sharabi O, Ruppel A, Vetter IR, Herrmann C, et al. (2010). What makes Ras an efficient molecular switch: a computational, biophysical, and structural study of Ras-GDP interactions with mutants of Raf. *J Mol Biol* 399: 422-435.
34. Wittinghofer A, Vetter IR (2011). Structure-function relationships of the G domain, a canonical switch motif. *Annual review of biochemistry* 80: 943-971.
35. Lartey J, Lopez Bernal A (2009). RHO protein regulation of contraction in the human uterus. *Reproduction* 138: 407-424.
36. Ali BR, Wasmeier C, Lamoreux L, Strom M, Seabra MC (2004). Multiple regions contribute to membrane targeting of Rab GTPases. *J Cell Sci* 117: 6401-6412.
37. Karnoub AE, Weinberg RA (2008). Ras oncogenes: split personalities. *Nature reviews Molecular cell biology* 9: 517-531.
38. Lam BD, Hordijk PL (2013) The Rac1 hypervariable region in targeting and signaling: a tail of many stories. *Small GTPases* 4: 78-89.
39. Michaelson D, Silletti J, Murphy G, D'Eustachio P, Rush M, et al. (2001). Differential localization of Rho GTPases in live cells: regulation by hypervariable regions and RhoGDI binding. *J Cell Biol* 152: 111-126.
40. Heasman SJ, Ridley AJ (2008). Mammalian Rho GTPases: new insights into their functions from in vivo studies. *Nature reviews Molecular cell biology* 9: 690-701.
41. Mulloy JC, Cancelas JA, Filippi MD, Kalfa TA, Guo F, et al. (2010). Rho GTPases in hematopoiesis and hemopathies. *Blood* 115: 936-947.
42. Jaiswal M, Dvorsky R, Ahmadian MR (2013). Deciphering the molecular and functional basis of Dbl family proteins: a novel systematic approach toward classification of selective activation of the Rho family proteins. *J Biol Chem* 288: 4486-4500.
43. Boureux A, Vignal E, Faure S, Fort P (2007). Evolution of the Rho family of ras-like GTPases in eukaryotes. *Mol Biol Evol* 24: 203-216.
44. Hall A (2012). Rho family GTPases. *Biochem Soc Trans* 40: 1378-1382.
45. Briggs MW, Sacks DB (2003). IQGAP1 as signal integrator: Ca²⁺, calmodulin, Cdc42 and the cytoskeleton. *FEBS Lett* 542: 7-11.
46. Johnson M, Sharma M, Henderson BR (2009). IQGAP1 regulation and roles in cancer. *Cell Signal* 21: 1471-1478.
47. Kim H, White CD, Sacks DB (2011). IQGAP1 in microbial pathogenesis: Targeting the actin cytoskeleton. *FEBS Lett* 585: 723-729.
48. Noritake J, Watanabe T, Sato K, Wang S, Kaibuchi K (2005). IQGAP1: a key regulator of adhesion and migration. *J Cell Sci* 118: 2085-2092.
49. White CD, Brown MD, Sacks DB (2009). IQGAPs in cancer: a family of scaffold proteins underlying tumorigenesis. *FEBS Lett* 583: 1817-1824.
50. Foroutannejad S, Rohner N, Reimer M, Kwon G, Schober JM (2014). A novel role for IQGAP1 protein in cell motility through cell retraction. *Biochem Biophys Res Commun* 448: 39-44.
51. Yuan H, Zhang H, Wu X, Zhang Z, Du D, et al. (2009). Hepatocyte-specific deletion of Cdc42 results in delayed liver regeneration after partial hepatectomy in mice. *Hepatology* 49: 240-249.
52. Ridley AJ (2004). Rho proteins and cancer. *Breast Cancer Res Treat* 84: 13-19.
53. Titus B, Schwartz MA, Theodorescu D (2005). Rho proteins in cell migration and metastasis. *Crit Rev Eukaryot Gene Expr* 15: 103-114.
54. Jaffe AB, Hall A (2005). Rho GTPases: biochemistry and biology. *Annu Rev Cell Dev Biol* 21: 247-269.
55. Nobes CD, Hall A (1995). Rho, rac, and cdc42 GTPases regulate the assembly of multimolecular focal complexes associated with actin stress fibers, lamellipodia, and filopodia. *Cell* 81: 53-62.
56. Wherlock M, Mellor H (2002). The Rho GTPase family: a Racs to Wrchs story. *J Cell Sci* 115: 239-240.
57. Neudauer CL, Joberty G, Taxis N, Macara IG (1998). Distinct cellular effects and interactions of the Rho-family GTPase TC10. *Curr Biol* 8: 1151-1160.
58. Tao W, Pennica D, Xu L, Kalejta RF, Levine AJ (2001). Wrch-1, a novel member of the Rho gene family that is regulated by Wnt-1. *Genes Dev* 15: 1796-1807.
59. Aspenstrom P, Fransson A, Saras J (2004). Rho GTPases have diverse effects on the organization of the actin filament system. *Biochem J* 377: 327-337.

60. Govek EE, Newey SE, Van Aelst L (2005). The role of the Rho GTPases in neuronal development. *Genes Dev* 19: 1-49.
61. Toliaas KF, Hartwig JH, Ishihara H, Shibasaki Y, Cantley LC, et al. (2000). Type I alpha phosphatidylinositol-4-phosphate 5-kinase mediates Rac-dependent actin assembly. *Curr Biol* 10: 153-156.
62. Wang F, Herzmark P, Weiner OD, Srinivasan S, Servant G, et al. (2002). Lipid products of PI(3)Ks maintain persistent cell polarity and directed motility in neutrophils. *Nat Cell Biol* 4: 513-518.
63. Olson MF, Ashworth A, Hall A (1995). An essential role for Rho, Rac, and Cdc42 GTPases in cell cycle progression through G1. *Science* 269: 1270-1272.
64. Yamamoto M, Marui N, Sakai T, Morii N, Kozaki S, et al. (1993). ADP-ribosylation of the rhoA gene product by botulinum C3 exoenzyme causes Swiss 3T3 cells to accumulate in the G1 phase of the cell cycle. *Oncogene* 8: 1449-1455.
65. Jaffe AB, Hall A (2002). Rho GTPases in transformation and metastasis. *Adv Cancer Res* 84: 57-80.
66. Malliri A, Collard JG (2003). Role of Rho-family proteins in cell adhesion and cancer. *Curr Opin Cell Biol* 15: 583-589.
67. Vega FM, Ridley AJ (2008). Rho GTPases in cancer cell biology. *FEBS Lett* 582: 2093-2101.
68. Boettner B, Van Aelst L (2002). The role of Rho GTPases in disease development. *Gene* 286: 155-174.
69. Sahai E, Marshall CJ (2002). RHO-GTPases and cancer. *Nat Rev Cancer* 2: 133-142.
70. Nadif Kasri N, Van Aelst L (2008). Rho-linked genes and neurological disorders. *Pflugers Arch* 455: 787-797.
71. Ambruso DR, Knall C, Abell AN, Panepinto J, Kurkchubasche A, et al. (2000). Human neutrophil immunodeficiency syndrome is associated with an inhibitory Rac2 mutation. *Proc Natl Acad Sci U S A* 97: 4654-4659.
72. DeGeer J, Lamarche-Vane N (2013). Rho GTPases in neurodegeneration diseases. *Exp Cell Res* 319: 2384-2394.
73. Preudhomme C, Roumier C, Hildebrand MP, Dallery-Prudhomme E, Lantoine D, et al. (2000). Nonrandom 4p13 rearrangements of the RhoH/TTF gene, encoding a GTP-binding protein, in non-Hodgkin's lymphoma and multiple myeloma. *Oncogene* 19: 2023-2032.
74. Kawazu M, Ueno T, Kontani K, Ogita Y, Ando M, et al. (2013). Transforming mutations of RAC guanosine triphosphatases in human cancers. *Proc Natl Acad Sci U S A* 110: 3029-3034.
75. Watson IR, Li L, Cabeceiras PK, Mahdavi M, Gutschner T, et al. (2014). The RAC1 P29S hotspot mutation in melanoma confers resistance to pharmacological inhibition of RAF. *Cancer Res* 74: 4845-4852.
76. Caye A, Strullu M, Guidez F, Cassinat B, Gazal S, et al. (2015). Juvenile myelomonocytic leukemia displays mutations in components of the RAS pathway and the PRC2 network. *Nat Genet* 12.
77. Stieglitz E, Taylor-Weiner AN, Chang TY, Gelston LC, Wang YD, et al. (2015). The genomic landscape of juvenile myelomonocytic leukemia. *Nat Genet* 12.
78. Chang TY, Dvorak CC, Loh ML (2014). Bedside to bench in juvenile myelomonocytic leukemia: insights into leukemogenesis from a rare pediatric leukemia. *Blood* 124: 2487-2497.
79. Niemeyer CM (2014). RAS diseases in children. *Haematologica* 99: 1653-1662.
80. Freeman JL, Abo A, Lambeth JD (1996). Rac "insert region" is a novel effector region that is implicated in the activation of NADPH oxidase, but not PAK65. *J Biol Chem* 271: 19794-19801.
81. Roberts PJ, Mitin N, Keller PJ, Chenette EJ, Madigan JP, et al. (2008). Rho Family GTPase modification and dependence on CAAX motif-signaled posttranslational modification. *J Biol Chem* 283: 25150-25163.
82. Jaiswal M, Fansa EK, Dvorsky R, Ahmadian MR (2013). New insight into the molecular switch mechanism of human Rho family proteins: shifting a paradigm. *Biol Chem* 394: 89-95.
83. Dvorsky R, Ahmadian MR (2004). Always look on the bright site of Rho: structural implications for a conserved intermolecular interface. *EMBO Rep* 5: 1130-1136.
84. Cherfils J, Zeghouf M (2013). Regulation of small GTPases by GEFs, GAPs, and GDIs. *Physiol Rev* 93: 269-309.
85. Rossman KL, Sondek J (2005). Larger than Dbl: new structural insights into RhoA activation. *Trends Biochem Sci* 30: 163-165.
86. Scheffzek K, Ahmadian MR (2005). GTPase activating proteins: structural and functional insights 18 years after discovery. *Cell Mol Life Sci* 62: 3014-3038.
87. Csepanyi-Komi R, Levay M, Ligeti E (2012). Rho/RacGAPs: embarrass de richesse? *Small GTPases* 3: 178-182.

88. Garcia-Mata R, Boulter E, Burridge K (2011). The 'invisible hand': regulation of RHO GTPases by RHOGDIs. *Nature reviews Molecular cell biology* 12: 493-504.
89. DerMardirossian C, Bokoch GM (2005). GDIs: central regulatory molecules in Rho GTPase activation. *Trends Cell Biol* 15: 356-363.
90. Burridge K, Wennerberg K (2004). Rho and Rac take center stage. *Cell* 116: 167-179.
91. Bishop AL, Hall A (2000). Rho GTPases and their effector proteins. *Biochem J* 2: 241-255.
92. Mackay DJ, Hall A (1998). Rho GTPases. *J Biol Chem* 273: 20685-20688.
93. Ihara K, Muraguchi S, Kato M, Shimizu T, Shirakawa M, et al. (1998). Crystal structure of human RhoA in a dominantly active form complexed with a GTP analogue. *J Biol Chem* 273: 9656-9666.
94. Diekmann D, Nobes CD, Burbelo PD, Abo A, Hall A (1995). Rac GTPase interacts with GAPs and target proteins through multiple effector sites. *Embo J* 14: 5297-5305.
95. Burbelo PD, Drechsel D, Hall A (1995). A conserved binding motif defines numerous candidate target proteins for both Cdc42 and Rac GTPases. *J Biol Chem* 270: 29071-29074.
96. Flynn P, Mellor H, Palmer R, Panayotou G, Parker PJ (1998). Multiple interactions of PRK1 with RhoA. Functional assignment of the Hr1 repeat motif. *J Biol Chem* 273: 2698-2705.
97. Fujisawa K, Madaule P, Ishizaki T, Watanabe G, Bito H, et al. (1998). Different regions of Rho determine Rho-selective binding of different classes of Rho target molecules. *J Biol Chem* 273: 18943-18949.
98. Dvorsky R, Blumenstein L, Vetter IR, Ahmadian MR (2004). Structural insights into the interaction of ROCK1 with the switch regions of RhoA. *J Biol Chem* 279: 7098-7104.
99. Blumenstein L, Ahmadian MR (2004). Models of the cooperative mechanism for Rho effector recognition: implications for RhoA-mediated effector activation. *J Biol Chem* 279: 53419-53426.
100. Diekmann D, Abo A, Johnston C, Segal AW, Hall A (1994). Interaction of Rac with p67phox and regulation of phagocytic NADPH oxidase activity. *Science* 265: 531-533.
101. Lapouge K, Smith SJ, Walker PA, Gambelin SJ, Smerdon SJ, et al. (2000). Structure of the TPR domain of p67phox in complex with Rac.GTP. *Mol Cell* 6: 899-907.
102. Jaffer ZM, Chernoff J (2002). p21-activated kinases: three more join the Pak. *Int J Biochem Cell Biol* 34: 713-717.
103. Bokoch GM (2003). Biology of the p21-activated kinases. *Annual review of biochemistry* 72: 743-781.
104. Citi S, Guerrero D, Spadaro D, Shah J (2014). Epithelial junctions and Rho family GTPases: the zonular signalosome. *Small GTPases* 5: 1-15.
105. Good MC, Zalatan JG, Lim WA (2011). Scaffold proteins: hubs for controlling the flow of cellular information. *Science* 332: 680-686.
106. Brown MD, Sacks DB (2006). IQGAP1 in cellular signaling: bridging the GAP. *Trends Cell Biol* 16: 242-249.
107. Mateer SC, Wang N, Bloom GS (2003). IQGAPs: integrators of the cytoskeleton, cell adhesion machinery, and signaling networks. *Cell Motil Cytoskeleton* 55: 147-155.
108. Kornfeld K, Hom DB, Horvitz HR (1995). The *ksr-1* gene encodes a novel protein kinase involved in Ras-mediated signaling in *C. elegans*. *Cell* 83: 903-913.
109. Schaeffer HJ, Catling AD, Eblen ST, Collier LS, Krauss A, et al. (1998). MP1: a MEK binding partner that enhances enzymatic activation of the MAP kinase cascade. *Science* 281: 1668-1671.
110. Luttrell LM, Ferguson SS, Daaka Y, Miller WE, Maudsley S, et al. (1999). Beta-arrestin-dependent formation of beta2 adrenergic receptor-Src protein kinase complexes. *Science* 283: 655-661.
111. Brown MD, Sacks DB (2009). Protein scaffolds in MAP kinase signalling. *Cell Signal* 21: 462-469.
112. Inder KL, Lau C, Loo D, Chaudhary N, Goodall A, et al. (2009). Nucleophosmin and Nucleolin Regulate K-Ras Plasma Membrane Interactions and MAPK Signal Transduction. *Journal of Biological Chemistry* 284: 28410-28419.
113. Tian T, Plowman SJ, Parton RG, Kloog Y, Hancock JF (2010). Mathematical modeling of K-Ras nanocluster formation on the plasma membrane. *Biophys J* 99: 534-543.
114. Shalom-Feuerstein R, Plowman SJ, Rotblat B, Ariotti N, Tian T, et al. (2008). K-ras nanoclustering is subverted by overexpression of the scaffold protein galectin-3. *Cancer Res* 68: 6608-6616.
115. Belanis L, Plowman SJ, Rotblat B, Hancock JF, Kloog Y (2008). Galectin-1 is a novel structural component and a major regulator of h-ras nanoclusters. *Mol Biol Cell* 19: 1404-1414.
116. Machesky LM (1998). Cytokinesis: IQGAPs find a function. *Curr Biol* 8: R202-205.
117. Watanabe T, Wang S, Kaibuchi K (2015). IQGAPs as Key Regulators of Actin-cytoskeleton Dynamics. *Cell Struct Funct* 40: 69-77.

118. Smith JM, Hedman AC, Sacks DB (2015). IQGAPs choreograph cellular signaling from the membrane to the nucleus. *Trends Cell Biol* 25: 171-184.
119. Hedman AC, Smith JM, Sacks DB (2015). The biology of IQGAP proteins: beyond the cytoskeleton. *EMBO reports* 16: 427-446.
120. Wang S, Watanabe T, Noritake J, Fukata M, Yoshimura T, et al. (2007). IQGAP3, a novel effector of Rac1 and Cdc42, regulates neurite outgrowth. *J Cell Sci* 120: 567-577.
121. Brandt DT, Grosse R (2007). Get to grips: steering local actin dynamics with IQGAPs. *EMBO Rep* 8: 1019-1023.
122. Schmidt VA, Scudder L, Devoe CE, Bernardis A, Cupit LD, et al. (2003). IQGAP2 functions as a GTP-dependent effector protein in thrombin-induced platelet cytoskeletal reorganization. *Blood* 101: 3021-3028.
123. White CD, Khurana H, Gnatenko DV, Li Z, Odze RD, et al. (2010). IQGAP1 and IQGAP2 are reciprocally altered in hepatocellular carcinoma. *BMC Gastroenterol* 10: 125.
124. Ho YD, Joyal JL, Li Z, Sacks DB (1999). IQGAP1 integrates Ca²⁺/calmodulin and Cdc42 signaling. *J Biol Chem* 274: 464-470.
125. Brill S, Li S, Lyman CW, Church DM, Wasmuth JJ, et al. (1996). The Ras GTPase-activating-protein-related human protein IQGAP2 harbors a potential actin binding domain and interacts with calmodulin and Rho family GTPases. *Mol Cell Biol* 16: 4869-4878.
126. Scheffzek K, Ahmadian MR, Wittinghofer A (1998). GTPase-activating proteins: helping hands to complement an active site. *Trends in biochemical sciences* 23: 257-262.
127. Ahmadian MR, Stege P, Scheffzek K, Wittinghofer A (1997). Confirmation of the arginine-finger hypothesis for the GAP-stimulated GTP-hydrolysis reaction of Ras. *Nat Struct Biol* 4: 686-689.
128. Noritake J, Fukata M, Sato K, Nakagawa M, Watanabe T, et al. (2004). Positive role of IQGAP1, an effector of Rac1, in actin-meshwork formation at sites of cell-cell contact. *Mol Biol Cell* 15: 1065-1076.
129. Jeong HW, Li Z, Brown MD, Sacks DB (2007). IQGAP1 binds Rap1 and modulates its activity. *J Biol Chem* 282: 20752-20762.
130. Ren JG, Li Z, Sacks DB (2007). IQGAP1 modulates activation of B-Raf. *Proc Natl Acad Sci U S A* 104: 10465-10469.
131. Roy M, Li Z, Sacks DB (2005). IQGAP1 is a scaffold for mitogen-activated protein kinase signaling. *Mol Cell Biol* 25: 7940-7952.
132. Weissbach L, Settleman J, Kalady MF, Snijders AJ, Murthy AE, et al. (1994). Identification of a human rasGAP-related protein containing calmodulin-binding motifs. *J Biol Chem* 269: 20517-20521.
133. Fukata M, Kuroda S, Fujii K, Nakamura T, Shoji I, et al. (1997). Regulation of cross-linking of actin filament by IQGAP1, a target for Cdc42. *J Biol Chem* 272: 29579-29583.
134. Bashour AM, Fullerton AT, Hart MJ, Bloom GS (1997). IQGAP1, a Rac- and Cdc42-binding protein, directly binds and cross-links microfilaments. *J Cell Biol* 137: 1555-1566.
135. Abel AM, Schuldt KM, Rajasekaran K, Hwang D, Riese MJ, et al. (2015). IQGAP1: insights into the function of a molecular puppeteer. *Mol Immunol* 65: 336-349.
136. Smith MJ, Hardy WR, Li GY, Goudreau M, Hersch S, et al. (2010). The PTB domain of ShcA couples receptor activation to the cytoskeletal regulator IQGAP1. *Embo J* 29: 884-896.
137. Roy M, Li Z, Sacks DB (2004). IQGAP1 binds ERK2 and modulates its activity. *J Biol Chem* 279: 17329-17337.
138. Andrews WJ, Bradley CA, Hamilton E, Daly C, Mallon T, et al. (2012). A calcium-dependent interaction between calmodulin and the calponin homology domain of human IQGAP1. *Mol Cell Biochem* 371: 217-223.
139. Mbele GO, Deloulme JC, Gentil BJ, Delphin C, Ferro M, et al. (2002). The zinc- and calcium-binding S100B interacts and co-localizes with IQGAP1 during dynamic rearrangement of cell membranes. *J Biol Chem* 277: 49998-50007.
140. Fukata M, Watanabe T, Noritake J, Nakagawa M, Yamaga M, et al. (2002). Rac1 and Cdc42 capture microtubules through IQGAP1 and CLIP-170. *Cell* 109: 873-885.
141. Kuroda S, Fukata M, Nakagawa M, Fujii K, Nakamura T, et al. (1998). Role of IQGAP1, a target of the small GTPases Cdc42 and Rac1, in regulation of E-cadherin-mediated cell-cell adhesion. *Science* 281: 832-835.
142. Li Z, Kim SH, Higgins JM, Brenner MB, Sacks DB (1999). IQGAP1 and calmodulin modulate E-cadherin function. *J Biol Chem* 274: 37885-37892.

143. Watanabe T, Wang S, Noritake J, Sato K, Fukata M, et al. (2004). Interaction with IQGAP1 links APC to Rac1, Cdc42, and actin filaments during cell polarization and migration. *Dev Cell* 7: 871-883.
144. Hart MJ, Callow MG, Souza B, Polakis P (1996). IQGAP1, a calmodulin-binding protein with a rasGAP-related domain, is a potential effector for cdc42Hs. *The EMBO journal* 15: 2997-3005.
145. Kuroda S, Fukata M, Kobayashi K, Nakafuku M, Nomura N, et al. (1996). Identification of IQGAP as a putative target for the small GTPases, Cdc42 and Rac1. *The Journal of biological chemistry* 271: 23363-23367.
146. Izumi G, Sakisaka T, Baba T, Tanaka S, Morimoto K, et al. (2004). Endocytosis of E-cadherin regulated by Rac and Cdc42 small G proteins through IQGAP1 and actin filaments. *The Journal of cell biology* 166: 237-248.
147. Kholmanskikh SS, Koeller HB, Wynshaw-Boris A, Gomez T, Letourneau PC, et al. (2006). Calcium-dependent interaction of Lis1 with IQGAP1 and Cdc42 promotes neuronal motility. *Nat Neurosci* 9: 50-57.
148. Brown MD, Bry L, Li Z, Sacks DB (2007). IQGAP1 regulates Salmonella invasion through interactions with actin, Rac1, and Cdc42. *The Journal of biological chemistry* 282: 30265-30272.
149. Sakurai-Yageta M, Recchi C, Le Dez G, Sibarita JB, Daviet L, et al. (2008). The interaction of IQGAP1 with the excyst complex is required for tumor cell invasion downstream of Cdc42 and RhoA. *The Journal of cell biology* 181: 985-998.
150. McCallum SJ, Wu WJ, Cerione RA (1996). Identification of a putative effector for Cdc42Hs with high sequence similarity to the RasGAP-related protein IQGAP1 and a Cdc42Hs binding partner with similarity to IQGAP2. *J Biol Chem* 271: 21732-21737.
151. Osman M (2010). An emerging role for IQGAP1 in regulating protein traffic. *ScientificWorldJournal* 10: 944-953.
152. Mataraza JM, Briggs MW, Li Z, Frank R, Sacks DB (2003). Identification and characterization of the Cdc42-binding site of IQGAP1. *Biochem Biophys Res Commun* 305: 315-321.
153. Ridley AJ, Schwartz MA, Burridge K, Firtel RA, Ginsberg MH, et al. (2003). Cell migration: integrating signals from front to back. *Science* 302: 1704-1709.
154. Mataraza JM, Briggs MW, Li Z, Entwistle A, Ridley AJ, et al. (2003). IQGAP1 promotes cell motility and invasion. *J Biol Chem* 278: 41237-41245.
155. Jacquemet G, Green DM, Bridgewater RE, von Kriegsheim A, Humphries MJ, et al. (2013). RCP-driven alpha5beta1 recycling suppresses Rac and promotes RhoA activity via the RacGAP1-IQGAP1 complex. *J Cell Biol* 202: 917-935.
156. Jacquemet G, Morgan MR, Byron A, Humphries JD, Choi CK, et al. (2013). Rac1 is deactivated at integrin activation sites through an IQGAP1-filamin-A-RacGAP1 pathway. *J Cell Sci* 126: 4121-4135.
157. Carmon KS, Gong X, Yi J, Thomas A, Liu Q (2014). RSPO-LGR4 functions via IQGAP1 to potentiate Wnt signaling. *Proc Natl Acad Sci U S A* 111: 17.
158. Liu F, Schaphorst KL, Verin AD, Jacobs K, Birukova A, et al. (2002). Hepatocyte growth factor enhances endothelial cell barrier function and cortical cytoskeletal rearrangement: potential role of glycogen synthase kinase-3beta. *FASEB J* 16: 950-962.
159. Tian Y, Tian X, Gawlak G, O'Donnell JJ, 3rd, Sacks DB, et al. (2014). IQGAP1 regulates endothelial barrier function via EB1-cortactin cross talk. *Mol Cell Biol* 34: 3546-3558.
160. Li Z, McNulty DE, Marler KJ, Lim L, Hall C, et al. (2005). IQGAP1 promotes neurite outgrowth in a phosphorylation-dependent manner. *J Biol Chem* 280: 13871-13878.
161. Kimura T, Yamaoka M, Taniguchi S, Okamoto M, Takei M, et al. (2013). Activated Cdc42-bound IQGAP1 determines the cellular endocytic site. *Mol Cell Biol* 33: 4834-4843.
162. Bhattacharya M, Sundaram A, Kudo M, Farmer J, Ganesan P, et al. (2014). IQGAP1-dependent scaffold suppresses RhoA and inhibits airway smooth muscle contraction. *J Clin Invest* 124: 4895-4898.
163. Wu Y, Tao Y, Chen Y, Xu W (2012). RhoC regulates the proliferation of gastric cancer cells through interaction with IQGAP1. *PLoS ONE* 7: 7.
164. Clark EA, Golub TR, Lander ES, Hynes RO (2000). Genomic analysis of metastasis reveals an essential role for RhoC. *Nature* 406: 532-535.
165. Zhang B, Chernoff J, Zheng Y (1998). Interaction of Rac1 with GTPase-activating proteins and putative effectors. A comparison with Cdc42 and RhoA. *J Biol Chem* 273: 8776-8782.
166. Elliott SF, Allen G, Timson DJ (2012). Biochemical analysis of the interactions of IQGAP1 C-terminal domain with CDC42. *World J Biol Chem* 3: 53-60.

167. Kurella VB, Richard JM, Parke CL, Lecour LF, Jr., Bellamy HD, et al. (2009). Crystal structure of the GTPase-activating protein-related domain from IQGAP1. *J Biol Chem* 284: 14857-14865.
168. Rittinger K, Walker PA, Eccleston JF, Nurmahomed K, Owen D, et al. (1997). Crystal structure of a small G protein in complex with the GTPase-activating protein rhoGAP. *Nature* 388: 693-697.
169. Nassar N, Hoffman GR, Manor D, Clardy JC, Cerione RA (1998). Structures of Cdc42 bound to the active and catalytically compromised forms of Cdc42GAP. *Nat Struct Biol* 5: 1047-1052.
170. Briggs MW, Li Z, Sacks DB (2002). IQGAP1-mediated stimulation of transcriptional co-activation by beta-catenin is modulated by calmodulin. *J Biol Chem* 277: 7453-7465.
171. Owen D, Campbell LJ, Littlefield K, Evetts KA, Li Z, et al. (2008). The IQGAP1-Rac1 and IQGAP1-Cdc42 interactions: interfaces differ between the complexes. *J Biol Chem* 283: 1692-1704.
172. Storck S, Shukla M, Dimitrov S, Bouvet P (2007). Functions of the histone chaperone nucleolin in diseases. *Subcell Biochem* 41: 125-144.
173. Mongelard F, Bouvet P (2007). Nucleolin: a multiFACeTed protein. *Trends Cell Biol* 17: 80-86.
174. Abdelmohsen K, Gorospe M (2012) RNA-binding protein nucleolin in disease. *RNA Biol* 9: 799-808.
175. Yun J-P, Chew EC, Liew C-T, Chan JYH, Jin M-L, et al. (2003). Nucleophosmin/B23 is a proliferate shuttle protein associated with nuclear matrix. *Journal of Cellular Biochemistry* 90: 1140-1148.
176. Lindstrom MS (2011). NPM1/B23: A Multifunctional Chaperone in Ribosome Biogenesis and Chromatin Remodeling. *Biochem Res Int* 2011: 195209.
177. Okuwaki M, Matsumoto K, Tsujimoto M, Nagata K (2001). Function of nucleophosmin/B23, a nucleolar acidic protein, as a histone chaperone. *FEBS Lett* 506: 272-276.
178. Grisendi S, Mecucci C, Falini B, Pandolfi PP (2006). Nucleophosmin and cancer. *Nature Reviews Cancer* 6: 493-505.
179. Hovanessian AG, Soundaramourty C, El Khoury D, Nondier I, Svab J, et al. (2010). Surface expressed nucleolin is constantly induced in tumor cells to mediate calcium-dependent ligand internalization. *PLoS ONE* 5: e15787.
180. Chan PK, Aldrich M, Cook RG, Busch H (1986). Amino acid sequence of protein B23 phosphorylation site. *J Biol Chem* 261: 1868-1872.
181. Leitinger N, Wesierska-Gadek J (1993). ADP-ribosylation of nucleolar proteins in HeLa tumor cells. *J Cell Biochem* 52: 153-158.
182. Galzio R, Rosati F, Benedetti E, Cristiano L, Aldi S, et al. (2012). Glycosylated nucleolin as marker for human gliomas. *J Cell Biochem* 113: 571-579.
183. Das S, Cong R, Shandilya J, Senapati P, Moindrot B, et al. (2013). Characterization of nucleolin K88 acetylation defines a new pool of nucleolin colocalizing with pre-mRNA splicing factors. *FEBS Lett* 587: 417-424.
184. Regnard C, Desbruyeres E, Huet JC, Beauvallet C, Pernollet JC, et al. (2000). Polyglutamylation of nucleosome assembly proteins. *J Biol Chem* 275: 15969-15976.
185. Swaminathan V, Kishore AH, Febitha KK, Kundu TK (2005). Human histone chaperone nucleophosmin enhances acetylation-dependent chromatin transcription. *Mol Cell Biol* 25: 7534-7545.
186. Okuwaki M (2007). The Structure and Functions of NPM1/Nucleophosmin/B23, a Multifunctional Nucleolar Acidic Protein. *Journal of Biochemistry* 143: 441-448.
187. Ginisty H, Sicard H, Roger B, Bouvet P (1999). Structure and functions of nucleolin. *J Cell Sci* 112: 761-772.
188. Taha MS, Nouri K, Milroy LG, Moll JM, Herrmann C, et al. (2014). Subcellular fractionation and localization studies reveal a direct interaction of the fragile X mental retardation protein (FMRP) with nucleolin. *PLoS ONE* 9: e91465.
189. Li YP, Busch RK, Valdez BC, Busch H (1996). C23 interacts with B23, a putative nucleolar-localization-signal-binding protein. *Eur J Biochem* 237: 153-158.
190. Kuo ML, den Besten W, Thomas MC, Sherr CJ (2008). Arf-induced turnover of the nucleolar nucleophosmin-associated SUMO-2/3 protease Senp3. *Cell Cycle* 7: 3378-3387.
191. Colombo E, Bonetti P, Lazzerini Denchi E, Martinelli P, Zamponi R, et al. (2005). Nucleophosmin is required for DNA integrity and p19Arf protein stability. *Mol Cell Biol* 25: 8874-8886.
192. Yun C, Wang Y, Mukhopadhyay D, Backlund P, Kolli N, et al. (2008). Nucleolar protein B23/nucleophosmin regulates the vertebrate SUMO pathway through SENP3 and SENP5 proteases. *J Cell Biol* 183: 589-595.
193. Bonetti P, Davoli T, Sironi C, Amati B, Pelicci PG, et al. (2008). Nucleophosmin and its AML-associated mutant regulate c-Myc turnover through Fbw7 gamma. *J Cell Biol* 182: 19-26.

194. Xiao J, Zhang Z, Chen GG, Zhang M, Ding Y, et al. (2009). Nucleophosmin/B23 interacts with p21WAF1/CIP1 and contributes to its stability. *Cell Cycle* 8: 889-895.
195. Colombo E, Alcalay M, Pelicci PG (2011). Nucleophosmin and its complex network: a possible therapeutic target in hematological diseases. *Oncogene* 30: 2595-2609.
196. Valdez BC, Perlaky L, Henning D, Saijo Y, Chan PK, et al. (1994). Identification of the nuclear and nucleolar localization signals of the protein p120. Interaction with translocation protein B23. *J Biol Chem* 269: 23776-23783.
197. Lindstrom MS (2012). Elucidation of motifs in ribosomal protein S9 that mediate its nucleolar localization and binding to NPM1/nucleophosmin. *PLoS ONE* 7: 20.
198. Duan Z, Chen J, Xu H, Zhu J, Li Q, et al. (2014). The nucleolar phosphoprotein B23 targets Newcastle disease virus matrix protein to the nucleoli and facilitates viral replication. *Virology* 452-453: 212-222.
199. Zoughlami Y, van Stalborgh AM, van Hennik PB, Hordijk PL (2013). Nucleophosmin1 is a negative regulator of the small GTPase Rac1. *PLoS ONE* 8: e68477.
200. Ma Z, Kanai M, Kawamura K, Kaibuchi K, Ye K, et al. (2006). Interaction between ROCK II and nucleophosmin/B23 in the regulation of centrosome duplication. *Mol Cell Biol* 26: 9016-9034.
201. Khurts S, Masutomi K, Delgermaa L, Arai K, Oishi N, et al. (2004). Nucleolin interacts with telomerase. *J Biol Chem* 279: 51508-51515.
202. Bhatt P, d'Avout C, Kane NS, Borowiec JA, Saxena A (2012). Specific domains of nucleolin interact with Hdm2 and antagonize Hdm2-mediated p53 ubiquitination. *Febs J* 279: 370-383.
203. Legrand D, Vigie K, Said EA, Ellass E, Masson M, et al. (2004). Surface nucleolin participates in both the binding and endocytosis of lactoferrin in target cells. *Eur J Biochem* 271: 303-317.
204. Hovanessian AG (2006). Midkine, a cytokine that inhibits HIV infection by binding to the cell surface expressed nucleolin. *Cell Res* 16: 174-181.
205. Said EA, Courty J, Svab J, Delbe J, Krust B, et al. (2005). Pleiotrophin inhibits HIV infection by binding the cell surface-expressed nucleolin. *Febs J* 272: 4646-4659.
206. Stepanova V, Lebedeva T, Kuo A, Yarovoi S, Tkachuk S, et al. (2008). Nuclear translocation of urokinase-type plasminogen activator. *Blood* 112: 100-110.
207. Feuerstein N, Chan PK, Mond JJ (1988). Identification of numatrin, the nuclear matrix protein associated with induction of mitogenesis, as the nucleolar protein B23. Implication for the role of the nucleolus in early transduction of mitogenic signals. *J Biol Chem* 263: 10608-10612.
208. Grisendi S, Bernardi R, Rossi M, Cheng K, Khandker L, et al. (2005). Role of nucleophosmin in embryonic development and tumorigenesis. *Nature* 437: 147-153.
209. Tanaka M, Sasaki H, Kino I, Sugimura T, Terada M (1992). Genes preferentially expressed in embryo stomach are predominantly expressed in gastric cancer. *Cancer Res* 52: 3372-3377.
210. Nozawa Y, Van Belzen N, Van der Made AC, Dinjens WN, Bosman FT (1996). Expression of nucleophosmin/B23 in normal and neoplastic colorectal mucosa. *J Pathol* 178: 48-52.
211. Shields LB, Gercel-Taylor C, Yashar CM, Wan TC, Katsanis WA, et al. (1997). Induction of immune responses to ovarian tumor antigens by multiparity. *J Soc Gynecol Investig* 4: 298-304.
212. Subong EN, Shue MJ, Epstein JI, Briggman JV, Chan PK, et al. (1999). Monoclonal antibody to prostate cancer nuclear matrix protein (PRO:4-216) recognizes nucleophosmin/B23. *Prostate* 39: 298-304.
213. Falini B, Mecucci C, Tiacci E, Alcalay M, Rosati R, et al. (2005). Cytoplasmic nucleophosmin in acute myelogenous leukemia with a normal karyotype. *N Engl J Med* 352: 254-266.
214. Ahn JY, Liu X, Cheng D, Peng J, Chan PK, et al. (2005). Nucleophosmin/B23, a nuclear PI(3,4,5)P(3) receptor, mediates the antiapoptotic actions of NGF by inhibiting CAD. *Mol Cell* 18: 435-445.
215. Qing Y, Yingmao G, Lujun B, Shaoling L (2008). Role of Npm1 in proliferation, apoptosis and differentiation of neural stem cells. *J Neurol Sci* 266: 131-137.
216. Bertwistle D, Sugimoto M, Sherr CJ (2004). Physical and functional interactions of the Arf tumor suppressor protein with nucleophosmin/B23. *Mol Cell Biol* 24: 985-996.
217. Koike A, Nishikawa H, Wu W, Okada Y, Venkiteraman AR, et al. (2010). Recruitment of phosphorylated NPM1 to sites of DNA damage through RNF8-dependent ubiquitin conjugates. *Cancer Res* 70: 6746-6756.
218. Shandilya J, Swaminathan V, Gadad SS, Choudhari R, Kodaganur GS, et al. (2009). Acetylated NPM1 localizes in the nucleoplasm and regulates transcriptional activation of genes implicated in oral cancer manifestation. *Mol Cell Biol* 29: 5115-5127.

219. Wang Z, Gall JM, Bonegio R, Havasi A, Illanes K, et al. (2013). Nucleophosmin, a critical Bax cofactor in ischemia-induced cell death. *Mol Cell Biol* 33: 1916-1924.
220. Christian S, Pilch J, Akerman ME, Porkka K, Laakkonen P, et al. (2003). Nucleolin expressed at the cell surface is a marker of endothelial cells in angiogenic blood vessels. *J Cell Biol* 163: 871-878.
221. Srivastava M, Pollard HB (1999). Molecular dissection of nucleolin's role in growth and cell proliferation: new insights. *FASEB J* 13: 1911-1922.
222. Fogal V, Sugahara KN, Ruoslahti E, Christian S (2009). Cell surface nucleolin antagonist causes endothelial cell apoptosis and normalization of tumor vasculature. *Angiogenesis* 12: 91-100.
223. Otake Y, Sengupta TK, Bandyopadhyay S, Spicer EK, Fernandes DJ (2005). Retinoid-induced apoptosis in HL-60 cells is associated with nucleolin down-regulation and destabilization of Bcl-2 mRNA. *Mol Pharmacol* 67: 319-326.
224. Otake Y, Soundararajan S, Sengupta TK, Kio EA, Smith JC, et al. (2007). Overexpression of nucleolin in chronic lymphocytic leukemia cells induces stabilization of bcl2 mRNA. *Blood* 109: 3069-3075.
225. Caudle WM, Kitsou E, Li J, Bradner J, Zhang J (2009). A role for a novel protein, nucleolin, in Parkinson's disease. *Neurosci Lett* 459: 11-15.
226. Hirano M, Kaneko S, Yamashita T, Luo H, Qin W, et al. (2003). Direct interaction between nucleolin and hepatitis C virus NS5B. *J Biol Chem* 278: 5109-5115.
227. Shimakami T, Honda M, Kusakawa T, Murata T, Shimotohno K, et al. (2006). Effect of hepatitis C virus (HCV) NS5B-nucleolin interaction on HCV replication with HCV subgenomic replicon. *J Virol* 80: 3332-3340.
228. Strang BL, Sinigalia E, Silva LA, Coen DM, Loregian A (2009). Analysis of the association of the human cytomegalovirus DNA polymerase subunit UL44 with the viral DNA replication factor UL84. *J Virol* 83: 7581-7589.
229. Sagou K, Uema M, Kawaguchi Y (2010). Nucleolin is required for efficient nuclear egress of herpes simplex virus type 1 nucleocapsids. *J Virol* 84: 2110-2121.
230. Greco A, Arata L, Soler E, Gaume X, Coute Y, et al. (2012). Nucleolin interacts with US11 protein of herpes simplex virus 1 and is involved in its trafficking. *J Virol* 86: 1449-1457.
231. Strang BL, Bender BJ, Sharma M, Pesola JM, Sanders RL, et al. (2012). A mutation deleting sequences encoding the amino terminus of human cytomegalovirus UL84 impairs interaction with UL44 and capsid localization. *J Virol* 86: 11066-11077.
232. Lymberopoulos MH, Pearson A (2007). Involvement of UL24 in herpes-simplex-virus-1-induced dispersal of nucleolin. *Virology* 363: 397-409.
233. Bertrand L, Pearson A (2008). The conserved N-terminal domain of herpes simplex virus 1 UL24 protein is sufficient to induce the spatial redistribution of nucleolin. *J Gen Virol* 89: 1142-1151.
234. Bertrand L, Leiva-Torres GA, Hyjazie H, Pearson A (2010). Conserved residues in the UL24 protein of herpes simplex virus 1 are important for dispersal of the nucleolar protein nucleolin. *J Virol* 84: 109-118.
235. Diaz JJ, Dodon MD, Schaerer-Uthurralt N, Simonin D, Kindbeiter K, et al. (1996). Post-transcriptional transactivation of human retroviral envelope glycoprotein expression by herpes simplex virus Us11 protein. *Nature* 379: 273-277.
236. Izumi RE, Valdez B, Banerjee R, Srivastava M, Dasgupta A (2001). Nucleolin stimulates viral internal ribosome entry site-mediated translation. *Virus Res* 76: 17-29.
237. Barel M, Meibom K, Charbit A (2010). Nucleolin, a shuttle protein promoting infection of human monocytes by *Francisella tularensis*. *PLoS ONE* 5: 0014193.
238. Barel M, Hovanessian AG, Meibom K, Briand JP, Dupuis M, et al. (2008). A novel receptor - ligand pathway for entry of *Francisella tularensis* in monocyte-like THP-1 cells: interaction between surface nucleolin and bacterial elongation factor Tu. *BMC Microbiol* 8: 1471-2180.
239. Suganuma M, Watanabe T, Yamaguchi K, Takahashi A, Fujiki H (2012). Human gastric cancer development with TNF-alpha-inducing protein secreted from *Helicobacter pylori*. *Cancer Lett* 322: 133-138.
240. Watanabe T, Hirano K, Takahashi A, Yamaguchi K, Beppu M, et al. (2010). Nucleolin on the cell surface as a new molecular target for gastric cancer treatment. *Biol Pharm Bull* 33: 796-803.
241. Tayyari F, Marchant D, Moraes TJ, Duan W, Mastrangelo P, et al. (2011). Identification of nucleolin as a cellular receptor for human respiratory syncytial virus. *Nat Med* 17: 1132-1135.
242. Sinclair JF, O'Brien AD (2002). Cell surface-localized nucleolin is a eukaryotic receptor for the adhesin intimin-gamma of enterohemorrhagic *Escherichia coli* O157:H7. *J Biol Chem* 277: 2876-2885.

243. Bevington JM, Needham PG, Verrill KC, Collaco RF, Basrur V, et al. (2007). Adeno-associated virus interactions with B23/Nucleophosmin: identification of sub-nucleolar virion regions. *Virology* 357: 102-113.
244. Samad MA, Okuwaki M, Haruki H, Nagata K (2007). Physical and functional interaction between a nucleolar protein nucleophosmin/B23 and adenovirus basic core proteins. *FEBS Lett* 581: 3283-3288.
245. Matthews DA (2001). Adenovirus protein V induces redistribution of nucleolin and B23 from nucleolus to cytoplasm. *J Virol* 75: 1031-1038.
246. Liu CD, Chen YL, Min YL, Zhao B, Cheng CP, et al. (2012). The nuclear chaperone nucleophosmin escorts an Epstein-Barr Virus nuclear antigen to establish transcriptional cascades for latent infection in human B cells. *PLoS Pathog* 8: 13.
247. Malik-Soni N, Frappier L (2014). Nucleophosmin contributes to the transcriptional activation function of the Epstein-Barr virus EBNA1 protein. *J Virol* 88: 2323-2326.
248. Lee SJ, Shim HY, Hsieh A, Min JY, Jung G (2009). Hepatitis B virus core interacts with the host cell nucleolar protein, nucleophosmin 1. *J Microbiol* 47: 746-752.
249. Jeong H, Cho MH, Park SG, Jung G (2014). Interaction between nucleophosmin and HBV core protein increases HBV capsid assembly. *FEBS Lett* 588: 851-858.
250. Mai RT, Yeh TS, Kao CF, Sun SK, Huang HH, et al. (2006). Hepatitis C virus core protein recruits nucleolar phosphoprotein B23 and coactivator p300 to relieve the repression effect of transcriptional factor YY1 on B23 gene expression. *Oncogene* 25: 448-462.
251. Huang WH, Yung BY, Syu WJ, Lee YH (2001). The nucleolar phosphoprotein B23 interacts with hepatitis delta antigens and modulates the hepatitis delta virus RNA replication. *J Biol Chem* 276: 25166-25175.
252. Lymberopoulos MH, Bourget A, Abdeljelil NB, Pearson A (2011). Involvement of the UL24 protein in herpes simplex virus 1-induced dispersal of B23 and in nuclear egress. *Virology* 412: 341-348.
253. Fankhauser C, Izaurralde E, Adachi Y, Wingfield P, Laemmli UK (1991). Specific complex of human immunodeficiency virus type 1 rev and nucleolar B23 proteins: dissociation by the Rev response element. *Mol Cell Biol* 11: 2567-2575.
254. Marasco WA, Szilvay AM, Kalland KH, Helland DG, Reyes HM, et al. (1994). Spatial association of HIV-1 tat protein and the nucleolar transport protein B23 in stably transfected Jurkat T-cells. *Arch Virol* 139: 133-154.
255. Li YP (1997). Protein B23 is an important human factor for the nucleolar localization of the human immunodeficiency virus protein Tat. *J Virol* 71: 4098-4102.
256. Adachi Y, Copeland TD, Hatanaka M, Oroszlan S (1993). Nucleolar targeting signal of Rex protein of human T-cell leukemia virus type I specifically binds to nucleolar shuttle protein B-23. *J Biol Chem* 268: 13930-13934.
257. Tsuda Y, Mori Y, Abe T, Yamashita T, Okamoto T, et al. (2006). Nucleolar protein B23 interacts with Japanese encephalitis virus core protein and participates in viral replication. *Microbiol Immunol* 50: 225-234.
258. Sarek G, Jarviluoma A, Moore HM, Tojkander S, Vartia S, et al. (2010). Nucleophosmin phosphorylation by v-cyclin-CDK6 controls KSHV latency. *PLoS Pathog* 6: 1000818.
259. Miyazaki Y, Takamatsu T, Nosaka T, Fujita S, Martin TE, et al. (1995). The cytotoxicity of human immunodeficiency virus type 1 Rev: implications for its interaction with the nucleolar protein B23. *Exp Cell Res* 219: 93-101.
260. Nouri K, J. MM, Milroy LG, Hain A, Dvorsky R, et al. (2015). Biophysical Characterization of Nucleophosmin Interactions with Human Immunodeficiency Virus Rev and Herpes Simplex Virus US11. *PLoS ONE* (in press).
261. Perea SE, Reyes O, Puchades Y, Mendoza O, Vispo NS, et al. (2004). Antitumor effect of a novel proapoptotic peptide that impairs the phosphorylation by the protein kinase 2 (casein kinase 2). *Cancer Res* 64: 7127-7129.
262. Perea SE, Reyes O, Baladron I, Perera Y, Farina H, et al. (2008). CIGB-300, a novel proapoptotic peptide that impairs the CK2 phosphorylation and exhibits anticancer properties both in vitro and in vivo. *Molecular and Cellular Biochemistry* 316: 163-167.
263. Rodriguez-Ulloa A, Ramos Y, Gil J, Perera Y, Castellanos-Serra L, et al. (2010). Proteomic profile regulated by the anticancer peptide CIGB-300 in non-small cell lung cancer (NSCLC) cells. *J Proteome Res* 9: 5473-5483.

264. Lussignol M, Queval C, Bernet-Camard MF, Cotte-Laffitte J, Beau I, et al. (2013). The herpes simplex virus 1 Us11 protein inhibits autophagy through its interaction with the protein kinase PKR. *J Virol* 87: 859-871.
265. Khoo D, Perez C, Mohr I (2002). Characterization of RNA determinants recognized by the arginine- and proline-rich region of Us11, a herpes simplex virus type 1-encoded double-stranded RNA binding protein that prevents PKR activation. *J Virol* 76: 11971-11981.
266. Dayton AI, Sodroski JG, Rosen CA, Goh WC, Haseltine WA (1986). The trans-activator gene of the human T cell lymphotropic virus type III is required for replication. *Cell* 44: 941-947.
267. Terwilliger E, Burghoff R, Sia R, Sodroski J, Haseltine W, et al. (1988). The art gene product of human immunodeficiency virus is required for replication. *J Virol* 62: 655-658.
268. Luo Y, Madore SJ, Parslow TG, Cullen BR, Peterlin BM (1993). Functional analysis of interactions between Tat and the trans-activation response element of human immunodeficiency virus type 1 in cells. *J Virol* 67: 5617-5622.
269. Pollard VW, Malim MH (1998). The HIV-1 Rev protein. *Annu Rev Microbiol* 52: 491-532.
270. Miyazaki Y, Nosaka T, Hatanaka M (1996). The post-transcriptional regulator Rev of HIV: implications for its interaction with the nucleolar protein B23. *Biochimie* 78: 1081-1086.
271. Cochrane AW, Perkins A, Rosen CA (1990). Identification of sequences important in the nucleolar localization of human immunodeficiency virus Rev: relevance of nucleolar localization to function. *J Virol* 64: 881-885.
272. Schaerer-Uthurralt N, Erard M, Kindbeiter K, Madjar JJ, Diaz JJ (1998). Distinct domains in herpes simplex virus type 1 US11 protein mediate post-transcriptional transactivation of human T-lymphotropic virus type I envelope glycoprotein gene expression and specific binding to the Rex responsive element. *J Gen Virol* 79: 1593-1602.
273. Nishiyama Y, Kurachi R, Daikoku T, Umene K (1993). The US 9, 10, 11, and 12 genes of herpes simplex virus type 1 are of no importance for its neurovirulence and latency in mice. *Virology* 194: 419-423.
274. Attrill HL, Cumming SA, Clements JB, Graham SV (2002). The Herpes Simplex Virus Type 1 US11 Protein Binds the Coterminally UL12, UL13, and UL14 RNAs and Regulates UL13 Expression In Vivo. *Journal of Virology* 76: 8090-8100.
275. Roller RJ, Roizman B (1991). Herpes simplex virus 1 RNA-binding protein US11 negatively regulates the accumulation of a truncated viral mRNA. *J Virol* 65: 5873-5879.
276. Xing J, Wu F, Pan W, Zheng C (2010). Molecular anatomy of subcellular localization of HSV-1 tegument protein US11 in living cells. *Virus Research* 153: 71-81.
277. Salsman J, Zimmerman N, Chen T, Domagala M, Frappier L (2008). Genome-wide screen of three herpesviruses for protein subcellular localization and alteration of PML nuclear bodies. *PLoS Pathog* 4: e1000100.
278. Brown SM, Harland J (1987). Three mutants of herpes simplex virus type 2: one lacking the genes US10, US11 and US12 and two in which Rs has been extended by 6 kb to 0.91 map units with loss of Us sequences between 0.94 and the Us/TRs junction. *J Gen Virol* 68 (Pt 1): 1-18.
279. Diaz-Latoud C, Diaz JJ, Fabre-Jonca N, Kindbeiter K, Madjar JJ, et al. (1997). Herpes simplex virus Us11 protein enhances recovery of protein synthesis and survival in heat shock treated HeLa cells. *Cell Stress Chaperones* 2: 119-131.
280. Hill TJ, Yirrell DL, Blyth WA (1986). Infection of the adrenal gland as a route to the central nervous system after viraemia with herpes simplex virus in the mouse. *J Gen Virol* 67 (Pt 2): 309-320.
281. Xu J, Yang Y, Sun J, Ding Y, Su L, et al. (2006). Expression of Toll-like receptors and their association with cytokine responses in peripheral blood mononuclear cells of children with acute rotavirus diarrhoea. *Clin Exp Immunol* 144: 376-381.
282. El Fatimy R, Tremblay S, Dury AY, Solomon S, De Koninck P, et al. (2012). Fragile X mental retardation protein interacts with the RNA-binding protein Caprin1 in neuronal RiboNucleoProtein complexes [corrected]. *PLoS One* 7: e39338.
283. Hoogeveen AT, Willemsen R, Oostra BA (2002). Fragile X syndrome, the Fragile X related proteins, and animal models. *Microsc Res Tech* 57: 148-155.
284. Santoro MR, Bray SM, Warren ST (2012). Molecular mechanisms of fragile X syndrome: a twenty-year perspective. *Annu Rev Pathol* 7: 219-245.
285. Bhakar AL, Dolen G, Bear MF (2012). The pathophysiology of fragile X (and what it teaches us about synapses). *Annu Rev Neurosci* 35: 417-443.

286. Iacoangeli A, Tiedge H (2013). Translational control at the synapse: role of RNA regulators. *Trends Biochem Sci* 38: 47-55.
287. Feng Y, Absher D, Eberhart DE, Brown V, Malter HE, et al. (1997). FMRP associates with polyribosomes as an mRNP, and the I304N mutation of severe fragile X syndrome abolishes this association. *Mol Cell* 1: 109-118.
288. Feng Y, Gutekunst CA, Eberhart DE, Yi H, Warren ST, et al. (1997). Fragile X mental retardation protein: nucleocytoplasmic shuttling and association with somatodendritic ribosomes. *J Neurosci* 17: 1539-1547.
289. Tamanini F, Meijer N, Verheij C, Willems PJ, Galjaard H, et al. (1996). FMRP is associated to the ribosomes via RNA. *Hum Mol Genet* 5: 809-813.
290. Corbin F, Bouillon M, Fortin A, Morin S, Rousseau F, et al. (1997). The fragile X mental retardation protein is associated with poly(A)⁺ mRNA in actively translating polyribosomes. *Hum Mol Genet* 6: 1465-1472.
291. Ceman S, O'Donnell WT, Reed M, Patton S, Pohl J, et al. (2003). Phosphorylation influences the translation state of FMRP-associated polyribosomes. *Hum Mol Genet* 12: 3295-3305.
292. Khandjian EW, Huot ME, Tremblay S, Davidovic L, Mazroui R, et al. (2004). Biochemical evidence for the association of fragile X mental retardation protein with brain polyribosomal ribonucleoproteins. *Proc Natl Acad Sci U S A* 101: 13357-13362.
293. Stefani G, Fraser CE, Darnell JC, Darnell RB (2004). Fragile X mental retardation protein is associated with translating polyribosomes in neuronal cells. *J Neurosci* 24: 7272-7276.
294. Wang H, Dichtenberg JB, Ku L, Li W, Bassell GJ, et al. (2008). Dynamic association of the fragile X mental retardation protein as a messenger ribonucleoprotein between microtubules and polyribosomes. *Mol Biol Cell* 19: 105-114.
295. Sidorov MS, Auerbach BD, Bear MF (2013). Fragile X mental retardation protein and synaptic plasticity. *Mol Brain* 6: 15.
296. Ramos A, Hollingworth D, Adinolfi S, Castets M, Kelly G, et al. (2006). The structure of the N-terminal domain of the fragile X mental retardation protein: a platform for protein-protein interaction. *Structure* 14: 21-31.
297. Sjekloca L, Pauwels K, Pastore A (2011). On the aggregation properties of FMRP--a link with the FXTAS syndrome? *FEBS J* 278: 1912-1921.
298. Darnell JC, Mostovetsky O, Darnell RB (2005). FMRP RNA targets: identification and validation. *Genes Brain Behav* 4: 341-349.
299. Siomi H, Siomi MC, Nussbaum RL, Dreyfuss G (1993). The protein product of the fragile X gene, FMR1, has characteristics of an RNA-binding protein. *Cell* 74: 291-298.
300. Zhang Y, O'Connor JP, Siomi MC, Srinivasan S, Dutra A, et al. (1995). The fragile X mental retardation syndrome protein interacts with novel homologs FXR1 and FXR2. *EMBO J* 14: 5358-5366.
301. Sjekloca L, Konarev PV, Eccleston J, Taylor IA, Svergun DI, et al. (2009). A study of the ultrastructure of fragile-X-related proteins. *Biochem J* 419: 347-357.
302. Lai D, Sakkas D, Huang Y (2006). The fragile X mental retardation protein interacts with a distinct mRNA nuclear export factor NXF2. *RNA* 12: 1446-1449.
303. Kim M, Bellini M, Ceman S (2009). Fragile X mental retardation protein FMRP binds mRNAs in the nucleus. *Mol Cell Biol* 29: 214-228.
304. Bardoni B, Sittler A, Shen Y, Mandel JL (1997). Analysis of domains affecting intracellular localization of the FMRP protein. *Neurobiol Dis* 4: 329-336.
305. Tamanini F, Bontekoe C, Bakker CE, van Unen L, Anar B, et al. (1999). Different targets for the fragile X-related proteins revealed by their distinct nuclear localizations. *Hum Mol Genet* 8: 863-869.
306. Zhang M, Wang Q, Huang Y (2007). Fragile X mental retardation protein FMRP and the RNA export factor NXF2 associate with and destabilize Nxf1 mRNA in neuronal cells. *Proc Natl Acad Sci U S A* 104: 10057-10062.
307. Kholodenko BN (2006) Cell-signalling dynamics in time and space. *Nature reviews Molecular cell biology* 7: 165-176.
308. Bhattacharyya RP, Remenyi A, Yeh BJ, Lim WA (2006). Domains, motifs, and scaffolds: the role of modular interactions in the evolution and wiring of cell signaling circuits. *Annual review of biochemistry* 75: 655-680.
309. Scott JD, Pawson T (2009). Cell signaling in space and time: where proteins come together and when they're apart. *Science* 326: 1220-1224.

310. Therrien M, Michaud NR, Rubin GM, Morrison DK (1996). KSR modulates signal propagation within the MAPK cascade. *Genes Dev* 10: 2684-2695.
311. Garrenton LS, Young SL, Thorner J (2006). Function of the MAPK scaffold protein, Ste5, requires a cryptic PH domain. *Genes Dev* 20: 1946-1958.
312. Schwartz MA, Madhani HD (2006). Control of MAPK signaling specificity by a conserved residue in the MEK-binding domain of the yeast scaffold protein Ste5. *Curr Genet* 49: 351-363.
313. Selyunin AS, Sutton SE, Weigele BA, Reddick LE, Orchard RC, et al. (2011). The assembly of a GTPase-kinase signalling complex by a bacterial catalytic scaffold. *Nature* 469: 107-111.
314. Yu X, Yu Y, Liu B, Luo K, Kong W, et al. (2003). Induction of APOBEC3G ubiquitination and degradation by an HIV-1 Vif-Cul5-SCF complex. *Science* 302: 1056-1060.
315. Kozubowski L, Saito K, Johnson JM, Howell AS, Zyla TR, et al. (2008). Symmetry-breaking polarization driven by a Cdc42p GEF-PAK complex. *Curr Biol* 18: 1719-1726.
316. Ruiz-Velasco R, Lanning CC, Williams CL (2002). The activation of Rac1 by M3 muscarinic acetylcholine receptors involves the translocation of Rac1 and IQGAP1 to cell junctions and changes in the composition of protein complexes containing Rac1, IQGAP1, and actin. *J Biol Chem* 277: 33081-33091.
317. Zhang SC NK, Amin E, Taha MS, Nakhaeizadeh H, Nakhaei-Rad S, Dvorsky R, Ahmadian M R (2014). Classical Rho Proteins: Biochemistry of Molecular Switch Function and Regulation. Wittinghofer, A (ed) Ras Superfamily small G Proteins, Biology and Mechanism, Vol 1 Springer, Chapter 14, pp 327-340.
318. Chow CR, Suzuki N, Kawamura T, Hamakubo T, Kozasa T (2013). Modification of p115RhoGEF Ser(330) regulates its RhoGEF activity. *Cell Signal* 25: 2085-2092.
319. Eberth A, Lundmark R, Gremer L, Dvorsky R, Koessmeier KT, et al. (2009). A BAR domain-mediated autoinhibitory mechanism for RhoGAPs of the GRAF family. *Biochem J* 417: 371-377.
320. Jaiswal M, Gremer L, Dvorsky R, Haeusler LC, Cirstea IC, et al. (2011). Mechanistic insights into specificity, activity, and regulatory elements of the regulator of G-protein signaling (RGS)-containing Rho-specific guanine nucleotide exchange factors (GEFs) p115, PDZ-RhoGEF (PRG), and leukemia-associated RhoGEF (LARG). *J Biol Chem* 286: 18202-18212.
321. Mitin N, Betts L, Yohe ME, Der CJ, Sondek J, et al. (2007). Release of autoinhibition of ASEF by APC leads to CDC42 activation and tumor suppression. *Nat Struct Mol Biol* 14: 814-823.
322. Moskwa P, Paclat MH, Dagher MC, Ligeti E (2005). Autoinhibition of p50 Rho GTPase-activating protein (GAP) is released by prenylated small GTPases. *J Biol Chem* 280: 6716-6720.
323. Rojas RJ, Yohe ME, Gershburg S, Kawano T, Kozasa T, et al. (2007). Galphaq directly activates p63RhoGEF and Trio via a conserved extension of the Dbl homology-associated pleckstrin homology domain. *J Biol Chem* 282: 29201-29210.
324. Yohe ME, Rossman K, Sondek J (2008). Role of the C-terminal SH3 domain and N-terminal tyrosine phosphorylation in regulation of Tim and related Dbl-family proteins. *Biochemistry* 47: 6827-6839.
325. Mayer S, Kumar R, Jaiswal M, Soykan T, Ahmadian MR, et al. (2013). Collybistin activation by GTP-TC10 enhances postsynaptic gephyrin clustering and hippocampal GABAergic neurotransmission. *Proc Natl Acad Sci U S A* 110: 20795-20800.
326. Locatelli F, Nollke P, Zecca M, Korthof E, Lanino E, et al. (2005). Hematopoietic stem cell transplantation (HSCT) in children with juvenile myelomonocytic leukemia (JMML): results of the EWOG-MDS/EBMT trial. *Blood* 105: 410-419.
327. Niemeyer CM, Arico M, Basso G, Biondi A, Cantu Rajnoldi A, et al. (1997). Chronic myelomonocytic leukemia in childhood: a retrospective analysis of 110 cases. European Working Group on Myelodysplastic Syndromes in Childhood (EWOG-MDS). *Blood* 89: 3534-3543.
328. Locatelli F, Niemeyer CM (2015). How I treat juvenile myelomonocytic leukemia. *Blood* 125: 1083-1090.
329. Emanuel PD (2014). Hallway gossip between Ras and PI3K pathways. *Blood* 123: 2751-2753.
330. Goodwin CB, Li XJ, Mali RS, Chan G, Kang M, et al. (2014). PI3K p110delta uniquely promotes gain-of-function Shp2-induced GM-CSF hypersensitivity in a model of JMML. *Blood* 123: 2838-2842.
331. Casteel DE, Turner S, Schwappacher R, Rangaswami H, Su-Yuo J, et al. (2012). Rho isoform-specific interaction with IQGAP1 promotes breast cancer cell proliferation and migration. *The Journal of biological chemistry* 287: 38367-38378.
332. Wennerberg K, Ellerbroek SM, Liu RY, Karnoub AE, Burrridge K, et al. (2002). RhoG signals in parallel with Rac1 and Cdc42. *J Biol Chem* 277: 47810-47817.

333. Prieto-Sanchez RM, Bustelo XR (2003). Structural basis for the signaling specificity of RhoG and Rac1 GTPases. *J Biol Chem* 278: 37916-37925.
334. Inoue M, Chang L, Hwang J, Chiang SH, Saltiel AR (2003). The exocyst complex is required for targeting of Glut4 to the plasma membrane by insulin. *Nature* 422: 629-633.
335. Inoue M, Chiang SH, Chang L, Chen XW, Saltiel AR (2006). Compartmentalization of the exocyst complex in lipid rafts controls Glut4 vesicle tethering. *Mol Biol Cell* 17: 2303-2311.
336. Chiang SH, Chang L, Saltiel AR (2006). TC10 and insulin-stimulated glucose transport. *Methods Enzymol* 406: 701-714.
337. Pommereit D, Wouters FS (2007). An NGF-induced Exo70-TC10 complex locally antagonises Cdc42-mediated activation of N-WASP to modulate neurite outgrowth. *J Cell Sci* 120: 2694-2705.
338. Dupraz S, Grassi D, Bernis ME, Sosa L, Bisbal M, et al. (2009). The TC10-Exo70 complex is essential for membrane expansion and axonal specification in developing neurons. *J Neurosci* 29: 13292-13301.
339. Fujita A, Koinuma S, Yasuda S, Nagai H, Kamiguchi H, et al. (2013). GTP hydrolysis of TC10 promotes neurite outgrowth through exocytic fusion of Rab11- and L1-containing vesicles by releasing exocyst component Exo70. *PLoS ONE* 8.
340. Ory S, Gasman S (2011). Rho GTPases and exocytosis: what are the molecular links? *Semin Cell Dev Biol* 22: 27-32.
341. Scheffzek K, Ahmadian MR, Kabsch W, Wiesmuller L, Lautwein A, et al. (1997). The Ras-RasGAP complex: structural basis for GTPase activation and its loss in oncogenic Ras mutants. *Science* 277: 333-338.
342. Grohmanova K, Schlaepfer D, Hess D, Gutierrez P, Beck M, et al. (2004). Phosphorylation of IQGAP1 modulates its binding to Cdc42, revealing a new type of rho-GTPase regulator. *J Biol Chem* 279: 48495-48504.
343. Le Clainche C, Schlaepfer D, Ferrari A, Klingauf M, Grohmanova K, et al. (2007). IQGAP1 stimulates actin assembly through the N-WASP-Arp2/3 pathway. *J Biol Chem* 282: 426-435.
344. Pratt SJ, Epple H, Ward M, Feng Y, Braga VM, et al. (2005). The LIM protein Ajuba influences p130Cas localization and Rac1 activity during cell migration. *J Cell Biol* 168: 813-824.
345. Nola S, Daigaku R, Smolarczyk K, Carstens M, Martin-Martin B, et al. (2011). Ajuba is required for Rac activation and maintenance of E-cadherin adhesion. *J Cell Biol* 195: 855-871.
346. Giraud S, Diaz-Latoud C, Hacot S, Textoris J, Bourette RP, et al. (2004). US11 of herpes simplex virus type 1 interacts with HIPK2 and antagonizes HIPK2-induced cell growth arrest. *J Virol* 78: 2984-2993.
347. Mulvey M, Arias C, Mohr I (2006). Resistance of mRNA translation to acute endoplasmic reticulum stress-inducing agents in herpes simplex virus type 1-infected cells requires multiple virus-encoded functions. *J Virol* 80: 7354-7363.
348. Kurki S, Peltonen K, Laiho M (2004). Nucleophosmin, HDM2 and p53: players in UV damage incited nucleolar stress response. *Cell Cycle* 3: 976-979.
349. Lindstrom MS, Zhang Y (2006). B23 and ARF: friends or foes? *Cell Biochem Biophys* 46: 79-90.
350. Hope TJ (1999). The ins and outs of HIV Rev. *Arch Biochem Biophys* 365: 186-191.
351. Benboudjema L, Mulvey M, Gao Y, Pimplikar SW, Mohr I (2003). Association of the herpes simplex virus type 1 Us11 gene product with the cellular kinesin light-chain-related protein PAT1 results in the redistribution of both polypeptides. *J Virol* 77: 9192-9203.
352. Mitrea DM, Grace CR, Buljan M, Yun MK, Pytel NJ, et al. (2014). Structural polymorphism in the N-terminal oligomerization domain of NPM1. *Proc Natl Acad Sci U S A* 111: 4466-4471.
353. DiMattia MA, Watts NR, Stahl SJ, Rader C, Wingfield PT, et al. (2010). Implications of the HIV-1 Rev dimer structure at 3.2 Å resolution for multimeric binding to the Rev response element. *Proc Natl Acad Sci U S A* 107: 5810-5814.
354. Taneva SG, Bañuelos S, Falces J, Arregi I, Muga A, et al. (2009). A Mechanism for Histone Chaperoning Activity of Nucleoplasmin: Thermodynamic and Structural Models. *Journal of Molecular Biology* 393: 448-463.
355. Jeang KT, Xiao H, Rich EA (1999). Multifaceted activities of the HIV-1 transactivator of transcription, Tat. *J Biol Chem* 274: 28837-28840.
356. Suhasini M, Reddy TR (2009). Cellular proteins and HIV-1 Rev function. *Curr HIV Res* 7: 91-100.
357. Cardarelli F, Serresi M, Bizzarri R, Giacca M, Beltram F (2007). In vivo study of HIV-1 Tat arginine-rich motif unveils its transport properties. *Mol Ther* 15: 1313-1322.

358. Lin MH, Sivakumaran H, Apolloni A, Wei T, Jans DA, et al. (2012). Nullbasic, a potent anti-HIV tat mutant, induces CRM1-dependent disruption of HIV rev trafficking. *PLoS ONE* 7: e51466.
359. Catez F, Erard M, Schaerer-Uthurralt N, Kindbeiter K, Madjar JJ, et al. (2002). Unique Motif for Nucleolar Retention and Nuclear Export Regulated by Phosphorylation. *Molecular and Cellular Biology* 22: 1126-1139.
360. Davidovic L, Durand N, Khalfallah O, Tabet R, Barbry P, et al. (2013). A novel role for the RNA-binding protein FXR1P in myoblasts cell-cycle progression by modulating p21/Cdkn1a/Cip1/Waf1 mRNA stability. *PLoS Genet* 9: e1003367.
361. Krueger DD, Bear MF (2011). Toward fulfilling the promise of molecular medicine in fragile X syndrome. *Annu Rev Med* 62: 411-429.
362. Wang T, Bray SM, Warren ST (2012). New perspectives on the biology of fragile X syndrome. *Curr Opin Genet Dev* 22: 256-263.
363. Darnell JC, Van Driesche SJ, Zhang C, Hung KY, Mele A, et al. (2011). FMRP stalls ribosomal translocation on mRNAs linked to synaptic function and autism. *Cell* 146: 247-261.

7 Acknowledgments

Firstly, I would like to express my sincere gratitude to my supervisor Prof. Dr. Reza Ahmadian for the continuous support of my Ph.D study and related research, for his patience, motivation, and immense knowledge. His guidance helped me in all the time of research and writing of this thesis. I would like to express the deep appreciation to my co-supervisor Prof. Dr. Lutz Schmitt for his precious support, kind help, and advices.

Thereafter, I thank Prof. Dr. Jurgen Scheller as a dean of the institute of Biochemistry and Molecular biology II for his supports and for providing researchers a warm atmosphere for the research. I would also thanks to Dr. Roland Piekorz, Dr. Lothar Gremer, Prof. Dr. David Timson, Prof. Dr. Carsten Münk, Anika Hain, Dr. Sander Smits, Dr. Lech-Gustav Milroy, Prof. Dr. Luc Brunsveld, Dr. Luitgard Nagel-Steger and Prof. Dr. Hélène Cavé for valuable discussion, collaboration, and nice help.

I would also like to thank to International Graduate School of Protein Science and Technology (iGRASP) and German Research Foundation through Collaborative Research Center 974 (Grant SFB 974) foundation for their financial support and, Prof. Dr. Jörg Pietruszka, Prof. Dr. Dieter Willbold, Prof. Dr Dieter Häussinger and our nice scientific coordinator Dr. Martina Holz for their supports. Thanks to all iGRASP fellows for discussion and also making funny moments during my PhD study.

Next, I thank my colleagues especially Ehsan Amin, Saeideh Nakhaei-Rad, Hossein Nakhaeizadeh, Rebecca Heinen, Jana Kremer, Dr. Jens Moll, Dr. Radovan Dvorsky, Dr. Eyad Kalawy Fansa, Dr. Si-Cai Zhang, Dr. Mohamed Saleh Taha, Dr. Madhurendra Singh, Alexander Lang, Niloufar Monhasery, and all other members of the institute for the valuable discussions, cooperation and happy moments.

I thank all kind staff in the institute of Biochemistry and Molecular biology II especially Petra Oprea Jeremic, Ilse Meyer, Freshteh Kamrani, Hakima Ezzahoini, Nadine Horstick-Muche, and Zeynep Tokyurek for their continuous support.

I thank my friends Omid Abbasi, Dr. Elmira Ghabraee, Dr. Hamed shaykhalishahi, Majid Ghorbanpour, Carolin Optiz, Kebria Hazaveh, and Mona Youhannayee for all helps and making unforgettable happy and funny moments during last 4 years.

Finally, my very special thanks go to my family. I would like to dedicate this thesis to my mother for her pure love, and the soul of my father who always encouraged me to have high expectations and to fight hard for what I want and believe. I thank my brothers and sisters for supporting me spiritually and giving me motivation throughout my life.

8 Curriculum Vitae

Personal details

Name	Kazem Nouri
Date of Birth	April 21 st 1984
Nationality	Iranian

Education

Since 2012	Ph.D. student in Biochemistry , Institute for Biochemistry and Molecular Biology II (IBMB2), Heinrich-Heine-University, Düsseldorf, Germany.
2011-2012	Ph.D. student in Biochemistry , Institute of Biochemistry and Biophysics (IBB), University of Tehran, Tehran, Iran.
2007-2010	M.Sc. in Biochemisrty , Institute of Biochemistry and Biophysics (IBB), University of Tehran, Tehran, Iran. GPA: 18.25 out of 20. (Thesis mark: 19.90 out of 20).
2003- 2007	B.Sc. in Biology , Faculty of Biological Sciences, Shahid Beheshti University, Tehran, Iran. GPA: 16.73 out of 20.

Research experience

Ph.D. student Thesis	Group of Prof. Dr. Reza Ahmadian Biochemical Characterization of RHO GTPases-IQGAPs and NPM1-US11/Rev interactions
M.Sc. student Thesis	Group of Prof. Dr. Razieh Yazdanparast Effects of intracellular purine nucleotide level on cellular fate toward differentiation and apoptosis

Honors and awards

Ranked first in PhD entrance exam of Biochemistry (University of Tehran)

Young Investigator grant of 36th FEBS Congress, Torino, Italy

Ranked the "3rd Position" among M.Sc. students of biochemistry at University of Tehran

Ranked as the "Top 5%" among B.Sc. students of biology at Shahid Beheshti University

Ranked as the "Top 2%" of national undergraduate entrance exam for Universities and Colleges in Iran

Presentation at conferences (poster)

Nouri K, Ahmadian MR (2015) New insights into the interaction between IQGAP1 and Rho family proteins. 29th Annual Symposium of The Protein Society, Barcelona, Spain.

Nouri K, Yazdanparast R (2011) Differentiation, apoptosis and reduction of intracellular GTP level in HL-60 and K562 cells upon treatment with a novel IMP dehydrogenase inhibitor. 36th FEBS congress Torino, Italy.

Nouri K, Yazdanparast R (2009) Effects of 3-hydrogenkwadaphnin (3-HK) on intracellular purine nucleotide contents of K562 cells. 17th ECDO Euroconference on Apoptosis, Paris, France.

Publications

1. Caye A, Strullu M, Guidez F, Cassinat B, Gazal S, Fenneteau O, Lainey E, **Nouri K**, Nakhaei-Rad S, et al., (2015) Juvenile myelomonocytic leukemia displays mutations in components of the RAS pathway and the PRC2 network. Nature Genetics 47:1334-40.
2. **Nouri K**, Fansa EK, Amin E, Nakhaei-Rad S, Dvorsky R, GremerR, Timson DJ, Schmitt, L, Häussinger D, Ahmadian MR. IQGAP1 interaction with RHO family proteins revisited: kinetic and equilibrium evidence for two distinct binding sites (in Preparation).
3. **Nouri K**, Moll JM, Milroy LG, Hain A, Dvorsky R, Amin E, Lenders M, Nagel-Steger L, Howe S, Smits SHJ, Hengel H, Schmitt L, Münk C, Brunsveld L, Ahmadian MR (2015) Biophysical Characterization of Nucleophosmin Interactions with Human Immunodeficiency Virus Rev and Herpes Simplex Virus US11. PLOS One (in press).
4. Zhang SC, **Nouri K**, Amin E, Taha MS, Nakhaeizadeh H, Nakhaei-Rad S, Dvorsky R, Ahmadian MR (2014) Classical Rho Proteins: Biochemistry of Molecular Switch Function and Regulation. In: Wittinghofer, A (ed) Ras Superfamily small G Proteins, Biology and Mechanism, Vol. 1 Springer, Chapter 14, 327-340.
5. Taha, MS, **Nouri K**, Milroy LG, Moll JM, Herrmann C, Brunsveld L, Piekorz RP, Ahmadian MR (2014) Subcellular fractionation and localization studies reveal a direct interaction of the fragile X mental retardation protein (FMRP) with nucleolin. PLoS ONE 9:e91465.
6. Thakur HC, Singh M, Nagel-Steger L, Kremer J, Prumbaum D, Kalawy FE, Ezzahoini H, **Nouri K**, et al., (2014) The centrosomal adaptor TACC3 and microtubule polymerase chTOG interact via defined C-terminal subdomains in an Aurora-A kinase independent manner. J. Biol. Chem. 289:74-88.
7. **Nouri K**, Yazdanparast R, Sarafnejad A (2011) Guanosine supplementation in K562 cells reduces the anti-proliferative and apoptotic effects of Gnidilatimonoein isolated from *Daphne mucronata*. Cell Biology International 35:1001-8.
8. Meshkini A, Yazdanparast R, **Nouri K** (2011) Intracellular GTP level determines cell's fate toward differentiation and apoptosis. Toxicology and Applied Pharmacology 253:188-96.
9. **Nouri K**, Yazdanparast R (2011) Effects of 3-hydrogenkwadaphnin on intracellular purine nucleotide contents and their link to K562 cell death. Food Chemistry 128(1):81-86.
10. **Nouri K**, Yazdanparast R (2011) Proliferation inhibition, cell cycle arrest and apoptosis induced in HL-60 cells by a natural diterpene ester from *Daphne mucronata*. DARU 19:145-153.

9 Declaration

I do solemnly declare that my thesis is presentation of original research performed according to the “Principles of Good Scientific Practice” set out by Heinrich-Heine University of Düsseldorf. This thesis does not contain the data already published in public domain and it has never been submitted or accepted by any other institutions for the award of any other degrees.

Düsseldorf, November 2015

Kazem Nouri